Defining the role of 14-3-3ζ in neuronal migration and neurogenesis

A thesis presented in partial fulfilment for the degree of Doctor of Philosophy in the School of Medicine of the University of Adelaide

August 2016

Eiman Osman Saleh
1602939

Supervisors
Dr Quenten Schwarz
Dr Hayley Ramshaw

Declaration

I certify that this work contains no material which has been accepted for the award of any other degree or diploma in my name, in any university or other tertiary institution and, to the best of my knowledge and belief, contains no material previously published or written by another person, except where due reference has been made in the text. In addition, I certify that no part of this work will, in the future, be used in a submission in my name, for any other degree or diploma in any university or other tertiary institution without the prior approval of the University of Adelaide and where applicable, any partner institution responsible for the joint-award of this degree.

I give consent to this copy of my thesis when deposited in the University Library, being made available for loan and photocopying, subject to the provisions of the Copyright Act 1968. I acknowledge that copyright of published works contained within this thesis resides with the copyright holder(s) of those works.

I also give permission for the digital version of my thesis to be made available on the web, via the University's digital research repository, the Library Search and also through web search engines, unless permission has been granted by the University to restrict access for a period of time.

Eiman O. Saleh

Acknowledgements

In the name of Allah (God), the Most Gracious and the Most Merciful.

All praises to Allah for the strengths and His blessing, in completing this thesis.

My PhD journey would not have been possible without the support of my family, mentors, colleagues and friends. Therefore, I would like to take this opportunity to extend my sincere gratitude and immeasurable appreciation to the people who have helped and supported me throughout this journey.

Foremost, a special thanks to my supervisors: Dr Quenten Schwarz and Dr Hayley Ramshaw who provided me an opportunity to join their laboratories, even though I had no background in neuroscience. I am thankful for all their continuous guidance, support and encouragement throughout the years.

To my lab colleagues, thank you for giving me your time, energy, and expertise- I am richer for it. Thank you all for helping me during different stages of my project and for being awesome lab colleagues. I truly loved the company of every one of you; I will cherish these memories forever.

A big thank you to members of the Schwarz's Lab:

Dr Sophie Wiszniak for helping me select the right international conference to go to. Dr Peter McCarthy for your constructive input during lab meeting. Samuela Kabbara for teaching me the lab system. Racheal Lumb for teaching me how to use the confocal spinning disc. Zarina Greenberg for making the lab

environment so much fun. Xiangjun Xu, I was so fortunate to share lab space with you and I am so thankful for your constant help no matter how busy you were; especially with getting the prefect brain sections, among other things. I truly appreciate it; without your super skills it would not have be possible to conduct this research.

A big thank you to members of the Ramshaw's Lab:

Nicole Wittwer for your countless help with protein experiments. Melanie Pudney for taking over genotyping mice towards the end of the project, you made my life a bit easier. Rebecca Wright (Krake), thank you for teaching me everything to do with breeding and maintaining the mouse colonies.

An extended thank you for all those who participated in this research, for whom without contribution this thesis would not be possible. A big thank you to all the collaborators, who without the work publication would not be possible.

Assoc Prof Natasha Harvey's group for their insightful comments and stimulating discussion during our combined lab meetings. Dr Lachlan Jolly for coming out of your way to teach me how to dissect and culture embryonic hippocampal neurons. All members of the Centre for Cancer Biology – the technical and office staff thank you for all your help. SA Pathology and the University of Adelaide staff for maintaining the mouse colonies.

Dr Winnie Kan, Victoria Arnet and Zarina Greenberg you for all your endless patience, support and encouragement- you are amazing friends. Thanks especially for listening about my experimental dilemmas.

I am especially grateful to my parents (Mariem Mirkab and Osman Ali) and siblings (Menal, Mohassin, Ahmed and Sanaa), for encouraging me in all of my pursuits and inspiring me to follow my dreams. Thank you for always believing and supporting me throughout this journey and my life in general. My parents, thank you for teaching me that my job in life was to learn, to be happy, and to know and understand myself; only then could I know and understand others. I also am grateful to Dr Hamid Adem for enlightening me the first glance of research and endless guidance.

Table of Contents

Declaration 1
Acknowledgements 2
Table of Contents 5
List of Figures 9
Abbreviations 11
Publications 14
Awards 15
Abstract 16

Chapter One: General Introduction 17
1.1 14-3-3 proteins 18
1.1.1 Structural information and protein interactions 19
1.1.2 Regulation 21
1.2 14-3-3 in brain function 23
1.2.1 14-3-3 proteins in neurological disorders 23
1.2.2 14-3-3 in schizophrenia 24
1.3 Brain development 27
1.3.1 The hippocampus 29
1.3.2 Hippocampal development 31
1.4 Mouse models 35
1.4.1 Schizophrenia mouse models 35
1.4.2 Disrupted in schizophrenia 1 (*DISC1*) 37
1.4.3 14-3-3ζ KO mouse model 38
1.5 Neuronal morphogenesis 40
1.5.1 Neurite outgrowth 42
1.5.2 Dendrite and spine morphogenesis 44
1.6 Neuronal migration 48
1.6.1 Molecular pathways regulating neuronal migration 51
1.6.2 Lissencephlay 1 (Lis1) 53
1.6.3 Nuclear distribution E-like homolog 1 (Ndel1) 53
1.7 Neurogenesis 54
1.7.1 Neurogenesis in the adult hippocampus 54
1.7.2 Links between disrupted adult neurogenesis and schizophrenia 57
1.7.3 Regulation of adult hippocampal neurogenesis 57
1.8 Aims of the thesis 61

Chapter Two: Material and Methods 63
2.1 Materials 64
2.2 Animal husbandry 65
2.2.1 Ethics 65
2.2.2 Strains and housing of mice 65
2.3 Animal and tissue preparation 66
2.3.1 Whole mouse perfusion fixation 66
2.3.2 Cryosectioning of mouse brain 66
2.3.3 Vibratome sectioning 67
2.3.4 EdU short-pulse labelling 67
2.4 Histology and immunohistochemistry 68
2.4.1 Nissl staining of brain sections 68
2.4.2 Immunostaining of brain sections 68
2.4.3 Golgi-cox impregnation 69
2.4.4 Biolistic labelling of neurons using gene gun 70
2.5 Hippocampal neuronal cultures 71
2.5.1 Glial feeder cultures 71
2.5.2 Preparation of glass coverslips for hippocampal cultures 72
2.5.3 Dissection of the E18.5 hippocampi 72
2.5.4 Hippocampal primary cell cultures 73
2.5.5 Glial feeder layer preparation for long-term hippocampal culture 74
2.5.6 Immunostaining of hippocampal primary cell cultures 75
2.5.7 Analysis of hippocampal neurons 75
2.6 Neurosphere culture 77
2.6.1 Neurosphere culture of hippocampal neural progenitor cells 77
2.6.2 Neurosphere migration assay 78
2.6.3 Analysis of the migration assay 79
2.6.4 Live imaging of the neurosphere migration assay using spinning disc confocal microscopy 80
2.6.5 Adhesion assay on neural progenitors 81
2.6.6 Nuclear-centrosome coupling 82
2.6.7 Transfection of neurospheres 83
2.6.8 Neurosphere proliferation and self-renewal assays 83
2.6.9 BrdU incorporation assay on neural progenitor cells from neurosphere cultures 85
2.6.10 Immunostaining of neurospheres with stem cells markers 86
2.7 Molecular biology protocols 88
2.7.1 Genomic DNA isolation and preparation 88
2.7.2 Mouse genotyping 88
2.7.3 Agarose gel electrophoresis 89

2.7.4 Constructs 90
2.7.5 DNA sequencing 90
2.7.6 Preparation of electrocompetent *E. coli* DH5α cells 91
2.7.7 Electroporation into *E. coli* DH5α cells 91
2.7.8 Large scale plasmid purification 92
2.8 Protein interaction analysis 93
2.8.1 HEK293T cell culture 93
2.8.2 Transfection of HEK293T cells 94
2.8.3 Protein extraction from cells and brain tissue 95
2.8.4 Protein quantitation using BCA protein assay 96
2.8.5 Immunoprecipitation 97
2.8.6 Sodium dodecyl sulphate polyacrylamide gel electrophoresis (SDS-PAGE) 98
2.8.7 Western blotting 99

Chapter Three: Characterization of 14-3-3ζ KO Mice 102
3.1 Introduction 103
3.2 Results 105
3.2.1 14-3-3ζ KO mice in the BALB/c and C57BL/6 backgrounds display hippocampal lamination defects similar to the 129/sv background 105
3.2.2 14-3-3ζ KO mice in the BALB/c and C57BL/6 backgrounds display disrupted mossy fibre circuit 109
3.2.3 The role of 14-3-3ζ in early phase neurite outgrowth 112
3.2.4 The role of 14-3-3ζ in dendrite morphogenesis 115
3.2.5 14-3-3ζ deficiency affects dendritic spine density 121
3.3 Discussion 126

Chapter Four: Defining the Role of 14-3-3ζ in Neuronal Migration 133
4.1 Introduction 134
4.2 Results 136
4.2.1 *In vitro* neuronal migration assay 136
4.2.2 14-3-3ζ is important for hippocampal neuronal progenitor cell migration 138
4.2.3 Live imaging reveals neuronal migration defects in 14-3-3ζ KO neurons 141
4.2.4 Effect of 14-3-3ζ KO in neuronal migration velocity and adhesion 143
4.2.5 Nuclear-centrosome coupling is disrupted in 14-3-3ζ deficient neurons 144
4.2.6 14-3-3ζ directly interacts with Ndel1 146
4.2.7 14-3-3ζ maintains Ndel1 phosphorylation 148
4.2.8 Expression of Ndel1 phosphomimetic in 14-3-3ζ KO neurons 151
4.3 Discussion 154

Chapter Five: The Role of 14-3-3ζ in Neurogenesis 158
5.1 Introduction 159
5.2 Results 161
5.2.1 Optimisation of neurosphere culture system 161
5.2.2 14-3-3ζ KO impairs neural stem/progenitor cell self-renewal *in vitro* 163
5.2.3 14-3-3ζ is required for neural stem/progenitor cell proliferation *in vitro* 166
5.2.4 Neurogenesis stage-specific cell marker expression in 14-3-3ζ KO neurospheres 169
5.2.5 Proliferation of neural stem/progenitor cells is decreased in 14-3-3ζ KO mice 171
5.2.6 14-3-3ζ KO mice have reduced expression of neurogenesis stage-specific cell markers *in vivo* 174
5.2.7 Neurogenesis stage-specific marker expression in adult mouse hippocampi 176
5.2.8 Investigating the molecular mechanism through which 14-3-3ζ controls neurogenesis 177
5.3 Discussion 178

Chapter Six: General Discussion and Conclusion 185
6.1 Discussion 186
6.2 Future studies and conclusion 191

References 193

Appendix 214
A.1 General solutions and buffers 215
A.2 Genotyping of mice 216
A.3 Hippocampal primary DIV21 neurons for dendritic spine density analysis 217
A.4 Preliminary analysis of dendritic spine in the 14-3-3ζ KO hippocampus via transmission electron microscopy revealed increase size compared to WT 218
A.5 Additional migration distance rescue experiments 220
A.6 Additional migration velocity data 223
A.7 BALB/c derived 14-3-3ζ deficient stem/progenitor cells also show reduced self-renewal *in vitro* 225

Published Papers 227

List of Figures

Figure 1. 1: Crystal structure of human 14-3-3 isoforms bound to peptide ligands..... 19
Figure 1. 2: Burden of diseases worldwide in 2004..... 24
Figure 1. 3: Illustration of mouse brain development after neural tube formation..... 28
Figure 1. 4: Hippocampal trisynaptic circuit in adult mouse brain. 30
Figure 1. 5: Mouse hippocampal development..... 34
Figure 1. 6: Schematic of neuronal morphogenesis. 41
Figure 1. 7: Signalling inputs regulating neurite outgrowth. 43
Figure 1. 8: Schematic of pyramidal neurons depicting atrophies in dendrite morphology and spines in brains of individuals with various disorders. 45
Figure 1. 9: Simplified schematic of steps involved in neuronal migration..... 50
Figure 1.10: Simplified schematic of the neuronal migration pathway and hippocampal lamination defects resulting from migration deficiencies. 52
Figure 1. 11: Developmental stages during adult hippocampal neurogenesis in the dentate gyrus. 56
Figure 1. 12: Canonical Wnt signaling pathway. 60

Figure 3.1: Hippocampal lamination defects in 14-3-3ζ KO mice. 108
Figure 3.2: Abnormal mossy fibre navigation in 14-3-3ζ KO mice..... 111
Figure 3.3: Early phase neurite outgrowth from 14-3-3ζ 129/sv hippocampal neurons. 113
Figure 3.4: Early phase neurite outgrowth from 14-3-3ζ BALB/c hippocampal neurons. 114
Figure 3.5: Dendrite morphogenesis of 14-3-3ζ 129/sv hippocampal neurons. 118
Figure 3 6: Dendrite morphogenesis of 14-3-3ζ BALB/c hippocampal neurons..... 119
Figure 3.7: Altered dendritic morphology in the hippocampus of 14-3-3ζ KO neurons in the 129/sv background..... 120
Figure 3.8: Golgi-cox staining of dendritic spines of cortical layer V pyramidal neurons of the 129/sv mice. 123
Figure 3.9: Reduced dendritic spine density in 14-3-3ζ KO 129/sv hippocampus. 124
Figure 3.10: Reduced dendritic spine density in 14-3-3ζ KO BALB/c hippocampus. 125

Figure 4.1: Neuronal migration assay. 137
Figure 4.2: Migration defects are associated with 14-3-3ζ deficiency in neuronal progenitor cells. 140
Figure 4.3: Live imaging of 14-3-3ζ WT and KO migrating neurons. 142
Figure 4.4: Mean migration velocity and adhesion assay of 14-3-3ζ KO neurons. 143
Figure 4.5: 14-3-3ζ deficient neurons have defective nuclear-centrosome coupling. 145
Figure 4.6: 14-3-3ζ interacts directly with Ndel1. 147
Figure 4.7: Ndel1 phosphorylation promotes interaction with 14-3-3ζ. 149
Figure 4.8: 14-3-3ζ KO leads to reduction in phosphorylated Ndel1 levels *in vivo*. 150
Figure 4. 9: 14-3-3ζ KO neuronal migration defect is rescued by Ndel1 phosphomimetic. 153
Figure 4.10: Model of 14-3-3 role to the neuronal migration pathway. 157

Figure 5. 1: Schematic of experimental procedure using the neurosphere culture system. 162
Figure 5. 2: 14-3-3ζ KO results in reduced stem/progenitor cell self-renewal *in vitro*. 165
Figure 5. 3: 14-3-3ζ KO results in reduced neural stem/progenitor cell proliferation *in vitro*. 167
Figure 5. 4: BrdU-incorporation demonstrates that 14-3-3ζ is important for neural stem/progenitor cells proliferation *in vitro*. 168
Figure 5. 5: Expression of neurogenesis stage-specific cell markers in neurospheres. 170
Figure 5. 6: Representative images of EdU short-pulse chase analysis of hippocampal dentate gyrus sections. 173
Figure 5. 7: 14-3-3ζ KO adult mice show reduced expression of neurogenesis stage-specific cell markers. 175
Figure 5. 8: 14-3-3ζ interaction with DCX and SOX2. 176
Figure 5. 9: 14-3-3ζ interaction with GSK3-3β and phosphorylated GSK-3β. 177
Figure 5. 10: A model for the stabilization mechanism of β-catenin by 14-3-3ζ to regulate neural stem/progenitor proliferation. 184

List of Tables

Table 2. 1: Sequence of primer set used for genotyping 14-3-3ζ mice. 89
Table 2. 2:Template for BCA protein assay based on a 96-well plate. 97
Table 2. 3: Recipes to make two separating gels based on protein molecular weight (MW). 99
Table 2. 4: Primary antibodies and dilutions used for western blotting. 100

Abbreviations

°C	Degrees Celsius
nM, µM, mM, M	Nano Molar, Micro Molar, Milli Molar, Molar
β, ε, γ, η, σ, τ, ζ	Beta, Epsilon, Gama, Eta, Sigma, Tau, Zeta
14-3-3	Tyrosine 3-monooxygenase/tryptophan5-monooxygenase activation protein
A	Alanine
ApoER2	Apolipoprotein E Receptor type 2
bFGF	Basic Fibroblast Growth Factor
bp	Base Pairs
BrdU	5-Bromodeoxyuridine
BSA	Bovine Serum Albumin
CA	Cornu Ammonis
CNS	Central Nervous System
Cdk5	Cyclin-Dependent Kinase 5
Dab1	Disabled 1
DAPI	4,6-diamidino-2-phenylindole
DCX	Doublecortin
DEAE	Diethylaminoethyl
DG	Dentate Gyrus
DISC1	Disrupted in schizophrenia 1
DIV	Days In Vitro
DMEM	Dulbecco's modified Eagle's medium
DMEM/F12	Dulbecco's modified Eagle's medium: Nutrient Mixture F-12
DMSO	Dimethyl sulfoxide
DNA	Deoxyribonucleic acid
dNTP	2'-deoxynucleotides (Adenine, Thymine, Guanine, or Cytosine)
E	Glutamic acid
E18.5	Embryonic day 18.5

EDTA	Disodium ethylenediamine tetracetate
EdU	5–ethynyl–2′–deoxyuridine
FCS	Fetal Calf Serum
g, mg, µg, ng	Gram(s), Miligram(s), Microgram(s), Nonogram(s)
GCL	Granule Cell Layer
GFAP	Glial Fibrillary Acidic Protein
GFP	Green Florescent Protein
GSK-3β	Glycogen Synthase Kinase 3β
HA-tag	Hemagglutinin Tag
HET	Heterozygous
IZ	Intermediate Zone
Kb	Kilo-base
kDa	Kilo-Dalton
KO	Knockout
L, mL, µL	Litre(s), Millilitre(s), Microlitre(s)
LB	Luria Bertani
Lis1	Lissencephaly 1
ML	Molecular Layer
MZ	Marginal Zone
Ndel1	Nuclear Distributed E-like Factor Homolog 1
NRG1	Neuregulin 1
OCT	Optimum Cutting Temperature
P#	Postnatal day #
PBS	Phosphate Buffered Saline
PCR	Polymerase Chain Reaction
PFA	Paraformaldehyde
PP2A	Protein phosphatase 2 A
PS	Penicillin/streptomycin
RPM	Revolutions Per Minute
RT	Room Temperature
S	Serine
SDS-PAGE	Sodium Dodecyl-Sulphate Polyacrylamide Gel Electrophoresis

SEM	Standard Error of the Mean
SGZ	Subgranule zone
SPL	Subplate
SVZ	Subventricular zone
T	Threonine
TAE	Tris-acetic-EDTA
TBST	Tris-Buffered Saline Tween-20
Tris	Tris[hydroxymethyl]aminomethane
U	Units
UV	Ultra Violet
v/v	Volume Per Volume
V	Volts
VLDLR	Very Low Density Lipoprotein Receptor
VZ	Ventricular Zone
WT	Wildtype
w/v	Weight Per Volume
X-gal	5-bromo-4-chloro-3-indolyl- beta-Dgalactopyranoside

Publications

RAMSHAW, H., XU, X., JAEHNE, E. J., MCCARTHY, P., GREENBERG, Z., **SALEH, E.**, MCCLURE, B., WOODCOCK, J., KABBARA, S., WISZNIAK, S., WANG, T. Y., PARISH, C., VAN DEN BUUSE, M., BAUNE, B. T., LOPEZ, A. & SCHWARZ, Q. 2013. Locomotor hyperactivity in 14-3-3zeta KO mice is associated with dopamine transporter dysfunction. Transl Psychiatry, 3, e327.

XU, X., JAEHNE, E. J., GREENBERG, Z., MCCARTHY, P., **SALEH, E**., PARISH, C. L., CAMERA, D., HENG, J., HAAS, M., BAUNE, B. T., RATNAYAKE, U., VAN DEN BUUSE, M., LOPEZ, A. F., RAMSHAW, H. S. & SCHWARZ, Q. 2015. 14-3-3zeta deficient mice in the BALB/c background display behavioural and anatomical defects associated with neurodevelopmental disorders. Sci Rep, 5, 12434.

JAEHNE, E. J., RAMSHAW, H. S., XU, X., **SALEH, E**., CLARK, S. R., SCHUBERT, K. O., LOPEZ, A. F., SCHWARZ, Q., BAUNE, B.T. 2015. In-vivo administration of clozapine affects behaviour but does not reverse dendritic spine deficits in the 14-3-3zeta KO mouse model of schizophrenia-like disorders. Pharmacol Biochem Behav. 138, 1-8.

Awards

School of medicine poster prize (2013), Faculty of health science postgraduate conference, Adelaide University.

Australian protein group student awards, (2013), Australian protein group, Adelaide.

Student travel award (2013), Australian Neuroscience Society, Melbourne.

Cell biology student poster prize (2012), Australian and New Zealand Society for Cell and Development Biology, Adelaide.

Abstract

Neuropsychiatric disorders such as schizophrenia have complex genetic traits and are believed to arise from defects in multiple genes within connected biological networks. One of the major limitations regarding the neurobiology of higher brain function and in studying complex psychiatric disorders is the necessity to use animal models to mimic the higher complexity of the human brain. Recently, *14-3-3ζ* has been associated with schizophrenia and our laboratory has previously demonstrated that mice lacking this gene have deficits reminiscent of the human condition. This thesis provides further evidence for 14-3-3ζ KO mice representing a unique and appropriate model to study the aetiology of schizophrenia and related disorders, with core focus on the orchestrated development of hippocampal neurons. Some of the key findings include; 1) the importance of 14-3-3ζ in controlling neuronal migration to promote hippocampal lamination, 2) the importance of 14-3-3ζ in controlling axonal pathfinding and dendritic spine formation, 3) the direct interaction of 14-3-3ζ with Cdk5/p35 phosphorylated Ndel1 to maintain Ndel1 phosphorylation and promote neuronal migration, and 4) the role of 14-3-3ζ in embryonic, early postnatal and adult neurogenesis, particularly in neural stem/progenitor cells proliferation and self-renewal. Taken together, this work provides novel insight to the functions of 14-3-3ζ in neuronal development and the aetiology of neuropsychiatric disorders.

Chapter One:

General Introduction

1.1 14-3-3 proteins

14-3-3 proteins are a family of highly conserved regulatory proteins expressed in eukaryotic organisms (Aitken et al., 1992, Berg et al., 2003). Moore and Perez (1967) first discovered these proteins during a systematic analysis of brain tissue based on their fraction number on DEAE-cellulose chromatography and their position on starch gel electrophoresis. 14-3-3 proteins are multifunctional and interact with over 100 protein partners. Despite this plethora of known binding proteins, in many cases the exact role of 14-3-3 in these interactions has remained obscure. However, there is extensive evidence indicating their involvement in multiple cellular processes such as cell cycle regulation, proliferation, migration, differentiation and apoptosis (Berg et al., 2003, Fu et al., 2000, Toyo-oka et al., 2003, Ikeda et al., 2008). Such diverse functions are thought to indicate their importance in human disease (Berg et al., 2003, Fu et al., 2000).

There are seven distinct mammalian isoforms of the 14-3-3 proteins (Figure 1.1) (Martin et al., 1993, Boston et al., 1982), where each isoform has been assigned a Greek letter (β, ε, γ, η, σ, τ, ζ) according to its sequential elution position after reverse-phase high-performance liquid chromatography (HPLC) (Aitken et al., 1992, Ichimura et al., 1988). Up to fifteen isoforms are present in plants and two isoforms have been identified in yeast, *Drosophila melanogaster* and *Caenorhabditis elegans* (Rosenquist et al., 2001, Wang and Shakes, 1996).

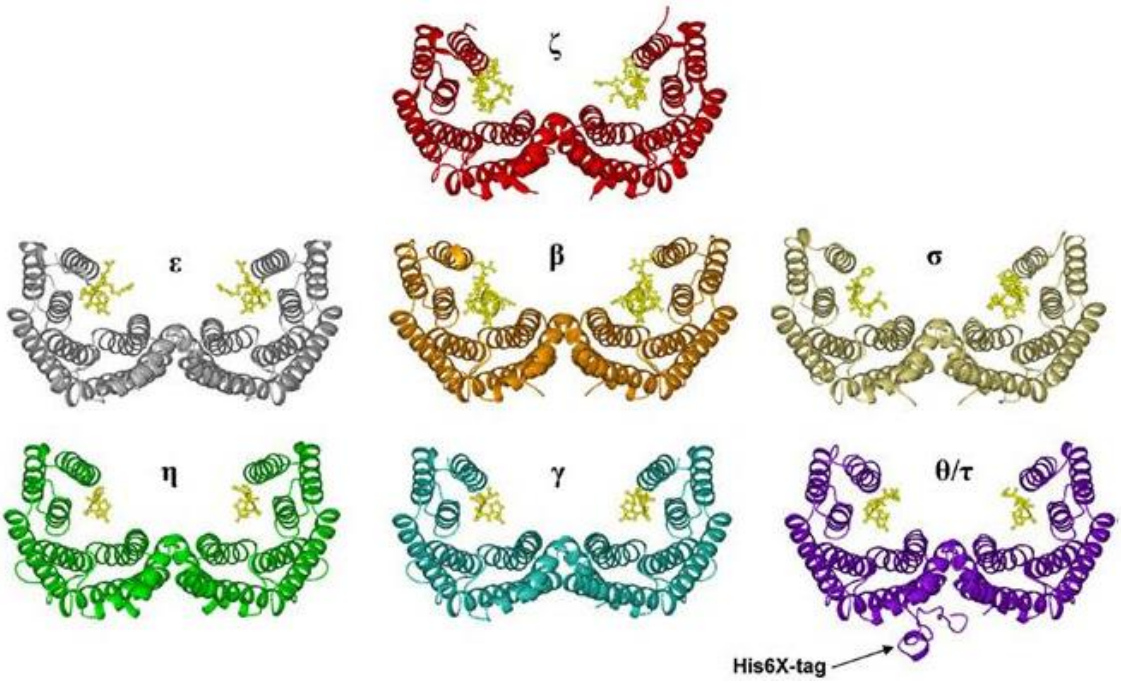

Figure 1. 1: Crystal structure of human 14-3-3 isoforms bound to peptide ligands.

A side view of each 14-3-3 isoforms in homodimeric form is shown according to the following scheme: red: zeta; grey: epsilon; orange: beta; tan: sigma; green: eta; blue: gamma; purple: tau. Dimerization occurs through salt bridges, as well as several buried polar and hydrophobic residues. The first salt bridge (Arg18-Glu89) and the hydrophobic/polar contacts (Leu12, Ala16, Ser58, Val62, Ile65, & Tyr82) are conserved in all human 14-3-3 isotypes. The second salt bridge (Glu5-Lys74) is absent in σ, η, ε, and γ isoforms, and the third salt bridge (Asp21-Lys85) is present in all human 14-3-3 structures except ε. In all models yellow residues represent phosphopeptide ligand except for ε which is a non-phosphopeptide ligand. Adapted from Gardino et al. (2006).

1.1.1 Structural information and protein interactions

14-3-3 proteins have molecular masses of around 30kDa and an isoelectric point of around 5 in the two-dimensional polyacrylamide gel electrophoresis (2D-PAGE) system (Aitken et al., 1992). The human 14-3-3ζ (Liu et al., 1995) and 14-3-3τ (Xiao et al., 1995) crystal structure revealed that these proteins exist in homo- or hetero-dimeric forms. Each monomer has a cup-like shape consisting of nine antiparallel α-helices (Berg et al., 2003, Fu et al., 2000) and there is an abundance

of acidic residues within their core conserved domains. The other human isoforms have subsequently been crystallized (reviewed in Gardino et al., 2006) and show similar structure (Figure 1.1).

The 14-3-3 dimers may bind to one target protein or to multiple target proteins via different motifs and hold them in multiprotein complexes (Skoulakis and Davis, 1998). Although the exact role of 14-3-3 dimerization is not completely understood, this phenomenon seems to be crucial for the function of this protein family. In fact, some isoforms prefer to adopt strictly homodimeric interactions such as human 14-3-3σ and 14-3-3γ while others preferentially form heterodimers such as human 14-3-3ε and all yeast 14-3-3 proteins (Gardino et al., 2006).

14-3-3 binding motifs generally contain phosphoserine/phosphothreonine consensus sequences recognized by the 14-3-3 proteins (Gardino et al., 2006, Berg et al., 2003). There are two high-affinity phosphorylation-dependent motifs: mode 1 (RSXpSXP) and mode 2 (RXXXpSXP, where pS represent phosphoserine/ threonine) (Gardino et al., 2006, Dougherty and Morrison, 2004). However, it should also be noted that a few proteins interact with 14-3-3 in a phosphorylation-independent manner. Regardless of whether the interactions are dependent on phosphorylation or not, all targets appear to interact with the same binding domain on 14-3-3, the conserved amphipathic groove (Berg et al., 2003, Fu et al., 2000, Liu et al., 1995). For example, the unphosphorylated ligand 5-phosphatase can bind to 14-3-3 with high affinity because it displays a model 1-like motif (Berg

et al., 2003). In this instance, it is likely that phosphorylation is overcome by the presence of multiple negatively charged Glutamate residues.

1.1.2 Regulation

The interaction of 14-3-3 proteins with their ligands is under tight control. Besides phosphorylation of target proteins, the status of 14-3-3 itself is also a critical determinant of this control. Mechanisms that regulate 14-3-3 include expression levels in cells, posttranslational modification, isoform specificity and subcellular localization (Takahashi, 2003, Fu et al., 2000).

The 14-3-3 family of proteins clearly have important role(s) in mammalian brain, where levels as high as 13.3μg/mL soluble protein (approximately 1%) were shown to exist in neuronal tissue (Baxter et al., 2002, Boston et al., 1982). All the 14-3-3 isoforms, with the exception of σ, are primarily but not exclusively expressed in neurons (Skoulakis and Davis, 1998). Their primarily neuronal expression pattern appears conserved in all animal species examined (Skoulakis and Davis, 1998, Aitken et al., 1995, Aitken et al., 1992, Ichimura et al., 1988). However, the expression pattern of 14-3-3 isoforms within the brain varies (Aitken et al., 1992).

It is noteworthy that the isoforms of 14-3-3 are highly expressed in pyramidal cells of the hippocampus, neurons of the cerebral cortex, olfactory bulb neurons, and Purkinje cells of the cerebellum (Takahashi, 2003, Skoulakis and Davis, 1998). There is a large degree of overlap in expression patterns among the isoforms but it is, as yet, undefined whether they are co-expressed in the same

cells**.** Variation in expression pattern and abundance within these brain regions may reflect functional differences or engagement of distinct signal-transduction pathways by different groups of cells.

Several kinases (sphingosine-dependent protein 1, casein kinase 1 and protein kinase Cs) have been reported to phosphorylate 14-3-3, suggesting that they could modulate the function of 14-3-3 isoforms (Takahashi, 2003). Among the mammalian isoforms, only 14-3-3τ and 14-3-3ζ are phosphorylated to give rise to the species initially designated as the α and δ isoforms, respectively (Fu et al., 2000). However, the role of phosphorylation in the physiological regulation of 14-3-3 function is not yet clear.

The presence of seven 14-3-3 isoforms also suggests possible roles for isoform-specific interactions with different target proteins to control different cellular processes. For example, overexpression of 14-3-3σ caused a G2 cell cycle arrest in colorectal carcinoma cells, whereas 14-3-3β overexpression did not (Fu et al., 2000). 14-3-3γ, but not other isoforms, was found to regulate P53, a tumour suppressor, by blocking its inhibitors and interacting with its regulatory proteins, such as mouse double minute X homolog (MDMX) (Jin et al., 2006). In addition, surface expression of voltage-gated Ca^{2+} channels have been reported to be significantly enhanced by 14-3-3τ (Liu et al., 2015).

1.2 14-3-3 in brain function

1.2.1 14-3-3 proteins in neurological disorders

The high expression of 14-3-3 proteins in the mammalian brain suggests that these proteins may be important contributors to neuronal development and in certain neuropathologies. The first physiological evidence of an essential role for 14-3-3 proteins in neuronal functions such as learning and memory was demonstrated in *Drosophila* (Skoulakis and Davis, 1998). Mutations in the binding motif of *Drosophila* 14-3-3ζ led to disruption of neuronal differentiation, synaptic plasticity, and behavioural plasticity, thereby establishing a role for these proteins in the development and function of the nervous system (Skoulakis and Davis, 1998). These effects on synaptic physiology and plasticity do not appear to be the result of decreased numbers of synaptic vesicles, but rather through a failure to regulate their function (localisation, turnover, ability to signal etc.) correctly.

In humans, several reports have indicated that 14-3-3ε has an important influence on neural migration. *14-3-3ε* is located in chromosomal region 17p13.3, that contains genes implicated in isolated lissencephaly sequence (ILS) and Miller-Dieker syndrome (MDS) (Dougherty and Morrison, 2004, Berg et al., 2003, Toyo-oka et al., 2003, Fu et al., 2000). ILS and MDS are diseases characterized by classical Lissencephaly (smooth brain), a neural migration defect that results in mental retardation and epilepsy. Additionally, 14-3-3 proteins are also found in the neurofibrillary tangles seen in patients with Alzheimer's disease (AD) (Berg et al., 2003, Layfield et al., 1996). 14-3-3 proteins have also been detected in the cerebrospinal fluid (CSF) of certain neurodegenerative diseases, such as scrapie,

bovine spongiform encephalopathy (BSE) and Creutzfeldt-Jakob disease (CJD) (Baxter et al., 2002, Hirsch et al., 1992).

1.2.2 14-3-3 in schizophrenia

Neuropsychiatric disorders such as schizophrenia, bipolar disorder and autism are the greatest cause of human suffering which comprise 13% of all reported diseases (Figure 1.2) (WHO, 2008). Unlike other chronic illnesses, these disorders often begin at a young age and require ongoing treatment throughout life making it an economic burden in terms of hospitalization, chronic treatment and rehabilitation, and lost productivity. Despite the negative effects of these disorders on public health, progress in understanding their pathophysiology has been frustratingly slow and the discovery of new therapeutic interventions is at a near standstill (Nestler and Hyman, 2010).

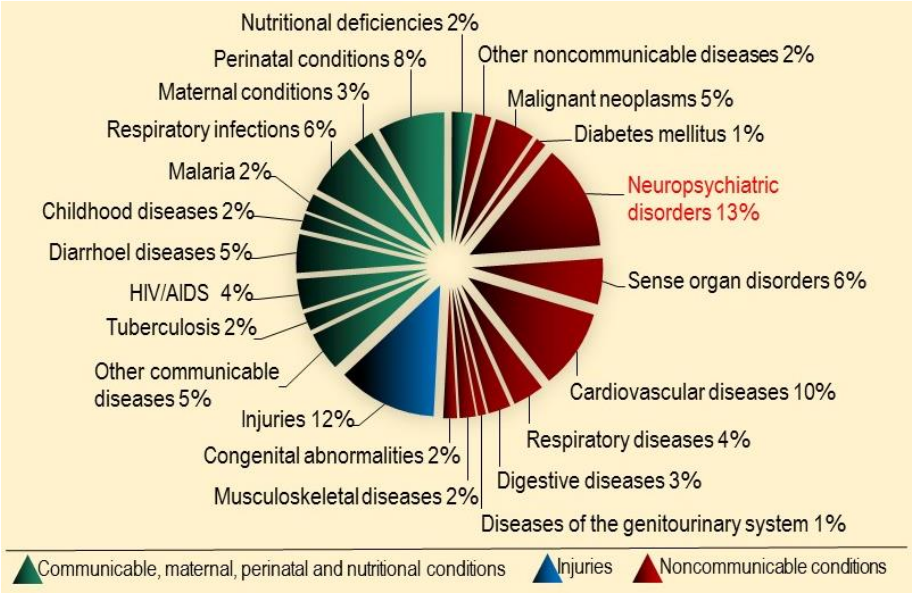

Figure 1. 2: Burden of diseases worldwide in 2004.

Neuropsychiatric disorders comprise 13% of all reported diseases and is the highest burden of disease among noncommunicable conditions. Figure was generated using data from WHO (2008).

Schizophrenia is the fourth leading cause of disability in the developed world affecting about 1% of the population and accounts for over one third of all mental illness, one of Australia's major medical issues (Miyamoto et al., 2003). Schizophrenia is characterized by positive symptoms of hallucinations, delusions, and thought disorder; negative symptoms of decreased motivation, altered expressivity, and an inability to experience pleasure (anhedonia); selective cognitive deficits in attention, learning, and memory; and comorbid features of depression, substance abuse, and suicide (Clapcote et al., 2007, Ross et al., 2006). Antipsychotics are an effective treatment for the positive symptoms of schizophrenia, but the illness continues to produce considerable disability (Miyamoto et al., 2003). The genetic cause of schizophrenia remains unknown despite extensive genetic linkage and association studies (Lewis and Levitt, 2002, Walsh et al., 2008).

Advances in the aetiology of schizophrenia provide resounding evidence of a neurodevelopmental origin, most likely arising from defects in neural migration and synapse formation (Harrison, 2004, Lewis and Levitt, 2002, Walsh et al., 2008). This evidence comes from *in vivo* and post mortem analyses as reviewed in Harrison (2004). The most consistent structural abnormalities found in schizophrenia include lateral and third ventricular enlargement; medial temporal lobe (hippocampal formation, subiculum, parahippocampal gyrus) volume reductions and superior temporal gyrus (STG) volume reductions (Harrison, 2004, Ross et al., 2006).

Linkage association studies of schizophrenia are increasingly providing evidence of the involvement of 14-3-3 proteins in this crippling disease. Single nucleotide polymorphism analysis in schizophrenia patients identified significant linkage to 14-3-3ζ compared to the other isoforms (Jia et al., 2004, Wong et al., 2005). Additionally, post-mortem schizophrenia brain samples revealed significant down-regulated mRNA (Middleton et al., 2005, Wong et al., 2005) and protein (English et al., 2011, English et al., 2009, Sivagnanasundaram et al., 2007, Focking et al., 2011, Schubert et al., 2015) levels of 14-3-3ζ in comparison to healthy controls.

More recently, a non-synonymous heterozygous point mutation in *14-3-3ζ* (14-3-3ζ-K115R) was identified in a schizophrenia patient by whole-exome sequencing analyses. This mutation leads to an alteration of a highly conserved lysine residue required for protein function (Fromer et al., 2014). In a related neurodevelopmental disorder, namely autism, a non-synonymous frame-shift mutation in *14-3-3ζ* (14-3-3ζ-fs220) results in premature truncation of the protein and loss of residues important for controlling protein-protein interactions (Toma et al., 2014). Moreover, 14-3-3ζ has been found to be part of the schizophrenia protein interaction network (Sun et al., 2010). Taken together, these findings identify 14-3-3ζ as a candidate risk factor of schizophrenia and associated disorders. On the basis of these reports, this thesis aimed to assess the causal relationship between 14-3-3ζ deficiency and the aetiology of schizophrenia and related neurodevelopmental disorders.

1.3 Brain development

Brain development occurs in a highly orchestrated sequence starting with neurulation from the ectoderm of the embryo (Jiang and Nardelli, 2015). Neurulation involves rapid proliferation of neuroepithelial cells (neural stem cells) of the ectoderm forming the neural plate that folds to form the neural tube. The differentiated cells in the neural tube positioned along the rostral or caudal portions eventually become the brain and spinal cord, respectively (Stiles and Jernigan, 2010). Following neurulation, the rostral portion of the neural tube swell to form three primary vesicles, namely the prosencephalon (forebrain), mesencephalon (midbrain), and rhombencephalon (hindbrain) (left image, Figure 1.3 i). These segments then give rise to five secondary vesicles by subdivision of the prosencephalon into the telencephalon and diencephalon, the rhombencephalon into the metencephalon and myelencephalon, while the mesencephalon remains undivided (right image, Figure 1.3 i)(Stiles and Jernigan, 2010).

The neuroepithelial cells migrate from their birth place to their final position to achieve lamination within all regions of the brain, forming complex internal structures (Figure 1.3 ii) (Hippenmeyer et al., 2010). They then mature to develop axons and dendrites allowing them to establish synaptic communication with other neurons leading to functional neuronal networks. The formation of the brain's general architecture is largely completed at birth, while maturation of the two principal glial cells, synaptogenesis and synapse pruning, and myelination occur postnatally (Jiang and Nardelli, 2015).

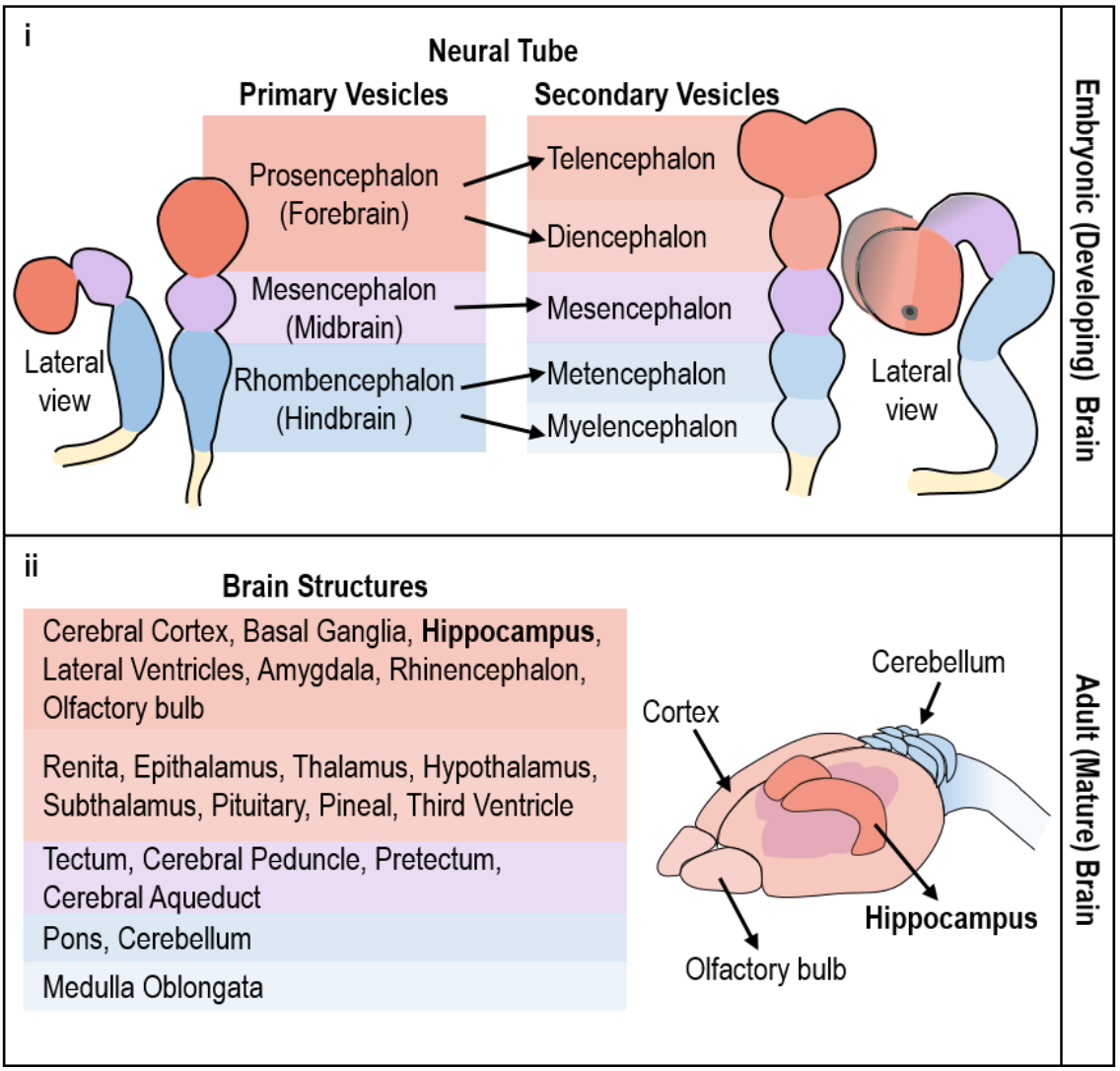

Figure 1. 3: Illustration of mouse brain development after neural tube formation.

(i) The neural tube develops into three primary vesicles at embryonic day (E) 10 that eventually forms the forebrain, midbrain, and hindbrain. The vesicles then give rise to five secondary vesicles, at E11.5, including the telencephalon, diencephalon, mesencephalon, metencephalon and myelencephalon. (ii) Within the mature adult brain these primitive regions develop into complex internal structures. Different colours represent the different brain regions.

1.3.1 The hippocampus

The hippocampus is a brain region derived from medial regions of the telencephalon and is known to play important roles in spatial memory and navigation (Belvindrah et al., 2014, Khalaf-Nazzal and Francis, 2013). It is located inside the medial temporal lobe and contains two main interlocking parts: cornu ammonis (CA) and the dentate gyrus (DG) (Figure 1.4). The primary neuronal layer of cornu ammonis is composed of glutamatergic excitatory pyramidal neurons which consist of only one layer of principal neurons. These neurons have different morphological and genetic properties, which divide it into the region of CA1 and CA3 where CA2 refers to the transitory region between the two anatomically define regions (Danglot et al., 2006). In contrast, the cells within the dentate gyrus are composed of granular neurons. Communication between the DG granular neurons and CA3 pyramidal neurons is achieved through precise axonal navigation and synaptic targeting.

The entorhinal cortex (EC), located in the parahippocampal gyrus, is the main interface between the hippocampus and other parts of the cerebral cortex. Within the hippocampus, the flow of information from the EC is largely unidirectional, with signals propagating through a series of tightly packed cell layers (Figure 1.4). EC axons project through the perforant path and innervate the granule cells of the DG. Mossy fibres from granule cells then pass information from the EC to thorny spines that exit from the proximal apical dendrite of CA3 pyramidal cells. The axons of CA3 pyramidal cells (Schaffer collaterals) then innervate CA1 pyramidal cells, which in turn innervate back to the EC and the subiculum.

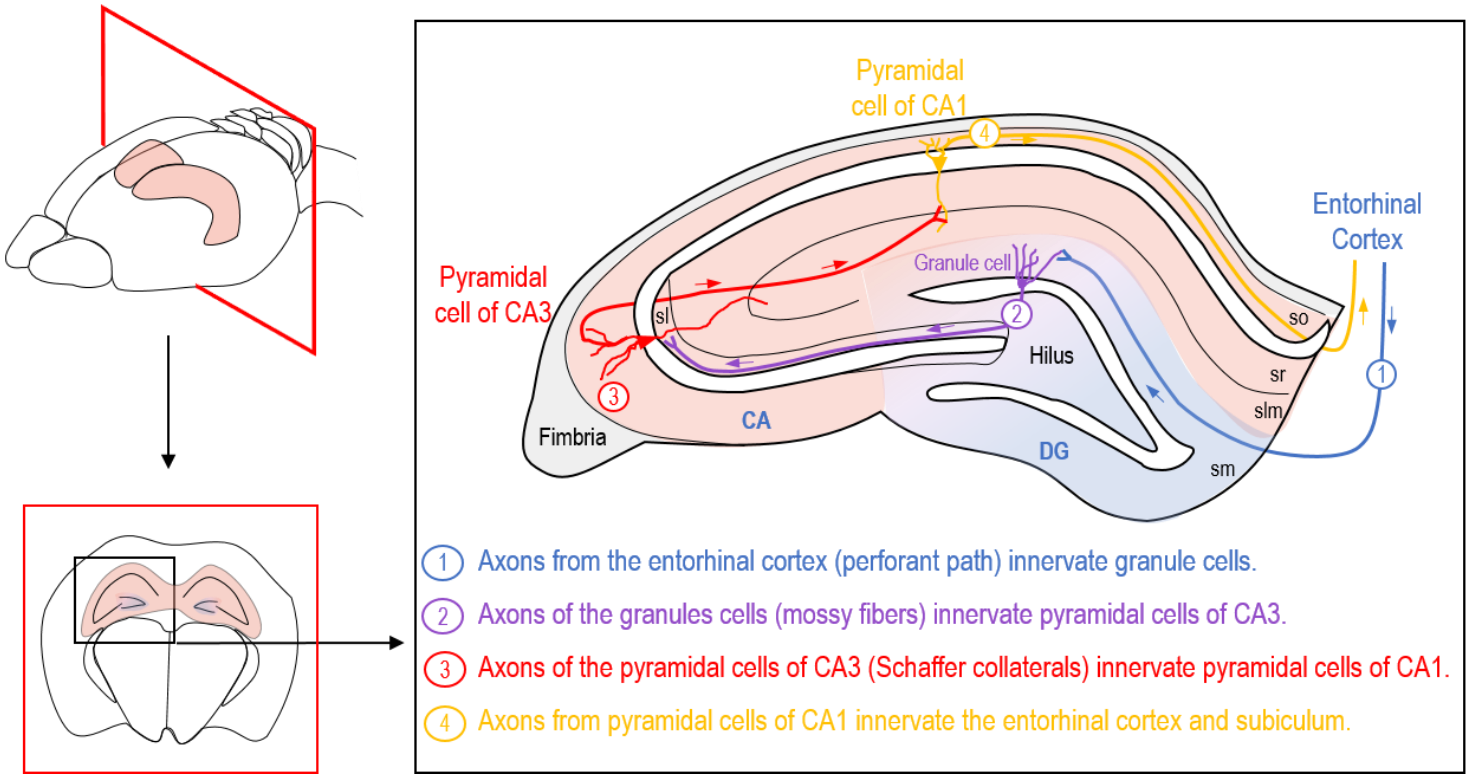

Figure 1. 4: Hippocampal trisynaptic circuit in adult mouse brain.

The pyramidal cells of the CA3 and CA1 regions along with the granule cells of the DG compose the trisynaptic loop. The entorhinal cortex projects to the granule cells by fibres collectively known as the perforant path (1). Mossy fibres from the granule cells in the DG synapse on pyramidal cells of CA3 (2). Pyramidal cells of CA3 sends signals to CA1 cells via Schaffer collaterals (3). Pyramidal cells of CA1 then synapse back to the entorhinal cortex and the subiculum (4). Cornu ammonis, CA in light orange; dentate gyrus, DG in blue; so, stratum oriens; sl, stratum lucidum; sr, stratum radiatum; slm, stratum lacunosum-moleculare; sm, stratum moleculare. Adapted and redrawn from Danglot et al. (2006).

1.3.2 Hippocampal development

The hippocampus begins to develop during early stages of embryogenesis and in mice only obtains its mature structure two weeks postnatally. At the earliest stages of its development neuroepithelial precursor cells within the ventricular zone (VZ) at the roof of the telencephalon exit the cell cycle and migrate radially towards their target layer where they settle in an inside-out fashion (Figure 1.5) (Belvindrah et al., 2014, Danglot et al., 2006, Marin et al., 2010). The neuroepithelium giving rise to the hippocampus consists of three subtypes; 1) the ammonic neuroepithelium which forms the pyramidal cells & large neurons of stratum oriens and stratum radiatum, 2) the dentate neuroepithelium which forms the granule cells & large neurons of stratum moleculare and hilus and 3) the glioepithelium which forms the glial cells of the future fimbria (Danglot et al., 2006).

In mice, CA3 pyramidal neurons are generated in the VZ at E14-15, while CA1 pyramidal neurons arise later at E15-E16. Ammonic neuroepithelial cells differentiate into young immature post-mitotic neurons which develop a transient multipolar morphology within the subventricular zone (SVZ) (Figure 1.5) (Hayashi et al., 2015, Wynshaw-Boris and Gambello, 2001). Upon gaining a bipolar morphology, these immature neurons migrate along radial glial scaffolds through the intermediate zone (IZ) towards the hippocampal plate (HP) (Belvindrah et al., 2014, Hayashi et al., 2015). Radial glial cells serve as ideal guide posts for this migration event as they extend their processes all the way from the VZ up to the marginal zone (MZ) (Belvindrah et al., 2014). Cajal-Retzius cells in the MZ are essential for this migration process as they secrete factors to help maintain radial

glial cell morphology and attract post-mitotic migrating neurons toward their final resting place (Belvindrah et al., 2014). The pyramidal cells reaching the hippocampal plate then polarise and initiate axonal formation and extension (Belvindrah et al., 2014).

The generation of the DG granule cells is unique as they are generated both within and outside of the VZ throughout brain development (Figure 1.5) (Danglot et al., 2006, Urban and Guillemot, 2014). At E14.5 in mice, dentate neuroepithelial cells proliferate and undergo initial differentiation within the VZ which is known as the primary matrix (1ry, Figure 1.5) (Belvindrah et al., 2014, Danglot et al., 2006, Khalaf-Nazzal and Francis, 2013). During later stages, neuroepithileial precursor cells of the DG migrate away from the VZ toward the dentate plate (DP) and give rise to the secondary matrix cell population (2ry, Figure 1.5) (Danglot et al., 2006, Khalaf-Nazzal and Francis, 2013, Urban and Guillemot, 2014). The first cells to arrive within the secondary matrix constitute the top blade of the dentate plate while the cells arriving at later stages give rise to the tertiary matrix cell population (3ry, Figure 1.5) (Danglot et al., 2006, Khalaf-Nazzal and Francis, 2013, Urban and Guillemot, 2014).

The first migration phase of immature granular neurons occurs independent of the Radial Glial cells through a tangential mode of migration, however, radial migration is later required for insertion into the granule plate (Khalaf-Nazzal and Francis, 2013). Although these cells are first detected in the dentate plate at around E18, the majority (~85%) only laminate the dentate gyrus postnatally (P1-2)(Khalaf-Nazzal and Francis, 2013). The tertiary matrix is the

only source of dentate progenitors and granule cells during postnatal stages of development, eventually becoming confined to the subgranular zone (SGZ) (Figure 1.11) (Khalaf-Nazzal and Francis, 2013, Urban and Guillemot, 2014). Notably, neurogenesis of granule precursor cells is retained throughout adulthood in the SGZ (section 1.7.1).

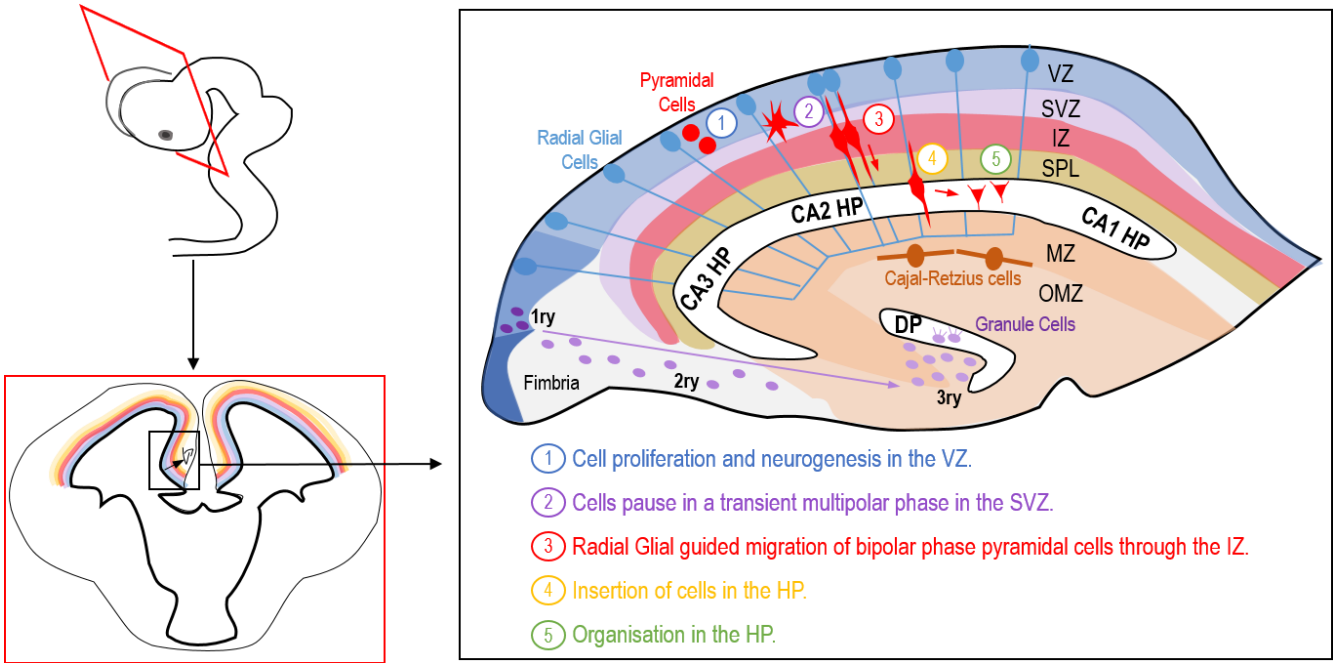

Figure 1. 5: Mouse hippocampal development.

Neuroepithelial precursor cells of pyramidal neurons proliferate within the VZ (1) before they pause in the SVZ to gain a multipolar morphology (2). They then develop a bipolar morphology allowing their migration to the IZ using Radial glial cells as scaffolds (3). Upon entering the HP, which occurs in a wave from CA3 to CA1, these cells will differentiate to form pyramidal neurons (4), and settle in their appropriate layer (5). CA1-3: Cornu ammonis 1-3; DG: dentate gyrus; VZ: ventricular zone (dark blue: glioepithelium; blue: dentate neuroepithelium & light blue: ammonic neuroepithelium); SVZ: sub-ventricular zone; IZ: intermediate zone; SPL: subplate; MZ: marginal zone; OMZ: outer marginal zone; HP: hippocampal plate: DP: dentate plate; 1ry, 2ry, 3ry: Primary, Secondary & Tertiary matrices, respectively; Red & purple arrows indicate pyramidal cell & granule cell migration path, respectively. Adapted and redrawn from Belvindrah et al. (2004) and Danglot et al. (2006).

1.4 Mouse models

1.4.1 Schizophrenia mouse models

One of the major limitations regarding the neurobiology of higher brain function and complex psychiatric disorders is the necessity to use animal models to mimic biological functions and the psychiatric state. As many of the symptoms used to establish psychiatric diagnoses in humans (e.g. hallucinations) are not easily replicated in animals this has provided a major obstacle to understanding disease pathogenesis. Nevertheless, disease models derived from plausible risk factors that exhibit a substantial degree of anatomical or behavioural pathology corresponding to human disease have provided profound insight to our understanding of the disease process (Johnstone et al., 2011).

In the context of schizophrenia, there is still a need to develop more comprehensive animal models that have the appropriate triad of face, construct and predictive validity (Jones et al., 2011, Wilson and Terry, 2010). Face validity is the degree of symptom homology between the animal model and human condition; such as deficits of information processing (e.g. prepulse inhibition) and cognitive function (e.g. working memory) (Jones et al., 2011, Wilson and Terry, 2010). Construct validity refers to the replication of the neurobiological and structural defects; such as neurotransmitter deficits, decreased hippocampal volume and synaptic connection (Jones et al., 2011, Wilson and Terry, 2010). Predictive validity is evaluation of the pharmacological effects to treatment by antipsychotics and potential new therapies (Jones et al., 2011, Wilson and Terry, 2010).

To develop mouse models of schizophrenia, many researchers have focused on examining behavioural tasks related to the disorder. For instance, prepulse inhibition (PPI) is a cross-species measurement of sensorimotor gating which is deficient in schizophrenic patients and which can also be used as a psychiatric-like measure in rodents (Young et al., 2010). Other common behaviour paradigms used for the study of schizophrenia in rodents include tests of locomotor hyperactivity (resulting from enhanced dopaminergic activity), and spatial learning and memory.

Many gene association studies have identified candidate risk factors for schizophrenia, of which the most replicated include DISC1, dysbindin and neuregulin-1 (Young et al., 2010). ENU-induced mutations in Exon 2 of *DISC1* in C57BL/6 mouse background resulted in disruption of PPI, hyperactivity and reduced anxiety (Clapcote et al., 2007). Another study in the same mouse background showed that a 25bp deletion in exon 6 of *DISC1*, resulted in working memory deficits but no locomotor hyperactivity or PPI disruption (Koike et al., 2006). The mutation of dysbindin in the DBA/2J mouse background resulted in decreased locomotor activity, social interaction deficit and higher dopamine turnover. However, no difference was found in PPI or spatial memory deficits (reviewed in Young et al., 2010). Neuregulin-1 heterozygous mice the in C57BL/6 mouse background have been reported to be mildly hyperactive and with impaired PPI (reviewed in van den Buuse 2010). Conversely, the 14-3-3ζ knockout (KO) mouse model, the focus of this thesis, has been shown to have striking behavioural and cognitive defects which include spatial memory deficits,

hyperactivity and disrupted sensorimotor gating which are reminiscent of the defects in schizophrenic patients (Cheah et al., 2012).

1.4.2 Disrupted in schizophrenia 1 (*DISC1*)

Over 130 genes have been reported to predispose to schizophrenia, but few have been replicated, and fewer still have been validated biologically (Clapcote et al., 2007, Ross et al., 2006). Among several independent studies, linkage to the gene, disrupted in schizophrenia 1 (*DISC1*) has been the most replicated (Johnstone et al., 2011). The *DISC1* gene was originally identified at the site of a balanced t(1;11) (q42.1;q14.3) chromosomal translocation that co-segregated with mental illness, including schizophrenia, in a large Scottish family (St Clair et al., 1990). Since this original finding, *DISC1* has also been implicated in a number of independent investigations on schizophrenic populations throughout the world (Ross et al., 2006). The DISC1 protein has no known enzymatic activity; rather it exerts its effect on multiple proteins through interactions that modulate their functional states and biological activities (Ross et al., 2006).

Although the precise functions of *DISC1* remain unclear, it is reported to be maximally expressed in the brain during development and to interact with numerous proteins required for neuronal migration, neurite outgrowth, axonal guidance and neuronal plasticity (Clapcote et al., 2007). DISC1 has been found to interact with several proteins which themselves are implicated in neuropsychiatric diseases such as lissencephaly-1 (Lis1) (section 1.6.2) and nuclear distribution E-like homolog 1 (Ndel1) (section 1.6.3) (Taya et al., 2007, Ross et al., 2006). Ndel1 and Lis1 play cooperative and critical roles in neuronal

proliferation, differentiation, and migration within the developing brain (Bradshaw and Porteous, 2010). These proteins bind directly to the candidate schizophrenia risk factor DISC1 (Bradshaw and Porteous, 2010, Taya et al., 2007, Brandon et al., 2004) which is essential for the re-localisation of Ndel1 and Lis1 from the cell body to the extending axon (Taya et al., 2007). Knock-down of either Ndel1 or Lis1 using siRNA in culture leads to reduced neurite outgrowth (Taya et al., 2007), while granule neurons from heterozygous Ndel1 or Lis1 knock-out mice show impaired migration *in vitro* (Toyo-Oka et al., 2005). Furthermore, 14-3-3ζ, the topic of this thesis, has been shown to interact with Ndel1, Lis1 and DISC1 (Toyo-oka et al., 2003, Cheah et al., 2012).

1.4.3 14-3-3ζ KO mouse model

14-3-3ζ KO mice were initially generated in the 129/sv background and then backcrossed into BALB/c and C57BL/6 backgrounds (Cheah et al., 2012). The 14-3-3ζ KO mice in all three genetic backgrounds are grossly normal with all male mice being infertile (to obtain litters of all genotypes heterozygous breeding pairs are therefore used). However, there are profound variations in terms of progeny survival between backgrounds. Knockout mice in the 129/sv background have notable growth retardation and moderate postnatal lethality which was completely rescued when backcrossed into the BALB/c background. Conversely, backcrossing into the C57BL/6 background caused a high rate of embryonic lethality with around 50% of knockout mice surviving into adulthood. 14-3-3ζ heterozygous (HET) mice in the 129/sv and BALB/c backgrounds were also found to breed better than mice in the C57BL/6 background (Hayley Ramshaw, personal communication).

Previous work in our laboratory has shown that 14-3-3ζ KO mice in the 129/sv background display anatomical defects associated with abnormal brain function (Cheah et al., 2012, Ramshaw et al., 2013). The anatomical defects are characterized by abnormal hippocampal lamination likely due to aberrant neuronal migration, aberrant mossy fibre navigation and increased excrescences on CA3 dendrites that is indicative of aberrant synapse formation. The behavioural defects were also reminiscent of schizophrenia-like symptoms including deficits in spatial learning and memory, reduced anxiety, locomotor hyperactivity and disrupted sensorimotor gating. Enhanced dopaminergic activity is known to underlie locomotor hyperactivity (van den Buuse, 2010) and was also observed in the 14-3-3ζ KO mice in the 129/sv background (Ramshaw et al., 2013). Recently, our lab undertook similar behavioural studies in the BALB/c background which showed spatial learning and memory defects similarly to the 14-3-3ζ KO 129/sv background. However, anxiety and locomotor hyperactivity were absent which may be due to the genetic makeup of BALB/c mice (van den Buuse, 2010, Xu et al., 2015).

1.5 Neuronal morphogenesis

The early processes of neuronal differentiation and morphogenesis have been well characterized in rodents using a highly reproducible hippocampal neuronal culture model (Dotti et al., 1988). The basic principle of neuronal morphogenesis is largely conserved between *in vivo* and *ex vivo* conditions, however notable discrepancies are also present (Arimura and Kaibuchi, 2007, Flynn, 2013). For example, neuronal cell bodies are not fixed in space *in vivo* as it they are in culture. Additionally, the presence of the extracellular signals from neighbouring cells is often lacking in culture.

As illustrated in Figure 1.6, neuronal morphogenesis is divided into five successive stages (Arimura and Kaibuchi, 2007, Flynn, 2013). Neurons isolated from embryonic rodent hippocampi initially have a spherical shape, rapidly attach to the substratum and develop several thin protrusions within a few minutes (stage 1, 0-6hrs). Neurite initiation commences when these protrusions transition into immature neurites which are morphologically equal in length (stage 2, 6-24hrs). Neuronal polarization then occurs when a single neurite with a large dynamic growth cone begins extending away from the cell body, later becoming an axon (stage 3, 24-72hrs). While the axon grows and differentiates, the remaining neurites continue to grow and arborize into morphologically distinct dendrites (stage 4, 3-4days). The neurons continue to develop into mature neurons through the formation of dendritic spines which mark functional synaptic connections with other neurons (stage 5, 7-28days).

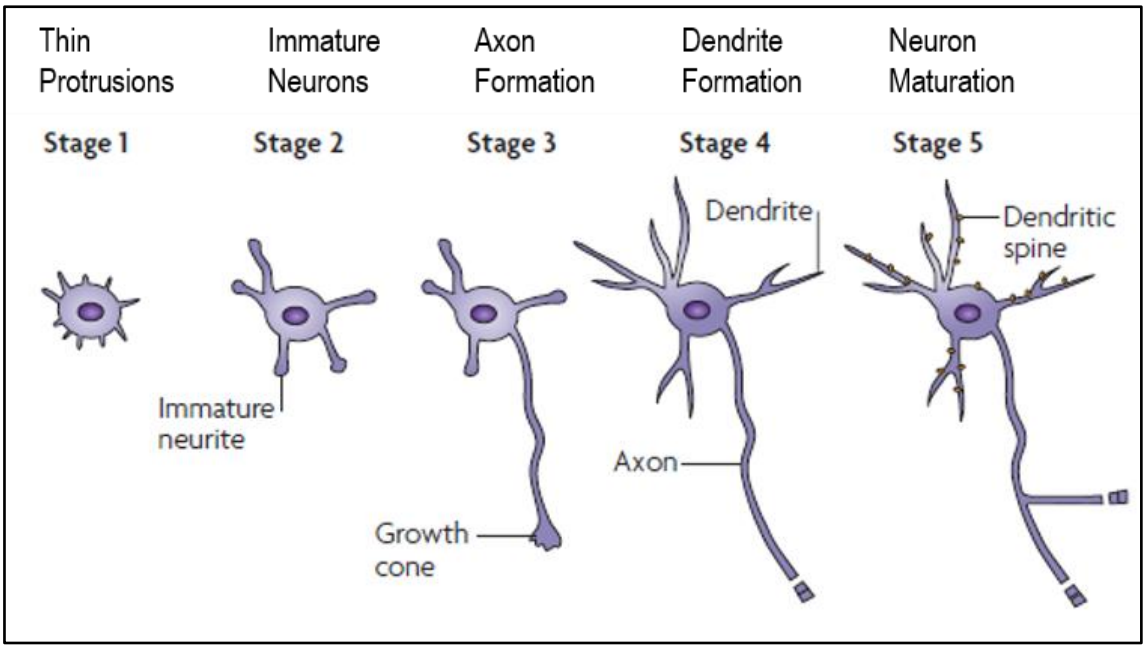

Figure 1. 6: Schematic of neuronal morphogenesis.

Cultured embryonic hippocampal neurons form thin protrusions when they attach to the substratum (Stage 1), and shortly after neurites begin to transition into immature neurites (Stage 2). One of the neurites with an enlarged growth cone elongates rapidly to form the axon (Stage 3). The remaining neurites continue to grow and branch to form dendrites (Stage 4), and in a final step of maturation, the axon and dendrites develop further with the formation of dendritic protrusions, or spines (Stage 5). Adapted and modified from Arimura & Kaibuchi (2007).

1.5.1 Neurite outgrowth

Aberrant neurite outgrowth contributes to morphological defects, inappropriate connections and abnormalities in brain function (Kiryushko et al., 2004). Many *in vitro* investigations of neurite extension have been achieved using cell lines of neuroepithelial origin (e.g. PC12 cells, neuroblastoma cells), where neurite outgrowth is induced by addition of exogenous growth factors (Kiryushko et al., 2004). Alternatively, primary cultures of rodent neurons have been used to study the dynamics of neurite outgrowth (Kiryushko et al., 2004). There are several factors that regulate neurite outgrowth such as extracellular matrix (ECM) associated molecules, cell adhesion molecules (CAMs), neurotrophic factors, repulsive, and attractive guidance cues (Figure 1.7) (Kiryushko et al., 2004).

14-3-3 proteins are known to interact with several of the molecules involved in neurite outgrowth, however, there are few studies investigating their potential roles in a neurite outgrowth setting (Graeser et al., 2002, Kajiwara et al., 2009, Marzinke et al., 2013, Ramser et al., 2010a, Ramser et al., 2010b, Tang et al., 1998, Rong et al., 2007). For example, although 14-3-3ζ has been demonstrated to directly interact with the cell adhesion molecule L1 which is essential for neurite outgrowth, whether 14-3-3ζ promotes outgrowth of hippocampal neurons remains unknown (Ramser et al., 2010b).

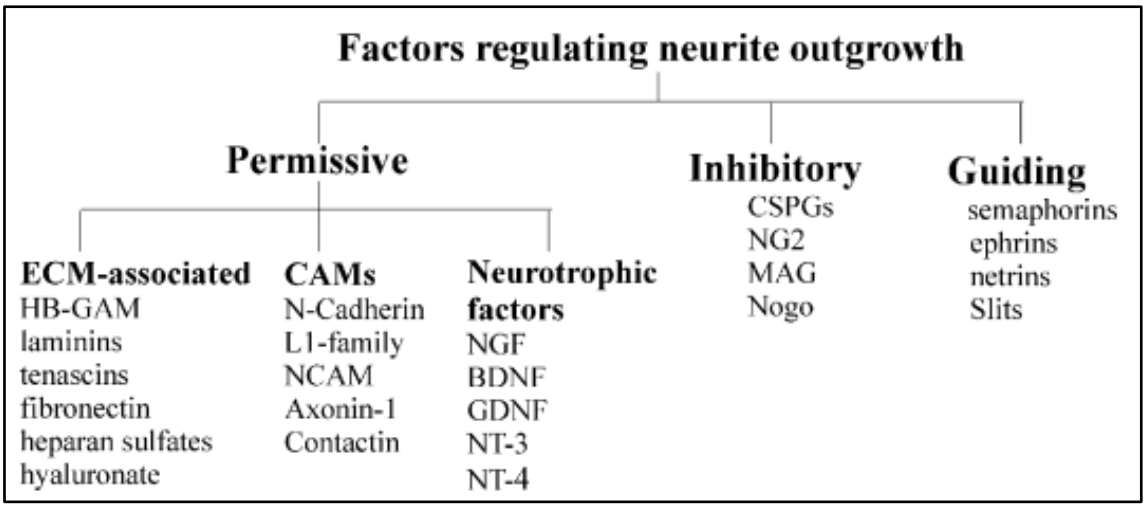

Figure 1. 7: Signalling inputs regulating neurite outgrowth.

These signals can be permissive (positive or attractive), negative (inhibitory or repulsive), or guiding (affecting the advance of the growth cone). Each signal may arise from either the extracellular matrix or the surface of other cells, or may be a diffusible secreted factor. ECM, extracellular matrix; CAMs, cell adhesion molecules. ECM: extracellular matrix; HB-GAM: heparin-binding growth-associated molecule, CAMs: cell adhesion molecules, NCAM: neural cell adhesion molecule, NGF: nerve growth factor, BDNF: brain-derived neurotrophic factor, GDNF: glial cell line-derived neurotrophic factor, NT-3: neurotrophin-3, NT-4: neurotrophin-4, CSPGs: chondroitin sulfate proteoglycans, NG2: neuron-glia antigen 2, MAG: myelin-associated glycoprotein. Taken from Kiryushko et al. (2004).

1.5.2 Dendrite and spine morphogenesis

Dendrite morphogenesis, a critical aspect of neural development, involves the development of dendritic branches that form dendritic arbors and spines required for proper brain function (Kulkarni and Firestein, 2012). Dendritic arborisation involves a highly dynamic process of branching and retraction to ensure that appropriate neural networks are formed (Kulkarni and Firestein, 2012). Alteration in hippocampal dendritic arborisation and spine number are known to contribute to various pathologies including neurological and neurodevelopmental disorders such as autism spectrum disorders, schizophrenia, bipolar disorder and Alzheimer's disease, as illustrated in Figure 1.8 (Jan and Jan, 2010, Koleske, 2013, Kulkarni and Firestein, 2012). Moreover, reduction of CA hippocampal dendritic spines has been correlated significantly with the degree of memory deficit in individual mice (Chen et al., 2010). Notably, mouse models of genes associated with schizophrenia, namely dysbindin, neuregulin-1 and DISC1, are reported to show reduced hippocampal spine density (Harrison, 2004, Jaaro-Peled et al., 2010, Penzes et al., 2011).

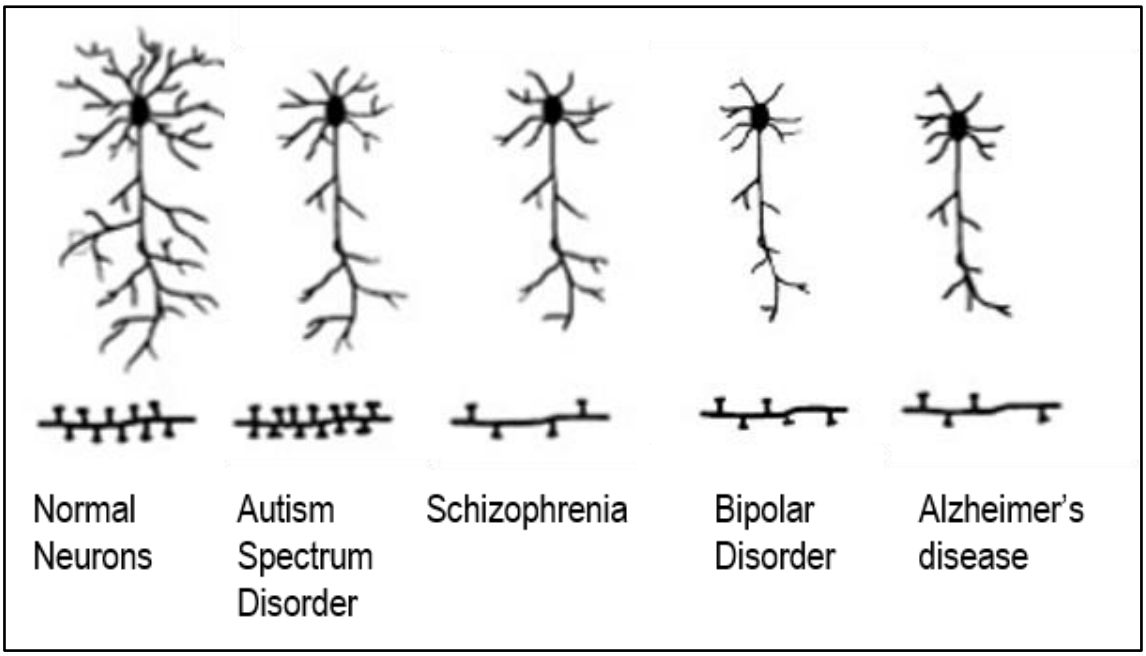

Figure 1. 8: Schematic of pyramidal neurons depicting atrophies in dendrite morphology and spines in brains of individuals with various disorders.

Autism spectrum disorder: decreased dendrite branching in CA1 and CA4 subregions of the hippocampus and higher spine density. Schizophrenia: neurons show reduced dendritic arbor and spine density in CA3 region of the hippocampus. Bipolar disorder: decreased dendrites and spine density have been observed in the CA3 region of hippocampus. Alzheimer's disease (AD): substantial alterations in the dendritic arbor characterized by significant reductions in the total dendrite lengths of apical and basal trees of CA1. In contrast, dentate gyrus granular neurons of the hippocampus show significant decreases in dendrite length of apical trees but non-significant decreases in basal tree lengths. Adapted and modified from Kulkarni & Firestein (2012).

Dendritic spines are small, actin-rich protrusions that receive excitatory input typically from one synapse (Koleske, 2013, Nimchinsky et al., 2002, Penzes et al., 2011). The head (surface) of the spine contains the postsynaptic density (PSD), a membrane-associated disc of electron dense material, consisting of receptors, organelles, cytoskeletal and adaptor proteins, and associated signalling molecules essential for synaptic function and plasticity (Jan and Jan, 2010, Nimchinsky et al., 2002). Some of these key proteins include, but not limited to, postsynaptic density protein 95 (PSD95), glutamate receptor interaction protein 1 (GRIP1) and filamentous actin (Jan and Jan, 2010). Dendritic spines are morphologically diverse and are classified based on the relative sizes of their head and neck, namely thin, stubby, mushroom- or cup-shaped (Koleske, 2013, Nimchinsky et al., 2002). Although their structures can be stable, they can undergo morphological remodelling during development and in adaptation to sensory stimuli or in learning and memory (Koleske, 2013, Nimchinsky et al., 2002, Penzes et al., 2011).

Reorganization of the neuronal cytoskeleton is required for proper dendritic morphogenesis; where actin and microtubule dynamics play a key role in shaping the dendritic arbor, spine development and plasticity (Jan and Jan, 2010, Kulkarni and Firestein, 2012). The actin and microtubule cytoskeleton require precise functioning of intricate signalling pathways which involves many intracellular proteins, molecular motor proteins, Rho-GTPase family members, and extracellular proteins (Jan and Jan, 2010). 14-3-3 proteins have been reported to interact with many of these molecules (Johnson et al., 2010), however their functional role in regulating the cytoskeleton *in vivo* is yet to be determined. For

example, the motor proteins from the kinesin superfamily (KIFs) play critical roles in the transport of cargo proteins along microtubules into the dendritic arbor. These cargo proteins include PSD proteins, neurotransmitter receptors, ion channels and specific messenger RNAs (Hirokawa and Takemura, 2005, Jan and Jan, 2010). KIF5 interacts with GRIP1 to regulate dendritic branching via allowing transport of ephrin receptors to dendrites (Hirokawa and Takemura, 2005, Hoogenraad et al., 2005, Setou et al., 2002). Recently, 14-3-3ζ has been reported to regulate the docking of KIF5 to GRIP1 in order to form proper dendrites (Geiger et al., 2014).

1.6 Neuronal migration

Correct neuronal migration is essential for ordering neurons into architectonic patterns and involves several coordinated events including leading process extension, nucleokinesis and trailing process retraction (illustrated in Figure 1.9) (Lambert de Rouvroit and Goffinet, 2001, Shu et al., 2004). Each of these steps are highly dependent on the microtubule network and any disruption within them can compromise cell motility (Shu et al., 2004). Many of these processes are regulated by 14-3-3 molecules (Angrand et al., 2006, Cheah et al., 2012, Gehler et al., 2004, Gohla and Bokoch, 2002, Toyo-oka et al., 2003, Yuan et al., 2004).

During the first step of neuronal migration, the neuron explores its microenvironment through thin protrusions (filopodia and lamellipodia) before extension of a leading process (Lambert de Rouvroit and Goffinet, 2001, Tsai and Gleeson, 2005). The leading process originates from the axonal growth cone or dendritic tips and its extension is controlled by attractive or repulsive cues acting on the plasma membrane (Lambert de Rouvroit and Goffinet, 2001, Tsai and Gleeson, 2005). Extension of the leading process is directed by microfilament polymerisation which is regulated by Rho-type small GTPases (Lambert de Rouvroit and Goffinet, 2001, Tsai and Gleeson, 2005). Once the leading edge is stabilized ahead of the soma, the nucleus and the cell body are displaced forward into the leading process in a cellular event referred to as nucleokinesis (Lambert de Rouvroit and Goffinet, 2001, Tsai and Gleeson, 2005).

During nucleokinesis the centrosome (also known as the microtubule organising centre) plays an essential role in coordinating interactions between the cytoskeleton and the nucleus. In the resting state, the centrosome is tightly coupled to the nucleus. During migration, the centrosome is positioned directly next to the nucleus at the side of the leading edge. As the leading edge extends the centrosome becomes uncoupled from the nucleus and moves towards the leading process (Marin et al., 2010). The nucleus is then translocated moving towards the centrosome, restoring the nucleus-centrosomal coupling (N-C coupling). This process is critically dependent on alteration in the actin and microtubules cytoskeletons and occurs in a saltatory pattern (Marin et al., 2010). The migrating neuron then retracts its trailing process, resulting in cell movement. This step does not, however, occur in all neuronal types. For example, pyramidal neurons retract their trailing process concurrently with nucleokinesis (Marin et al., 2010). At the end of migration as the neurons reach their final destination, they are ordered into architectonic patterns allowing proper connection and functioning of neural circuits (Lambert de Rouvroit and Goffinet, 2001).

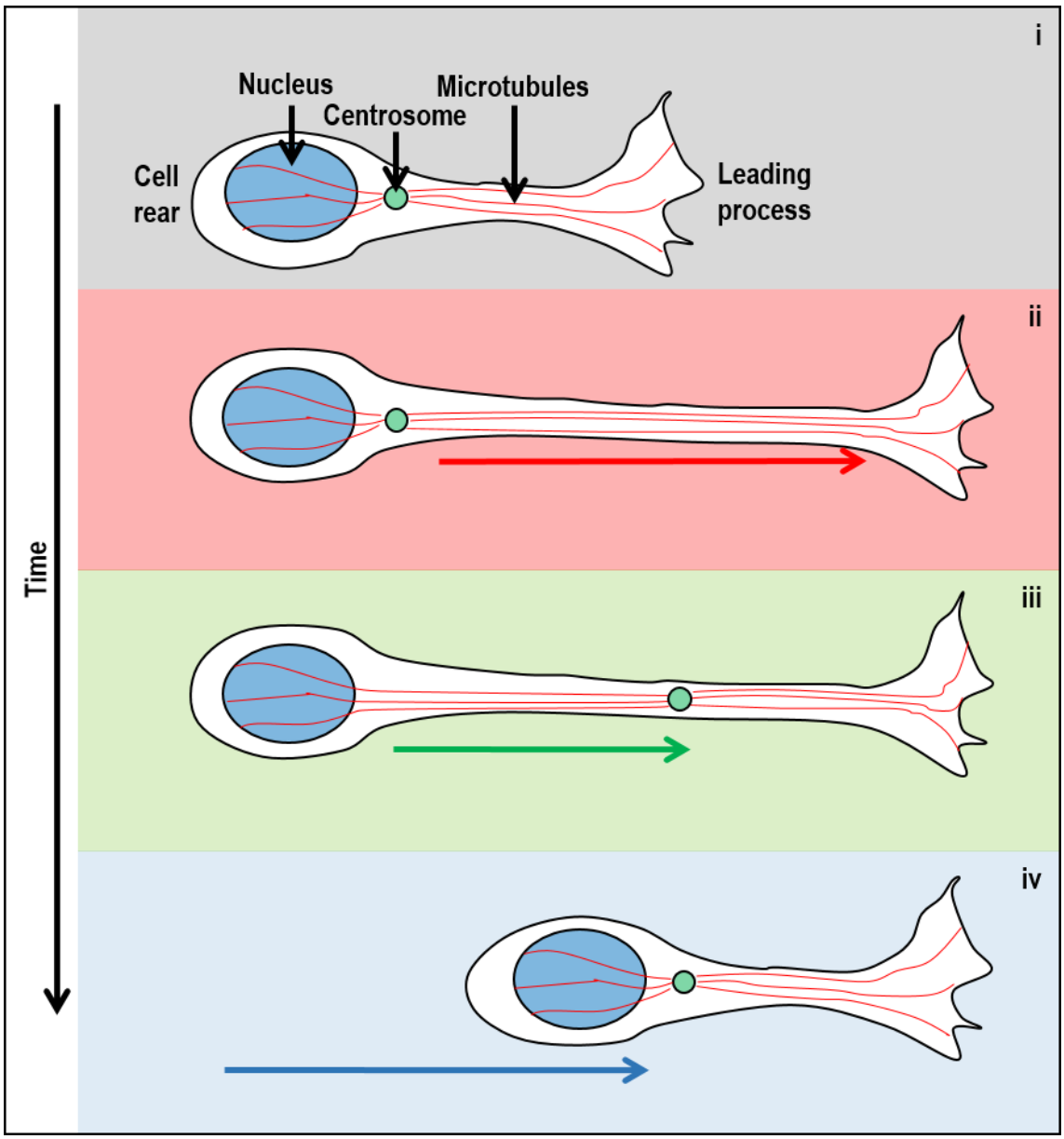

Figure 1. 9: Simplified schematic of steps involved in neuronal migration.

Neurons receive external cues inducing neuronal migration (i) leading to polarized extension of the leading process (red arrow) (ii). Forward movement of the centrosome into the leading process (green arrow) (iii), followed by translocation of the nucleus (blue arrow) towards the leading process (iv) and retraction of the cellular rear process. Neuronal migration is the result of repeating these events. Adapted and redrawn from Tsai and Gleeson (2005).

1.6.1 Molecular pathways regulating neuronal migration

Neuronal migration is regulated by three overlapping yet independent pathways/complexes namely, the Reelin pathway, Cdk5/p35 pathway and Ndel1/Lis1/dynein complex (Figure 1.10 i). Reelin is a large extracellular protein secreted by Cajal-Retzius cells to guide post-mitotic migrating neurons toward the mantle zone (Wynshaw-Boris and Gambello, 2001). The Reelin signalling pathway is also important for the organisation and layering of migrating neurons throughout the CNS (Lambert de Rouvroit and Goffinet, 2001). Neuronal migration is initiated when Reelin binds to cell surface receptors such as the very low density lipoprotein receptor (VLDLR) and ApoE receptor type 2 (ApoER2) leading to activation of intracellular factors such as Disabled 1 (Dab1) tyrosine kinase adaptor (Lambert de Rouvroit and Goffinet, 2001, Wynshaw-Boris and Gambello, 2001). Dab1 activation leads to a cascade of downstream signalling which results in the activation of the cyclin-dependent kinase (Cdk5) to promote binding with its coactivator p35 (Lambert de Rouvroit and Goffinet, 2001). Cdk5/p35 phosphorylates microtubule associated proteins such as Ndel1 and double cortin (DCX) (Niethammer et al., 2000, Tanaka et al., 2004b). Cdk5 phosphorylated Ndel1 forms a complex with Lis1 and the dynein motor to sustain microtubule bundles and facilitate N-C coupling (Feng et al., 2000, Niethammer et al., 2000, Sasaki et al., 2000).

Several studies have shown that disruption of molecules within the neuronal migration pathway leads to hippocampal lamination defects with varying degrees of severity (Figure 1.9 ii). For example, Reelin mutant mice displayed severe fragmentation, layering, and heterotopic organisation of pyramidal neurons

throughout all CA regions, including diffuse organisation of DG granule cells (Belvindrah et al., 2014). Mutations in the Cdk5 activator p35 results in loosely arranged CA pyramidal neurons and DG granule cells (Belvindrah et al., 2014). Like the Reelin mutant mice, although not as severe, Lis1 deficiency leads to fragmentation and layering of the CA pyramidal neurons, as well as diffusely packed DG granule cells (Belvindrah et al., 2014, Fleck et al., 2000).

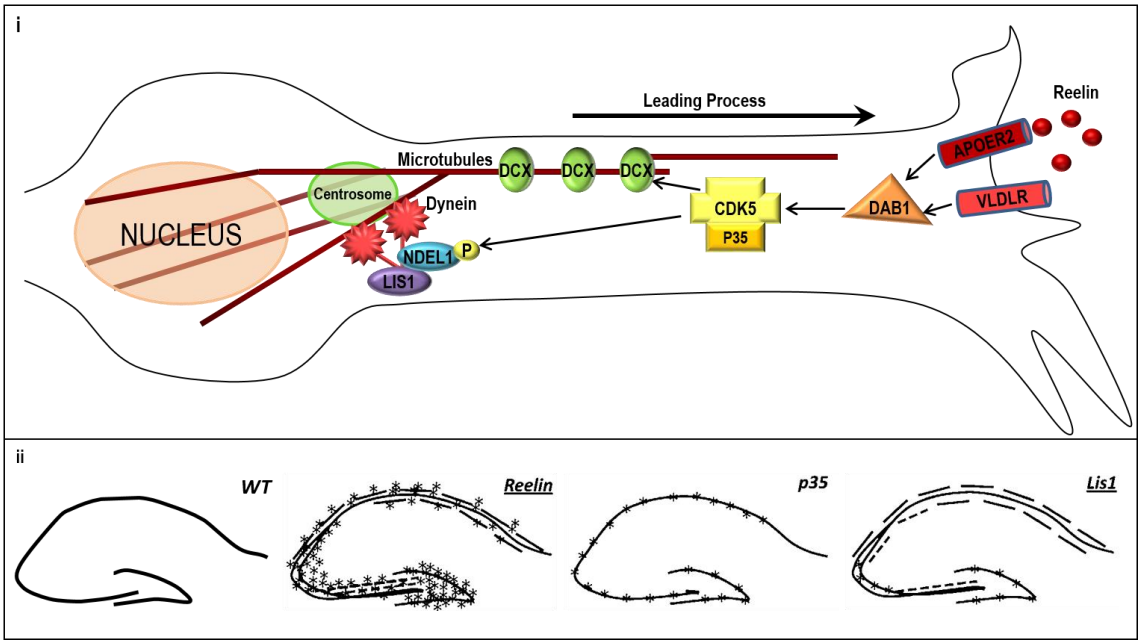

Figure 1.10: Simplified schematic of the neuronal migration pathway and hippocampal lamination defects resulting from migration deficiencies.

(i) Extracellular Reelin binds to the membrane-bound receptors (APOER2 & VLDLR), which stimulate the intracellular signalling molecules (Dab1, Cdk5/p35) to activate microtubule associated proteins (DCX, Ndel1, Lis1, dynein) facilitating neuronal migration. Adapted and modified from Keays at al. (2007). (ii) A selections of hippocampal lamination defects arising from deficiency in molecules involved in the neuronal migration pathway compared to WT. Broken lines indicate degrees of fragmentation. Asterisks indicate either heterotopic cells or diffusely packed cells. Adapted and modified from Belvindrah et al. (2014).

1.6.2 Lissencephlay 1 (Lis1)

Lis1 is a key molecule in the neuronal migration pathway (Reiner et al., 1993, Wynshaw-Boris and Gambello, 2001). In humans, mutations in *Lis1* leads to the neurodevelopmental disorder lissencephlay which is characterised by a smooth brain formation due to cell autonomous neuronal migration defects leading to abnormal patterning of neurons in the cortex and hippocampal layers (Feng and Walsh, 2001, Reiner, 2013, Tsai and Gleeson, 2005). In mice, null mutation of *Lis1* is embryonically lethal, while HET mice display severe neuronal migration defects in the cortical layers, hippocampus and olfactory bulb (Gambello et al., 2003, Reiner et al., 1993, Fleck et al., 2000, Hirotsune et al., 1998).

1.6.3 Nuclear distribution E-like homolog 1 (Ndel1)

Ndel1 is a coiled-coiled protein first identified as a Lis1 interaction partner (Feng et al., 2000, Feng and Walsh, 2001, Niethammer et al., 2000). In mice, complete removal of *Ndel1* leads to embryonic lethality, where loss of function leads to impairment of neuronal migration in the cortex and hippocampus (Feng and Walsh, 2004, Hippenmeyer et al., 2010, Sasaki et al., 2005, Shu et al., 2004, Youn et al., 2009). Ndel1 phosphorylation mediated by Cdk5/p35 is essential for binding with Lis1 and modulates its interaction with the dynein motor protein which is required for proper N-C coupling (Niethammer et al., 2000, Sasaki et al., 2000). Moreover, 14-3-3ε binding to Cdk5/p35 phosphorylated Ndel1 has previously been shown to be required to maintain Ndel1 phosphorylation (Toyo-oka et al., 2003).

1.7 Neurogenesis

Neurogenesis is the process by which neural stem/progenitor cells generate mature neurons. This process was traditionally thought to occur only during early embryonic and postnatal stages, however, more recently active neurogenic zones have also been identified in restricted areas of the adult brain (Hayashi et al., 2015, Ming and Song, 2011, Urban and Guillemot, 2014). While neurogenesis occurs at high rates throughout embryonic and early postnatal development, the percentage of neural population generated throughout adulthood is comparatively small (Stiles and Jernigan, 2010). The major neurogenic regions in the adult brain include the subventricluar zone (SVZ) adjacent to the lateral ventricle and the subgranular zone (SGZ) in the DG of the hippocampus (Hayashi et al., 2015, Ming and Song, 2011), a central region affected in the 14-3-3ζ KO mice (Cheah et al., 2012). Neurons generated in the SVZ migrate via the rostral migratory stream to the olfactory bulb where they become interneurons while dentate granule cells generated in the SGZ migrate to the nearby granular layer (Stiles and Jernigan, 2010). Neural stem cells from the SVZ and the SGZ can be isolated and cultured *in vitro* as neurospheres (section 2.6) generating self-renewing cells that can differentiate into neurons (Ming and Song, 2011, Reif et al., 2006, Urban and Guillemot, 2014).

1.7.1 Neurogenesis in the adult hippocampus

Adult neurogenesis in the DG of the hippocampus involves a well-defined series of events in which a small number of neural stem cells (~10%) differentiate into functional neurons and incorporate into the existing circuitry (Figure 1.11)

(Reif et al., 2007). The undifferentiated precursor cells that give rise to the granule dentate cells are found in the SGZ of the DG, where they extend a single radial process towards the molecular layer hence giving them the name radial glia-like cells (type I cells). These cells are found in quiescent (slow dividing) state, expressing GFAP, nestin and SOX2. Upon activation, the radial glia-like cells proliferate giving rise to both non-radial precursor (type II cell) and intermediate progenitor cells (Ming and Song, 2011, Reif et al., 2006, Reif et al., 2007, Urban and Guillemot, 2014). In contrast, during embryonic neurogenesis these cells are highly proliferative giving rise to a radial glia-like cell and an intermediate progenitor cell (Urban and Guillemot, 2014).

In adult neurogenesis, the non-radial precursor (type II cell) and intermediate progenitor cells express nestin and SOX2 but not GFAP and undergo a limited number of cell divisions followed by commitment to a neural lineage to generate neuroblasts (type III cells) (Ming and Song, 2011, Reif et al., 2006, Urban and Guillemot, 2014). Neuroblasts are proliferative cells expressing doublecortin (DCX) but not nestin and become immature neurons that migrate a small distance through the inner GCL, located just above the SGZ (Ming and Song, 2011, Reif et al., 2006, Urban and Guillemot, 2014). The immature neurons extend their dendrites and axons toward the molecular layer (ML) and CA3 region through the hilus, respectively. These neurons eventually differentiate into dentate granule cells which integrate structurally and functionally into the pre-existing hippocampal trisynaptic circuit (section 1.3.1, Figure 1.4) (Ming and Song, 2011).

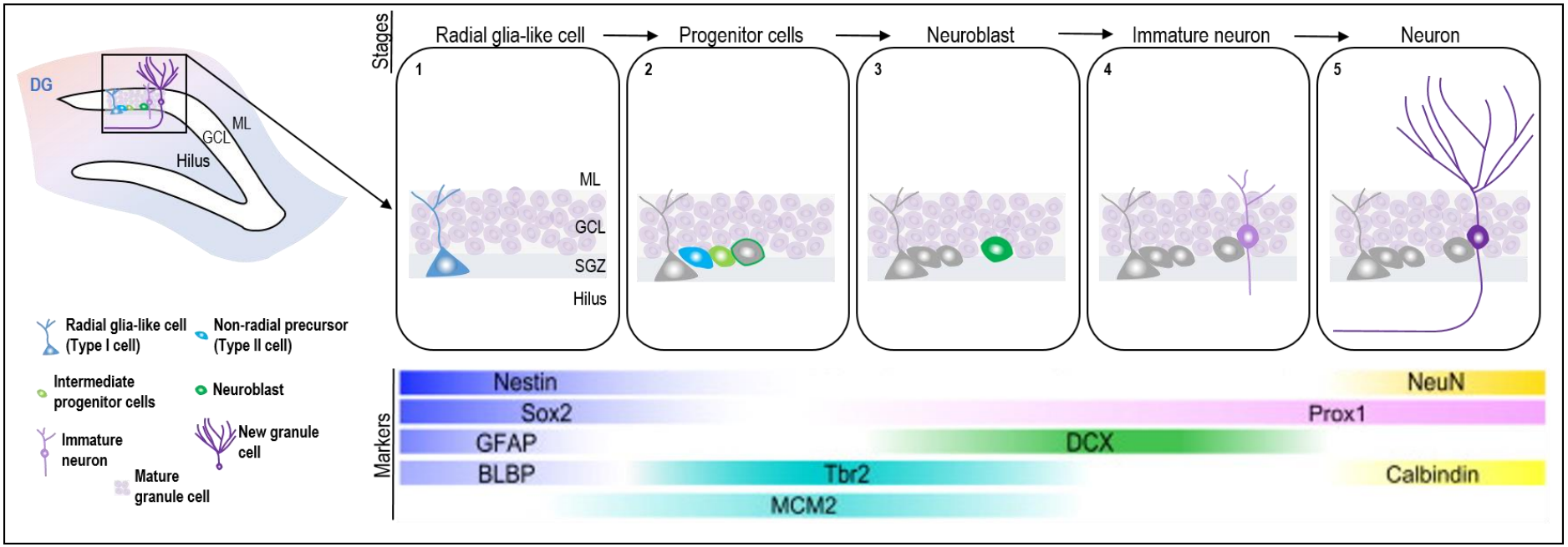

Figure 1. 11: Developmental stages during adult hippocampal neurogenesis in the dentate gyrus.

Quiescent radial glia-like cells (dark blue) in the SGZ are activated (1) leading to their proliferation to give rise to non-radial precursor (light blue) and intermediate progenitor cells (light green) (2). The latter develop into neuroblast that migrate into the GCL (3) and becomes an immature neuron which starts to integrate into the inner GCL (4). Differentiation of the immature neuron into functional dentate granule cell allows it to integrate into the pre-existing hippocampal trisynaptic circuit (5). The expression of stage-specific markers is indicated. DG: dentate gyrus; SGZ: subgranular zone; GCL: granule cell layer; ML: molecular layer; GFAP: glial fibrillary acidic protein; BLBP: brain lipid-binding protein; DCX: doublecortin; NeuN: neuronal nuclei. Adapted and redrawn from Ming and Song (2011).

1.7.2 Links between disrupted adult neurogenesis and schizophrenia

Adult hippocampal neurogenesis contributes to cognitive functions important for spatial learning and memory, known to be disrupted in neuropsychiatric disorders such as schizophrenia (Reif et al., 2006). Neuroimaging studies in schizophrenia patients revealed reduced hippocampal volume of 4-8% (Nelson et al., 1998, Shenton et al., 2001) that was correlated with the degree of cognitive dysfunction (Gur et al., 2000, Sanfilipo et al., 2002). Although absolute cell numbers within the hippocampus have not been calculated, several reports also demonstrate significant reduction in hippocampal cell proliferation and neurogenesis in post-mortem schizophrenia brain samples (Allen et al., 2015, Reif et al., 2006, Reif et al., 2007). These studies suggest that deficits in adult neurogenesis may contribute to the cognitive dysfunction seen in schizophrenia patients. Notably, DISC1 has been shown to play important roles in hippocampal neurogenesis in embryonic, postal and adult mice brains through various signalling pathways (reviewed by Wu et al., 2013).

1.7.3 Regulation of adult hippocampal neurogenesis

Tight regulation of hippocampal neurogenesis is crucial given its functional implications in the adult brain. Several signalling pathways, including the AKT signalling pathway, GABA signalling pathway, GSK3β signalling pathway, WNT signalling pathway, and NMDA-R signalling pathway have been implicated in regulating different aspects of adult neurogenesis from the activation of quiescent stem cells through to maturation and integration within mature neuronal

networks (Ming and Song, 2011, Urban and Guillemot, 2014, Varela-Nallar and Inestrosa, 2013, Wu et al., 2013).

Wnt proteins are a family of large glycoproteins that interact with cell-surface receptors to activate different downstream signalling cascades. While the canonical pathway generally leads to gene transcriptional changes as a result of altered β-catenin activity, the non-canonical or β-catenin-independent pathway induces either an increase in intracellular calcium concentration or activation of the c-Jun-N-terminal kinase (JNK) cascade (Varela-Nallar and Inestrosa, 2013). The canonical Wnt signalling pathway regulates both embryonic and adult neurogenesis by promoting proliferation and neural fate specification (Ming and Song, 2011, Urban and Guillemot, 2014, Varela-Nallar and Inestrosa, 2013). In the absence of ligand (Figure 1.12 i) the destruction complex composed of multiproteins including APC (adenomatous polyposis coli), axin, casein kinase I (CKI) and glycogen synthase kinase 3β (GSK-3β) phosphorylates β-catenin (Varela-Nallar and Inestrosa, 2013, Wu et al., 2013). This in turn results in β-catenin ubiquitination and degradation by the proteasome (Varela-Nallar and Inestrosa, 2013, Wu et al., 2013).

Wnt ligand binding to the frizzled receptor and the low density lipoprotein receptor-related protein 5/6 (LRP5/6) at the cell-surface membrane (Figure 1.12 ii) leads to inhibition of the destruction complex and stabilization of β-catenin (Reif et al., 2007, Wu et al., 2013). β-catenin subsequently translocates to the nucleus (Varela-Nallar and Inestrosa, 2013) where it associates with transcription factors such as lymphoid enhancer factor (LEF) and the T cell factor (TCF) to drive

expression of renewal and proliferative genes (Wu et al., 2013). GSK-3β is inactivated when phosphorylated by the AKT serine/threonine-specific protein kinase at serine 9 (Chang et al., 2012). Not surprisingly, several 14-3-3 proteins have been reported to directly interact with GSK-3β at serine 9 with functional implications including promotion of mouse embryonic stem cell proliferation and neural survival (Chang et al., 2012, Mwangi et al., 2006, Yuan et al., 2004). However, the role of 14-3-3 protein in neural stem cell proliferation during neurogenesis is yet to be examined.

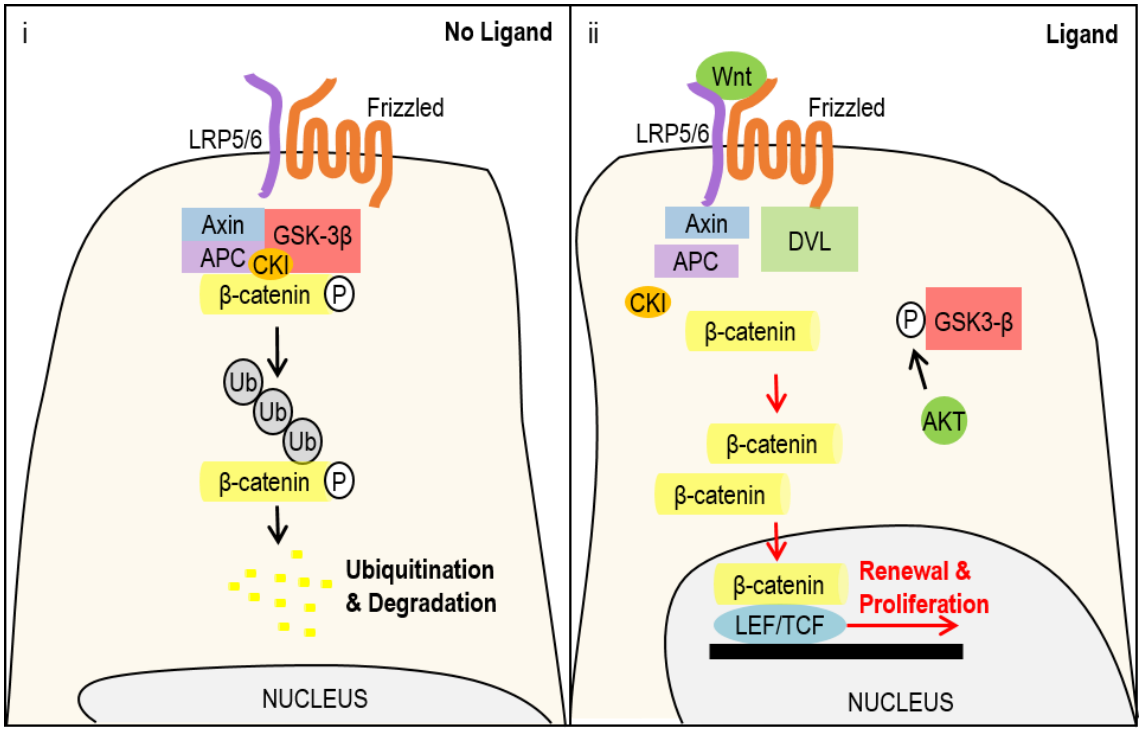

Figure 1. 12: Canonical Wnt signaling pathway.

(i) In the absence of ligand, β-catenin is associated with the destruction complex (CKI, GSK-3β, APC, Axin) where it is phosphorylated and targeted for ubiquitination and proteasomal degradation.

(ii) Binding of the Wnt ligand to the frizzled-LRP5/6 receptor complex results in dishevelled (DVL) activation which displaces GSK-3β from the destruction complex and therefore stabilizes β-catenin. β-catenin translocates into the nucleus and associates with LEF/TCF proteins activating renewal and proliferative genes. Black arrows represent negative function; red arrows represent positive function.

1.8 Aims of the thesis

The overall aim of this thesis were: 1) to provide evidence that 14-3-3ζ KO mice serve as an appropriate model of neuropsychiatric disorders such as schizophrenia, 2) to gain insights into the molecular mechanism through which 14-3-3ζ controls neuronal development, and 3) to explore the developmental mechanism underlying the onset of neuropsychiatric disorders.

More specifically, the aims of the work undertaken were:

- To address if the defects previously observed in the 129/sv 14-3-3ζ KO mice are conserved across different genetic backgrounds, namely BALB/c and C57BL/6, and not due to genetic diversity (chapter 3).
- To determine if the structural hippocampal defects previously observed in the 14-3-3ζ KO mice are accompanied by additional defects characteristic of schizophrenia, including neurite outgrowth, dendrite morphogenesis and spine formation (chapter 3).
- To explore the molecular mechanism by which 14-3-3ζ may modulate neuronal migration (chapter 4).
- To explore the role of 14-3-3ζ in regulating the maintenance and differentiation of neural stem/progenitor cells within the hippocampus (chapter 5).

The principal findings of the first aim in chapter 3 revealed that the hippocampal lamination defects of 14-3-3ζ KO mice are replicated among three independent mouse backgrounds, albeit with varying degree of severity. This was

accompanied by aberrant connectivity demonstrated by the misrouting in the mossy fibre circuit and reduced dendritic spine density. Results presented in chapter 4, using an *in vitro* neurosphere culture system, show that 14-3-3ζ is essential for proper neuronal migration and nucleus-centrosome coupling. Further, it was found that 14-3-3ζ directly interacts with Cdk5/p35 phosphorylated Ndel1 to maintain Ndel1 phosphorylation and thereby modulate neuronal migration. Chapter 5 demonstrated that 14-3-3ζ plays a pivotal role in hippocampal embryonic, postnatal and adult neurogenesis, given that its loss leads to reduction in neural stem/progenitor cell proliferation and self-renewal.

In conclusion, these results identify an important role for 14-3-3ζ in the formation and function of the hippocampus. Additionally, this work provides strong support to the notion that 14-3-3ζ KO mice are an appropriate animal model for disorders such as schizophrenia. 14-3-3ζ KO mice therefore represent an ideal model for further investigations into the aetiology of neuropsychiatric disorders and offer an exciting pre-clinical resource for the analysis of new therapeutic interventions. Although this work presents inroads to the molecular functions of 14-3-3ζ in hippocampal development there is still much to learn about the mechanisms by which this scaffolding protein modulates molecular pathways to control these processes.

Chapter Two:

Material and Methods

2.1 Materials

Chemicals used were primarily supplied by Chem-Supply, Sigma, Merk, Life Technologies, Promega, MP Biomedicals, BD Biosciences, RCI Labscan, Neurotechnologies and Thermo Fisher Scientific, unless otherwise stated. Surgical materials were supplied from Fine Science Tools, BD Biosciences, Swann-Morton and Cutisoft. Sectioning and staining materials were supplied from ProSciTech, Molecular Probes, EMS, Tissue-Tek, Ibidi, Sigma, Vector Laboratories and Invitrogen, unless otherwise stated. Recipes for the general solutions and buffers can be found in Appendix A.1.

All culture media and supplements were supplied from Life Technologies, Roche Applied Science, Sigma, Worthington Biochemicals, and Peprotech, unless otherwise stated. Sterile tissue culture plasticware was supplied from BD Biosciences and Millipore. Molecular biology reagents and purification kits were supplied from New England Biolabs, Promega, Sigma, Bioline and Qiagen. All primers were ordered from GeneWorks.

2.2 Animal husbandry

2.2.1 Ethics

All experimental protocols presented in this thesis were conducted in accordance with the guidelines of the Animal Ethics Committee of SA Pathology and the University of Adelaide. Animals used for experiments included; 1) E18.5 foetuses obtained from pregnant dams used for hippocampal cultures (section 2.5.3) and neurosphere cultures (section 2.6.1), 2) postnatal pups (P1-P3) for glial cultures (section 2.5.1), 3) postnatal day 7, 14, and 30 mice for EdU short-pulse chase labelling (section 2.4.5), and 4) adult mice for immunohistochemistry (section 2.4) and protein lysates (section 2.8.3).

2.2.2 Strains and housing of mice

14-3-3ζ KO mice in 129/sv background were generated carrying a gene trap construct that contains the βGeo reporter gene disrupting 14-3-3ζ expression which was previously described in Cheah et al. (2012). These mice were also backcrossed into BALB/c or C57BL/6 mouse backgrounds over ten generations. Animals used for this study were obtained from the littermate offspring of heterozygous breeding pairs and were maintained under a 12hr light/dark cycle and fed with regular rodent's chow and tap water. Genotypes were determined by PCR amplification of genomic tail DNA or DNA from the E18.5 brains (sections 2.7.1 & 2.7.2). The wild-type (WT) allele amplified a band of 288bp and the mutant gene trapped allele amplified a band of 165bp (Appendix A.2).

2.3 Animal and tissue preparation

2.3.1 Whole mouse perfusion fixation

Postnatal mice were perfuse-fixed according to a procedure described by Gage et al. (2012). Briefly, mice were anesthetized using sodium pentobarbitone (Nembutal) prior to surgical procedure. Toe pinch-response was used to determine depth of anaesthesia. A small incision in the diaphragm was made exposing the pleural cavity. The sides of the ribcage up to the collarbone were cut and the tip of the sternum was lifted away using a haemostat which was then placed over the head, exposing the heart. A perfusion needle (19G) was inserted to the left ventricle at the apex of the heart and a small incision was made to the right aorta. The vascular system was first flushed with 1x PBS followed by fixation with 4% PFA. Brains were harvested, post-fixed in 4% PFA overnight at 4°C followed by infiltration of 20% sucrose at 4°C overnight. Brains were transferred into square disposable embedding moulds (EMS), embedded into OCT (Tissuse-Tek) and frozen using liquid nitrogen. Samples were stored at -80°C or -20°C until use.

2.3.2 Cryosectioning of mouse brain

A cryostat (Leica CM1950) was used for cryosectioning of mouse brain samples. The chamber and stage temperatures were set to -22°C and -20°C, respectively. OCT frozen brain samples (section 2.3.1) stored in the -80°C freezer were either equilibrated in -20°C freezer the day before sectioning or for 30min in the chamber. The sample was removed from the mould and mounted on the block holder using OCT. Excess OCT was trimmed using a single edge razor. The sample was clamped to the block holder, aligned, sectioned coronally (10µm), anterior to

posterior, and collected onto positively charged plus slides (Thermo Scientific). Slides were stored in -20°C, until use.

2.3.3 Vibratome sectioning

A microtome (Leica VT1200) was used to generate thick sections from either fixed (sections 2.4.3) or live (section 2.4.4) brain tissue. Briefly, brain samples were mounted onto a metal platform with superglue and allowed to dry for 20min. The sample was covered with 1x PBS and fresh razor blades were used for sectioning. Using a paintbrush, floating brain sections were transferred into a well of a 24-well plate containing 1x PBS. Plates were sealed using Parafilm (Bemis) and stored at 4°C until use.

2.3.4 EdU short-pulse labelling

EdU short-pulse labelling was used to study proliferating cells in P7, P14 and P30 mouse brains, using a protocol adapted from Zeng et al. (2010). Briefly, 10mg/ml EdU (Invitrogen) stock was prepared in sterile 1x PBS and stored in -20°C. Pre-warmed EdU was intraperitoneally injected into the mice (100mg/kg EdU per bodyweight). Brains were isolated from humanely killed mice after 2hrs, fixed in 4% PFA overnight at 4°C then infiltrated with 20% sucrose solution at 4°C overnight. Brain samples were then embedded in OCT, frozen using liquid nitrogen and stored at -20°C until sectioned (section 2.3.2). Sections were stained for EdU-positive cells using Click-it EdU Imaging Kit (Invitrogen), following the manufacturer's protocol. Images were taken by confocal laser microscopy (LSM 510 META, Zeiss) and processed with ZEN imaging software (Zeiss).

2.4 Histology and immunohistochemistry

2.4.1 Nissl staining of brain sections

Nissl staining was based on a protocol by Paul et al. (2008). Briefly, Nissl stain consisting of 0.1% cresyl violet (Sigma) in a total of 50ml MilliQ water equilibrated with a few drops of glacial acetic acid was freshly prepared and filtered. Brain sections (section 2.3.2) were dehydrated in 1:1 ratio of ethanol/chloroform overnight, followed by series rehydration in 100%, 75%, 50%, 25% ethanol to distilled water for 5min each. Samples were then Nissl stained for 2-5min and rinsed quickly with distilled water. Sections were differentiated in 95% ethanol then dehydrated in 100% ethanol for 5min each. To clear the samples, they were placed in xylene for 5min and then mounted using Leica CV mount (Leica) and covered with an 18X18mm coverslip (ProSciTech). Images were taken using a stereo microscope (SZX10, Olympus) with bright field settings and processed with OpenLab 2.2 software (Improvision).

2.4.2 Immunostaining of brain sections

Frozen brain sections (section 2.3.2) were defrosted at room temperature (RT) before immunostaining. Using a PAP pen (Vector Laboratories) barriers were created on the slides around the brain sections to contain the solutions. First, brain sections were rehydrated in 1x PBS for 30min, followed by treatment with 1x PBT (0.1% Tween-20 in 1x PBS) for 10min at RT. Sections were then placed in block solution (10% normal goat serum in 1x PBT) for 30min at RT. Primary antibodies were prepared by dilution in block solution and added to brain sections 1hr at RT. Primary antibodies used include: rabbit polyclonal to calbindin (D-28K) (1:500,

Millipore), mouse monocolonal to SOX2 (1:250, Cell Signalling) and rabbit polyclonal to doublecortin (1:400, Cell Signalling). For the negative control slide, no primary antibodies were added to sections, instead block solution alone was used with the same secondary antibodies. Excess antibody was washed off three times with 1x PBT for 5min each. The appropriate Alexa Fluor-labelled secondary antibodies (1:200, Molecular Probes) were diluted in 1x PBS and added to brain sections for 1hr at RT. After four washes with 1x PBS, sections were post-fixed with 4% PFA for 10min and mounted with Prolong Gold antifade reagent with DAPI (Molecular Probes). Samples were imaged using confocal laser microscopy (LSM 510 META, Zeiss) and processed using ZEN imaging software (Zeiss).

2.4.3 Golgi-cox impregnation

Adult mouse brains were isolated and subjected to Golgi-cox impregnation using a FD Rapid Golgi Stain kit (Neurotechnologies) according to the manufacturer's protocol. Briefly, fixed brains were immersed in impregnation solution containing mercuric chloride, potassium dichromate and potassium chromate for 24hrs before the solution was replaced and they were left for 2 weeks at RT in the dark. Brain tissues were then transferred to solution C and store at 4°C in the dark for at least 48hrs, with replacement of solution C at first 24hrs of immersion or the following day. A vibratome (section 2.3.3) was used to make 200μm thick sections and samples were kept in 1x PBS at 4°C until use. Sections were first rinsed with MilliQ water twice then placed in a mixture containing 1 part solution D, 1 part solution E and 2 parts MilliQ water for 10min. Sections were rinsed and went through a series of dehydration in 50%, 75%, 95% to 100% ethanol. Sections were cleared in xylene for 5min, mounted with Leica CV

mount (Leica) and covered with an 18X18mm coverslip (ProSciTech). Images were captured with a 40x objective plus 1.6x magnification using an inverted microscope (IX81, Olympus) with bright field settings and processed with CellR software (Olympus).

2.4.4 Biolistic labelling of neurons using gene gun

For spine formation analysis, live brain sections were labelled with lipophilic dyes using a gene gun method based on a protocol by Seabold et al. (2010). Briefly, bullets were made containing gold particles coated with lipophilic dyes DiI (orange fluoresce) or DiO (green fluoresce) (Molecular Probes). Thick 300μm brain slices were cut using a vibratome (section 2.3.3) and placed in 1x PBS at 4°C until use. Slices were washed three times with 1x PBS then were moved using a paintbrush to the centre of a fresh well of a 24-well plate. Coated bullets were shot through a 3μm filter membrane using a Helios Gene Gun system (Bio-Rad) at 200psi helium gas pressure by placing the gun at a distance of 1.5cm between the sample and the end of the barrel. Slices were washed with 1x PBS three times and stored in 1x PBS for 24hrs at RT to allow the dye to spread along the dendrites and spines. The following day slices were moved onto a glass slide, with the labelled side facing up and mounted with Prolong Gold antifade reagent with DAPI (Molecular Probes) and covered with 18X18mm coverslip (ProSciTech) sealed with clear nail polish. Using a confocal laser microscopy (LSM510 META, Zeiss), z-stack images of the dendritic spines were acquired with a 63x water immersion objective. Images were processed using ZEN imaging software (Zeiss); spines on over 30 dendrites were manually counted 100-500μm from the cell body from each mouse.

2.5 Hippocampal neuronal cultures

2.5.1 Glial feeder cultures

Glial feeder cultures were prepared 1 week prior to hippocampal cultures (section 2.5.4) using a modified protocol adapted from Kaech and Banker (2006) and Viesselmann et al. (2011). Briefly, postnatal WT mouse pups (P1-P3) were humanely killed by decapitation, and the cerebrum was isolated. In a biohazard hood, tissues were finely minced and then dissociated in a solution of 2.5% Trypsin with 1% (w/v) DNAse1 in Hank's Balanced Salt Solution (HBSS) by incubation at 37°C for 5min with occasional mixing. Tissues were triturated using a 10ml pipette, and then returned to the water bath for an additional 10-15min. Cell suspension was passed through a 50µm cell strainer to remove un-dissociated tissues and collected in a 50ml falcon tube. The cell suspension was centrifuged for 5min at 1500rpm and the cell pellet was resuspended in 1ml of glial growth media consisting of Eagle's Minimum Essential Medium (MEM) supplemented with 0.3% (v/v) D-glucose (Sigma), 1mM pyruvate, 10% (v/v) Fetal Calf Serum (FCS), 100units/ml Penicillin/Streptomycin (PS). Cells were counted and $7.5x10^6$cells were plated per $75cm^2$ flask containing 15-20ml of growth media. After 2-3 days in culture, the loosely attached cells were dislodged by knocking the flask by hand; the media was then removed and replaced with fresh glial growth media. Glial cells were harvested 1-2 weeks after growth for co-culture with hippocampal neuronal cultures (section 2.5.5).

2.5.2 Preparation of glass coverslips for hippocampal cultures

Round 18mm glass coverslips (ProSciTech) were washed then autoclaved before use. For long-term cultures (DIV10 & DIV21), paraffin wax dots were applied onto the coverslips to generate feet to suspend the coverslips above the glial feeder layer (section 2.5.5). Paraffin wax was melted in a 65°C water bath and three dots were applied onto each coverslip in a triangular pattern using a small paint brush. Coverslips were placed in 10cm dishes and were sterilized under UV light for 30min then washed with 1x PBS before substrate treatment. Coverslips were coated with poly-L-lysine (Sigma) for 1hr at RT, and washed with 1x PBS twice. Coverslips were covered in 1x PBS, sealed with Parafilm and stored at 4°C until use.

2.5.3 Dissection of the E18.5 hippocampi

Pregnant mice were humanely killed by cervical dislocation and the embryos were removed from the uterus. Embryos were quickly decapitated and their heads were collected in ice cold dissection medium (1x HBSS and 200mM Hepes in MilliQ water). The head was placed onto the lid of a 10cm dish and using forceps the skin was peeled away and the skull plate removed. The brain was scooped out and place into a 10cm dish containing ice cold dissection medium. Under a stereo microscope (SZX10, Olympus), the cerebral hemispheres were removed and the remaining brain was cut in half. The thalamus was removed exposing the hippocampus in both halves of the brain, followed by removal of meninges. The hippocampi were isolated and placed in eppendorf tubes with

appropriate media (section 2.5.5 or 2.6.1). Note that some of the remaining brain tissue was kept for genotyping (sections 2.7.1 & 2.72).

2.5.4 Hippocampal primary cell cultures

Hippocampal primary cell cultures were prepared as previously described by Kaech and Banker (2006). Briefly, hippocampi isolated from E18.5 embryos described in section 2.5.3 were placed into 500µL of Neural-Feed media (Neurobasal media supplemented with 2% (v/v) B27, 2mM L-glutamine, 100units/ml PS) on ice until dissociation. The remaining tissue from the brain was kept at 4°C until use for genotyping the embryos (sections 2.7.1 & 2.7.2). In a biohazard hood, the neural-feed media was removed and the hippocampus was minced with sterile scissors. Tissue was washed twice with pre-warmed neat Neurobasal media to remove traces of B27 and PS. Supernatant was removed and tissue was resuspended with 900µL neat Neurobasal media plus 10µL of 2.5% Trypsin for tissue dissociation. After 5min incubation at 37°C, 1µL of 10mg/ml DNAse1 was added and the tissue was incubated for another 10min. Tissue was then washed with Neural-Seed media (Neurobasal supplemented with 2% B27, 2mM L-glutamine, 10% FCS, 100units/ml PS) twice. The tissue was triturated using fire polished glass pipette in 1ml of Neural-Seed media. The cell suspension was passed through a 50µm cell strainer, and transferred to a fresh tube. Cells were counted and plated on substrate coated 18mm round glass coverslips (section 2.5.2) which were placed into wells of a 12-well plate.

The number of cells plated varied depending on experiments to be undertaken. For low density cultures, $5x10^4$cells/well on 18mm round glass

coverslips in a 12-well plate were used for DIV3 (3 days *in vitro*) and DIV10 (10 days *in vitro*) cultures. High density cultures of $1.5x10^5$cells/well on 18mm round glass coverslips containing paraffin feet (section 2.5.2) in a 12-well plate were used for DIV21 (21 days *in vitro*) cultures. Hippocampal cell cultures were grown at 37°C flushed with 5% CO_2 for 4-6hrs then the media was changed to Neural-Feed. Half the culture medium was renewed every 4 days. Cultures of DIV10 and DIV21 were co-cultured with glia (section 2.5.5). Neurons were fixed in 4% PFA after 3, 10 or 21 DIV before being subjected to immunostaining (section 2.5.6) and analysis (section 2.5.7).

2.5.5 Glial feeder layer preparation for long-term hippocampal culture

Long-term hippocampal cultures of more than 7 days required neutrotophic support from glia for survival *in vitro*. Thus, DIV10 and DIV21 cultures (section 2.5.4) were co-cultured in 10cm dishes containing a glial monolayer. A week prior to co-culture, glial cultures from section 2.5.1 were first rinsed with 5ml of pre-warmed Trypsin/EDTA (Invitrogen) solution. The solution was removed and 2ml was added following incubation at 37°C for 2min. Trypsinization was stopped by adding 5ml of neat MEM media and cells were detached by repeated pipetting. Cell suspension was transferred into 15ml conical tubes and centrifuged at 1000rpm for 8min. Cell pellets were then resuspended into 10ml of growth media and $5x10^5$cells in 12.5ml of growth media were plated per 10cm dish. Growth media was changed every 2-3 days (section 2.5.4). The growth media was replaced by conditioned hippocampal culture growth media

three days prior to co-culture. Coverslips with hippocampal cultures were then suspended above the glial feeder layer with the help of the paraffin feet.

2.5.6 Immunostaining of hippocampal primary cell cultures

PFA fixed hippocampal neurons of DIV3 and DIV10 cultures (sections 2.5.4) were washed in 1x PBS for 30min followed by treatment with 1x PBT (0.1% Tween-20 in 1x PBS) for 10min at RT. Neurons were blocked in block solution (10% normal goat serum in 1x PBT) for 30min at RT. Hippocampal neurons were incubated with mouse monoclonal anti-MAP2 (1:200, Chemicon) diluted in block solution for 1hr at RT. For negative control, no primary antibody was added to sections, instead plain block solution was used. Excess antibody was washed off three times with 1x PBT for 5min each. The appropriate Alexa Fluor-labelled secondary antibody (1:200, Molecular Probes) diluted in 1x PBS was added to the neurons for 1hr at RT. Neurons were washed four times with 1x PBS, post-fixed with 4% PFA for 10min and mounted with Prolong Gold antifade reagent with DAPI (Molecular Probes). Neurons from DIV3 cultures were imaged at 20x magnification and DIV10 at 10x magnification using inverted microscope (IX71, Olympus) and processed with AnalySIS getIT software (Olympus). Images of a scale bar were taken at 10x and 20x magnification to calibrate the images for analysis in section 2.5.7.

2.5.7 Analysis of hippocampal neurons

Hippocampal neurons from DIV3 and DIV10 were analysed using ImageJ software after appropriate calibration (for DIV3 neurons 20x magnification was used and, for DIV10 the 10x magnification was used). For scale calibration in

ImageJ the appropriate scale bar slide image was used to draw a straight line of 100μm. The set scale dialog box from the Analyze tab was opened where a distance in pixels was automatically filled based on the line that was drawn. The known distance (i.e. 100) and the unit of scale (i.e. μm) were filled and applied to all images opened within that session.

For neurite outgrowth analysis, DIV3 hippocampal neurons were used to measure the length, number of bifurcations and total number of neurites per neuron. NeuronJ tool in the ImageJ software was used to measure the length of the neurites, whereas the number of bifurcations and total number of neurites per neuron were counted manually. For dendrite morphology analysis, DIV10 hippocampal neurons were used to look at the dendrite complexity. MAP2 positive neurites were quantified using the Sholl Analysis tool in the ImageJ software. Dendrites crossing concentric circles where drawn at 5μm intervals around neuron's cell body and the number of dendrite crossings the concentric circles were measured. For spine analysis, DIV21 neurons were labelled with lipophilic dyes using a gene gun as described in section 2.4.4 prior to fixation.

2.6 Neurosphere culture

2.6.1 Neurosphere culture of hippocampal neural progenitor cells

Neurosphere cell cultures were prepared based on protocols described by Chen et al. (2007) and Giachino et al. (2009). Briefly, dissociation media consisting of 1x HBSS supplemented with 15units/ml papain (Worthington Biochemicals), 1.7mM L-cysteine and 0.6mM EDTA was freshly made and filter sterilized. Hippocampi isolated from E18.5 embryos described in section 2.5.3 were incubated with pre-warmed dissociation media for 20min at 37°C. Pre-warmed neat Dulbecco's Modified Eagle Medium: Nutrient Mixture F-12 with Glutamax (DMEM/F12) media was used to wash out the papain within the dissociation solution twice. Cells were then dissociated in 500µL neurosphere growth media (DMEM/F12 supplemented with 2% B27, 20ng/ml EGF, 20ng/ml hFGF, 100units/ml PS) using a fire polish glass pipette ~20-25 times, avoiding the introduction of air bubbles. Cells were plated at constant density of 10,000cells/well in uncoated 24-well plates or 500cells/well in uncoated 96-well plates and incubated at 37°C flushed with 5% CO_2.

Neurospheres initially take longer to develop therefore the first passage was undertaken 10 days post culture while following passages were undertaken every 6 days thereafter. When passaging, neurospheres were transferred into a 15ml tube then centrifuged at 1500rpm for 5min. The supernatant was carefully removed, 500µL of TrypLE Express (without phenol red) was added and incubated at 37°C for 20min. Neurospheres were centrifuged at 1500rpm for 5min and the cell pellet was resuspended in growth media (500µL). Using a fire polished glass

pipette neurospheres were triturated to a single cell suspension. Cells were plated and incubated at 37°C flushed with 5% CO_2.

2.6.2 Neurosphere migration assay

A grid was drawn at the bottom of a 22mm glass bottom dish (ProSciTech). Dishes were coated with poly-L-lysine (Sigma) for 30min at RT. Dishes were washed with 1x PBS then coated with 10ng/ml laminin (Invitrogen) diluted in neat DMEM/F12 medium for 1hr at RT. Dishes were washed with 1x PBS twice and stored at 4°C, covered in 1x PBS, until use. The 1x PBS was replaced with ~100-200µL (just enough to cover the bottom of the dish) of pre-warmed media containing DMEM/F12 supplemented with 2% B27 and 100units/ml PS.

Only neurospheres from the third or fourth passage were used for migration assays. Neurospheres were transferred to a well of a 6-well plate and using a dissecting microscope single neurospheres was transferred to a square within the grid drawn on the base of a 22mm glass bottom dish (ensuring neurospheres are not in close proximity to each another). Neurospheres were incubated for 30min allowing them to adhere to the substrate followed by addition of 500µL of media and incubation at 37°C with 5% CO_2. Neurospheres were left to migrate for 24hrs before media removal and wash with 1x PBS. Neurospheres were fixed with pre-warmed 4% PFA for 10min and washed with 1x PBS prior to mounting with Prolong Gold antifade reagent with DAPI. Neurospheres were imaged at 20x magnification using an inverted microscope (IX71, Olympus) and processed with AnalySIS getIT software (Olympus).

2.6.3 Analysis of the migration assay

Photoshop CS3 software (Adobe Systems) was used to prepare the images from section 2.6.3 before being analysed using ImageJ software. A template of scale bars (50, 100, 200, 300 and 400μm) was generated and saved as tiff file. Images of the DAPI stained neurons from the migration assay in section 2.6.2 were opened in Photoshop and the images were converted to grey scale. The scale bars were then dragged to the image and aligned against the edge of the original neurosphere (Figure 4.1 viii). The original neurosphere was then traced by using the freehand tool and deleted since the DAPI staining is too bright within this region. The central deleted region was coloured black and the image was duplicated. The free transform tool was used on the original image to drag the outlined sphere to the first scale bar of 50μm whilst holding the alt button to increase size of the selection area in scale. That first bin area was copied from the duplicated image, pasted in a new file and saved ensuring the background colour is also black. The free transform tool was selected on the original image and the process was repeated to generate images for the remaining bins.

Once all bins were generated for each area and neurosphere per genotype, the images were then analysed in ImageJ. Images were opened in ImageJ and inverted. The threshold was adjusted and number of nuclei within that bin were counted by using Analyze Particle Tool. The 50μm bin images however were counted manually as the cells overlapped and the program was unable to produce accurate counts. The raw data was transferred to Excel (Microsoft) and plotted using histograms.

2.6.4 Live imaging of the neurosphere migration assay using spinning disc confocal microscopy

Migration assays were undertaken as described in section 2.6.2 with the following modifications. A line on the centre of the 22mm glass bottom dish was drawn instead of a grid. WT neurospheres were isolated and placed on one side of the dish and KO neurospheres on the other. Once neurospheres adhered to the substrate treated glass bottom dish, media was added and the dish was inserted into the spinning disc confocal microscope (CV1000, Yokogawa). While the dish was left to equilibrate, the scanning parameters were adjusted. Images were set to be taken every 30min z-stacked for 24hrs at 40x magnification of each neurosphere (at least 3 neurospheres per group per experiment). Once experiments were completed movies were generated using the CV1000 software (CV1000, Yokogawa).

Movies generated from live imaging were analysed using the Manual Tracking tool to track individual neurons in the ImageJ software. The appropriate scale was set using the set scale tool under analyse in the main tabs. The time interval parameter was set to 30min in the tracking window. Individual neurons were tracked using the add track tool by tracing it in each frame. The end track tool was used to end tracking of that individual neuron. This process was repeated for each neuron. The result folder was saved then opened in the Chemotaxic and Migration Tool (Ibidi) which generates a summary of the raw data generated by tracking the neurons. In the setting tab, the time interval was adjusted to 30min and the X/Y calibration to μm. The data set saved from the Manual Tracking was

imported through the import dataset tool which included all frame slices (the 48 images in the movie). The imported data was then selected and all settings applied within the apply settings tool. To generate statistical values from the dataset, the Show Info tool was selected which resulted in a summary of the mean migration distance, mean velocity and directionality of the neurons. An animated plot or a plot graph of the neurons tracked can be generated using the plot feature tab by clicked animate plot or plot graph, respectively.

2.6.5 Adhesion assay on neural progenitors

The cell adhesion assay was performed based on a modified version of the protocol described by Humphries (2009). Briefly, in 96-well plates a few wells were left empty for obtaining background measurements and the rest were coated with poly- L-lysine (Sigma) for 30min at RT then washed with 1x PBS. Plates were then coated with 10ng/ml laminin (Invitrogen) diluted in DMEM/F12 for 1hr at RT. Wells were washed twice with wash buffer (0.1% (v/v) Bovine Serum Albumin (BSA) in DMEM/F12) then blocked with block buffer (0.5% (v/v) BSA in DMEM/F12) for 45-60min in a 37°C incubator with 5% CO2. Wells were washed with wash buffer and placed in 4°C covered in wash buffer until use.

A single cell suspension of neurospheres from the third passage (section 2.6.1) was generated and $4x10^4$cells/ml were seeded per well. In each well 50µL of the cell suspension was added and plates were incubated in the 37°C incubator with 5% CO2 at for either 10min or 60min. Plates were gently agitated for 10-15secs to remove loosely attached cells and washed 2-3 times with 1x PBS. Cells were fixed with 4% PFA at RT for 10-15min and washed with wash buffer. Cells

were stained with 50µL crystal violet (5mg/ml in 2% ethanol) for 10min and washed twice with wash buffer. Plates were turned upside down and allowed to dry completely before addition of 100µL 1% SDS in MilliQ water and incubation at RT for 30min. Absorbance was measured at 550nm using a plate reader (Biotek) and analysed using KC4 data analysis software (Biotek). The data was plotted in histograms using Excel (Microsoft).

2.6.6 Nuclear-centrosome coupling

For nuclear-centrosome (N-C) coupling experiments, migration assays were performed as described in section 2.6.2. After 24hrs of migration neurospheres were fixed with pre-warmed 4% PFA for 10min and washed with 1x PBS prior immunostaining with mouse monoclonal antibody to γ-tubulin (1:500, Sigma) and Prolong Gold antifade reagent with DAPI to label the centrosome and nucleus, respectively. Immunostaining was undertaken based on the method described in section 2.4.2. Samples were imaged using confocal laser microscopy (LSM 510 META, Zeiss) and processed using ZEN imaging software (Zeiss). For measurement of the distance between the nucleus and centrosome, images were opened in ZEN imaging software and the graphics tag at the bottom of the screen was selected. The line icon was used to measure the distance between the nucleus and the centrosome. The measurements were recorded and plotted using histograms in Excel (Microsoft).

2.6.7 Transfection of neurospheres

Neurospheres were transfected using the Nucleofection Amaxa kit (Lonza) based on a modified protocol from Viesselmann et al. (2011). First, 12-well plates were prepared by adding growth media (300µL/well) and left to equilibrate in a 37°C incubator flushed with 5% CO_2. Neurospheres were then isolated from either the third or fourth passage and were dissociated into single cell suspension as described in section 2.6.1. Cells were seeded at a density of $5x10^6$ cells/transfection and the supernatant was removed. Nucleofection solution was prepared freshly by mixing 82µL solution A + 18µL of solution B (Lonza) and 10-20µg of Qiagen endotoxin-free prepared GFP tagged plasmid DNA (sections 2.7.4 & 2.7.8) was added to the solution. Nucleofection/DNA solution was added to the cell pellet and transferred to the electroporation cuvette. The cuvette was inserted into a Nucleofector device (Lonza) and program A33 was used to electroporate the cells. The cuvette was quickly removed and 500µL growth media was added to the cells. The cells were then transferred to a well of the equilibrated 12-well plates containing 300µL of growth media. Transfected cells were incubated overnight at 37°C incubator with 5%CO_2, with a change of growth media the following day. GFP positive neurospheres were isolated 72hrs post transfection and used for migration assay as described in section 2.6.4.

2.6.8 Neurosphere proliferation and self-renewal assays

Neural progenitors were isolated from the hippocampus of E18.5 embryos and cultured in suspension for 10 days until they formed neurospheres as described in section 2.6.1. Neurospheres were then passaged at a constant density

of 10,000cells/well in 24-well plates or 500cells/well in 96-well plates over three passages every 6 days.

For neurosphere size examination, third passage neurospheres cultured in 24-well plates were imaged using an inverted microscope (CKX41, Olympus) with bright field settings. At least 4 images at 10x magnification were taken per well and three wells per sample. For analysis the images were opened in ImageJ software and the appropriate scale was set using the set scale tool under the analyze tab. The circle tool was used to draw a circle around the neurosphere to measure total neurosphere area.

To determine the total number of neurospheres, neural stem/progenitor cells were plated at a density of 500cells/well in 96-well plates and grown for 6 days. The number of neurospheres formed was counted under an inverted microscope (CKX41, Olympus) under bright field setting. This was repeated for the neurospheres from the second and third passages.

To determine the total cell number of neurospheres within a well, 1000cells/well were cultured in uncoated 24-well plates. Six days post culture from the first passage, all neurospheres within a well were isolated and dissociated into a single cell suspension and the viable cells within that well were counted using a haemocytometer. This was then repeated for the second and third passages.

2.6.9 BrdU incorporation assay on neural progenitor cells from neurosphere cultures

BrdU (5-bromodeoxyuridine) incorporation assay was used to determine the proliferation rate of the neural progenitor cells in neurosphere cultures. Neurospheres were mechanically dissociated to produce a single cell suspension as described in section 2.6.1. The dissociated cells were then cultured (10,000cells/well) on poly-L-lysine (Sigma) and laminin (Invitrogen) coated 24-well plates for 48hrs. The media was then replaced with media supplemented with 10μM BrdU (Sigma) and incubated for an additional hour. The media was removed and the cells were fixed with ice cold 70% ethanol for 20min at RT. The cells were then washed twice with 1x PBS and once with wash buffer (0.5% BSA in 1x PBS).

The DNA was denatured by incubating the cells in 2M HCl for 30min at RT and washed once in wash buffer for 2min with gentle shaking. HCl was then neutralised by adding 0.1M Borax (pH 8.5) for 5min at RT with shaking, followed by two washes in wash buffer for 2min each. Cells were blocked with 0.5% BSA and 0.5% Tween-20 in 1x PBS for 30min. Rat monoclonal anti-BrdU (1:250, Ab6326) diluted in block solution was added to the cells for 1hr at RT, followed by three washes in wash buffer. Secondary donkey anti-rat Alexa-488 conjugated antibody (1:250, Invitrogen) diluted in block buffer was then added for 1hr at RT. Cells were washed three times with wash buffer and mounted in Prolong Gold antifade reagent with DAPI. Four images/well and three wells/genotype were taken on an inverted microscope (IX71, Olympus) at 40x magnification and

processed with AnalySIS getIT software (Olympus). Images were analysed using the Analyze Particle Tool in ImageJ software. The raw data was analysed and plotted in histograms as percentage of BrdU-positive cells relative to DAPI using Excel (Microsoft).

2.6.10 Immunostaining of neurospheres with stem cells markers

For immunohistochemistry with stem cell markers, first passage (primary) neurospheres from section 2.6.1 were processed in suspension in Eppendorf tubes. Half the media was removed from the free-floating neurospheres and the same amount of pre-warmed 4% PFA was added and incubated for 10min at RT. Neurospheres were washed with 1x PBS then permeabilized with 1x PBT (0.1% Tween-20 in 1x PBS) for 10min at RT. Neurospheres were blocked in 10% normal goat serum in 1x PBT for 30min at RT. Primary antibodies were prepared by dilution in block solution and added to neurospheres for 1hr at RT. Primary antibodies including mouse monocolonal to Nestin (1:250, Abcam) and rabbit polyclonal to doublecortin (1:400, Cell Signalling) were added to the same sample. Primary antibodies were washed off three times with 1x PBT for 5min each. A combination of donkey anti-mouse Alexa-488 and donkey anti-rabbit Alex-555 conjugated secondary antibodies (1:200, Invitrogen) were diluted in 1x PBS and added to the neurospheres for 1hr at RT. After four washes with 1x PBS, neurospheres were stained with DAPI diluted in methanol. Neurosphere were post-fixed with 4% PFA for 10min, then washed and maintained with 1x PBS at 4°C until imaging.

To avoid altering 3D structure of the neurospheres, they were mounted on a slide containing a rectangular well cut out of three layers of electrical tape. Excess PBS was then carefully removed by touching the corner of a Kimwipe (Kimtech Science) on the slide drawing off the liquid. 95% glycerol was then added to the cells and samples covered using an 18/18mm cover slide. Using a confocal laser microscopy (LSM510 META, Zeiss), z-stacks of the neurospheres were acquired and processed using ZEN imaging software (Zeiss).

2.7 Molecular biology protocols

2.7.1 Genomic DNA isolation and preparation

Genomic DNA was isolated from either E18.5 brains or mouse tails. Briefly, tails were incubated overnight at 55°C in 500µL DNA lysis buffer (1MTris-HCl pH 8.5, 0.5M EDTA, 4M NaCl and 10% SDS in MilliQ water) and 0.2mg/ml Proteinase K then centrifuged at 13000rpm for 10min. Supernatant was transferred into fresh Eppendorf tubes and 500µL isopropanol was mixed with the samples. Samples were centrifuged for 5min at 13000rpm and pellets were carefully rinsed with 70% ethanol followed by centrifugation for 3min at 13000rpm. Supernatant was removed and pellet was air dried on the bench top. DNA was resuspended in 300µL of TE buffer (1M Tris-HCl pH 8.5 and 0.5M EDTA in MilliQ water) and heated for 30min at 65°C. DNA samples were stored at 4°C until use.

2.7.2 Mouse genotyping

Genomic DNA was prepared as described in section 2.7.1 and genotyping was preformed using primers listed in Table 2.1. PCR reactions were performed using GeneAMP PCR system 2700 (Applied Biosystems) in 200µL thin-walled PCR tubes. The PCR mix contained 100ng genomic DNA, 12.5µL GoTaqGreen (Promega), 8µM forward primer, 8µM reverse primer and the mixture was brought up to 25µL by addition of sterile MilliQ water.

PCR cycling involved heating the reaction at 94°C for 2min for the activation of the polymerase; followed by 40 cycles of denaturing at 94°C for 1min, annealing at 46°C for 2min, elongation at 65°C for 5min; the final elongation cycle

was at 65°C for 10min and samples were held at 4°C. PCR products were run on 1% agarose gels (section 2.7.3). The expected PCR product from 14-3-3ζ WT allele was 288bp and 14-3-3ζ KO allele was 165bp, while 14-3-3ζ HET allele displayed both PCR products (see Appendix A.2 for gel).

Allele	Forward Primer	Reverse primer
14-3-3ζ WT	5'-GAA CTT CAG ATC TGG TGA C-3'	5'- GAT TGT ACT CAA AAT GGT GGA C-3
14-3-3ζ KO	5'-GCG TTA CTT AAG CTA GCT TGC-3'	

Table 2. 1: Sequence of primer set used for genotyping 14-3-3ζ mice.

2.7.3 Agarose gel electrophoresis

1-3% (w/v) agarose gels were made depending on the samples. Agarose gels were prepared using agarose powder in 1x TAE buffer (40mM Tris-Base, 0.11% glacial acetic acid, 1mM EDTA, pH 8.0 in MilliQ water). To each lane in the gel, a mixture of 10µL PCR product and 2µL 10x DNA loading buffer (Invitrogen) was added. Low molecular weight DNA Ladder (Invitrogen) was used as a marker to determine band sizes. Gels were electrophoresed at a voltage of 85-90 volts for 20-40min using a Bio-Rad gel electrophoresis system. The gel was stained in 0.5µg/ml ethidium bromide bath followed by imaging on GelDoc-It Imaging System (UVP).

2.7.4 Constructs

The Rc/CMV-14-3-3ζ-Myc and Rc/CMV-14-3-3ζ-IRES-GFP with ampicillin (AMP) resistance were generously provided by Joanna Woodcock (Centre for Cancer Biology, AUS). The pEGFP-C1-Ndel1 with kanamycin (KAN) resistance was kindly supplied by Daisuke Tsuboi (Nagoya University, Japan). The quadruple Ndel1 mutant plasmid (S198A, T219A, S231A, & S242A) denoted Ndel14A-IRES-GFP (AMP) and Ndel1 phosphomimetic plasmid (S198E, T219E, & S231E) denoted Ndel13E-IRES-GFP (AMP) were already available in our laboratory. DNA concentration was determined using a NanoDrop spectrophotometer, according to the manufacturer's instructions.

2.7.5 DNA sequencing

Plasmids (section 2.7.4) were sent for sequencing to ensure that they were accurate. Samples were prepared based on the Sanger sequencing protocol from the Australian Genome Research Facility (AGRF). Briefly, 20µL reaction mixture consisting of 4µL 5x RD Buffer, 1µL BDT, 1µL appropriate primer (10ng/µL), 1µL plasmid DNA (200-400ng) from section 2.7.4 and 13µL sterile MilliQ water were prepared in 200µL thin-walled PCR tubes. The mixtures were reacted in GeneAMP PCR system 2700 (Applied Biosystems) using the following cycle: 94°C for 2min and 30x cycles of 94°C for 10secs, 50°C for 10secs and 60°C for 4min. Samples were held at 4°C until clean up. The 20µL samples were transferred into Eppendorf tube, followed by the addition of 50µL of 75% isopropanol and 1µL of glycogen. Samples were incubated for 30min at RT and centrifuged at 13000rpm for 15min at 4°C. Pellets were carefully washed with 500µL of 75% isopropanol

and centrifuged at 13000rpm for 5min at 4°C. Pellets were dried by incubation at 37°C for 5min and sent for sequencing at the AGRF. Sequences were processed using the BioEdit sequencing alignment software (Ibis Biosciences).

2.7.6 Preparation of electrocompetent *E. coli* DH5α cells

A starter culture was prepared containing 10mL of Luria Bertani (LB) media and *E. coli* DH5α cells (from -80°C glycerol stock), incubated overnight at 37°C with shaking at 180rpm. The overnight culture was used to inoculate 400mL LB culture until the optical density reached ~0.4-0.8. The cells were cooled on ice for 30min, followed by centrifugation at 5,000xg for 10min at 4°C using a super-speed centrifuge (Avanti J-26XPI, Beckman Coulter). The pellet was then transfer to 50mL falcon tubes and centrifuged using a bench centrifuge (Heraeus) ~3,600xg for 15min at 4°C. The pellet was resuspended in 20mL of ice-cold 10% glycerol with 1mM Hepes and centrifuged ~3,600xg for 15min at 4°C. The cells were then resuspended in 400µL of ice cold 10% glycerol and 25µL aliquots were placed in pre-cooled Eppendorf tubes. Cells were snap frozen in liquid nitrogen and stored at -80°C.

2.7.7 Electroporation into *E. coli* DH5α cells

Luria Bertani (LB) media was kindly made by the LSC staff at the Centre for Cancer Biology. LB agar plates were prepared by heat dissolving 0.375g of Bactiological Agar in 25ml of sterilized LB per plate. The LB agar media was cooled before addition of the appropriate antibiotic (100µg/µL AMP or 50µg/µL KAN)

and 0.1% (w/v) glucose. The LB agar media was poured into petri dishes and allowed to set under aseptic conditions.

To 25µL of electrocompetent *E. coli* DH5α cells, 1-2µL of the DNA was added and transferred to the cuvette. The cells were electroporated at 2 volts and quickly 200µL of pre-warmed LB media was added to the cuvette. The electroporated cells were transferred to fresh Eppendorf tubes and incubated at 37°C for 1hr. Electroporated cells were then spread plated onto LB agar plates containing appropriate antibiotics, and incubated at 37°C overnight. Plates containing transformed colonies were sealed with Parafilm and stored at 4°C.

2.7.8 Large scale plasmid purification

A starter culture was prepared using a single transformed colony from section 2.5.7, containing the desired plasmids, inoculated in 5mL of LB media with the appropriate antibiotics (100µg/µL AMP or 50µg/µL KAN) for ~8hrs at 37°C with agitation (180rpm). The starter culture was diluted (1:1000) into 200mL of selective LB media and incubated overnight at 37°C with agitation (180rpm). For glycerol frozen stocks, 1mL of culture was mixed with 100µL of 80% glycerol in cryovial, snap frozen in liquid nitrogen and stored at -80°C. The remaining culture was used for plasmid purification using EndoFree Plasmid Maxi-Prep Kit (Qiagen) following the manufacture's protocol. DNA concentration was determined using a NanoDrop spectrophotometer according to the manufacturer's instructions. Aliquots of 50µL Endofree plasmid DNA were stored at -20°C and working stock was stored at 4°C. Samples were checked on agarose gels (section 2.7.3).

2.8 Protein interaction analysis

2.8.1 HEK293T cell culture

The human embryonic kidney 293T (HEK293T) cells were cultured in the biohazard hood using aseptic technique. A cryovial containing HEK293T cells from the liquid nitrogen storage was quickly thawed in a 37°C water bath followed by immediate transfer of cells into the 3mL of pre-warmed HEK293T culture media (Dulbecco's Modified Eagle Medium (DMEM) supplemented with 10% FCS and 100units/ml PS). Cells were centrifuged at 15000rpm for 3min and the cell pellet was washed in 3mL of neat DMEM media to remove any traces of dimethyl sulfoxide (DMSO) from the cells. Cells were centrifuged again at 15000rpm for 3min and the cell pellet was resuspended into 1mL of HEK293T culture media and transferred into a sterilised 75cm^2 flask containing 10mL of pre-warmed HEK293T culture media. Cells were incubated at 37°C with 5% CO_2.

For maintenance, cells were left to reach 80-90% confluence prior to passaging (generally 2-3 times a week). Cell monolayers was carefully rinsed twice with sterile 1x PBS, then treated with 1.5mL of TrypLE Express (with no phenol red) for 2min at 37°C in order to detach cells. Trypsinized cells were gently triturated to generate a single cell suspension and 3mL of neat DMEM media was then added for inhibition of trypsin from further digestion. Cells were centrifuged at 15000rpm for 3min and the cell pellet was then resuspended in 1mL of HEK293T culture media and cultured into a new 75cm^2 flask at 1:10 or 1:15 ratio of cell suspension: media. Cells were incubated at 37°C incubator with 5% CO_2.

For cell storage, cells were isolated by trypsinization as described above. HEK293T cells with a density of $1x10^5$cells/mL were resuspended in freezing media consisting of 10% DMSO and 90% FCS. Cells were aliquoted into cryovials and placed in a Mr. Frosty with isopropanol at -80°C for 24hrs to allow gradient freezing of cells. Cells were places in liquid nitrogen for long term storage.

2.8.2 Transfection of HEK293T cells

For transfection, HEK293T cells were seeded at a density of $2x10^5$cells/well in a 6-well plate in DMEM supplemented with 10% FCS without antibodies. The following day 4µg of Endofree plasmid DNA (section 2.7.10) was mixed with 250µL of pre-warmed OptiMEM media in an Eppendorf tube. In another Eppendorf tube 10µL Lipfectamine 2000 (Invitrogen) was added to 240µL of pre-warmed OptiMEM media. The solutions were incubated at RT for 5min, and then mixed together. After 30min at RT the 500µL transfection solution was added carefully dropwise to the cells and incubated for 4hr in the 37°C incubator flushed with 5% CO_2. The media was then replaced with HEK293T culture media and incubated for another 48hrs. In the case where the vectors had fluorescent tags, transfected HEK293T cells were visualised using an inverted microscope (IX71, Olympus) to calculate transfection efficiency. For protein extraction (section 2.8.3), transfected cells were either lysed immediately or 2hr post treatment with 0.5µM Okadaic acid or FTY720 to inhibit or activate PP2A, respectively. The Okadaic acid and FTY720 were generously provided by Jason Powell (Centre for Cancer Biology, AUS).

2.8.3 Protein extraction from cells and brain tissue

NP-40 lysis buffer (10mM Tris-HCl pH 7.4, 137mM NaCl, 10% glycerol and 1% NP-40 in MilliQ water) was prepared and stored at 4°C. The protease and phosphatase inhibitors: 10mM β-glycerol phosphate, 2mM sodium vanadate, 2mM sodium fluoride, 2mM phenylmethylsulfonyl fluoride, 10mM sodium pyrophosphate, 1μg/ml leupeptin, 5μg/ml aprotinin, one complete mini EDTA-free protease inhibitor cocktail tablet were added freshly to the NP-40 lysis buffer on the day of protein extraction.

For cell lysis, transfected HEK293T cells (section 2.8.2) were carefully washed first with pre-warmed media then with pre-warmed 1x PBS. Ice cold NP-40 lysis buffer with the appropriate inhibitors was added to the cells and transferred into a microfuge tube. Cells were lysed at 4°C for 30min, then centrifuged at 13000rpm for 10min at 4°C. The supernatant was transferred into a fresh Eppendorf tube and the protein lysate was stored at -20°C until use (sections 2.8.4-2.8.7).

For brain tissue lysis, either the hippocampus alone or the whole brain of snap frozen or fresh samples were manually homogenized, using a disposable homogenization pestle, in NP-40 lysis buffer with the protease and phosphatase inhibitors. Tissue was left to lysis 4°C for 30min with shaking. Supernatant was collected by centrifuging samples at 13000rpm for 10min at 4°C. Protein lysates were stored at -20°C until use (sections 2.8.4-2.8.7).

2.8.4 Protein quantitation using BCA protein assay

The Pierce BCA protein assay kit (Thermo Fisher Scientific) was used for all protein quantitation following the manufacture's protocol. Briefly, a set of protein standards using bovine serum albumin (BSA) diluted in 1x PBS were prepared (0µg/mL, 0.125µg/mL, 0.25µg/mL, 0.5µg/mL, 1µg/mL, 2µg/mL, 5µg/mL, & 10µg/mL) and stored in -20°C until use. Protein lysates from section 2.8.3 were also prepared by diluting them in neat NP-40 lysis buffer using a 1:10 and 1:50 dilutions. The BCA working reagent was prepared by mixing 50 parts of reagent A with 1 part of reagent B (Thermo Fisher Scientific). The BSA protein standards and protein lysate (10µL) were aliquoted into the appropriate wells in a 96-well plate, in duplicates (for template see Table 2.2).

To each well, 200µL/well of BCA mixture was added and mixed carefully avoiding bubbles. The plate was incubated at 37°C for 30min followed by measurement of absorbance at 540nm using a microplate reader (Biotek) and processed using KC4 data analysis software (Biotek). A standard graph was generated using the known BSA protein concentrations by plotting the blank-corrected 540nm measurement versus their concentration in µg/ml. The concentration of the protein lysates was then determined using the standard curve multiplied by the dilution factor used.

BSA 0µg/mL	BSA 0µg/mL	BLANK	BLANK	BLANK	BLANK						
BSA 0.125µg/mL	BSA 0.125µg/mL	BLANK	BLANK	BLANK	BLANK						
BSA 0.25µg/mL	BSA 0.25µg/mL	sample 1 neat	sample 1 neat	sample 2 neat	sample 2 neat						
BSA 0.5µg/mL	BSA 0.5µg/mL	sample 1 1:10	sample 1 1:10	sample 2 1:10	sample 2 1:10						
BSA 1µg/mLl	BSA 1µg/mL	sample 1 1:50	sample 1 1:50	sample 2 1:50	sample 2 1:50						
BSA 2µg/mL	BSA 2µg/mL	sample 3 neat	sample 3 neat	sample 4 neat	sample 4 neat						
BSA 5µg/mL	BSA 5µg/mL	sample 3 1:10	sample 3 1:10	sample 4 1:10	sample 4 1:10						
BSA 10µg/mL	BSA 10µg/mL	sample 3 1:50	sample 3 1:50	sample 4 1:50	sample 4 1:50						

Table 2. 2:Template for BCA protein assay based on a 96-well plate.

All samples are loaded in duplicates, side by side. The first two columns consist of the BSA protein standard. Protein lysate samples are loaded neat and diluted (1:10 and 1:50). Colour code represents protein concentration: lighter colours represent low protein concentration, while darker the colours represent higher protein concentration.

2.8.5 Immunoprecipitation

Prior to immunoprecipitation, 50µL/sample of a 50% protein-A sepharose slurry was washed twice with ice cold 1x PBS. For load control, 5% of the protein lysates from the transfected HEK293T cells (sections 2.8.3) were kept for later use as input. The remaining protein lysates were precleared with protein-A sepharose beads for 30min at 4°C with constant rotation of samples to prevent any non-specific protein binding to the beads. At the same time, 1µL of mouse monoclonal anti-Myc (9E10, Cell Signalling) was incubated with 50µL of beads for 30min at 4°C with rotation. This was then centrifuged at 13000rpm at 4°C for 10min to remove excess unbound antibody. The precleared protein lysate was centrifuged for 15min at 4°C and the supernatant was transferred to the antibody bound beads for immunoprecipitation overnight at 4°C with constant shaking.

Immunoprecipitated proteins and lysates were separated using SDS-PAGE (section 2.8.6), followed by transfer of gels to nitrocellulose membranes for western blot analysis by immunoblotting (section 2.8.7).

2.8.6 Sodium dodecyl sulphate polyacrylamide gel electrophoresis (SDS-PAGE)

SDS-PAGE gel electrophoresis was used to separate protein samples according to their size. Polyacrylamide gels were prepared using various gel concentrations depending on the molecular weight of the protein of interest (see Table 2.3). Separating gels were prepared in duplicates by mixing the appropriate concentrations of 30% of acrylamide (Bio-Rad) with MilliQ water and Tris buffer (1.5M Tris-base and 0.4% SDS in MilliQ water). 20µL TEMED and 40µL fresh 10% ammonium persulphate (APS) were added to the acrylamide/buffer mixture prior to pouring into the gel cassettes, leaving the top 3cm free for stacking gel. To ensure a smooth even surface of the separating gel MilliQ water was carefully overlaid on top of the acrylamide/buffer mixture without excessive mixing. The separating gel was left to set for at least 1hr. Once set, the MilliQ water overlay was discarded, the gel was rinsed MilliQ water and thoroughly drained. Stacking gels were prepared by mixing 1.6mL 30% acrylamide, 5.9mL MilliQ water and 2.5mL Tris buffer (0.5MTris-base and 0.4% SDS in MilliQ water). 20µL TEMED and 60µL fresh 10% APS were added to the mixture prior to pouring it into the cassette. A lane comb was inserted to the cassette and the stacking gel was left to set for at least 30min. Polyacrylamide gels were kept damp and stored in 4°C until use.

Upon use, the comb was removed from the gels and the wells were flushed using 1x SDS running buffer (25mM Tris-base, 190mM Glycine and 0.1% SDS in MilliQ water). Gels were assembled in the running apparatus and covered with 1x SDS running buffer. Load buffer was prepared by freshly adding 5% 2-mecarptoethanol to 6x SDS-loading dye (0.5M Tris, 20% Glycerol, 4% SDS and bromophenol blue in MilliQ water). Protein samples (25-40µg per lane) from sections 2.8.3 & 2.8.5 were prepared by adding 1x load buffer and incubated at 100°C for 5min. Precision plus protein standard (Bio-Rad) and protein samples was loaded to gels. Gels were electrophoresed at ~10mA until dyes entered the separating gel then increased to 25 mA, per gel, for 40-60min.

MW Range	Gel (%)	30% Acrylamide (mL)	MilliQ water (mL)	Lower Buffer (mL)
70-200kDa	5	2.7	9.3	4
40-150kDa	7.5	4	8	4
20-100kDa	10	5.3	6.7	4
10-70kDa	12.5	6.7	5.3	4
8-50kDa	15	8	4	4

Table 2. 3: Recipes to make two separating gels based on protein molecular weight (MW).

2.8.7 Western blotting

After SDS-PAGE (section 2.8.6) proteins from the gel were transferred to nitrocellulose membranes in transfer buffer (25mM Tris-base, 190mM Glycine and 20% methanol in MilliQ water) at 25mA for 1.5hr. Following protein transfer, nitrocellulose membranes were bathed in block solution consisting of 1% skim milk in 1x TBST (10mM TrisHCl, 100 mM NaCl and 0.1% Tween I MilliQ water) for 30-60min at RT or overnight at 4°C with shaking. Membranes were washed with

block solution three times for 10min each at RT with shaking. Membranes were then incubated with primary antibodies (see Table 2.4) diluted in the block solution overnight at 4°C with shaking. The following day membranes were washed three times with 1x TBST for 10min at RT with shaking. The appropriate horseradish peroxidase-conjugated secondary antibodies (1:20,000, Pierce-Thermo Scientific) diluted in 1x PBS were added to the membranes and incubated for 1hr at RT with shaking. Membranes were washed three times with 1x PBS for 15min each at RT with shaking. Immunoreactive proteins were visualized by Amersham ECL detection reagent (Life Science) on a Luminescent Image Analyzer (LAS-4000, Fujifilm) and images were processed with Multi Gauge Ver3.0 (Fujifilm). Protein bands were quantified using ImageQuant Software (Life Science) and were plotted on histograms using Excel.

Primary Antibody	Host Species	Dilutions	Source	Protein Size
Ndel1	Mouse	1:1000	Millipore	38.4kDa
14-3-3 (C16)	Rabbit	1:1000	Santa Cruz	27kDa
pNdel1 (N219T)	Mouse	1:1000	MBL	42kDa
β-actin (AC-15)	Mouse	1:5000	Sigma	42kDa
α-tubulin	Rabbit	1:5000	Abcam	52kDa
SOX2 (L1D6A2)	Mouse	1:1000	Cell Signalling	35kDa
DCX	Rabbit	1:1000	Cell Signalling	45kDa
GSK-3β (27C10)	Rabbit	1:1000	Cell Signalling	46kDa
pGSK-3β (Ser9)	Rabbit	1:1000	Cell Signalling	46kDa

Table 2. 4: Primary antibodies and dilutions used for western blotting.

2.9 Statistical analysis

In all studies, statistical analysis was performed using either GraphPad (Prism) or Excel (Microsoft) software. Data was analysed using Student's t-test and either one- or two-way analysis of variance (ANOVA). All statistical calculations are presented as mean ± SEM and a p-value of ≤0.05 was taken as significant.

Chapter Three:

Characterization of 14-3-3ζ KO Mice

3.1 Introduction

Mouse models have been employed to study human disease for roughly the last one hundred years (Wade and Daly, 2005). These models have provided indispensable tools to improve our understanding of the cause and progression of diseases and lead to the evaluation of drug candidates in the hope of discovering potential therapeutics. Since their first introduction to medical research hundreds of inbred mouse backgrounds have been generated where each background has considerable genetic variation akin to that across human populations. To understand the pathogenic roles of genetic mutations across varied human patient populations it is therefore useful to compare any mutation across several genetic backgrounds (Hardouin and Nagy, 2000). Indeed, an increasing number of reports are showing that the genetic profile of the mouse background can modulate the phenotype of a given single mutation (Chalfin et al., 2014). Therefore, it is important to examine whether the phenotype observed in one mouse background can be recapitulated in another.

The 129/sv mouse background has been widely used by many researchers as the bulk of embryonic stem cells used for derivation of genetic defects were generated from 129/sv mice (Chalfin et al., 2014, Lusis et al., 2007). The 129/sv background generally breed poorly and are reported to have altered anatomy and behaviour compared to other mouse backgrounds such as C57BL/6 and BALB/c (Sellers, 2012, Rivera and Tessarollo, 2008). Therefore, backcrossing into C57BL/6 background for at least ten generations is widely accepted and has been reported to decrease adverse phenotypes (Sellers, 2012, Rivera and Tessarollo, 2008). The

C57BL/6 background is considered the gold standard in biological studies as they are known to breed well, live long, and be permissive to the expression of most genetic mutations (Rivera and Tessarollo, 2008, Johnson, 2012). Similarly, the BALB/c background is widely used as it serves as a general purpose animal model and is known to breed well (Johnson, 2012). Notably, the 129/sv, BALB/c and C57BL/6 have also been shown to have markedly different behavioural phenotypes resulting from their genetic diversity (Sellers, 2012, Rivera and Tessarollo, 2008).

Previous work published by our group (Cheah et al., 2012) has shown that 14-3-3ζ KO mice in the 129/sv background have anatomical and behavioural defects akin to those seen in schizophrenia. To address if these defects are conserved across different genetic backgrounds or if they are specific to the 129/sv background here I examined whether the hippocampal defects are reproduced in the BALB/c and C57BL/6 backgrounds. Furthermore, I also extended these previous studies to examine if the structural defects of the hippocampus are accompanied by additional defects characteristic of schizophrenia, including aberrant neurite outgrowth, aberrant dendrite morphogenesis and aberrant spine formation.

3.2 Results

3.2.1 14-3-3ζ KO mice in the BALB/c and C57BL/6 backgrounds display hippocampal lamination defects similar to the 129/sv background

Our laboratory has previously shown that the anatomy of the brain in 14-3-3ζ KO mice in the 129/sv background appears grossly normal, with the exception of mild hippocampal defects which were first noticeable before hippocampal maturation at P0 and maintained throughout adulthood (Cheah et al., 2012). As such, for this part of the project I specifically focused on the formation of the hippocampus. To determine whether the observed hippocampal defects were purely due to 14-3-3ζ deficiency and not through epistatic interactions with the 129/sv mouse genetic background, we selected two additional and genetically dissimilar mouse backgrounds, namely BALB/c and C57BL/6, which were backcrossed with the 14-3-3ζ mice over ten generations. This was done to ensure that the mice were more than 99% pure-bred for each strain, so that any differences observed between WT and KO mice would result from the transgene itself and not genetic variance between mice within the same background.

From the 14-3-3ζ 129/sv, BALB/c and C57BL/6 mouse backgrounds at least 4 adult mice per group/genotype were collected and perfuse fixed (section 2.3.1). Brains were then isolated and fixed in 4% PFA overnight prior to coronal sectioning (section 2.3.2) and at least 10 sections per sample were Nissl stained (section 2.4.1). Nissl stain is a cresyl violet acetate solution which is used to stain

Nissl substances (rough endoplasmic reticulum) in neurons and is commonly used to identify the neuronal structures in the brain and spinal cord (Paul et al., 2008).

In the 14-3-3ζ KO 129/sv adult mouse hippocampus I was able to confirm that the pyramidal neurons in the CA3 region were malpositioned in the stratum radiatum and the stratum oriens, instead of their usual resting place in the stratum pyramidale, resulting in a bilaminar layer instead of a single cell layer (arrowheads, Figure 3.1 ii). Moreover, the pyramidal neurons at the CA2 region were ectopically positioned in the stratum oriens (asterisks, Figure 3.1 ii). The granule cells are generally tightly packed in the DG, however, in the 14-3-3ζ KO mouse hippocampus they appeared to be diffusely packed (arrows and box, Figure 3.1 ii). These observations are consistent with that previously reported in Cheah et al. (2012).

Consistent with my findings in the 14-3-3ζ KO 129/sv background initial low-resolution histological examination of Nissl stained sections in the 14-3-3ζ KO BALB/c and C57BL/6 backgrounds revealed that the morphology of the brain was grossly normal (not shown) (Xu et al., 2015). The hippocampal defects were also replicated in both BALB/c and C57BL/6 backgrounds (Figure 3.1 iv & vi, respectively), however the degree of severity varied as discussed below. Moreover, the hippocampal defect observed was evident throughout the rostro-caudal extent of the hippocampus in all mouse backgrounds (not shown).

The neuronal mispatterning in the 14-3-3ζ KO BALB/c hippocampus was found to be most severe among the three backgrounds (Figure 3.1 iv). In the

BALB/c background, the CA3 pyramidal neurons formed a discontinuous bilaminar structure that failed to merge with the pyramidal layer at the CA2 region (open arrowhead, Figure 3.1 iv) (Xu et al., 2015). Moreover, in contrast to the 129/sv background, in both BALB/c and C57BL/6 backgrounds the malpositioned pyramidal neurons were observed throughout all CA regions (CA1-3) (asterisks, Figure 3.1 iv & v). Although mild, the diffuse compactions of the granular neurons in the DG were also conserved across all backgrounds (arrows and box, Figure 3.1 ii, iv & v). An observation arising from the analysis of all three backgrounds that had not previously been documented for 14-3-3ζ KO mice is the altered shape of the DG. Thus, my analyses highlight that the DG is smaller in 14-3-3ζ KO mice and that the shape is more circular compared to the normal v-shaped structure in WT animals. Another notable difference amongst the backgrounds is that 14-3-3ζ KO in the BALB/c background had enlarged ventricles which were not observed in either the 129/sv or C57BL/6 backgrounds (not shown) (Xu et al., 2015).

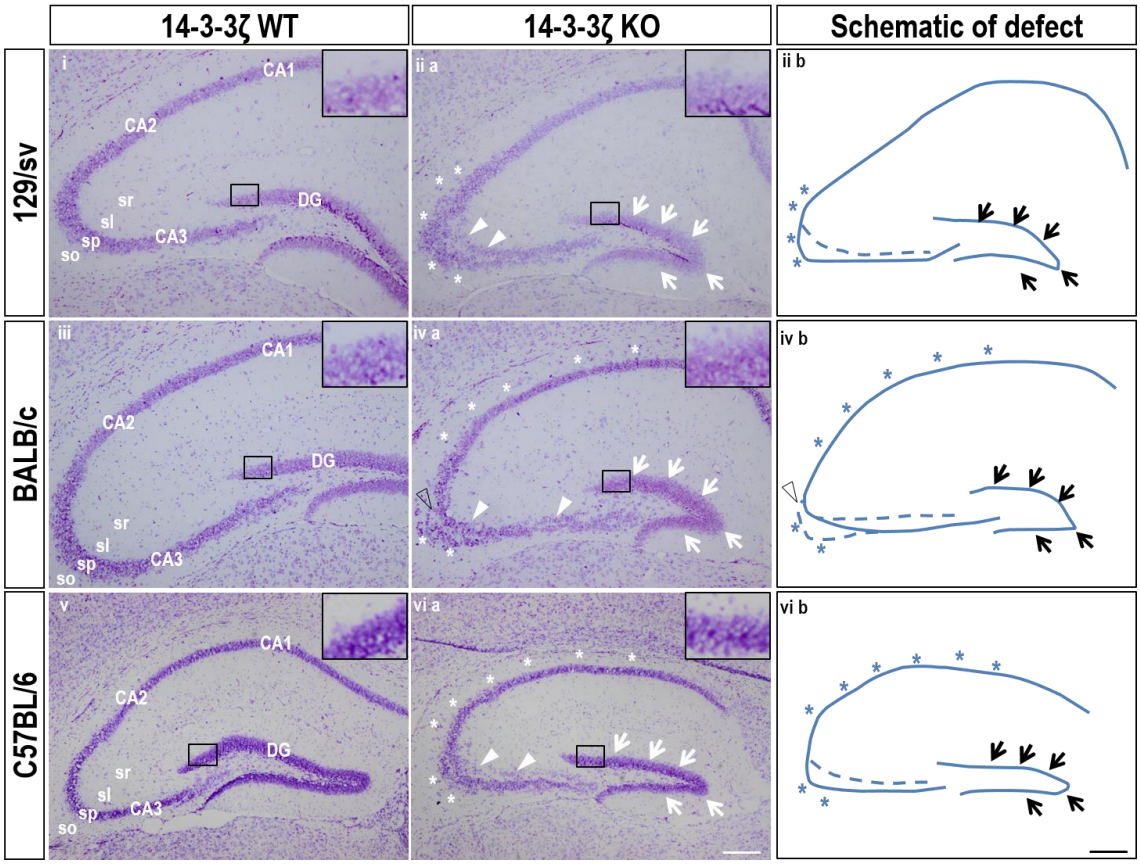

Figure 3.1: Hippocampal lamination defects in 14-3-3ζ KO mice.

Nissl staining of the hippocampus of 14-3-3ζ WT (i, iii, v) and KO (ii, iv, vi) mice from adult 129/sv (i, ii), BALB/c (iii, iv), and C57BL/6 (v, iv) mouse backgrounds. Arrowheads highlight the duplicated layer of the hippocampal pyramidal neurons. Asterisks highlight the ectopically positioned pyramidal neurons. Arrows highlight the loosely arranged granule cells in the DG. Open arrowheads indicate a break in the usually continuous laminar organisation of the CA region. Box shows high magnification of DG revealing diffuse compaction of the granule neurons in the 14-3-3ζ KO mice compared to WT. CA: cornus ammonus; DG: dentate gyrus; so: stratum oriens; sp: stratum pyramidale; sl: stratum lucidum; sr: stratum radiatum. Scale bar 50μm.

3.2.2 14-3-3ζ KO mice in the BALB/c and C57BL/6 backgrounds display disrupted mossy fibre circuit

I next examined whether the hippocampal trisynaptic circuit (see section 1.3.1) was also disrupted at the level of the mossy fibre connection between the DG and CA3 pyramidal neurons as shown previously in the 129/sv background (Cheah et al., 2012). Normally, mossy fibres emanate from the DG granule cells and bifurcate to precisely navigate on either side of CA3 pyramidal neurons. The supra- and infrapyramidal mossy fibre tracts span along the stratum lucidum and stratum oriens layers on either side of the stratum pyramidale of CA3, respectively (arrowheads, Figure 3.2 i, iii & v) (Cheah et al., 2012). In 14-3-3ζ KO mice in the 129/sv background, the suprapyramidal mossy fibre tract navigated along the stratum lucidum layer of the CA3 pyramidal neurons while the infrapyramidal tract was completely misrouted and navigated amongst the stratum pyramidale (Figure 3.2 ii).

To determine whether this phenotype is conserved across the BALB/c and C57BL/6 mouse backgrounds, adult mouse brains were isolated and sectioned as detailed above and immunostained (section 2.4.2) with anti-calbindin, a mossy fibre marker (Figure 3.2). Consistently, the segregation of mossy fibres into supra- and infrapyramidal tracts was disrupted in the BALB/c and C57BL/6 backgrounds (Figure 3.2 iv & vi, respectively). In both the 129/sv and C57BL/6 backgrounds, the suprapyramidal tract navigated along the stratum lucidum, while the infrapyramidal mossy fibre tract aberrantly navigated amongst the CA3 stratum pyramidale layer (arrows, Figure 3.2 iv & vi, respectively). While the

suprapyramidal branch navigates to the site of the CA2/3 boundary in WT and 14-3-3ζ KO brains of the 129/sv and C57BL/6 backgrounds, my analysis revealed that the suprapyramidal branch is prematurely arrested in 14-3-3ζ KOs in the BALB/c background (asterisk, Figure 3.2 iv).

Notably, my analyses of hippocampal structure and mossy fibre tracts in three independent backgrounds demonstrate that the anatomical defects arising from 14-3-3ζ deficiency are largely conserved and independent of background differences. In our breeding of 14-3-3ζ KO mice in each of these backgrounds we noticed that mice in the C57BL/6 background did not breed as well as the other lines. As such, I therefore chose to focus on the 129/sv and the BALB/c mouse backgrounds in the subsequent experiments.

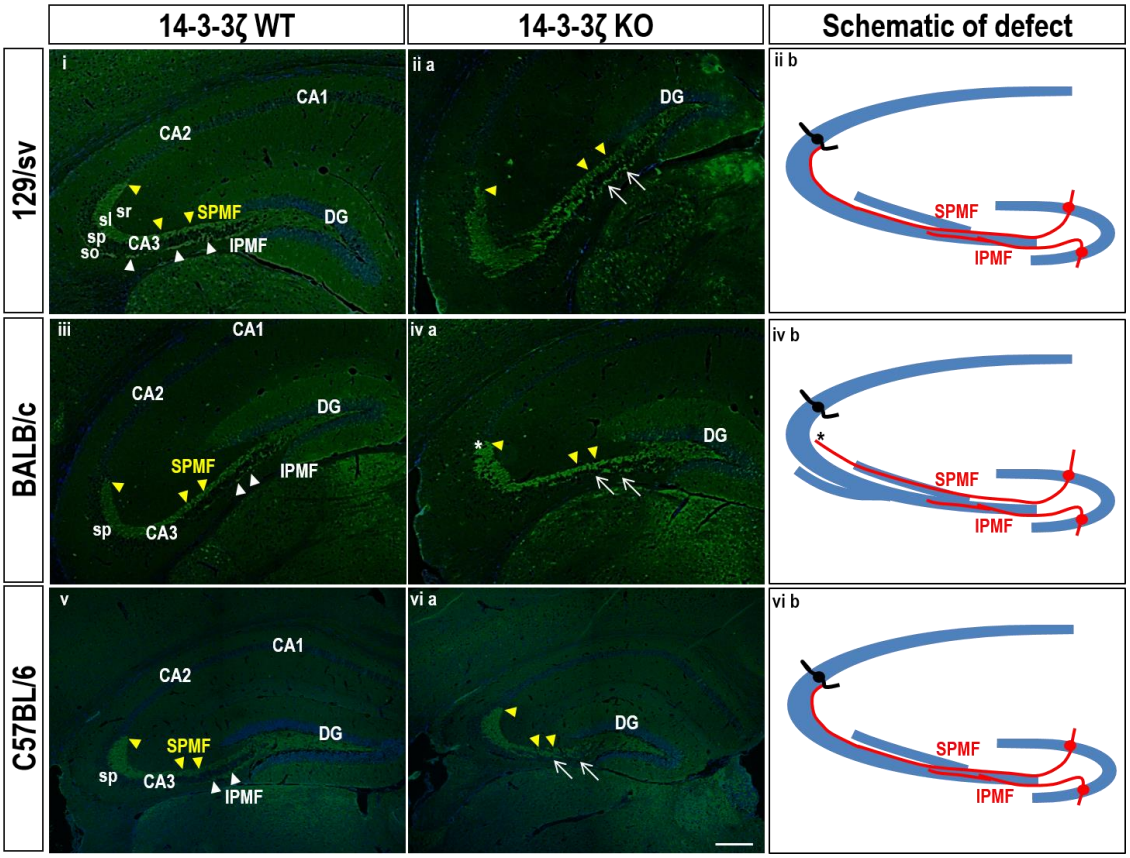

Figure 3.2: Abnormal mossy fibre navigation in 14-3-3ζ KO mice.

Calbindin immunostaining of the suprapyramidal (SPMF, yellow arrowheads) and the infrapyramidal (IPMF, white arrowheads) mossy fibre trajectories in WT (i, iii & v) and KO (ii, iv & vi) mice from adult 129/sv (i, ii), BALB/c (iii, iv), and C57BL/6 (v, iv) mouse backgrounds. Similar to WT controls, 14-3-3ζ KO neurites initially bifurcate into the SPMF and IPMF branches after navigating away from the DG. However, the IPMF branch of KO mice navigated aberrantly among the pyramidal cell somata (sp, white arrows). In addition, the diffuse SPMF branch of the 14-3-3ζ KO mice invaded the duplicated pyramidal cell layer in CA3 stratum pyramidale. Asterisk indicates shortening of the SPMF in the 14-3-3ζ KO BALB/c mouse background (iv). CA: cornus ammonus; DG: dentate gyrus; so: stratum oriens; sp: stratum pyramidale; sl: stratum lucidum; sr: stratum radiatum. Scale bar 50µm.

3.2.3 The role of 14-3-3ζ in early phase neurite outgrowth

To examine whether 14-3-3ζ may play a role in the early phase of neurite outgrowth, hippocampal neurons were isolated from WT, HET and KO E18.5 hippocampi from both 129/sv and BALB/c mouse backgrounds (section 2.5.3). Hippocampal neurons were plated in 12-well plates ($5x10^4$cells/well) and cultured for 3 days *in vitro* (DIV3) (section 2.5.4) before they were immunostained with anti-MAP2 and imaged using on a confocal microscope (section 2.5.6). MAP2, microtubule-associated protein 2, a neuron-specific protein that can be used as a neuronal marker, is known to be important for the earliest phases of neurite formation as it is involved in microtubule assembly during neurite outgrowth by stabilizing the microtubules (Flynn, 2013, Kulkarni and Firestein, 2012, Jan and Jan, 2010). Thus, MAP2 is enriched in the neurites of DIV3 hippocampal neurons but as the neuron matures (DIV10) it is only expressed in dendrites and not axons and thereby can also be used as a dendrite marker in more mature hippocampal neurons.

WT, HET and KO 14-3-3ζ MAP2 positive DIV3 hippocampal neurons from both the 129/sv and BALB/c backgrounds were quantified by measuring the number of neurites originating from the soma, the length of neurites and the number of bifurcations using the NeuronJ tool in ImageJ (section 2.5.7). My analysis demonstrated no significant difference between genotypes in both 129/sv (Figure 3.3) and BALB/c (Figure 3.4) backgrounds for all quantitative measures. This result most likely indicates that 14-3-3ζ is not essential for early neurite outgrowth, or conversely that other 14-3-3 isoforms may be able to compensate for its function in this process.

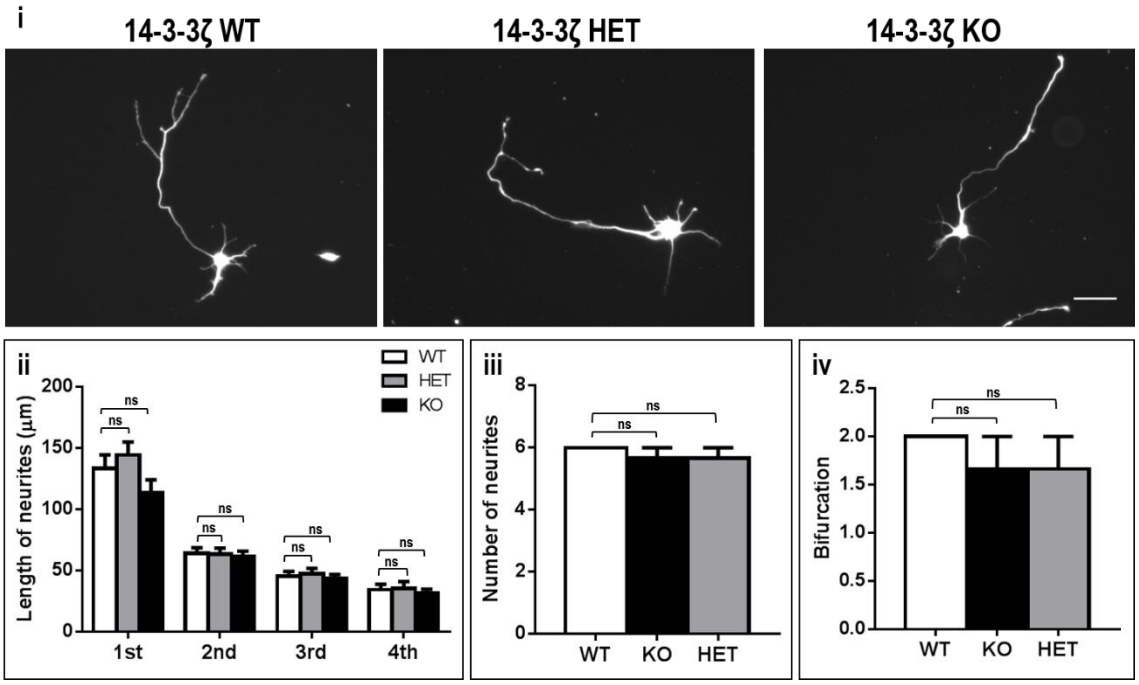

Figure 3.3: Early phase neurite outgrowth from 14-3-3ζ 129/sv hippocampal neurons.

(i) Hippocampal neurons isolated from E18.5 14-3-3ζ WT, HET and KO mice and cultured for 3 days *in vitro* (DIV3) followed by immunostaining with an anti-MAP2 antibody. Scale bar 50µm. (ii) Lengths of the first, second, third and fourth longest neurites at DIV3 were measured in 14-3-3ζ WT (white bar), HET (grey bar) and KO (black bar) neurons (mean ± SEM, n=3). (iii) Total neurite numbers at DIV3 and (iv) bifurcation were analysed (mean ± SEM, n=3). The average number of neurons analysed is as follows: WT n=64, HET n=60 and KO n=52. ns indicates that no significant difference was observed.

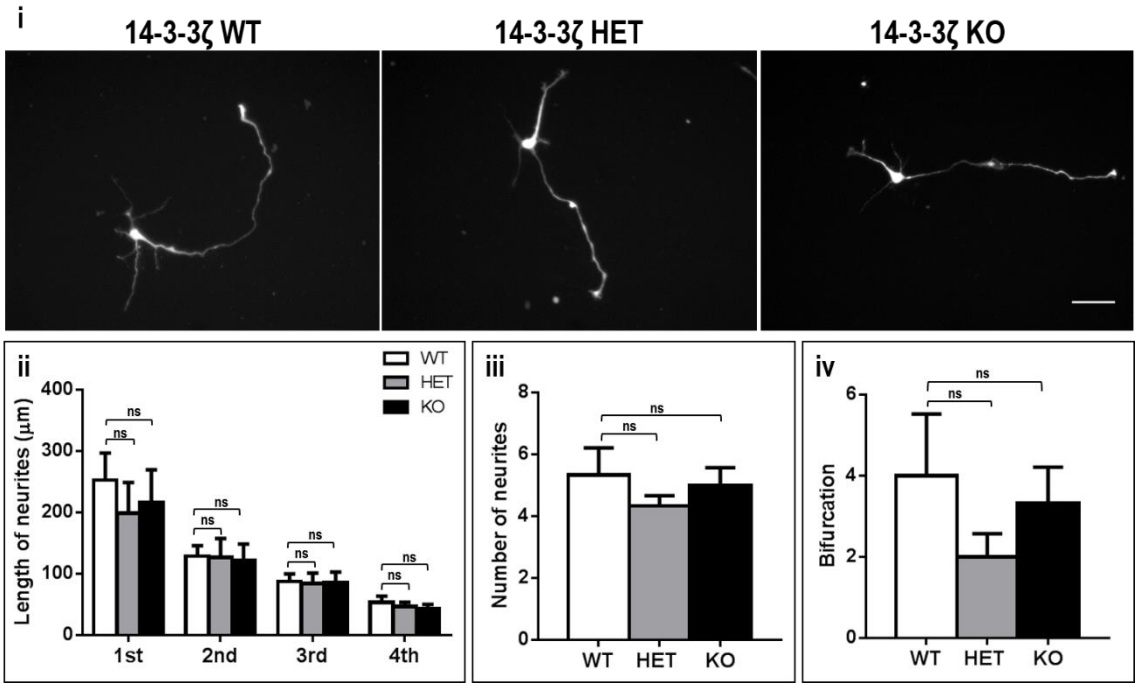

Figure 3.4: Early phase neurite outgrowth from 14-3-3ζ BALB/c hippocampal neurons.

(i) Hippocampal neurons isolated from E18.5 14-3-3ζ WT, HET and KO mice and cultured for 3 days *in vitro* (DIV3) followed by immunostaining with an anti-MAP2 antibody. Scale bar 50µm. (ii) Lengths of the first, second, third and fourth longest neurites at DIV3 were measured in 14-3-3ζ WT (white bar), HET (grey bar) and KO (black bar) neurons (mean ± SEM, n=3). (iii) Total neurite numbers at DIV3 and (iv) bifurcation were analysed (mean ± SEM, n=3). The average number of neurons analysed is as follows: WT n=59, HET n=57 and KO n=41. ns indicates that no significant difference was observed.

3.2.4 The role of 14-3-3ζ in dendrite morphogenesis

To study the function of 14-3-3ζ in dendrite morphogenesis, we analysed DIV10 primary hippocampal neurons isolated from E18.5 14-3-3ζ WT, HET and KO mice from the 129/sv and BALB/c backgrounds, as introduced above. Long-term hippocampal cultures of more than 7 days required neurotrophic support from glia for survival *in vitro*. Therefore, hippocampal neurons were cultured on glass cover slides and placed in a well of a 24-well plate ($5x10^4$cells/well) then at DIV3 were transferred to 10cm dishes containing astrocyte islands (sections 2.5.1-2.5.5). Hippocampal neurons were fixed and immunostained with anti-MAP2 at DIV10 (section 2.5.6). Only neurites positive for MAP2 were quantified to exclude axons from the analysis. Dendrite complexity was calculated by Sholl analysis (Sholl, 1953), where dendrites crossing concentric circles drawn at 5μm intervals around the neuron cell bodies and the number of dendrite crossings the concentric circles were measured using the Sholl Analysis tool in ImageJ.

Although no significant differences were noted, the HET and KO neurons isolated from the 129/sv mouse background showed a trend toward more immature dendrites as compared to WT, indicated by reduced dendrite complexity compared to WT neurons (Figure 3.5 i). The peak number of dendrites in WT neurons was identified at a 60μm distance from the cell body while the HET neurons showed a peak at 35μm and the KO neurons appear to plateau after the 40μm crossing (Figure 3.5 ii). Comparison of dendrite number at a 60μm distance from the cell bodies (as it was the peak crossing for the WT neurons) yielded lower values for both HET and KO neurons; however, this was not significant (Figure 3.5 iii).

Neurons isolated from the BALB/c mouse background showed contrasting results from the 129/sv mouse background (Figure 3.6). In terms of peak dendrite number, WT neurons showed the highest number of dendrites at a 60μm distance from the cell body while the HET neurons showed a peak at 45μm and the KO at 55μm (Figure 3.6 ii). However, when comparing the crossings at a 60μm distance from the cell bodies (as it was the peak crossing for the WT neurons) HET and KO neurons yielded significantly higher values compared to WT (Figure 3.6 iii, $p<0.05$). The contrasting results in these experiments may have arisen from differences in the genetic profiles or simply the nature of the experimental protocol. Here we used high density neuronal cultures which could have affected the dendritic complexity; it is known that plating density may influence the rate of neuronal maturation and hence dendritic complexity. Therefore, an alternative experimental approach is to use autaptic neuronal cultures, where a single neuron is cultured on a glial bed.

Although it appeared that the dendrite complexity is reduced in both 14-3-3ζ HET and KO neurons compared to WT in the 129/sv background, due to contrasting results in the BALB/c background I was unable to make any solid conclusion. As such, I decided to analyse the dendrite complexity using an *in vivo* system. Thus, adult mouse brains from 14-3-3ζ WT and KO mice in the 129/sv background were isolated, coronally sectioned (sections 2.3.2) and at least ten sections were Golgi-cox stained (section 2.4.3). Golgi-cox staining is a modified silver stain that reveals morphological traits of neurons in brain slices by randomly labelling a limited number of cells (~1%) in their entirety, thereby showing detailed arborisation of the dendritic tree (Pilati et al., 2008).

Upon visual examination of pyramidal cells in stratum radiatum and stratum lacunosum moleculare of the CA1 region of hippocampus, it was clearly obvious that the dendrites of the 14-3-3ζ KO neurons have reduced complexity in terms of branching (Figure 3.7 iii & iv). Furthermore, it appeared that the thickness of the apical dendrites is reduced and they appear longer in the length compared to WT (arrowheads, Figure 3.7 iii & iv). Manual tracing of these neurons clearly demonstrates the altered dendritic complexity between 14-3-3ζ KO and WT mice (Figure 3.7 v & vi). Taken together with my *in vitro* finding, this result suggests that 14-3-3ζ might play a role in dendrite arborisation *in vivo*. Further analysis of the phenotype is required to provide a definitive conclusion on the role of 14-3-3ζ in dendrite formation, and to determine if there are indeed quantitative differences in alternative backgrounds as may be predicted from my *in vitro* analyses.

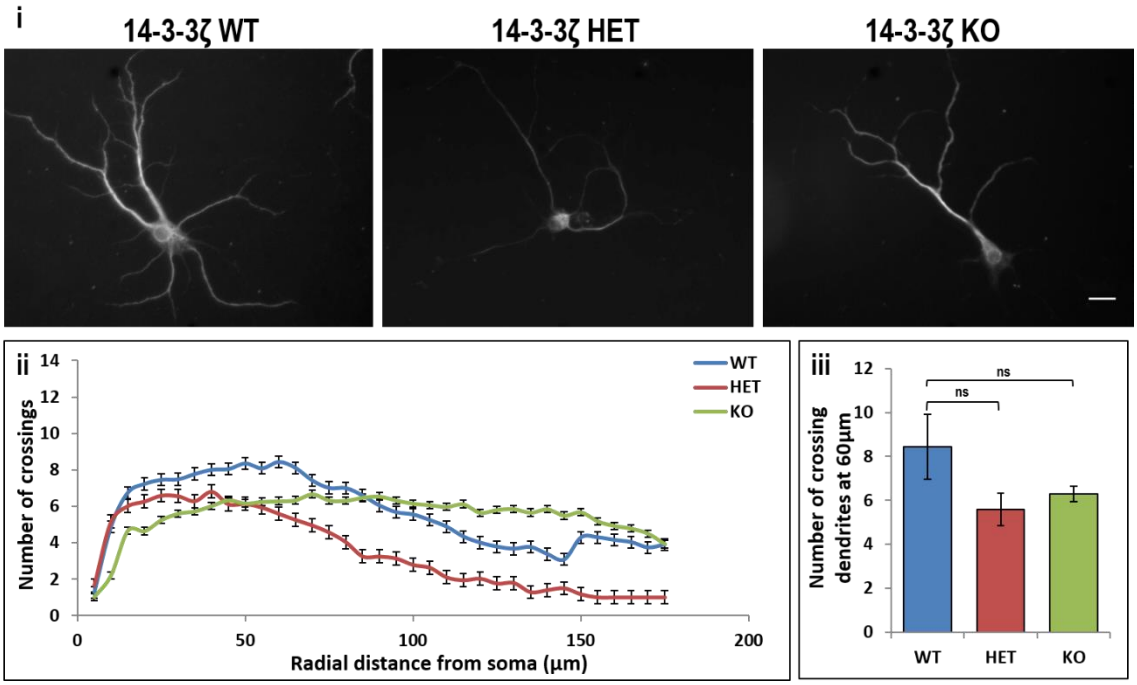

Figure 3.5: Dendrite morphogenesis of 14-3-3ζ 129/sv hippocampal neurons.

(i) Immunostaining of 14-3-3ζ WT, HET and KO hippocampal neurons at DIV10 using an anti-MAP2 antibody. Scale bar 50µm. (ii) Sholl analysis and quantification of the number of crossings within 175µm radius from the soma (mean ± SEM, n=3). (iii) Number of crossings at 60µm (mean± SEM, n=3). The average number of neurons analysed is as follows: WT n=16, HET n=11 and KO n=13. ns indicates that no significant difference was observed.

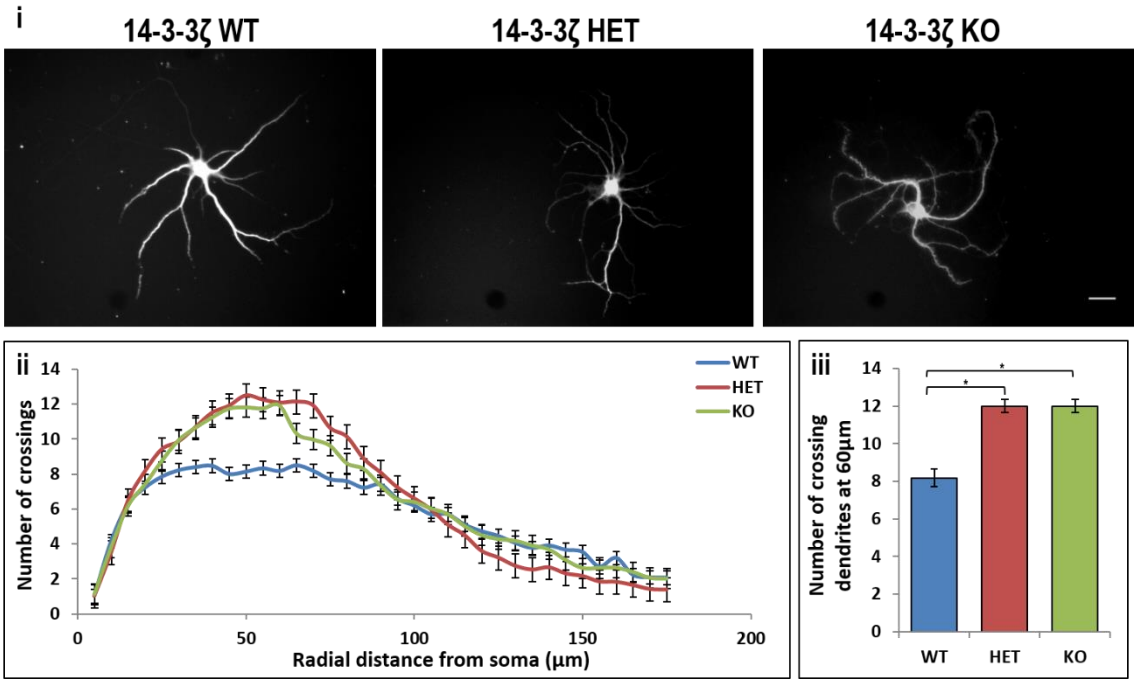

Figure 3 6: Dendrite morphogenesis of 14-3-3ζ BALB/c hippocampal neurons.

(i) Immunostaining of 14-3-3ζ WT, HET and KO hippocampal neurons at DIV10 using an anti-MAP2 antibody. Scale bar 50µm. (ii) Sholl analysis and quantification of the number of crossings within 175µm radius from the soma (mean ± SEM, n=3). (iii) Number of crossings at 60µm (mean± SEM, n=3). The average number of neurons analysed is as follows: WT n=11, HET n=12 and KO n=14. Asterisks indicate p-value < 0.05.

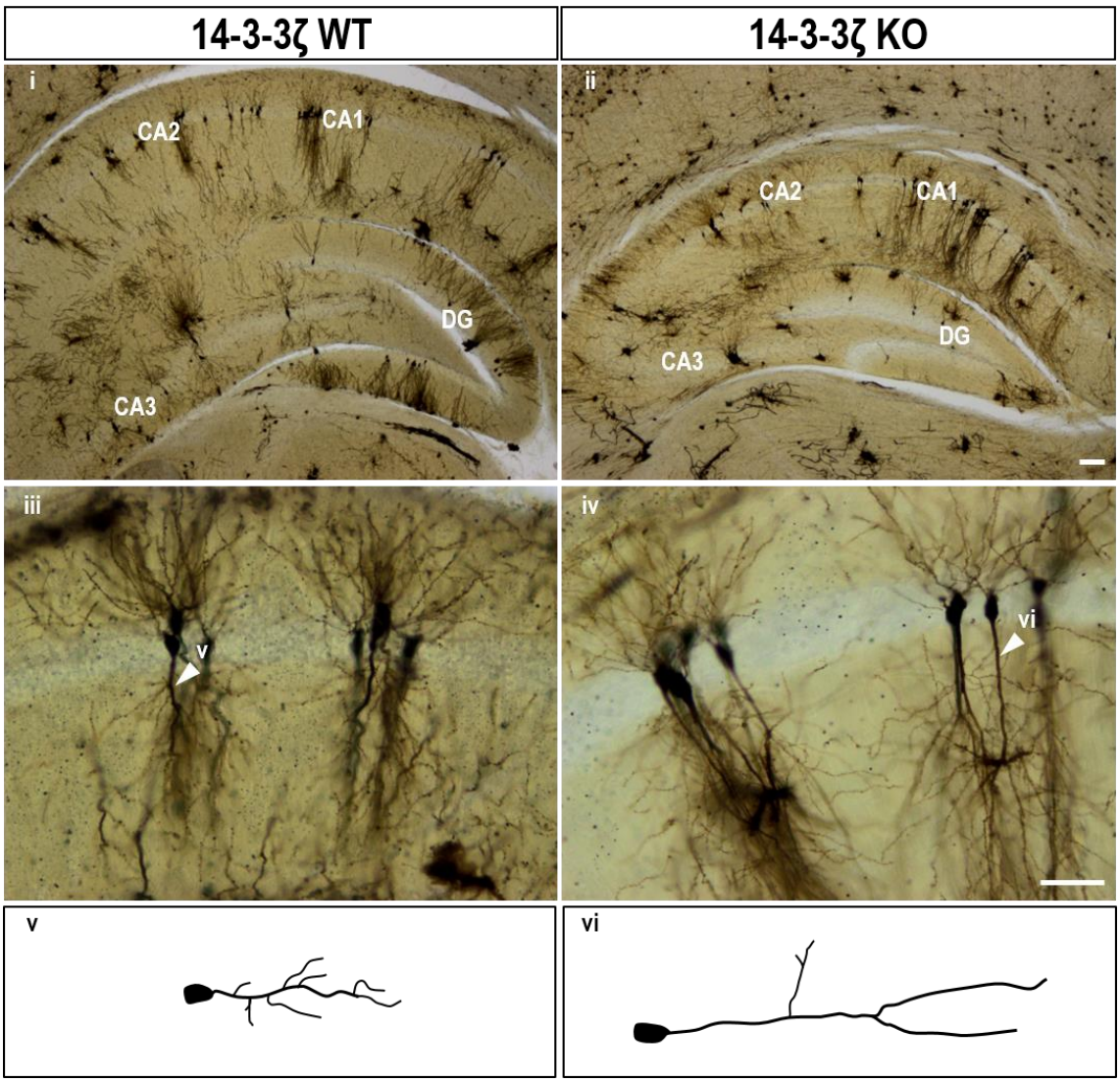

Figure 3.7: Altered dendritic morphology in the hippocampus of 14-3-3ζ KO neurons in the 129/sv background.

(i-ii) Low magnification of Golgi-cox stained 129/sv adult brain sections showing an overview of 14-3-3ζ WT (i) and KO (ii) hippocampal neurons. CA: cornus ammonus; DG: dentate gyrus. Scale bar 100μm. (iii-iv) High magnification images of 14-3-3ζ KO CA1 hippocampal neurons (iv) show reduction in dendrite complexity accompanied with the thinning of the apical dendrite width compared to WT (iii). Arrowhead indicates apical dendrite. Scale bar 50μm. (v-vi) Manually traced neurons demonstrating altered apical dendritic complexity between KO (vi) and WT (v) mice. n=3 for each genotype.

3.2.5 14-3-3ζ deficiency affects dendritic spine density

As reduced dendritic complexity, synapse number and spine formation are hallmark features of neurodevelopmental disorders such as schizophrenia, I also wanted to determine if dendritic spine density was altered in 14-3-3ζ KO mice. In my first analyses I initially planned to measure the number of spines forming in 14-3-3ζ WT and KO neurons grown for 21 days *in vitro* (sections 2.5.4 & 2.5.5). However, due to technical issues and large variability in spine numbers (Appendix A.3), I decided to instead utilise the Golgi-cox impregnation technique (section 2.4.3). Initially, I examined spines at the apical dendrites on cortical layer V pyramidal neurons as they were clearer to image and more spread out compared to the hippocampal neurons. We observed that 14-3-3ζ KO cortical pyramidal neurons showed reduced dendritic spines compared to WT neurons (Figure 3.8).

In my hands the Golgi-cox impregnation method labelled vast numbers of hippocampal neurons (Figure 3.7 i & ii) which precluded the analysis of dendritic spines in this area. Accordingly, I decided to utilise a gene gun method where thick vibratome sections of the adult mouse brain (sections 2.3.3) were labelled with lipohilic fluorescent dyes using a gene gun (section 2.4.4). Following lipophilic dye labelling neuronal dendrites were imaged at 63x magnification on a confocal laser microscope allowing us to generate 3D reconstructed images from z-stacks. For spine density quantification, the number of spines along equivalent lengths of dendritic segments proximal to the cell body were quantified.

Similar to my Golgi-cox stain analysis of layer V cortical pyramidal neurons, this technique demonstrated that both the dendritic spines of the CA3 pyramidal

neurons and DG neurons were significantly reduced (CA, p=0.01; DG, p=0.01, Figure 3.9) in the 129/sv mouse background. Consistently, we also observed that the 14-3-3ζ KO hippocampal neurons from the BALB/c mouse background showed reduced dendritic spine density compare to WT neurons (CA, p=0.05; DG, p=0.19, Figure 3.10). To examine this further, transmission electron microscopy (TEM) studies were commenced to address if the positioning and synapse type (excitatory or inhibitory) are also altered in the 14-3-3ζ KO mice compared to WT (Appendix A.4). However, due to time limitations TEM experiments were not completed.

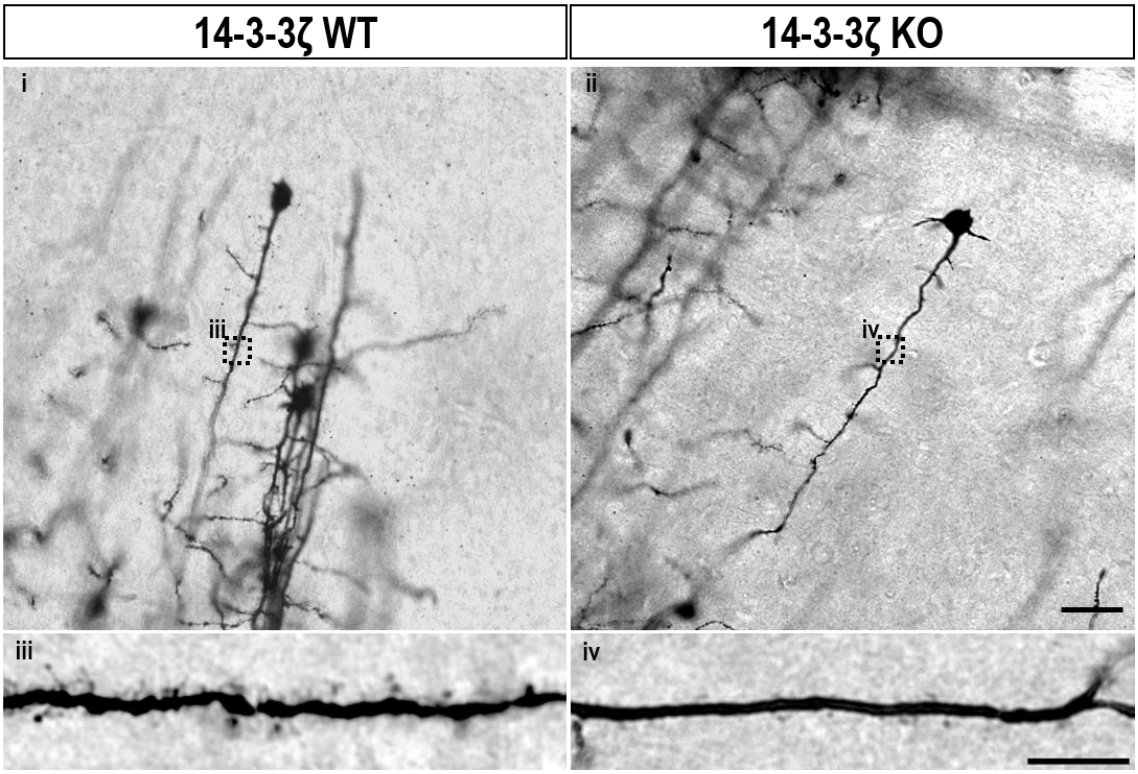

Figure 3.8: Golgi-cox staining of dendritic spines of cortical layer V pyramidal neurons of the 129/sv mice.

Low magnification of Golgi-cox stained sections of 129/sv adult brain layer V cortical pyramidal neurons from 14-3-3ζ WT (i) and KO (ii). Scale bar 100μm. High magnification of 14-3-3ζ KO neurons (iv) show reduction in spine density compared to WT (iii). Scale bar 20μm. n=3 for each genotype. This work was published in Jaehne et al. (2015).

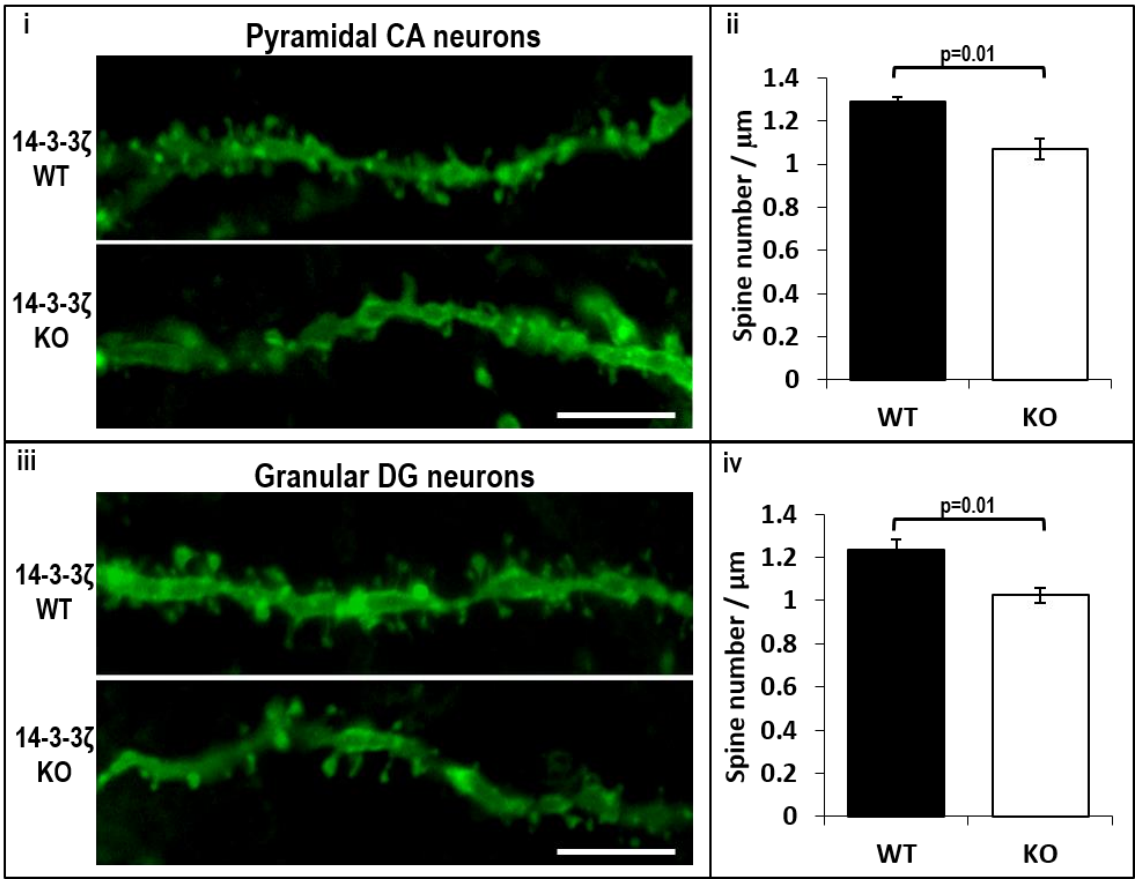

Figure 3.9: Reduced dendritic spine density in 14-3-3ζ KO 129/sv hippocampus.

(i) Pyramidal neurons in the CA3 region of the hippocampus have reduced dendritic spines in 14-3-3ζ KO mice. (ii) Quantitation of dendritic spines identifies a significant reduction in pyramidal neurons of 14-3-3ζ KO neurons compared to WT. Error bars indicate mean ± SEM (WT n=3, KO n=3; over 30 dendrites counted/mouse). (iii) Granular cells in the DG of the hippocampus also show reduced dendritic spine density in 14-3-3ζ KO mice. (iv) Quantitation of dendritic spines reveals significant reduction in the DG of 14-3-3ζ KO mice compared to WT. Error bars indicate mean ± SEM (WT n=3, KO n=3; over 30 dendrites counted/mouse). Scale bar 20µm. CA: cornus ammonus; DG: dentate gyrus. This work was published in Jaehne et al. (2015).

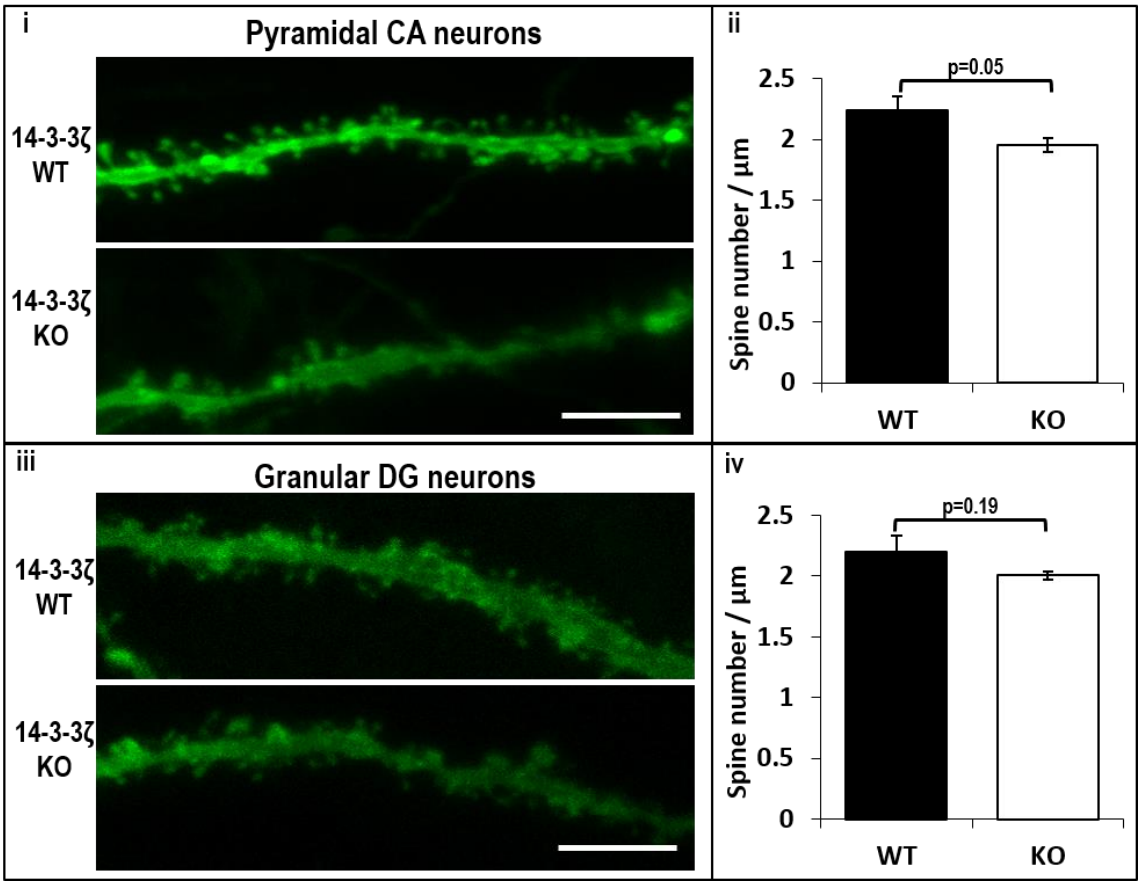

Figure 3.10: Reduced dendritic spine density in 14-3-3ζ KO BALB/c hippocampus.

(i) Pyramidal neurons in the CA of the hippocampus have reduced dendritic spines in 14-3-3ζ KO mice. (ii) Quantitation of dendritic spines identifies a significant reduction in pyramidal neurons of 14-3-3ζ KO neurons compared to WT. Error bars indicate mean ± SEM (WT n=3, KO n=5; over 30 dendrites counted/mouse). (iii) Granular cells in the DG of the hippocampus also show reduced dendritic spines in 14-3-3ζ KO mouse. (iv) Quantitation of spine number of granular cells reveals that there are no significant differences in the DG of 14-3-3ζ KO mice compared to WT. Error bars indicate mean ± SEM (WT n=3, KO n=4; over 30 dendrites counted/mouse). Scale bar 20µm. CA: cornus ammonus; DG: dentate gyrus. This work was published in Xu et al. (2015).

3.3 Discussion

The variable penetrance of genetic mutations in human disease is complex and may be partially explained by epistatic genetic interactions between the mutation itself and the genetic background of the host. Mouse models provide important tools to help understand human disease and to develop new therapeutics. Therefore, it is critical to select an appropriate mouse model in the correct genetic background to investigate a specific biological phenomenon. In this chapter I examined the phenotypic diversity of 14-3-3ζ KO in three commonly used mouse backgrounds, namely 129/sv, BALB/c and C57BL/6 to evaluate their relevance to model specific components of schizophrenia and related neuropsychiatric disorders.

There has been an increasing number of reports detailing the involvement of 14-3-3 proteins in the aetiology of schizophrenia (as discussed in section 1.2.2). Thus, it is important to select an appropriate animal model that enables in depth investigation of the role 14-3-3ζ plays in this crippling disease and other neurodevelopmental disorders. Previous work in our laboratory demonstrated that 14-3-3ζ KO mice in 129/sv background displayed anatomical and behavioural defects reminiscent of a schizophrenia-like phenotype (Ramshaw et al., 2013, Cheah et al., 2012). Notably, these mice have hippocampal defects characterised by mispatterning of the hippocampal pyramidal neurons and misrouting of the mossy fibres (Cheah et al., 2012). My findings now demonstrate that 14-3-3ζ KO mice in the BALB/c and C75BL/6 backgrounds display a similar phenotype to the 129/sv background, albeit with varying degree of severity, suggesting that the traits

observed are due to direct consequence of 14-3-3ζ deficiency and not due to other genetic intrusion. The mild phenotypic variability observed among the different backgrounds therefore make the analysis of 14-3-3ζ KO mice a highly appropriate model to investigate certain neuropathologies associated with schizophrenia and associated disorders. The spectrum of phenotypic severity and viability of 14-3-3ζ KO mice, like in humans, was influenced by the genetic heterogeneity of the background strain. For instance, 14-3-3ζ KO mice in the BALB/c and C75BL/6 backgrounds had an increase in the numbers of ectopically positioned pyramidal neurons in all subfields of the hippocampus and not just the CA3 region as previously observed in the 129/sv background (Figure 3.1). The mispositioned pyramidal neurons in the hippocampus strongly suggest a role of 14-3-3ζ in neuronal migration. Notably, the hippocampal lamination defect is similar to mouse mutants of protein known to play a role in neuronal migration (Belvindrah et al., 2014), which I have investigated in more detail in chapter 4.

This study also identified aberrantly enlarged lateral ventricles in 14-3-3ζ KO mice in the BALB/c background that did not extend to the other ventricles. As increased ventricular size is commonly associated with schizophrenia (Jaaro-Peled et al., 2010, Harrison, 2004), this provides even further credence to the use of 14-3-3ζ KO mice as a model for the human condition. While the reasons of why the lateral ventricle defects would be specific to one background are unclear, BALB/c mice have been reported to have a larger brain size compared to other backgrounds (Brodkin, 2007). It may therefore be possible that any changes in ventricle size could be exacerbated in this background. Regardless of why, this finding warrants further detailed investigation of the ventricles over time and in

each of the genetic backgrounds. Notably, ventricle enlargement has previously been associated with developmental defects in neurogenesis and the reduced compaction of DG granule cells in 14-3-3ζ KO mice (Figure 3.1) observed in all mouse backgrounds suggests its potential role in neurogenesis, which is examined more closely in chapter 5.

The anatomy of the hippocampus complements its function and its disruption contributes to several neurological diseases such as Alzheimer's disease, epilepsy, depression and schizophrenia (Tamminga et al., 2010). In schizophrenic patients, several studies have reported reduction of hippocampal size, ventricular enlargement and alteration of the synaptic circuitry, density and connectivity (Jaaro-Peled et al., 2010, Harrison, 2004). Miscommunication between neurons is also a major underlying cause of many neurological disorders and misrouting of neurons can lead to such events. Mossy fibres are known to mediate connectivity between the DG granular cells the CA3 pyramidal neurons in the hippocampus and are crucial for higher-order memory formation (Crusio and Schwegler, 2005). Alteration of the mossy fibre circuit is known to correlate with neuronal disorders, making it one of the most powerful synaptic structures in the brain (Wilke et al., 2014, Knoll et al., 2006). However, the exact molecular mechanisms which dictate the formation of the mossy fibre circuits are not completely understood.

Misrouting of the hippocampal mossy fibres was observed in 14-3-3ζ KO in both the BALB/c and C57BL/6 backgrounds, as previously seen in the 129/sv mice (Figure 3.2), suggesting axonal guidance abnormalities which warrants further

investigation. Although the misrouting of the mossy fibres in the 14-3-3ζ KO mouse brain is subtle, it was highly reproducible between biological replicates among each of the mouse backgrounds. Moreover, the suprapyramidal mossy fibres emanating from the DG were also shortened in the BALB/c background (Figure 3.2 iv). The length of the mossy fibres is known to directly correlate with improved memory performance (Crusio and Schwegler, 2005). Consistent with the mossy fibre defects, behavioural studies of the 14-3-3ζ KO in the 129/sv and BALB/c backgrounds also revealed memory deficits (Cheah et al., 2012, Xu et al., 2015).

Analysis of pyramidal hippocampal neuron development indicated that 14-3-3ζ does not play an essential role in initial neurite outgrowth (Figures 3.3 & 3.4), possibly due to redundancy of other 14-3-3 proteins which may provide a compensatory function. For future studies, a dominant negative approach may be useful to bypass this compensatory effect of other 14-3-3 proteins. It is also possible that the pathways mediated by 14-3-3ζ are non-responsive to the extracellular matrix, namely laminin, used in this experimental system. In future experiments it would therefore be worthwhile analysing different substrates that are known to mediate neurite outgrowth such as L1, a cell adhesion molecule. In fact, 14-3-3 was shown to act as a switch between positive and negative modulation of neurite outgrowth stimulated by retinoic acid, cell adhesion molecules (L1 & NCAM), and nerve growth factor (NGF) (Marzinke et al., 2013, Ramser et al., 2010a, Ramser et al., 2010b, Kajiwara et al., 2009, Rong et al., 2007, Tang et al., 1998).

Following initial neurite extension, neurons become specialised by the differentiation of their neurites into axons and dendrites. Dendrite morphogenesis has been correlated with neuronal function and is affected in many neurodevelopmental disorders such as autism spectrum disorders, and schizophrenia (Kulkarni and Firestein, 2012). Schizophrenia patients have been reported to have reductions in dendritic arbor size of their hippocampal pyramidal neurons (Kolomeets et al., 2007). This led me to examine the dendritic morphogenesis of the 14-3-3ζ deficient hippocampal neurons. The dendrite complexity of 14-3-3ζ KO hippocampal neurons from the 129/sv background was reduced in both *in vitro* and *in vivo* settings (Figures 3.5 & 3.7). In contrast, dendritic arborisation of the 14-3-3ζ KO hippocampal neurons from the BALB/c background was enhanced *in vitro* (Figure 3.6). This contrasting result could reflect a true difference in genetic background of the mice and warrants further *in vivo* analysis to address the role of 14-3-3ζ in dendrite arborisation. In combination with the fact that 14-3-3ζ has been reported to interact with Glutamate Receptor Interacting Protein 1 (GRIP1) to regulate dendrite morphogenesis in mouse embryonic cultured hippocampal neurons (Geiger et al., 2014), my findings in the 129/sv background support the notion that 14-3-3ζ is essential for dendrite formation.

As synaptic density is consistently reduced in schizophrenic brain samples I also analysed the synaptic density in 14-3-3ζ KO mice by counting the number of spines in hippocampal neurons (Xu et al., 2015). Proper synapse formation is essential for the establishment of functional neuronal circuitry and ultimately behaviour. Synapses occur on small protrusions along dendrites called dendritic

spines, where a single spine accommodates a single synapse (Penzes et al., 2011, Nimchinsky et al., 2002). Reduction of CA hippocampal dendritic spines has been correlated with the degree of memory deficit in individual mice (Chen et al., 2010). Dendritic spine density of the CA pyramidal neurons and DG granular cells of 14-3-3ζ KO 129/sv mice was significantly lower (CA p=0.01; DG p=0.01) than that of WT (Figures 3.9). The reduction in dendritic spine density was also apparent in the 14-3-3ζ KO BALB/c mice (Figures 3.10). However, only the dendritic spine density of the CA pyramidal neurons was significantly reduced and not the DG granular cells (CA p=0.05; DG, p=0.19). Consistently, the 129/sv 14-3-3ζ KO mice display a more severe memory deficit compared to the BALB/c background (129/sv $p<0.001$; BALB/c $p<0.05$) (Cheah et al., 2012, Xu et al., 2015). Not only does the latter agree with the notion that the degree of spine loss correlates significantly with the degree of memory defect, it also suggests a potential role for 14-3-3ζ in spine density regulation.

Developmental disturbances of synapse formation resulting in improper transmission and plasticity have been implicated in schizophrenia and provide solid support to the suggestion of a neurodevelopmental basis for the disorder (Walsh et al., 2008, Camargo et al., 2007, Harrison, 2004, Lewis and Levitt, 2002). Schizophrenia associated genes, such as DISC1, ERBB4 and NRG1, encode proteins that have also been implicated in synapse formation and/or function (Walsh et al., 2008). Notably, 14-3-3ζ has been reported to interact with several proteins found in the post synaptic density such as DISC1, HOMER and SPIN90 (Cheah et al., 2012, Angrand et al., 2006, Heverin et al., 2012) and proteins involved in actin polymerisation such as cofilin (Gohla and Bokoch, 2002). Indeed, 14-3-3ζ has

recently been suggested to control phosphorylation of serine 3 on cofilin to mediate spine formation (Gohla and Bokoch, 2002).

In summary, this chapter has demonstrated that 14-3-3ζ KO mice have largely conserved phenotypes in three independent backgrounds thereby supporting the notion that the phenotype observed is due to deficiency of the gene itself and not from genetic interactions. Furthermore, these results highlight an important role for 14-3-3ζ in brain development and provide further support to the neurodevelopmental basis of schizophrenia and associated disorders. As I have verified that the phenotypes arising from 14-3-3ζ deficiency are conserved across genetic backgrounds, I have therefore focused the rest of my mechanistic studies in this thesis in one genetic background (i.e. 129/sv mouse background).

Chapter Four:

Defining the Role of 14-3-3ζ in Neuronal Migration

4.1 Introduction

Precise control of neuronal migration from the ventricular zone to their final destination within the hippocampal plate is essential for establishing brain architecture (Marin et al., 2010, Reiner, 2013). This process is regulated by a complex molecular pathway that involves extracellular guidance cues (Reelin) binding to membrane-bound receptors (APOER2, VLDLR) to stimulate intracellular signalling molecules (Dab1, Cdk5, p35) which activate microtubule associated proteins (DCX, Lis1, Ndel1, dyneins) to sustain microtubule bundles and facilitate neuronal migration (Keays, 2007, Wynshaw-Boris and Gambello, 2001) (see section 1.6 for more detail).

Defects in several proteins involved in the neuronal migration pathway have been associated with neurological disorders such as lissencephaly, mental retardation, epilepsy, schizophrenia and autism. This direct link to human disorders makes the molecular basis for neuronal migration an area of intense investigation. For example, single nucleotide polymorphism analysis in an American population of schizophrenic patients identified significant linkage to *Ndel1* (Burdick et al., 2008), while expression analyses on post-mortem schizophrenia brain samples revealed significant down-regulation of *Ndel1* and *Lis1* (Lipska et al., 2006). Given that *14-3-3ζ* is also associated with schizophrenia (discussed in section 1.2.2) and that my analyses identified 14-3-3ζ KO mice display phenotypic similarity to Ndel1 and Lis1 deficient mice (sections 1.6.2 & 1.6.3) this suggests a potential role for this protein in the neuronal migration pathway.

14-3-3 proteins predominantly bind to target proteins through recognition of consensus phosphorylated serine (S) or threonine (T) residues (section 1.1.1). Proteins can be phosphorylated by kinases, such as Cdk5, and dephosphorylated by phosphatases, such as PP2A, causing alteration of the protein's activity and function (Dephoure et al., 2013). To study the roles of S/T phosphorylation in protein function the use of molecular variants in which the S/T phosphorylated residues are replaced with alternative amino acids has been widely used. Thus, replacement of the S/T residues with alanine (A) renders this site phospho-dead and therefore acts as a loss-of-function mutant. Conversely, replacement of the S/T with glutamic acid (E) mimics the phosphorylation state and acts as a gain-of-function mutant (Dephoure et al., 2013). However, although mutants in which S/T is replaced with E act as a phosphomimetic in functionality, in many cases they do not bind adaptor proteins such as 14-3-3 proteins as the E does not fully replicate the phosphorylation state and fit into the binding pocket (Dephoure et al., 2013).

Ndel1 is known to have three specific S/T phosphorylation sites (S198, T219 & S231) and two weak phosphorylation sites (S242 & T245) which are recognised by Cdk5/p35 (Niethammer et al., 2000). Our collaborators have previously shown that 14-3-3ε interacts with Ndel1 and this is completely abrogated in a triple Ndel1 mutant (S198A, T219A & S231A) (Toyo-oka et al., 2003). By investigating the phosphorylation dynamics of Ndel1 in the absence of 14-3-3ε they also found that 14-3-3ε maintains Ndel1 phosphorylation in cortical neurons to control binding to Lis1 and the dynein motor complex (Toyo-oka et al., 2003). This chapter investigates whether 14-3-3ζ, like 14-3-3ε, interacts with Cdk5/p35 phosphorylated Ndel1 to modulate hippocampal neuronal migration.

4.2 Results

4.2.1 *In vitro* neuronal migration assay

Using a BrdU-pulse chase technique in 14-3-3ζ KO mice, our lab has previously reported that 14-3-3ζ plays an important role in neuronal migration of hippocampal neurons (Cheah et al., 2012). To explore whether 14-3-3ζ plays a cell autonomous role in neuronal migration and to define its the mechanistic role within this pathway, I established an *in vitro* migration assay where neuronal progenitors were isolated from the hippocampus of E18.5 14-3-3ζ WT, HET, and KO mice (Figure 4.1 i & ii, section 2.6). These cells were cultured in spherical cellular re-aggregates, known as neurospheres, (Figure 4.1 iii) over three to four passages (Figure 4.1 iv & v) then transferred to poly-L-lysine and laminin-coated 22mm glass bottom dishes and allowed to migrate radially (Figure 4.1 vi & vii, sections 2.6.1 & 2.6.2). After 24hrs, migration distance was measured by both manual and automated techniques using ImageJ as described in sections 2.6.3 and 2.6.4 (Figure 4.1 viii). To examine any differences in neuronal migration rate, I counted the number of neurons in concentric circles (bins) surrounding the edge of the initial neurosphere (Figure 4.1 viii). Of note, in these experiments DAPI was used to label migrating cells relying on the assumption that all migrating cells are actually neurons. While not completed here, clarification that these cells are indeed neurons would require labelling for DCX or other neuronal markers.

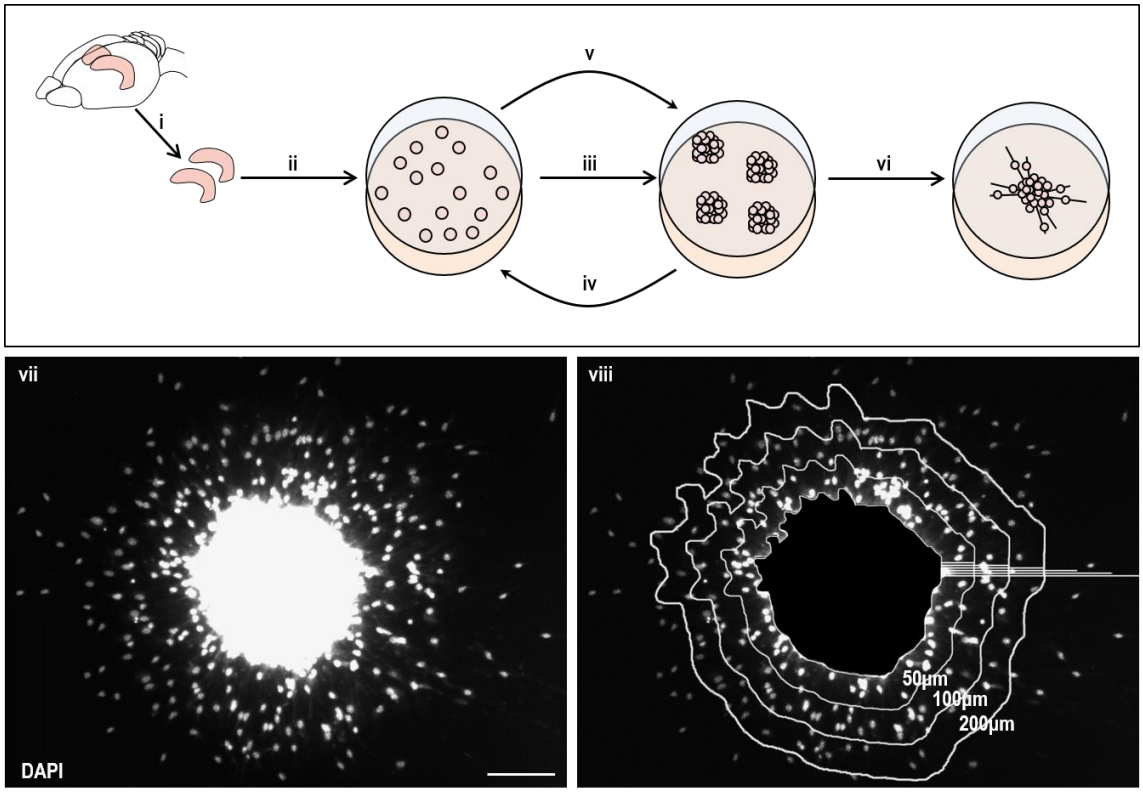

Figure 4.1: Neuronal migration assay.

(i-vi) Diagram illustrating the experimental procedure undertaken for the neuronal migration assay. The hippocampus is dissected from E18.5 embryos (i) to isolate neuronal progenitor cells which are cultured as a single cell suspension (ii). These cells then proliferate and form neurospheres (iii) which are passaged several times (iv-v) before being used for migration assays. Neurospheres grown for at least 3-4 passages are isolated and cultured on ploy-L-lysine and laminin treated 22mm glass bottom dishes (vi) for 24hrs. (vii, viii) DAPI staining of neurospheres after 24hrs migration period. Scale bar 100µm. (viii) Migration distance of each neuron was sorted in 50, 100, 200, 300, & 400µm bins using Photoshop (vii). The 50µm bin was analysed manually with the rest analysed using ImageJ. White lines indicate corresponding migration distances from the edge of the original neuronsphere.

4.2.2 14-3-3ζ is important for hippocampal neuronal progenitor cell migration

DAPI staining of neuropheres after 24hrs of migration revealed reduced migration in the 14-3-3ζ KO hippocampal neurons compared to HET and WT (Figure 4.2 i-iii). Quantification of migration revealed that the 14-3-3ζ KO hippocampal neurons display aberrant migration characterised by the leftward shift of the distribution bins (Figure 4.2 vi). This effect was also identified in 14-3-3ζ HET hippocampal neurons which displayed an intermediate leftward shift (Figure 4.2 v) compared to the KO neurons (Figure 4.2 iv). Furthermore, the mean migration distance of the 14-3-3ζ KO and HET hippocampal neurons was significantly reduced compared to WT neurons ($p<0.001$, Figure 4.2 vii). Analysing the data from the HET mice, I determined that there is a significant dose dependent effect in neuronal migration similar to that reported for Lis1, Ndel1 and 14-3-3ε deficient neurons (Gambello et al., 2003, Hirotsune et al., 1998, Sasaki et al., 2000, Tanaka et al., 2004a, Toyo-oka et al., 2003, Youn et al., 2009).

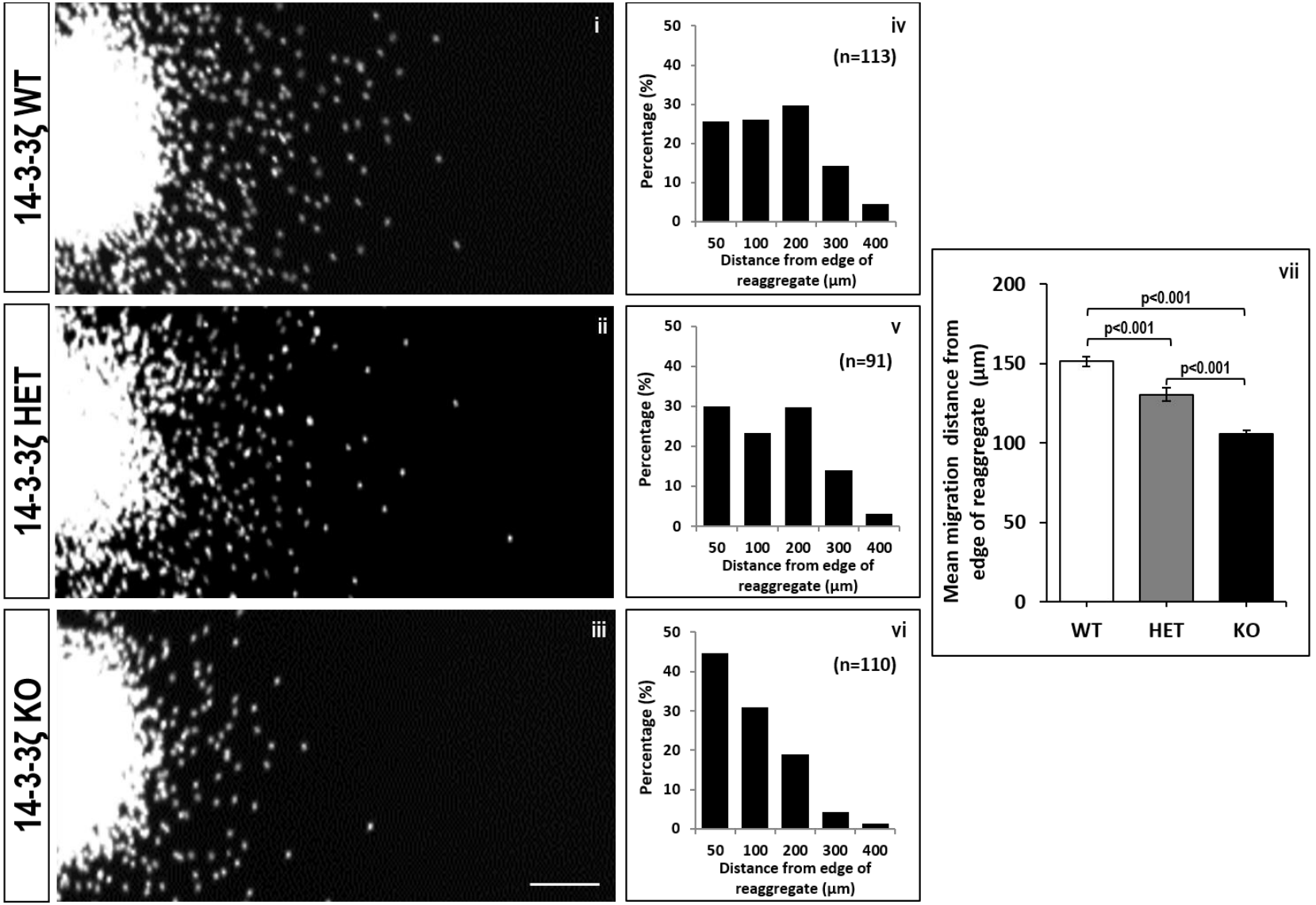
14-3-3ζ WT
14-3-3ζ HET
14-3-3ζ KO
i
ii
iii
iv
(n=113)
v
(n=91)
vi
(n=110)
Percentage (%)
Distance from edge of reaggregate (µm)
vii
Mean migration distance from edge of reaggregate (µm)
p<0.001
p<0.001
p<0.001
WT
HET
KO

Figure 4.2: Migration defects are associated with 14-3-3ζ deficiency in neuronal progenitor cells.

(i-vii) *In vitro* neurosphere migration assay using neuronal progenitor cells isolated from E18.5 embryos of 14-3-3ζ WT, HET and KO hippocampi and cultured as neurospheres. (i-iii) DAPI staining of neurospheres after 24hrs migration on ploy-L-lysine and laminin treated glass bottom dish. Scale bar 100μm. (iv-vi) Migration distance of each neuron was sorted in 50-100μm bins. Compared to WT neurons (iv), 14-3-3ζ KO neurons (vi) displayed a shift in the bin distribution towards the left and the HET neurons (v) displayed a slight shift towards the left. n is the number of neurospheres measured for each examination. (vii) Mean migration distance was determined for all genotypes. Error bars indicate SEM of neurosphere number (WT n=113, HET n=91, KO n=110).

4.2.3 Live imaging reveals neuronal migration defects in 14-3-3ζ KO neurons

To examine the migration dynamics in the 14-3-3ζ KO neurons, I repeated the migration assays and observed them in real-time using a spinning disc confocal microscope (section 2.6.4). Since our spinning disc microscope only accommodated one dish at a time, I cultured 14-3-3ζ WT and KO neurospheres in different areas of the same dish. Thus, I first completed experiments to determine that the same migration defects observed in the 14-3-3ζ KO neurons as observed above (Figure 4.2) were reproduced using this experimental design. Movies were generated from the live imaging and used to track individual migrating neurons with Manual Tracking tool in ImageJ software (Figure 4.3 i & ii, Movie 4.1, section 2.6.4). Consistent with my previous result (Figure 4.2), I observed a significant migration delay in the 14-3-3ζ KO neurons ($p=0.01$; Figure 4.3 v, Movie 4.2). In addition, the presence of 14-3-3ζ WT neurons in the same dish was unable to rescue the migration defect of the 14-3-3ζ KO neurons, suggesting a cell-autonomous role for 14-3-3ζ in altering neuronal migration. Furthermore, I confirmed that the migration delay observed was not due to the 14-3-3ζ KO neurons having defects in their directionality as they moved similarly to WT neurons (WT $D=0.7$, KO $D=0.7$; Figures 4.3 iii & iv, respectively).

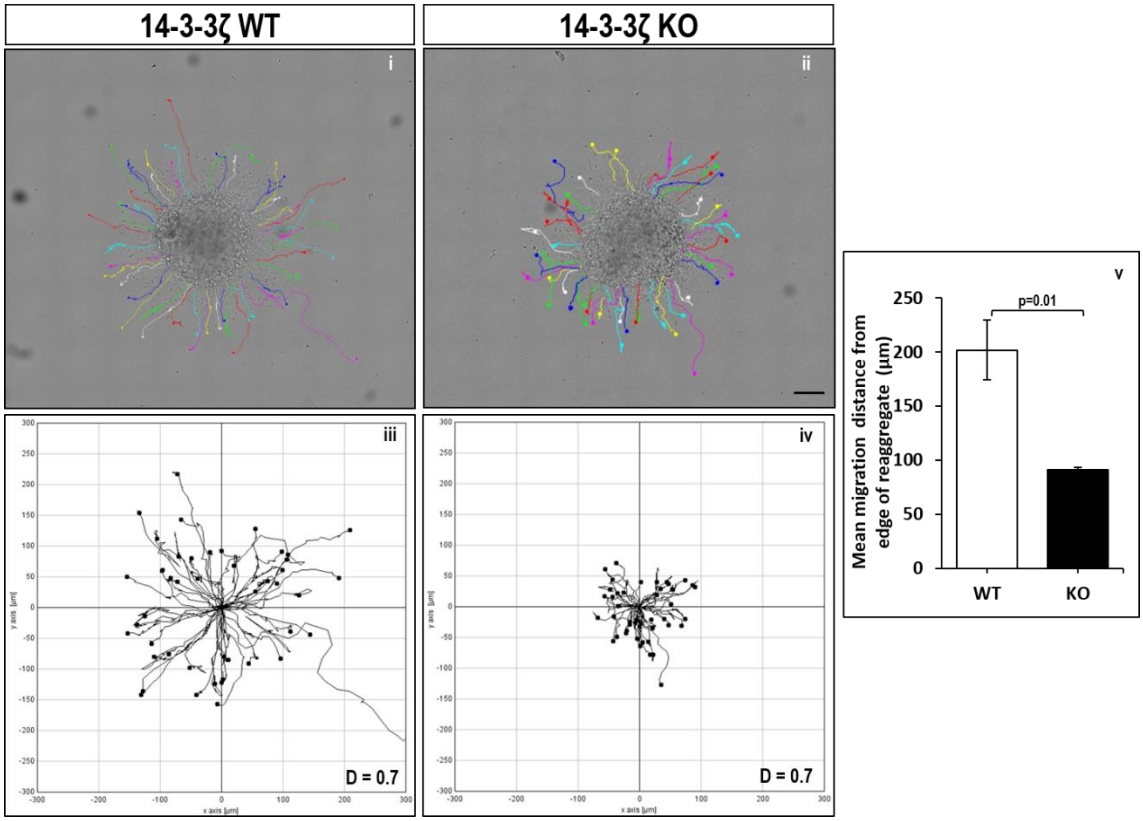

Figure 4.3: Live imaging of 14-3-3ζ WT and KO migrating neurons.

To further examine the migration dynamics in the 14-3-3ζ KO neurons I have analysed the migration in real time using a spinning disc confocal microscope (Cell Voyager, CV1000, Yokogawa). Snap shot of the neuropsphere migration assay of 14-3-3ζ WT (i) and KO (ii) neuronal progenitors at ~22hrs. Each line represents a neuron that has been manually tracked. Scale bar 100µm. (iii-iv) Migration directionality plots indicate no directionality defect in the 14-3-3ζ KO (iii) neurons compared to WT (vi). Each line represents a neuron. Note that the plots have comparable scale bars. D= directionality correlation. (v) Quantification of the mean migration distance. Error bars indicate SEM of neurosphere number (WT n=4, KO n=4).

4.2.4 Effect of 14-3-3ζ KO in neuronal migration velocity and adhesion

Previous studies have shown that Lis1 and Ndel1 deficient cortical neurons have reduced migration velocity (Youn et al., 2009) and therefore we questioned whether 14-3-3ζ KO hippocampal neurons would have a similar defect. Using the data from the spinning disc microscope I found that 14-3-3ζ KO neurons have a significant decrease in mean migration velocity (p=0.03, Figure 4.4 i). I also examined the neurons ability to adhere to laminin using an adhesion assay described in section 2.6.5. A single cell suspension of neurons from either 14-3-3ζ KO or WT neurospheres were plated on laminin for 10 or 60min then the number of cells adhered to the substrate was measured (section 2.6.5). 14-3-3ζ KO neurons were able to adhere normally at the 10min time point, but had increased adherence compared to WT at 60min (Figure 4.4 ii).

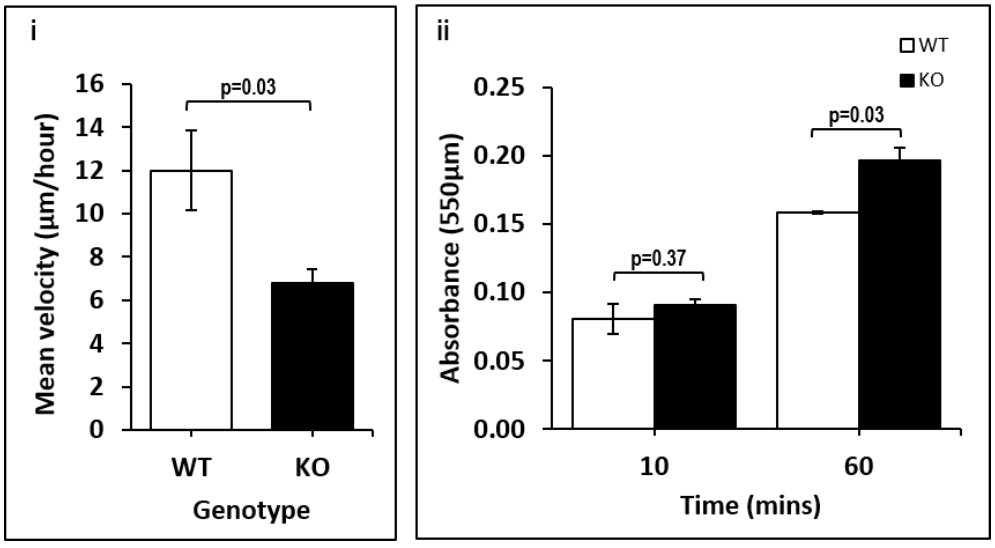

Figure 4.4: Mean migration velocity and adhesion assay of 14-3-3ζ KO neurons.

(i) 14-3-3ζ KO neurons show a significant reduction in mean migration velocity compared to WT. Error bars indicate SEM from neurosphere number (WT n=4, KO n=4; average of 145 neurons were measured per sample). (ii) Adhesion assay on laminin, 10 or 60min after plating. Error bars indicate SEM (WT n=2, KO n=2).

4.2.5 Nuclear-centrosome coupling is disrupted in 14-3-3ζ deficient neurons

An important mechanism in neuronal migration is nuclear-centrosome (N-C) coupling (Lambert de Rouvroit and Goffinet, 2001). Tanaka et al. (2004a) have previously shown that under normal conditions microtubules in migrating neurons couple the leading process to the centrosome and the centrosome to the nucleus (Figure 4.5 i). This process allows the translocation of the nucleus during neuronal migration. Lis1 and Ndel1 deficient neurons have been reported to have uncoupling of the nucleus to the centrosome (Shu et al., 2004, Tanaka et al., 2004a). Thus, I wanted to determine whether deficiency of 14-3-3ζ would result in the same phenotype, given that my data suggest that it may be involved in the same neuronal migration pathway. A neuronal migration assay was undertaken as previously reported in section 2.6.2 followed by fixation with 4% PFA during the active phase of migration. 14-3-3ζ WT and KO neurons were stained with DAPI and γ-tubulin to label the nucleus and centrosome, respectively (section 2.6.6). Neurons were imaged and analysed using confocal laser microscope as described in section 2.6.6. Quantitation of the distance between the nucleus and centrosome demonstrates a dose dependent requirement of 14-3-3ζ in maintaining N-C distance (Figure 4.5; WT v HET, $p<0.001$; WT v KO, $p<0.001$; HET v KO, $p=0.01$).

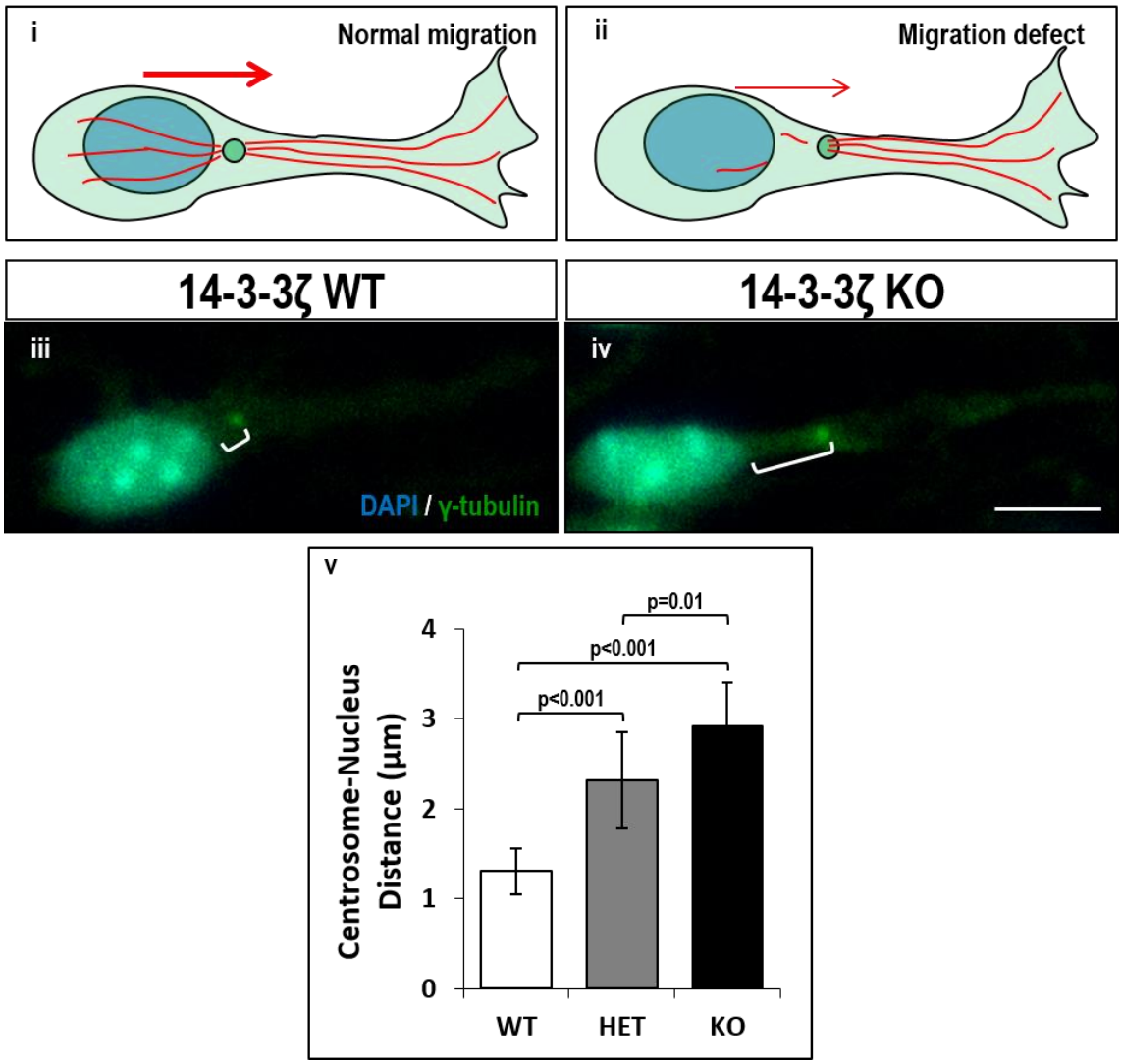

Figure 4.5: 14-3-3ζ deficient neurons have defective nuclear-centrosome coupling.

(i-ii) Schematic illustrating nuclear-centrosome (N-C) coupling under normal migration (i) and during migration defects induced by lack of Ndel1 and/or Lis1 (ii). (iii-iv) Migrating neurons were stained for DAPI (blue) and γ-tubulin (green) to identify nuclei and centrosomes, respectively. 14-3-3ζ KO neurons (iv) display increased nucleus-centrosome distance compared to WT (iii). Scale bar 10µm. (v) 14-3-3ζ KO neurons displayed N-C coupling defects characterized by the extended distance between the nucleus and centrosome. Similar results were obtained from two separate experimental trials. Error bars indicate SEM from neurosphere number (WT n=24, HET n=18, KO n=22; 200 neurons were measured per sample).

4.2.6 14-3-3ζ directly interacts with Ndel1

Given that my analysis of 14-3-3ζ KO hippocampal neurons suggests its involvement in the neuronal migration pathway and that other members of the 14-3-3 family interact with Ndel1, I next examined if 14-3-3ζ interacts with Ndel1 using an exogenous co-immunoprecipitation assay. HEK293T cells were individually transfected or co-transfected with expression constructs consisting 14-3-3ζ Myc tagged (14-3-3ζ-Myc) and one of native Ndel1 GFP tagged (Ndel1-GFP), quadruple Ndel1 mutant with IRES GFP (Ndel14A; S198A, T219A, S231A, & S242A) or phosphomimetic Ndel1 IRES GFP tagged (Ndel13E; S198E, T219E, & S231E), as described in sections 2.8.1 - 2.8.3. Cell lysates were immunoprecipitated with anti-Myc antibodies on sepharose-A beads (sections 2.8.4 & 2.8.5) and analysed by immunoblotting with antibodies against anti-Ndel1 (sections 2.8.6 & 2.8.7). My analysis indicated that 14-3-3ζ-Myc interacts with Ndel1-GFP, and this interaction is compromised with both Ndel14A and Ndel13E (Figure 4.6 ii). This result suggests that 14-3-3ζ, similar to 14-3-3ε (Toyo-oka et al., 2003), is able to directly interact with Ndel1 and this interaction is reduced when the Cdk5/p35 S/T phosphorylation sites (S198, T219, S231, & S242) are altered.

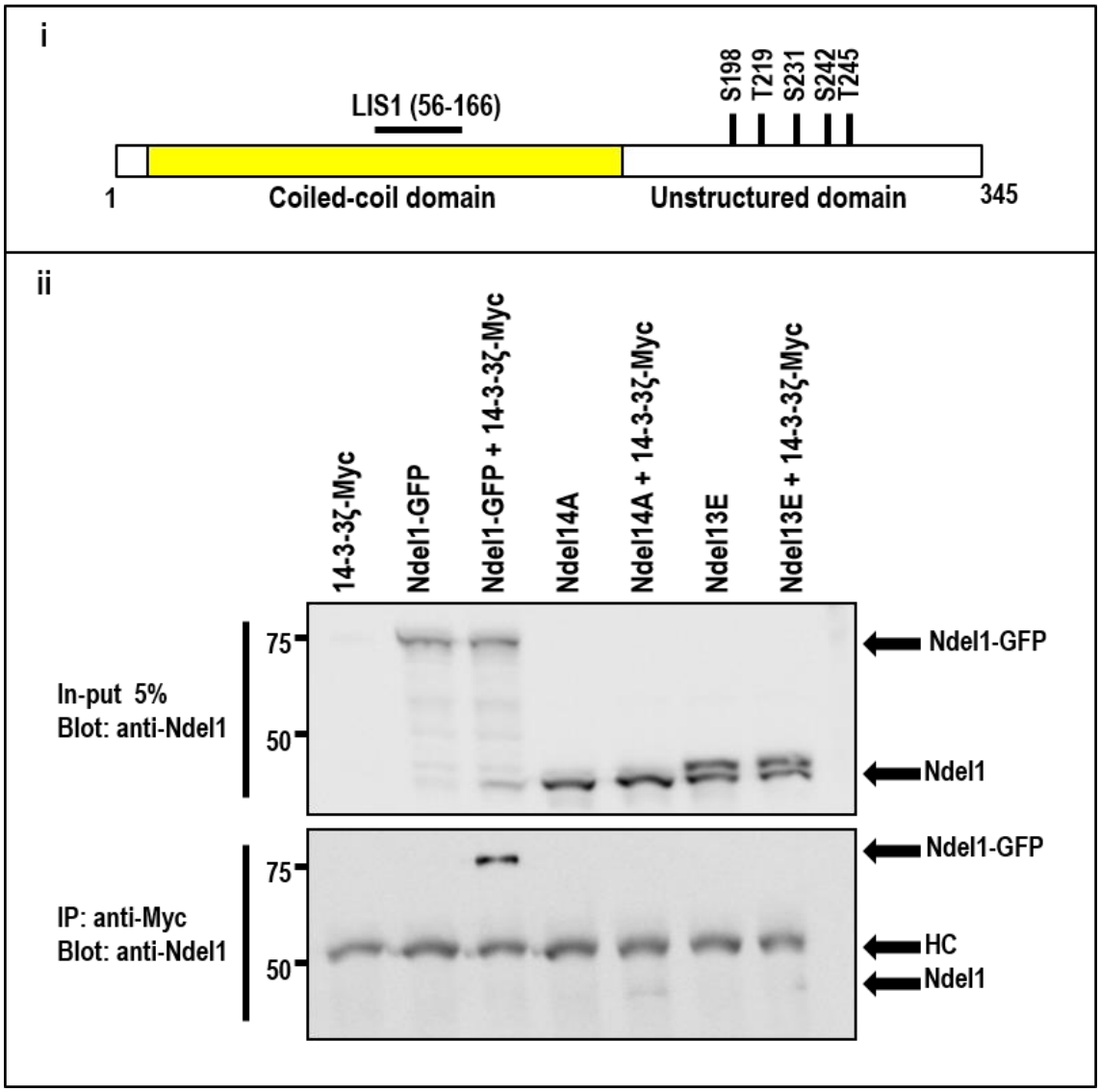

Figure 4.6: 14-3-3ζ interacts directly with Ndel1.

(i) A schematic of Ndel1 indicating the coiled-coil domain, Lis1 recognition domain and Cdk5/p35 S/T phosphorylation sites. (ii) *In vitro* co-immunoprecipitation assays using recombinant proteins for 14-3-3ζ Myc tagged (14-3-3ζ-Myc) and native Ndel1 GFP tagged (Ndel1-GFP) or quadruple Ndel1 mutant IRES GFP (Ndel14A) or Ndel1 phosphomimetic IRES GFP (Ndel13E). Proteins were pulled down by using Myc antibodies and analysed by immunoblotting with antibodies recognising Ndel1. HC, antibody heavy chain.

4.2.7 14-3-3ζ maintains Ndel1 phosphorylation

To further confirm that 14-3-3ζ interaction with Ndel1 is dependent on Ndel1 phosphorylation, I performed another co-immunoprecipitation assay where the HEK293T cells were treated with either the PP2A inhibitor, Okadaic acid to increase Ndel1 phosphorylation, or the PP2A activator, FTY720 to decrease Ndel1 phosphorylation prior to cell lysis (section 2.8.2). Inhibition of PP2A resulted in increased Ndel1 interaction with 14-3-3ζ (Figure 4.7 i & ii). Conversely, activation of PP2A resulted in decreased Ndel1 interaction with 14-3-3ζ (Figure 4.7 i & iii). This result demonstrates that Ndel1 phosphorylation at S198, T219, S231, and S242 is crucial for 14-3-3ζ interaction. This finding is in strong agreement with that reported for 14-3-3ε (Toyo-oka et al., 2003) and the findings of Johnson et al. (2010) who showed that HA-Ndel1 binds directly to 14-3-3, and that this interaction is abolished by dephosphorylation with PP2A.

To determine whether 14-3-3ζ KO has an effect on the levels of Ndel1 phosphorylation *in vivo*, I next isolated protein lysates from 14-3-3ζ WT and KO hippocampi or whole brain (sections 2.8.3 & 2.8.4) and probed for phosphorylated Ndel1 and total Ndel1 (Figure 4.8, i) (sections 2.8.6 & 2.8.7). My analysis indicated that the loss of 14-3-3ζ leads to reduction in phosphorylated Ndel1 levels without affecting the total levels of Ndel1 (Figure 4.8 ii & iii, respectively). This result suggests that 14-3-3ζ may play a protective role for phosphorylated Ndel1 from being targeted by phosphatases, such as PP2A.

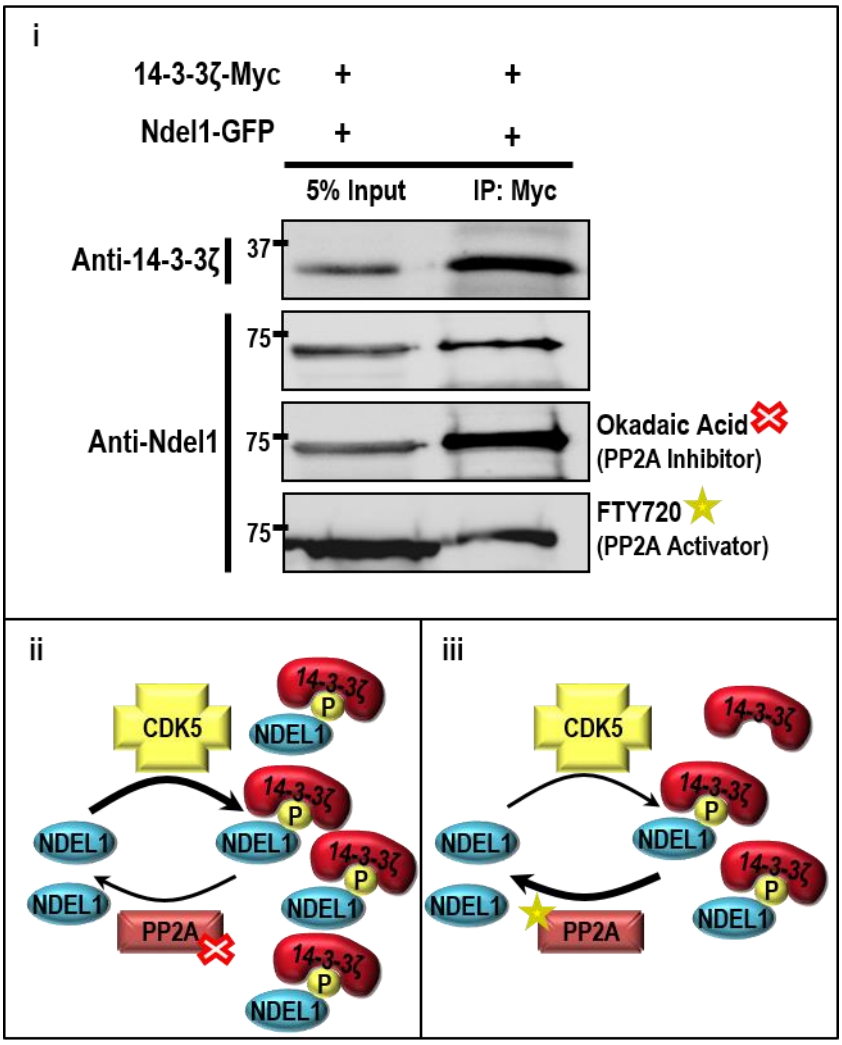

Figure 4.7: Ndel1 phosphorylation promotes interaction with 14-3-3ζ.

(i) Co-immunoprecipitation assays from cells treated with either Okadaic acid (PP2A inhibitor) to inhibit Ndel1 dephosphorylation or FTY720 (PP2A activator) to increase Ndel1 dephosphorylation an hour prior to lysis. Western blots were probed with either Anti-14-3-3ζ or Anti-Ndel1. (ii-iii) Schematic of effects of PP2A inhibitor (ii) and activator (iii) on Ndel1 phosphorylation status and 14-3-3ζ interaction.

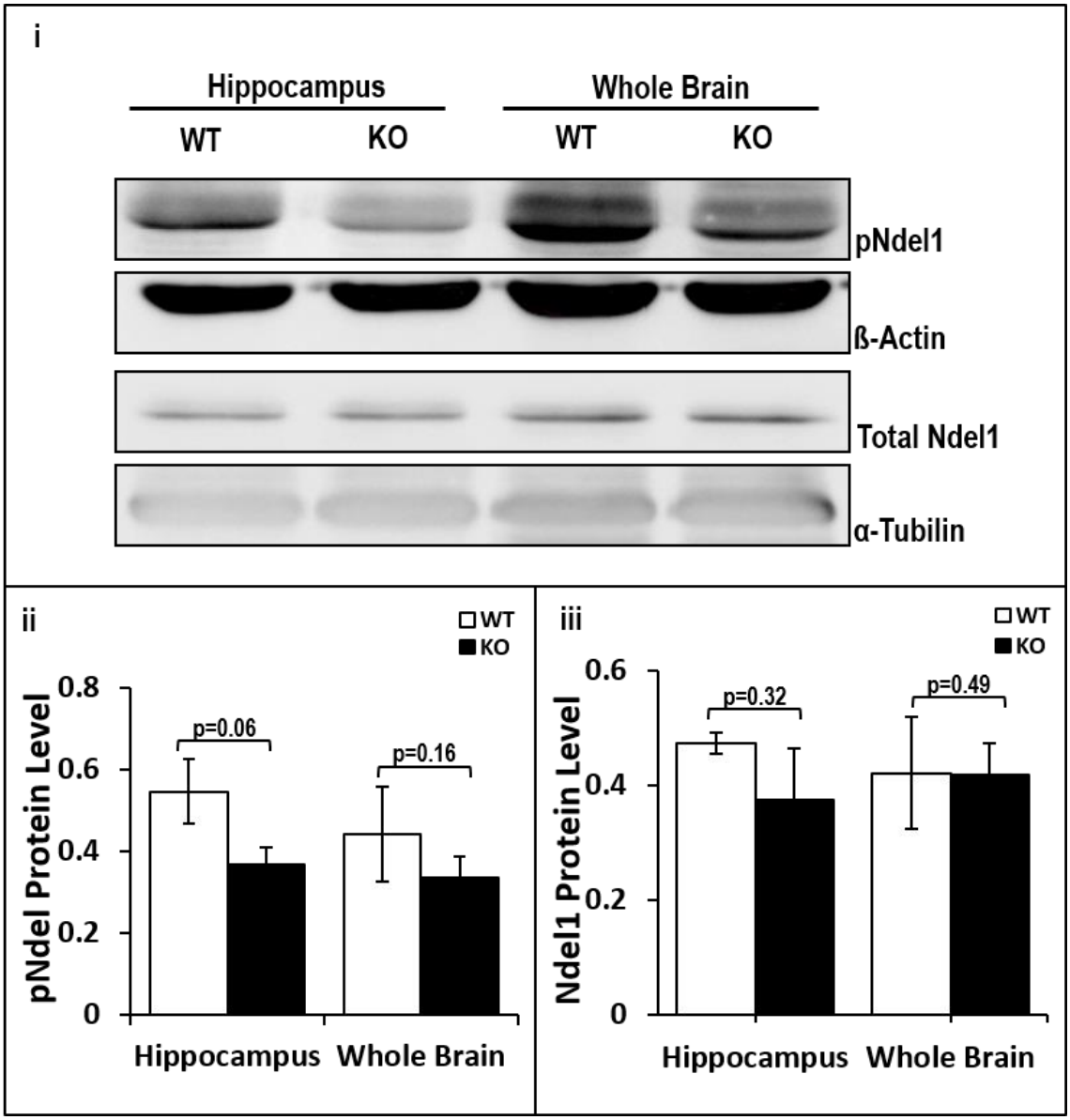

Figure 4.8: 14-3-3ζ KO leads to reduction in phosphorylated Ndel1 levels *in vivo*.

(i) Western-blot analysis of protein lysates from adult hippocampi or whole brains using antibodies against pNdel1 or Ndel1. Quantification of pNdel1 (ii) and Ndel1 (iii) protein levels in the presence and absence of 14-3-3ζ. Error bars indicate SEM (pNdel1: hippocampus WT n=2 KO n=3, whole brain WT n=3 KO n=3, Ndel1: hippocampus WT n=3 KO= n=3, Ndel1 whole brain WT n=4 KO n=4).

4.2.8 Expression of Ndel1 phosphomimetic in 14-3-3ζ KO neurons

To test the notion that 14-3-3ζ maintains Ndel1 phosphorylation to control neuronal migration I next examined whether the constitutively active Ndel1 phosphomimetic (Ndel13E) was sufficient to rescue the migration defect observed in 14-3-3ζ KO neurons. Neuronal progenitor cells isolated from 14-3-3ζ WT and KO hippocampi were electroporated with vectors consisting of either GFP alone, wild type 14-3-3ζ with IRES GFP, native Ndel1 GFP tagged, Ndel1 phosphomimetic with IRES GFP (Ndel3E), or Ndel1 quadruple mutant with IRES GFP (Ndel14A), as described in section 2.6.7. Migration of transfected neurons was quantitated by analysis of GFP positive cells in real time on a spinning disc confocal microscope (section 2.6.4). Movies generated from images taken at 30min intervals (Movie 4.3) were processed using the Manual Tracking tool in ImageJ (section 2.6.4).

Albeit that several electroporation parameters were tested to optimise transfection efficiency only a small number of cells could be transfected in each neurosphere (i.e. ~10-50/neurosphere). Analysis of GFP transfected neurons (WT n=19, KO n=19) identified a trend toward KO neurons migrating less than controls but lacked power to show significance, likely due to the small number of neurons transfected in this assay (Appendix A.5). However, by pooling this data with my previous spinning disc analysis (Figure 4.3) there was a clear reduction in migration distance of KO compared to WT neurons ($p<0.001$, Figure 4.9 i). Transfection of KO neurospheres with wild type 14-3-3ζ resulted in a complete reversal of the migration defect therefore confirming that a lack of 14-3-3ζ leads to the migration phenotype ($p=0.004$, Figure 4.9 iii). Analysis of KO neurons transfected with either native Ndel1 or Ndel1 phosphomimetic (Ndel13E) also

showed that the migration phenotype can be reversed by increasing the absolute levels or phosphorylated levels of Ndel1 (Ndel1 $p<0.001$, Ndel13E $p=0.01$; Figure 4.9 iii). Surprisingly, I also found that the Ndel1 quadruple mutant (Ndel14A) was able to increase the migration of KO neurons ($p<0.001$; Figure 4.9 iii). In contrast, I was unable to identify any significant differences in mean migration velocity using this assay (Appendix A.6).

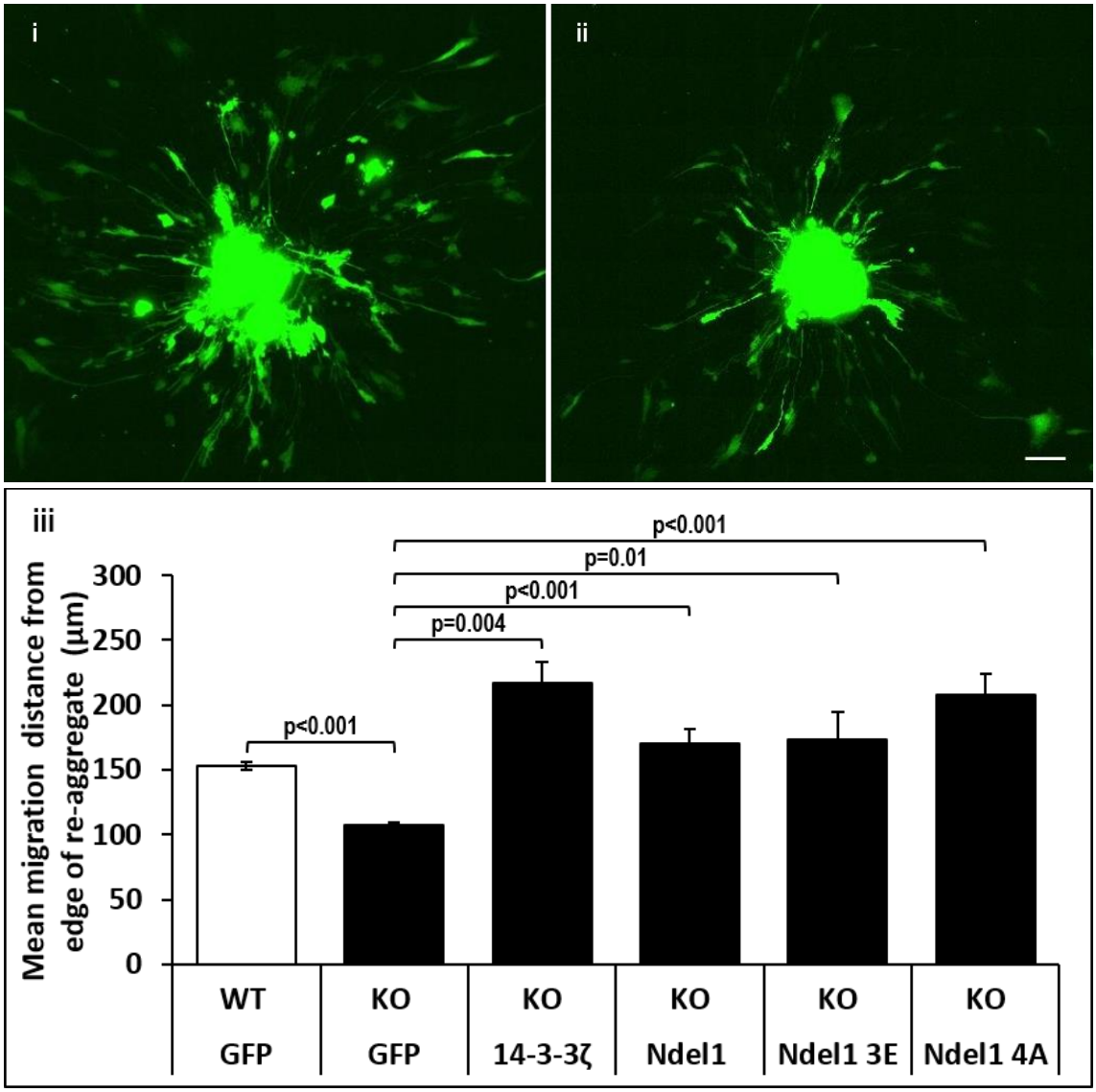

Figure 4. 9: 14-3-3ζ KO neuronal migration defect is rescued by Ndel1 phosphomimetic.

Example of transfected WT (i) and KO (ii) neurospheres with empty vector consisting of GFP alone. (iii) Mean migration distance from the edge of the re-aggregate was determined for all conditions. Error bars indicate SEM of neurosphere number (WT GFP n=120, KO GFP n=117, KO 14-3-3ζ n=4, Ndel1 n=8, KO Ndel1 3E n=15, KO Ndel1 4A n=14 KO). Ndel1 3E: Ndel1 phosphomimetic, Ndel1 4A: Ndel1 quadruple mutant.

4.3 Discussion

Correct positioning of neurons within the brain is essential to establish complex networks for normal brain function. Indeed, many neurodevelopmental disorders, such as lissencephaly, epilepsy and schizophrenia, have been directly linked to neuronal mispositioning (Keays, 2007, Reiner, 2013, Tsai and Gleeson, 2005). Our previous analysis of 14-3-3ζ KO mice found that CA pyramidal neurons within the hippocampus are mispositioned and that this is accompanied with misrouted dentate mossy fibres and reduced synaptic density (chapter 3). While previous birth-dating studies suggested that these mispositioning defects may arise from aberrant migration (Cheah et al., 2012), whether 14-3-3ζ controls neuronal migration remained to be determined. Thus, in this chapter I have established an *in vitro* neuronal migration assay to address if and how 14-3-3ζ plays a role in hippocampal neuronal migration.

Proper neuronal migration is crucial for correct neuronal positioning and is controlled by a highly regulated series of cellular events involving leading process extension, nucleokineses (N-C coupling) and trailing process retraction. Disruption of any of these processes can compromise cell motility (section 1.6) (Lambert de Rouvroit and Goffinet, 2001, Shu et al., 2004). My results demonstrate, for the first time, that 14-3-3ζ is required cell autonomously for neuronal migration. I found that 14-3-3ζ deficient neurons display delayed neuronal migration (Figure 4.2) in addition to perturbed N-C coupling (Figure 4.5) in a dose-dependent manner, similar to that reported in Lis1 and Ndel1 deficient neurons (Gambello et al., 2003, Hirotsune et al., 1998, Sasaki et al., 2000, Tanaka et al., 2004a, Toyo-oka et al.,

2003, Youn et al., 2009, Shu et al., 2004). Providing clues to the molecular mechanisms by which 14-3-3ζ controls neuronal migration, I found that 14-3-3ζ binds to phosphorylated Ndel1 (Figures 4.6 & 4.7) and that in the absence of 14-3-3ζ the levels of phosphorylated Ndel1 are perturbed in hippocampal neurons. This therefore suggests that 14-3-3ζ binds to Ndel1 to maintain its phosphorylation levels to control migration, similar to that reported for 14-3-3ε (Toyo-oka et al., 2003). Moreover, the migration defect observed could also be a result of 14-3-3ζ KO neurons displaying increased adherence (Figure 4.4 ii), however this notion requires further investigation.

My co-immunoprecipitation assays with native and mutant versions of Ndel1 show that 14-3-3ζ interaction is dependent on the Cdk5/p35 serine and threonine phosphorylation sites (Figure 4.6). Interestingly, in my migration assays I found that native Ndel1 and quadruple Ndel1 mutant (Ndel4A; S198A, T219A, S231A, & S242A) reduced the migration defects of 14-3-3ζ KO neurons to a similar extent as phosphomimetic Ndel1 (Ndel13E; S198E, T219E, & S231E) (Figure 4.9). In addition to Cdk5/p35 dependent phosphorylation of S198, T219, & S231, Ndel1 has also been reported to be phosphorylated by Aurora A at S251 (Mori et al., 2007). Johnson et al. (2010) have shown that interactions between 14-3-3 and Ndel1 are reduced in the presence of serine to alanine mutations at S251 and S336 and even further reduced in the presence of alanine mutations of S198, T219, S231, S251 and S336. It is therefore possible that a phosphorylation hierarchical system is in place where phosphorylation of S198, T219 and S231 are first required to allow phosphorylation of S251 and S336 to modulate interactions with 14-3-3. Alternatively, it is also possible that several 14-3-3 molecules are required

to interact with different Ndel1 phosphorylated sites. To decipher these possibilities, it will be important to expand these migration assays with a series of Ndel1 mutants removing all of the potential serine/threonine phosphorylation sites.

Although my data fit with the idea that 14-3-3ζ controls neuronal migration by maintaining the levels of Ndel1 phosphorylation (Figure 4.10), there are also important differences in the phenotypes between mice lacking these proteins. Notably, Ndel1 heterozygous mice have profound migration defects in multiple neuronal subclasses (Shu et al., 2004). To date we have only seen defects in hippocampal neurons, which may be due to functional redundancy of other 14-3-3 proteins. However, it will be of interest analyse additional neuronal sub-classes to address if there are more widespread defect in the 14-3-3ζ KO mice.

14-3-3 proteins are known to function as either homo- or heterodimers. Given that 14-3-3ε functions only as a heterodimer this may suggest that 14-3-3ζ and 14-3-3ε preferentially heterodimerise to play a role in hippocampal neuronal migration. In support of this notion, our collaborators have recently generated 14-3-3ζ and 14-3-3ε double KO mice which have cortical lamination defects (Toyo-oka et al., 2014). It would also be of interest to examine if these mice display more severe hippocampal lamination defect compared to the 14-3-3ζ KO mice.

The role of 14-3-3ζ in neuronal migration is in strong agreement with 14-3-3ζ KO mice modelling many of the anatomical defects associated with neurodevelopmental disorders such as schizophrenia. Understanding the

mechanisms by which 14-3-3ζ controls neuronal development therefore offers the hope of understanding the origins of these disorders and also toward the generation of novel diagnostics and therapeutics for these disorders. During the course of my project there were several reports of *14-3-3ζ* mutations in schizophrenia and autism adding weight to the notion of a pivotal role for the 14-3-3ζ / Ndel1 axis in the pathogenesis of neurodevelopmental disorders. It will now be of interest to test the pathogenicity of these mutations using migration assays as described in this chapter.

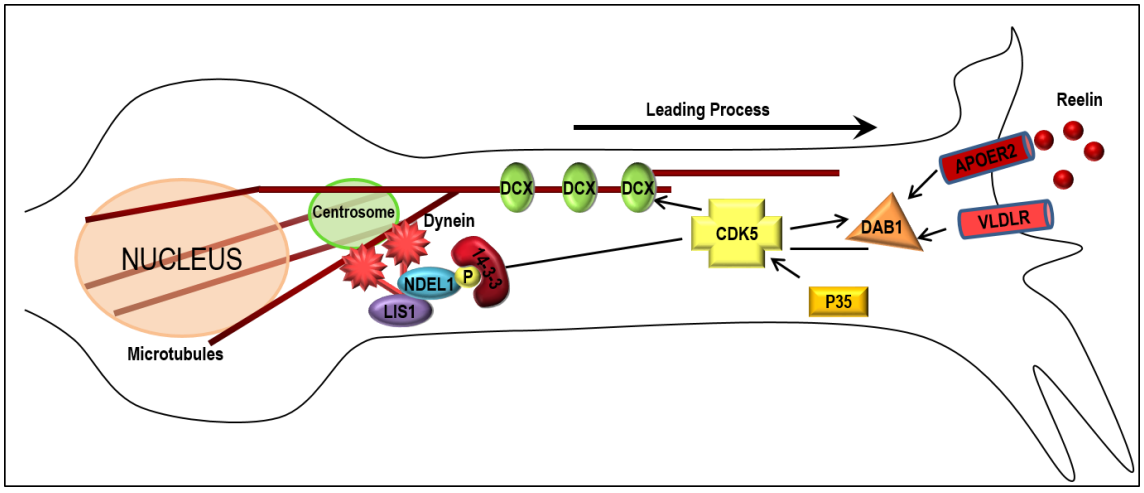

Figure 4.10: Model of 14-3-3 role to the neuronal migration pathway.

Schematic of the molecular pathway required for neuronal migration. Extracellular Reelin binds to the membrane-bound receptors APOER2 and VLDLR, which stimulate the intracellular signalling molecule Dab1. Phosphorylated Dab1 interacts with Lis1. Cdk5 is activated by p35 and phosphorylates the microtubule stabilizer DCX and Ndel1. Phosphorylated Ndel1 complexes with Lis1 and dynein, which act to sustain microtubule bundles and facilitate nucleokinesis. Adapted and redrawn from Keays (2007).

Chapter Five:

The Role of 14-3-3ζ in Neurogenesis

5.1 Introduction

Neural stem cells give rise to the entire central nervous system (brain and spinal cord) during embryonic and early postnatal development (section 1.3). These cells transition from proliferative and multipotent precursors into fully differentiated neurons through a process known as neurogenesis (section 1.7) (Ming and Song, 2011, Reif et al., 2006, Urban and Guillemot, 2014). Neurogenesis also persists in restricted areas of the adult brain including the subventricular zone (SVZ) adjacent to the lateral ventricle and the subgranular zone (SGZ) of the hippocampal dentate gyrus (Hayashi et al., 2015, Ming and Song, 2011).

Hippocampal dentate gyrus adult neurogenesis is critical for certain aspects of learning and memory throughout life and has been implicated in neuropsychiatric disorders such as schizophrenia (section 1.7.2). Several reports demonstrate significant reduction in hippocampal cell proliferation and neurogenesis in post-mortem schizophrenia brain samples (Allen et al., 2015, Reif et al., 2006, Reif et al., 2007). Moreover, several studies also report structural abnormality including enlargement of the lateral ventricles and reduced hippocampal volume in schizophrenia patients (Harrison, 2004, Jaaro-Peled et al., 2010, Ross et al., 2006). As highlighted in chapter 3, our 14-3-3ζ KO mouse model displays reduced size of the hippocampal dentate gyrus, aberrant compaction of granular cells and enlarged lateral ventricles compared to WT which are characteristic of perturbed neurogenesis.

Neural stem cells can be isolated from the SVZ and SGZ and expanded in culture systems known as neurospheres (Chen et al., 2007, Giachino et al., 2009). Neurospheres are composed of several cell populations where only ~1-5% have stem-cell like properties. The sequential culture and expansion of stem-cell like neuronal progenitors from neurospheres therefore provides an indicator of the ability of the cells to proliferate and self-renew (Chen et al., 2007, Giachino et al., 2009). In this chapter, I have utilised the *in vitro* neurosphere culture system to examine the contribution of 14-3-3ζ in hippocampal neural stem cell proliferation and self-renewal. I also extended these studies to determine if neurogenesis is perturbed in the 14-3-3ζ KO hippocampi *in vivo*.

5.2 Results

5.2.1 Optimisation of neurosphere culture system

To determine if the loss of 14-3-3ζ affects neural stem cell properties I utilised the neurosphere culture system (section 2.6) as it allows examination of three neural stem cell characteristics including proliferation, self-renewal and multipotency. Neurosphere cultures are highly sensitive to the procedure and thus it was important to ensure that the culture system was optimal and reproducible. For optimisation of the culture system, various cell densities, passage frequency, and concentration of mitogens (i.e. EGF, hFGF) were tested which resulted in the following experimental protocol. Neural stem/progenitor cells were isolated from E18.5 14-3-3ζ WT and KO mouse hippocampi and plated as a single cell suspension (Figure 5.1 i, sections 2.6.1). Cells were cultured at a constant density of 10,000cells/well in 24-well plates or 500cells/well in 96-well-plates, depending on the assay. As neurospheres initially take longer to form, the first passage was undertaken 10 days post culture while following passages were undertaken every 6 days thereafter (Figure 5.1 ii). Experimental analyses were made 6 days post neurosphere passage; analysis made from the first, second and third passages will be addressed as primary, secondary and tertiary neurospheres, respectively (Figure 5.1 iii, section 2.6.8). Note that no experiments exceeded the fourth passage since an extended number of passages leads to both complexity and reduction in the neurogenic capacity of the neurospheres.

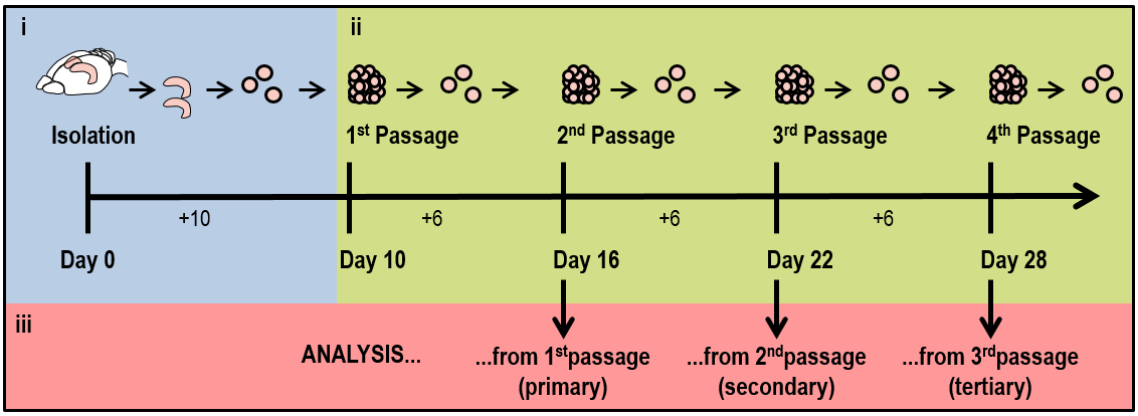

Figure 5. 1: Schematic of experimental procedure using the neurosphere culture system.

(i) Neuronal progenitors are isolated from the hippocampus of 14-3-3ζ WT and KO E18.5 embryos and plated as a single cell suspension. These cultures were grown for 10 days until they formed neurospheres. (ii) Neurospheres are passaged every 6 days for a maximum of four passages. (iii) Neurospheres from the 1st, 2nd and 3rd passages are used to analyse the neurosphere size, total neurosphere number and the total cell number.

5.2.2 14-3-3ζ KO impairs neural stem/progenitor cell self-renewal *in vitro*

Neural stem/progenitor cells possess the ability self-renew, thus examination of the number of neurospheres over several passages allows assessment to whether the 14-3-3ζ KO would influence neurosphere formation. A serial passage neurosphere-forming assay was performed in which the neural stem/progenitor cells were plated at a low density with a set number of single cells (500cells/well in uncoated 96-well plate) and left to form primary neurospheres. The primary neurospheres were then dissociated and re-cultured with stem/progenitors cells going on to develop into secondary neurospheres. This process was repeated to generate tertiary neurospheres. The ability to form neurospheres after each passage is an indicator of self-renewal. For this experiment following each passage, the number of primary, secondary and tertiary neurospheres formed in culture were measured (section 2.6.8).

A reduction in neurosphere number from 14-3-3ζ KO culture compared to WT was apparent upon visual examination of the wells (Figure 5.2 i). Quantification of the total neurosphere number generated from 500 stem/progenitor cells revealed a significant reduction in the primary, secondary and tertiary neurosphere formation in the 14-3-3ζ KO compared to WT ($p=0.003$, $p=0.001$, $p=0.005$, respectively; Figure 5.2 ii). This result demonstrates that 14-3-3ζ KO neural stem/progenitors have decreased capacity to generate neurospheres following serial subcloning, suggesting impaired self-renewal capabilities. Notably, passaging 14-3-3ζ KO derived neurospheres for 10 passages, the longest time

studied, always resulted in fewer neurospheres compared to WT at every passage (data not shown).

To further demonstrate the effect of 14-3-3ζ on self-renewal of neural stem/progenitors, I measured the total number of viable cells after neurosphere formation. Briefly, 10,000 cells/well in 24-well plates were cultured from 14-3-3ζ WT and KO embryonic hippocampi for 6 days. Primary neurospheres within that well were dissociated and the total number of viable cells was measured, followed by re-culturing of cells to generate secondary and tertiary neurospheres (section 2.6.8). Interestingly, the total neural stem/progenitors cell number from the 14-3-3ζ KO primary, secondary and tertiary neurospheres was reduced compared to WT ($p=0.08$, $p=0.12$, $p=0.04$, respectively; Figure 5.2 iii). Notably, this was also seen in the BALB/c derived neural stem/progenitor cells (Appendix A.7). Taken together, these results are best explained by a reduction in neurosphere-forming cells, which stimulate a decreased number of neurospheres that form, and thus the total number of cells in the culture. Additionally, it also could be a result in reduction of proliferation which is investigation in the next section (section 5.2.3).

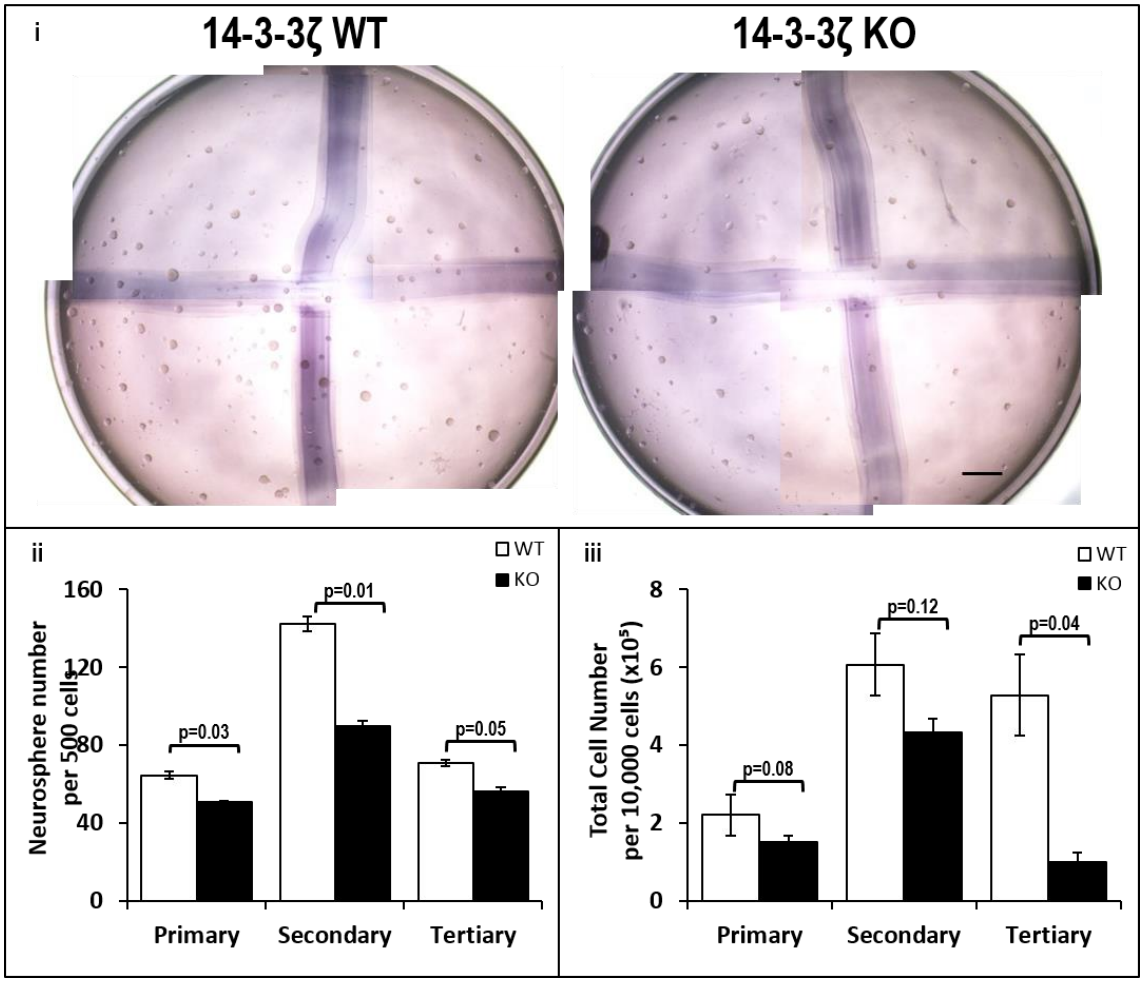

Figure 5. 2: 14-3-3ζ KO results in reduced stem/progenitor cell self-renewal *in vitro*.

(i) Representative bright-field images showing a well of a 96-well plate with neurospheres cultured for 6 days from E18.5 14-3-3ζ WT and KO hippocampi. Scale bar 200μm. (ii)Quantification of the number of neurospheres forming from 500 stem/progenitors cells reveals reduced neurosphere number in the 14-3-3ζ KO compared to WT (mean± SEM; WT n=3, KO n=3; three wells/sample were analysed). (iii) Quantification of the total cell number of stem/progenitor cells per well reveals a reduced number of stem/progenitor in 14-3-3ζ KO culture compared to WT (mean± SEM; WT n=3, KO n=4; two wells/sample were analysed).

5.2.3 14-3-3ζ is required for neural stem/progenitor cell proliferation *in vitro*

Reduced neurosphere size was also apparent in 14-3-3ζ KO neurospheres compared to WT (Figure 5.2 i), suggestive of reduced proliferation. Thus, to determine if 14-3-3ζ affects neural stem/progenitors cell proliferation, I examined size of the neurospheres as an indicator of their proliferative capabilities by culturing 10,000cells/well in uncoated 24-well plates for 6 days from E18.5 hippocampi of 14-3-3ζ WT and KO mice (sections 2.6.1. & 2.6.8). 14-3-3ζ WT and KO derived tertiary neurospheres were imaged and the neurospheres area (μm^2) was measured using ImageJ as described in section 2.6.8. Upon visual examination, it was apparent that the 14-3-3ζ KO derived tertiary neurospheres were smaller in size compared to WT (Figure 5.3 i). Quantification of the neurosphere size by measuring its area revealed that 14-3-3ζ KO derived neurospheres are significantly smaller in size compared to WT ($p=0.05$, Figure 5.3 ii), suggesting a potential role for 14-3-3ζ in neural stem/progenitor proliferation.

For direct examination of proliferation, tertiary neurospheres were subjected to a BrdU-incorporation assay (section 2.6.9). Briefly, neurospheres were dissociated into single cells suspension, plated on poly-L-lysine and laminin coated 24-well plates (10,000 cells/well) for 48hrs. BrdU was then added to the media for 1hr prior to fixation. BrdU is a nucleotide analogue it is incorporated into the DNA of cells undergoing DNA synthesis and therefore acts as a marker of proliferation. Cells were stained with anti-BrdU antibody and DAPI, followed by imaging and quantification using the Analyze Particle Tool in ImageJ (section

2.6.9). The percentage of BrdU-positive cells from 14-3-3ζ KO derived neurospheres was significantly lower than WT (p=0.05, Figure 5.4 ii).

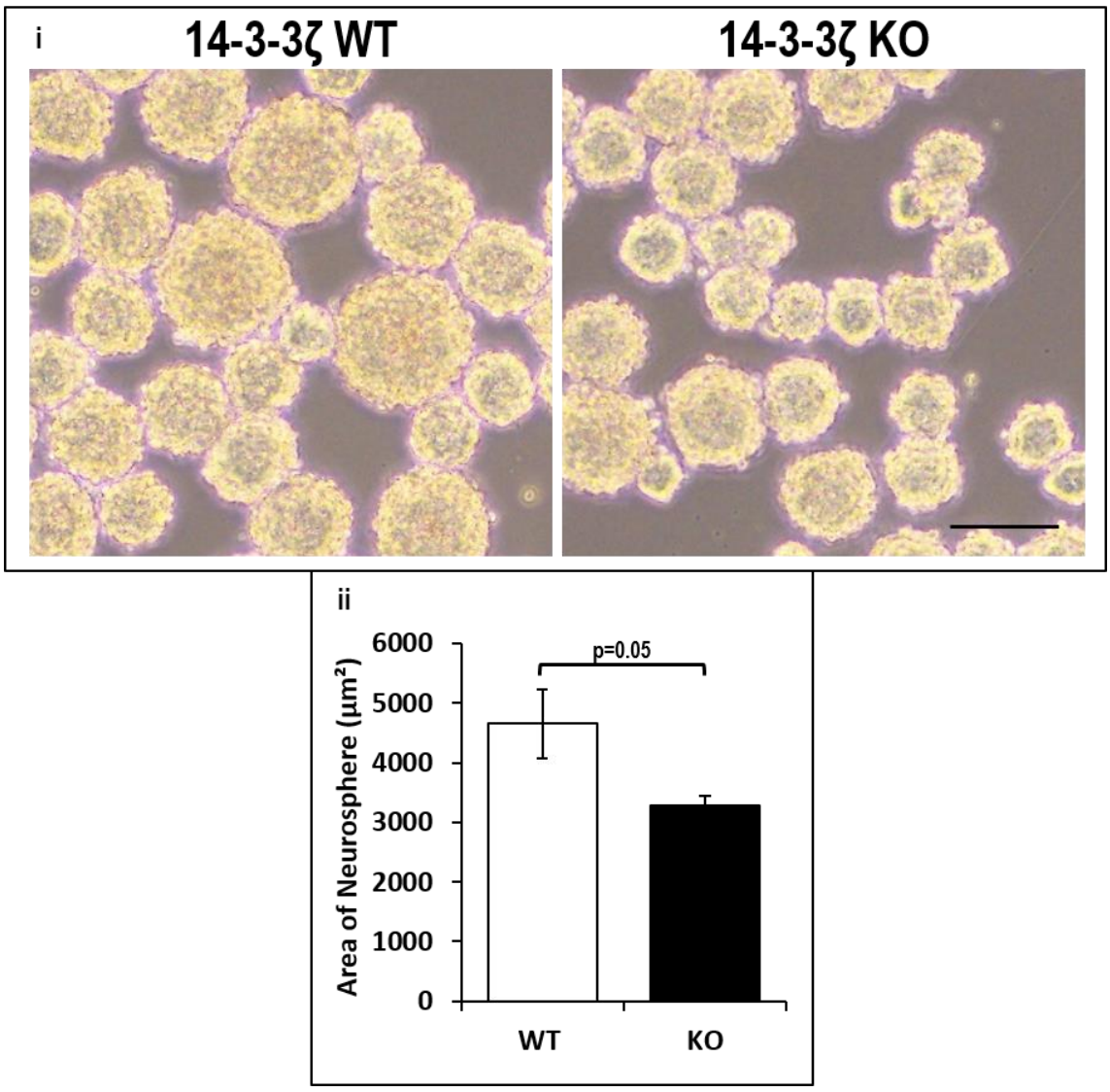

Figure 5. 3: 14-3-3ζ KO results in reduced neural stem/progenitor cell proliferation *in vitro*. (1-ii) Morphological examination of bright field images of neurospheres from the third passage of 14-3-3ζ WT (i) and KO (ii) E18.5 hippocampi. Scale bar 100µm. (iii) Quantification of the neurosphere area reveals significant reduction in neurosphere size in 14-3-3ζ KO compared to WT, indicating reduced proliferation of the neural stem/progenitor cells (mean± SEM; WT n=3, KO n=4; three wells/sample and three images/well were analysed).

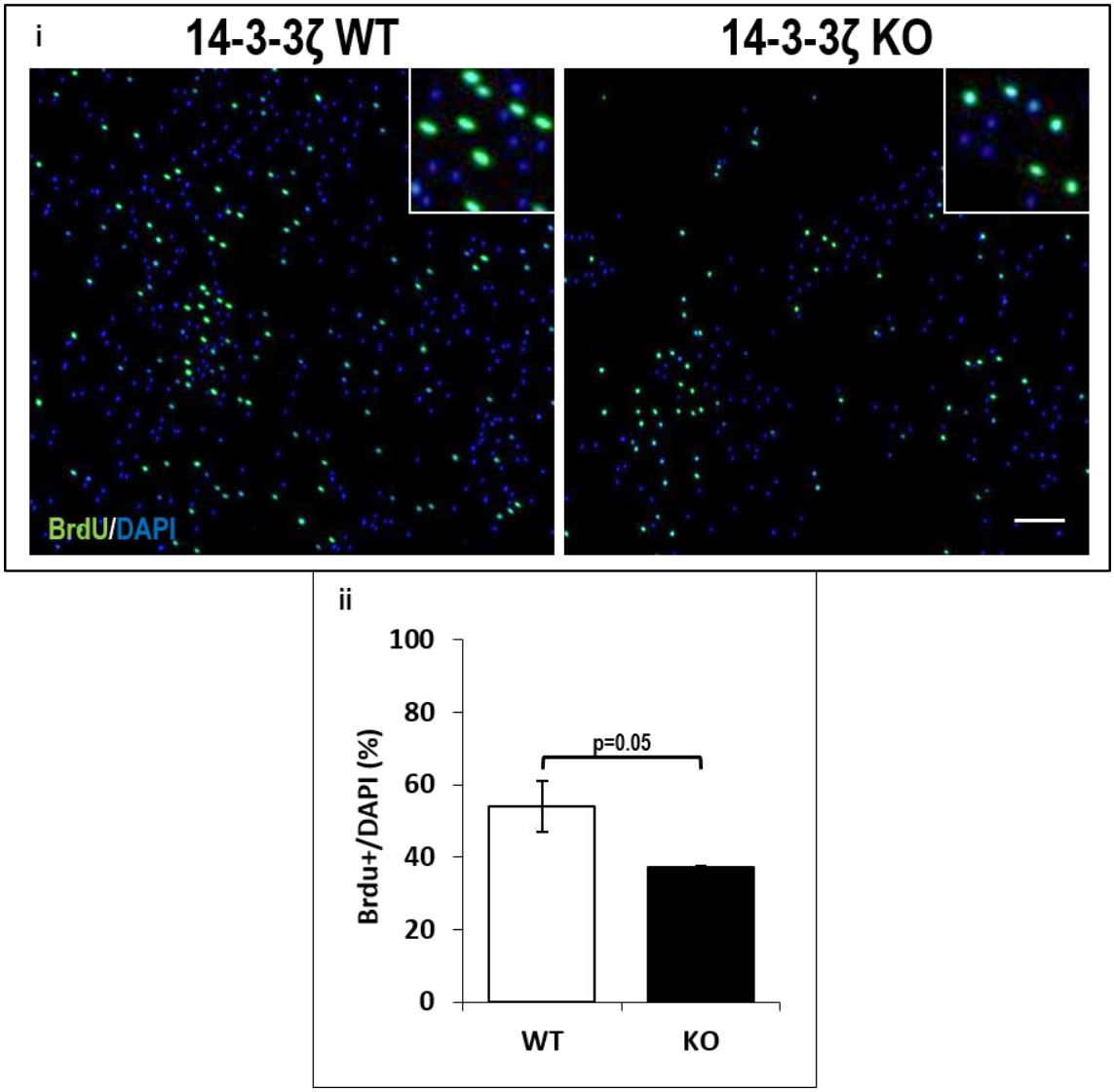

Figure 5. 4: BrdU-incorporation demonstrates that 14-3-3ζ is important for neural stem/progenitor cells proliferation *in vitro*.

(i) Images of neural stem/progenitor cells labelled by BrdU from E18.5 14-3-3ζ WT and KO hippocampi. Rectangular box indicates area of higher magnification. Scale bar 20μm. (ii) Statistical analysis of 14-3-3ζ KO samples reveals a significant reduction in the number of BrdU-positive cells compared to WT (mean± SEM; n=2; four images/well and four wells/ genotype were analysed).

5.2.4 Neurogenesis stage-specific cell marker expression in 14-3-3ζ KO neurospheres

I next examined the expression of neurogenesis stage-specific cell markers (illustrated in Figure 1.11), including Nestin, an intermediate filament protein associated with neural stem/progenitor cells, and doublecortin (DCX), a marker expressed in neuroblasts/immature neurons in neurospheres derived from 14-3-3ζ WT and KO embryos. Briefly, primary neurospheres were isolated and processed in suspension by fixation in 4% PFA followed by immunostaining with Nestin and DCX antibodies (section 2.6.10). Primary neurospheres were used for this assay as these were found to contain the highest number of neuronal stem-like progenitors in my previous assays (i.e. see the total number or neurospheres generated from primary and secondary neurospheres in Figure 5.2 ii).

Immunoflorescence analysis of 14-3-3ζ WT and KO derived primary neurospheres confirmed expression of the neurogenesis stage-specific cell markers Nestin and DCX (Figure 5.5 i & ii). For statistical analysis, fluorescent intensity of Nestin and DCX within the neurospheres was normalised to DAPI. As expected, the 14-3-3ζ WT derived primary neurospheres showed significantly higher Nestin fluorescent intensity compared to DCX, indicating a higher number of neural stem/progenitor cells compared to the neuroblasts/immature neurons, respectively ($p=0.01$; Figure 5.5 iii). In contrast, 14-3-3ζ KO derived primary neurospheres showed similar levels of neural stem/progenitor cells to neuroblasts/immature neurons, demonstrated by the similar levels of Nestin and DCX ($p=0.325$; Figure 5.5 iii). Interestingly, 14-3-3ζ KO derived primary

neurospheres exhibited a significant reduction in Nestin fluorescent intensity compare to WT neurospheres (p=0.001; Figure 5.5 iii), while DCX remained unchanged (p=0.283; Figure 5.5 iii). Together, this staining is suggestive of reduced neuronic capacity of the neurospheres.

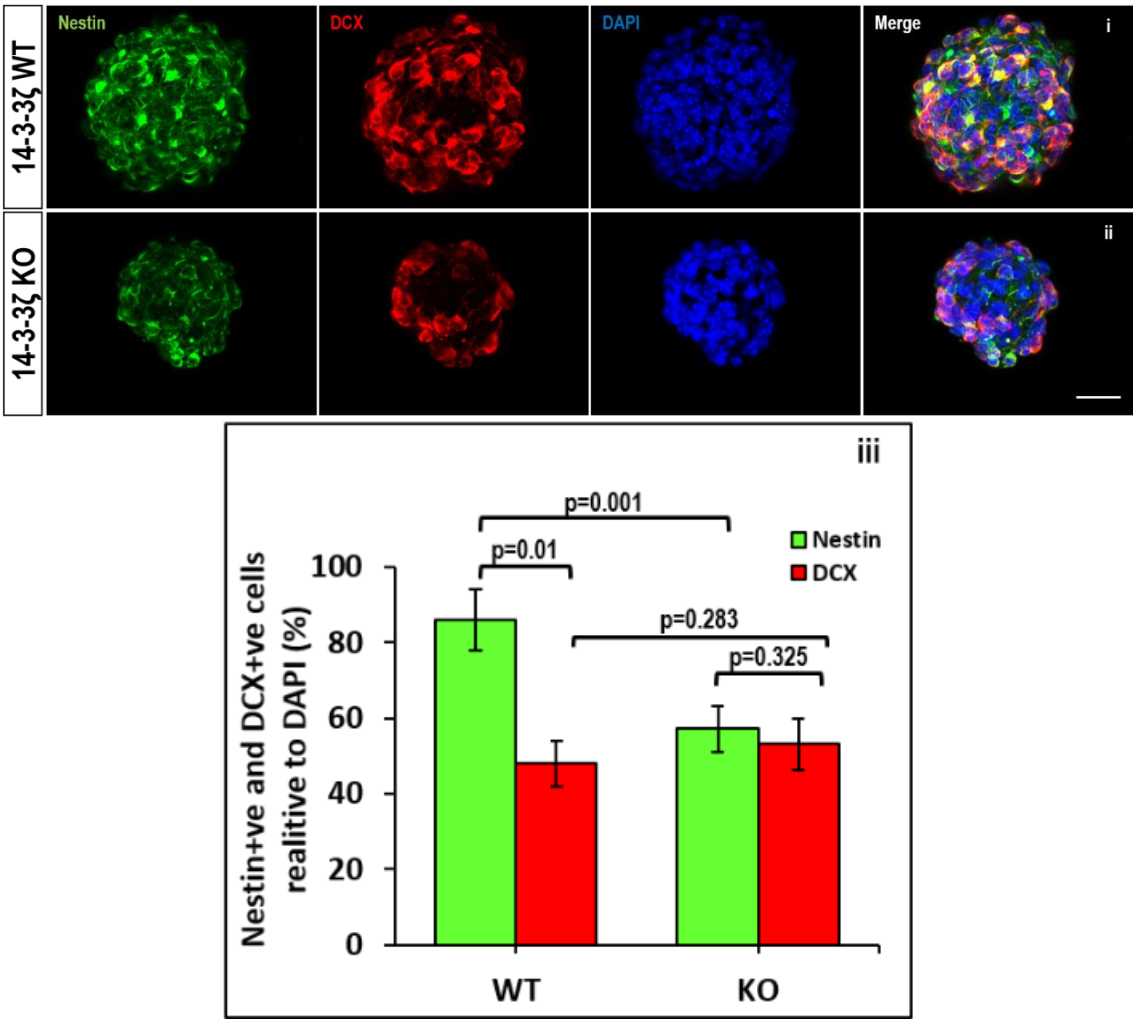

Figure 5. 5: Expression of neurogenesis stage-specific cell markers in neurospheres.

Representative z-stacked images of primary neurospheres isolated from E18.5 14-3-3ζ WT (i) and KO (ii) hippocampi stained with neurogenesis stage-specific cell markers. Green: Nestin (stem/progenitor cells), Red: DCX (neuroblasts/immature neurons), Blue: nucleus. Scale bar 20µm. (iii) Statistical analysis of fluorescent intensity of Nestin and DCX normalised to DAPI within the neurospheres (mean± SEM of neurosphere number; WT n=10, KO n=10).

5.2.5 Proliferation of neural stem/progenitor cells is decreased in 14-3-3ζ KO mice

To examine if the *in vitro* findings are recapitulated *in vivo*, short-pulse labelling with the nucleotide analogue EdU was performed to identify proliferating cells within the dentate gyrus. Briefly, EdU was administered intraperitoneally (100mg/kg EdU per bodyweight) into P7, P14 and P30 14-3-3ζ WT and KO mice (section 2.3.4). Brains were isolated after 2hrs and fixed in 4% PFA overnight prior to coronal sectioning (section 2.3.2). At least 8 sections/sample were immunostained for EdU-positive cells using Click-it EdU Imaging Kit form Invitrogen (section 2.3.4).

14-3-3ζ KO mice showed a marked reduction in EdU labelled cells at all ages examined (P7, P14 & P30) (Figure 5.6 i-vi), indicating that 14-3-3ζ is required to maintain hippocampal stem/progenitor proliferation *in vivo*. Quantitative analysis of proliferating cells within the DG revealed a significant reduction in the number of EdU-positive cells in the 14-3-3ζ KO P7, P14 and P30 mice compared to WT ($p=0.02$, $p=0.05$ & $p=0.01$, respectively; Figure 5.6 vii). This result is consistent with the *in vitro* data, showing that 14-3-3ζ KO results in significant reduction in hippocampal neural progenitor cell proliferation compared to WT in early postnatal and adult neurogenesis. Moreover, as the mice age a major decrease in the number of proliferative cells in the DG was also identified as previously reported by others (Figure 5.6 vii).

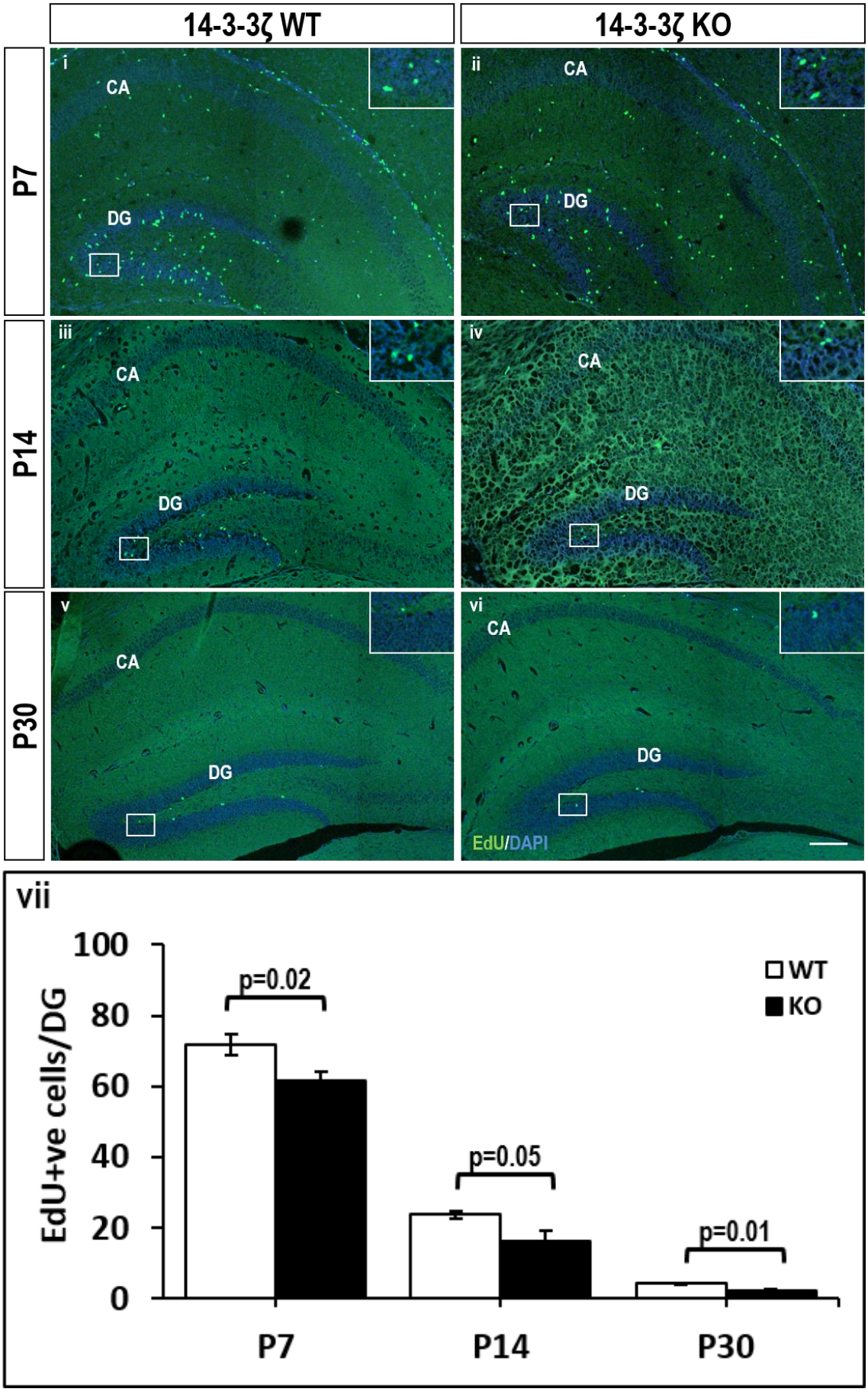
14-3-3ζ WT
14-3-3ζ KO
P7
P14
P30
i
ii
iii
iv
v
vi
CA
DG
EdU/DAPI
vii
EdU+ve cells/DG
100
80
60
40
20
0
p=0.02
p=0.05
p=0.01
WT
KO
P7
P14
P30

Figure 5. 6: Representative images of EdU short-pulse chase analysis of hippocampal dentate gyrus sections.

Staining for EdU-positive cells in 14-3-3ζ WT (i, iii, v) and KO (ii, iv, vi) dentate gyrus at different ages.. Scale bar 50μm. Boxed image shows high magnification of DG. Green: EdU-positive cells; Blue: DAPI staining of nucleus; DG: dentate gyrus. (vii) Statistical analysis of the number of EdU-positive cells in P7, P14, and P30 DG reveals a significant decrease in neural progenitor cell proliferation in 14-3-3ζ KO mice compared to WT (mean± SEM; P7 WT n=4, KO n=3; P14 WT n=3, KO n=3; P30 WT n=2, KO n=3).

5.2.6 14-3-3ζ KO mice have reduced expression of neurogenesis stage-specific cell markers *in vivo*

To determine if the reduction in neural stem/progenitor proliferation is also associated with a depletion of neurogenesis, I examined expression of SOX2 (labels same cell population as Nestin) and DCX in the dentate gyrus of adult mice. Briefly, adult brains were isolated and stored in 4% PFA overnight prior to coronal sectioning and at least 10 sections per sample were stained with SOX2 and DCX antibodies (section 2.4.2). Due to non-specific background staining I was unable to quantify the level of SOX-positive cells, however, visual examination suggested that SOX2-positive cell may be reduced in 14-3-3ζ KO mice (Figure 5.7 ii) compared to WT (Figure 5.7 i). DCX-positive cells were also reduced in the 14-3-3ζ KO dentate gyrus (Figure 5.7 iii) compared to WT (Figure 5.7 iv). Quantitative analysis revealed a significant decrease in the number of DCX-positive cells in the 14-3-3ζ KO dentate gyrus compared to WT ($p<0.001$; Figure 5.7 v). This data provides further evidence for a role for 14-3-3ζ in hippocampal neurogenesis.

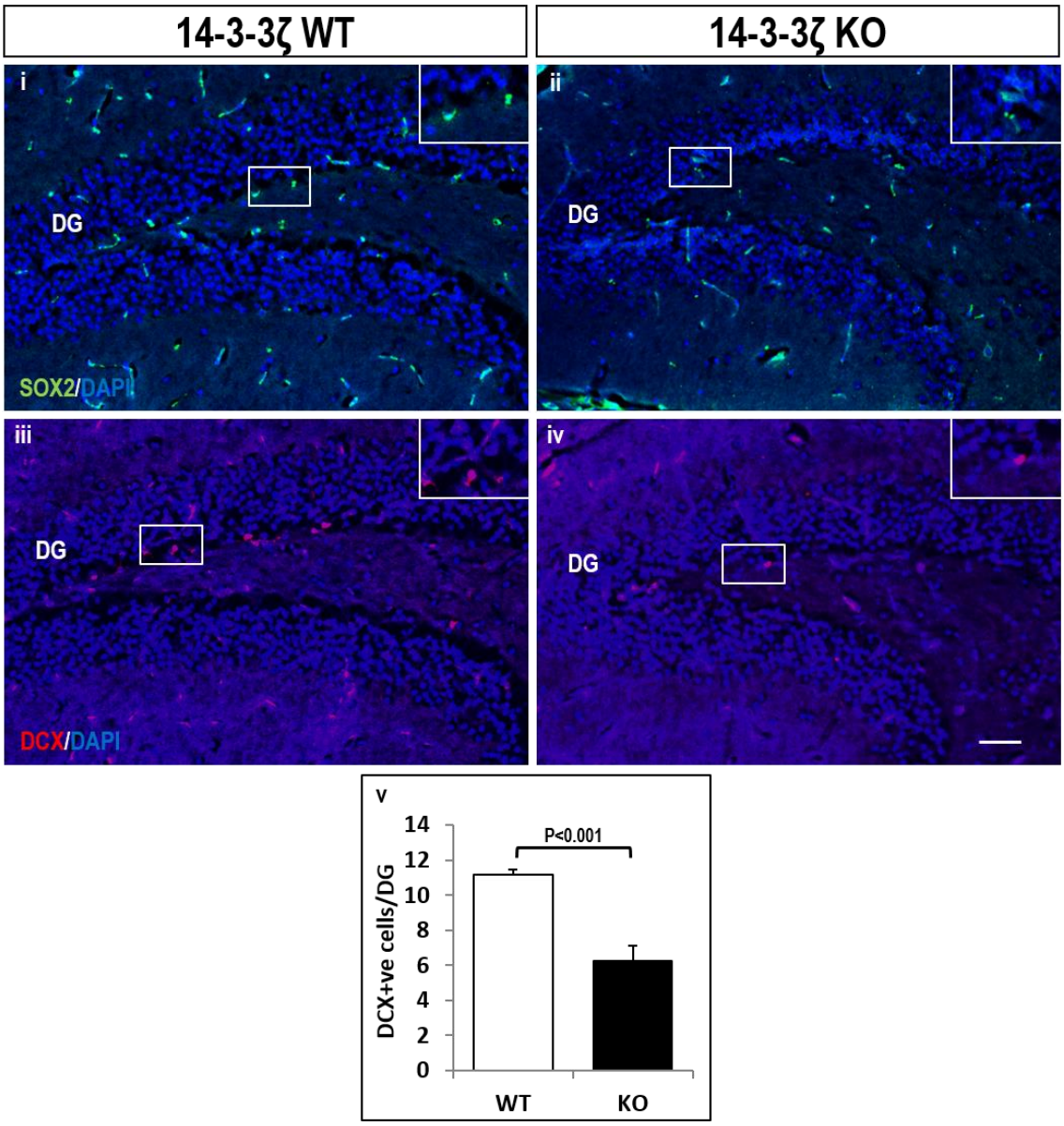

Figure 5. 7: 14-3-3ζ KO adult mice show reduced expression of neurogenesis stage-specific cell markers.

Immunohistochemical analysis of dentate gyrus in 14-3-3ζ WT (i, iii) and KO (ii, iv) adult mice stained with antibodies against SOX2 (i & ii) and DCX (iii & iv). SOX2: green, DCX: red, Nuclei (DAPI): blue. Scale bar 50µm. (v) Quantitative analysis reveals a significant reduction of the number of DCX-positive cell in the 14-3-3ζ KO DG compared to WT (mean± SEM; n=2). DG: dentate gyrus, DCX: doublecortin.

5.2.7 Neurogenesis stage-specific marker expression in adult mouse hippocampi

To further examine the expression of stage-specific neurogenesis markers the protein levels of SOX2 (which equivalent to Nestin) and DCX were quantitated by western blot. Briefly, protein lysates were obtained from 14-3-3ζ WT and KO adult hippocampi (sections 2.8.3 & 2.8.4) and run on SDS-PAGE gels (section 2.8.6) prior to immunoblotting (section 2.8.7) for SOX2 and DCX (Figure 5.8 i). My analysis showed that in the adult 14-3-3ζ KO mouse hippocampi DCX and SOX2 protein levels are reduced compared to WT (Figure 5.8).

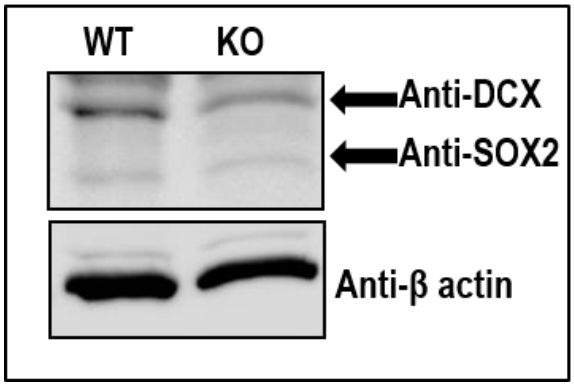

Figure 5. 8: 14-3-3ζ interaction with DCX and SOX2.

(i) Western blotting analysis of the protein levels of DCX and SOX2 in 14-3-3ζ KO adult hippocampal lysate. WT n=2; KO n=3. DCX: 45kDa, SOX2: 35kDa, β-Actin: 42kDa.

5.2.8 Investigating the molecular mechanism through which 14-3-3ζ controls neurogenesis

14-3-3 proteins have been reported to directly interact with GSK-3β with functional implications such as promotion of mouse embryonic stem cell proliferation and neural survival (Chang et al., 2012, Mwangi et al., 2006, Yuan et al., 2004). Thus, to elucidate the mechanism by which 14-3-3ζ may regulate neurogenesis I investigated whether 14-3-3ζ KO has an effect on the levels of GSK-3β and phosphorylated GSK-3β *in vivo*. Briefly, protein lysates isolated from the hippocampus of 14-3-3ζ WT and KO adult mice (sections 2.8.3 & 2.8.4) were analysed by Western Blot with probing for total GSK-3β (Figure 5.9 i) and phosphorylated GSK-3β (Figure 5.9 ii) (sections 2.8.6 & 2.8.7). Surprisingly, loss of 14-3-3ζ in adult mouse hippocampi showed dramatic changes in total GSK-3β (Figure 5.9 i) which was not replicated for phosphorylated GSK-3β (Figure 5.9 ii).

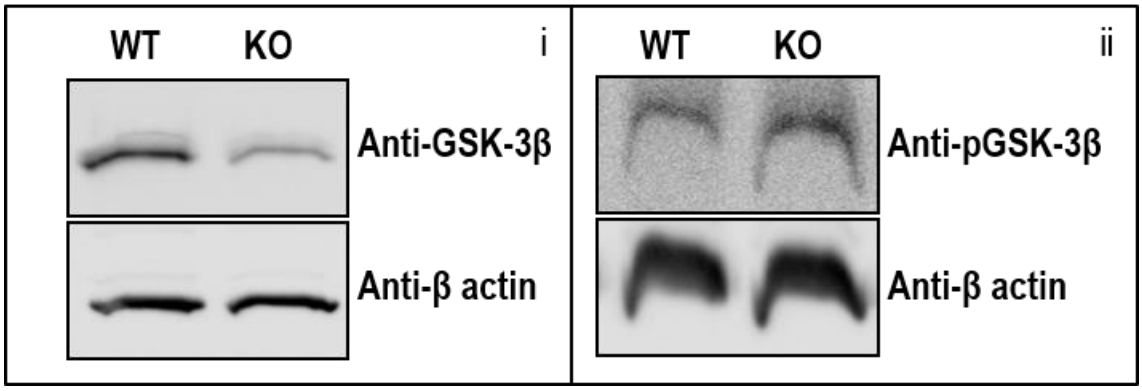

Figure 5. 9: 14-3-3ζ interaction with GSK3-3β and phosphorylated GSK-3β.

Western blotting analysis of the protein levels of GSK3-3β (i) and pGSK3-3β (ii) in 14-3-3ζ KO adult hippocampal lysate compared to WT. WT n=2; KO n=3. GSK3-3β: 46kDa, pGSK3-3β: 46kDa, β-Actin: 42kDa.

5.3 Discussion

It is becoming widely accepted that many neuropsychiatric disorders, such as schizophrenia, have a neurodevelopmental origin where the onset of the disorder may arise during embryonic development as a result of perturbed neural stem cell specification, growth, expansion or differentiation (Walsh et al., 2008, Camargo et al., 2007, Harrison, 2004, Lewis and Levitt, 2002). In schizophrenia patients, several studies have reported reduction of hippocampal volume size (Nelson et al., 1998, Shenton et al., 2001) and ventricular enlargement (Harrison, 2004, Jaaro-Peled et al., 2010, Ross et al., 2006). The reduction in hippocampal volume in some patients has also been shown to correlate with the degree of cognitive dysfunction (Gur et al., 2000, Sanfilipo et al., 2002). Our previous analysis of 14-3-3ζ KO mice revealed reduced dentate gyrus size and enlarged ventricles (chapter 3), which lead to my hypothesis that 14-3-3ζ may also have a role in regulating the fundamental properties of neural stem/progenitor cell renewal and/ or maintenance.

Neural stem cells are characterised by their multipotency, ability to proliferate and self-renew. Using neurosphere assays, I have now demonstrated that 14-3-3ζ is important for proper embryonic neural stem/progenitor cell proliferation and self-renewal *in vitro* (Figures 5.2-5.4). Moreover, the number of neural stem/progenitor (Nestin+) cells in the 14-3-3ζ KO derived neurospheres was significantly reduced compare to WT, while the level of neuroblasts/immature (DCX+) was unchanged (Figure 5.5). This result suggests that 14-3-3ζ KO derived neurospheres have reduced neurogenic capacity compared to WT, potentially

resulting from premature cell cycle exit leading to differentiation of the cells. Due to time limitation, the latter has not been tested directly using neurosphere differentiation assays, although there are now a number of studies that support this notion. Recent work by our collaborators using embryonic cortical derived neurospheres from conditional double (ζ/ε) 14-3-3 KO mice showed increased differentiation of neural progenitor cells into neurons compared to WT (Toyo-oka et al., 2014). Moreover, Mao et al. (2009) have shown that DISC1 knockdown in embryonic mouse brain caused premature neuronal differentiation at the expense of the progenitor pool. Previous work in our laboratory has shown that 14-3-3ζ interact with DISC1 (Cheah et al., 2012) and accordingly this interaction may be important for embryonic neuronal differentiation, which is yet to be examined.

As mentioned above, 14-3-3ζ KO results in reduced cell proliferation compared to WT, which may arise from altered cell cycle or apoptosis. To determine whether 14-3-3ζ KO neural progenitor cells prematurely exit the cell cycle during embryonic hippocampus development, *in vivo* BrdU cell cycle analysis can be used (proliferating progenitor cell, BrdU+; cell cycle exit, BrdU+/Ki67–). Alteration in the frequency of cell division, asymmetric (one progenitor cell and one neuron) versus symmetric cell division (two progenitor cells), could also lead to reduced cell proliferation. Frequency of asymmetrical cell division can be examined by measuring the cell division angle or spindle orientation. Alternatively, a more direct test is pair-cell analysis combined with immunostaining with cell division specific marker (neuron–neuron, both TuJ1+; neuron–progenitor, one TuJ1+ and one SOX2+; progenitor–progenitor, both TuJ1-/SOX2+). While increased apoptosis could be a factor in the reduced cell

proliferation observed, tunnel assay on 14-3-3ζ KO embryonic, early postnatal and adult hippocampi showed no sign of cell death compared to WT (Cheah et al. 2012). Moreover, no difference in cell viability was observed in both hippocampal neuron and neurosphere cultures when using trypan blue exclusion assay (data not shown).

Hippocampal neurogenesis is downregulated across ageing, which is thought to be mediated by a reduction of the neural stem cell pool and increased state of quiescence in the remaining cells (Urban and Guillemot, 2014, Varela-Nallar and Inestrosa, 2013). The age related decline of neural stem/progenitor proliferation was apparent in the 14-3-3ζ WT and KO mice hippocampus (Figure 5.6 vii). Additionally, 14-3-3ζ KO resulted in a consistent reduction of hippocampal cell proliferation across all ages examined therefore indicating an important role for this molecule in neurodevelopment (Figure 5.6). There are reports demonstrating significant reduction in hippocampal cell proliferation and neurogenesis in post-mortem schizophrenia brain samples (Allen et al., 2015, Reif et al., 2006, Reif et al., 2007). Similarity, 14-3-3ζ KO mice also showed reduced hippocampal cell proliferation, however its correlation with the degree of cognitive dysfunction reported in these mice (Cheah et al., 2012, Xu et al., 2015) is yet to be examined.

The rate and balance between the sequential stages of neurogenesis is crucial, where perturbation in one stage can affect another. Neurogenic markers (illustrated in Figure 1.11) are used to assess whether the reduced cell proliferation in neurogenic regions such as the DG, result in deficits in

hippocampal neurogenesis. My studies indicate that neural stem/progenitor (SOX2+) cells and neuroblast/immature neurons (DCX+) are reduced in the hippocampus of 14-3-3ζ KO mice (Figure 5.7). It will now be important to fully quantitate neural stem (SOX2+/GFAP+), proliferating neural stem cells (SOX2+/GFAP+/Ki67+) and differentiated neurons (TuJ1+) in these mice. Moreover, SOX2 and DCX protein levels were reduced in 14-3-3ζ KO hippocampal lysate compared to WT (Figure 5.8).

Hippocampal neurogenesis is tightly regulated through several signalling pathways (section 1.7.3). To provide clues to the molecular mechanisms by which 14-3-3ζ may regulate hippocampal neurogenesis I chose to examine the GSK-3β/β-catenin signalling pathway as 14-3-3 proteins are known to directly interact with GSK-3β (Chang et al., 2012, Mwangi et al., 2006, Yuan et al., 2004). At the basal state (Figure 1.12 i), β-catenin is associated with the destruction complex (which includes GSK-3β) where it is phosphorylated and targeted for ubiquitination and proteasomal degradation. Wnt activation (Figure 1.12 ii) results in a signalling cascade which in turn causes release and stabilization of β-catenin, leading to its translocation into the nucleus to upregulate the transcription of proliferative and renewal genes. Meanwhile, GSK-3β is targeted for phosphorylation by AKT serine/threonine-specific protein kinase at serine 9 inhibiting its activity (Figure 1.12 ii).

Unexpectedly, the total GSK-3β level was decreased (Figures 5.9 i) while phosphorylated GSK-3β was unchanged (Figures 5.9 ii) in the 14-3-3ζ KO adult hippocampal lysate. The molecular mechanisms that control neurogenesis during

embryonic development also play important roles in adult neurogenesis, however, essential differences exist in the biological responses of neural precursors in the embryonic and adult contexts. Therefore, 14-3-3ζ may function in regulating adult neural/progenitor cell proliferation through interaction with GSK-3β during embryonic and not adult stages, which is yet to be examined.

The hippocampus is composed of several cell populations where only a small percentage represent the neural stem cells, therefore a better approach would be to use neurosphere protein lysates to examine if loss of 14-3-3ζ has any implication in protein required for neurogenesis. Of interest, β-catenin and αN-catenin were both downregulated in 14-3-3 conditional double (ζ/ε) KO embryonic cortical derived neurospheres compared to WT (Toyo-oka et al., 2014). Moreover, 14-3-3ζ was shown to directly interact with β-catenin in intestinal stem cells, resulting in its stabilisation and enhancing it transactivation action (Tian et al., 2004). Future studies are needed to identify cellular and molecular mechanisms by which 14-3-3ζ controls the developmental decisions made at distinct stages of neurogenesis (Figure 5.10). It has been reported that DISC1 directly interacts with GSK-3β to inhibit its activity leading to reduced β-catenin phosphorylation and stabilization, thereby promoting neural progenitor proliferation (Mao et al., 2009). Therefore, during neural stem proliferation 14-3-3 may potentially act through the GSK-3β/β-catenin signalling pathway by either direct interaction with β-catenin or GSK-3β or indirectly through interactions with DISC1, given that it has been previously shown to interact with DISC1 (Cheah et al., 2012). We also need to have a better understanding between the relationships of

adult hippocampal neurogenesis and cognitive outcome. Future studies should also look at neurogenesis in other brain regions, i.e. SVZ of the lateral ventricles.

In summary, this study presents *in vitro* and *in vivo* evidence revealing a novel role for 14-3-3ζ in hippocampal embryonic, postnatal and adult neurogenesis. Thus, 14-3-3ζ KO mice are an appropriate animal model that would enables in depth investigation of crippling diseases with neurodevelopmental origin, such as schizophrenia, and offer potential avenues for therapeutic intervention. For example, induction neurogenesis may be sufficient to rescue the cognitive impairment associated with neuropsychiatric disorders. There is still a lot to learn about factors regulating neurogenesis and how neurogenesis is affect throughout the course of neuropsychiatric illness such as schizophrenia (Allen et al., 2015).

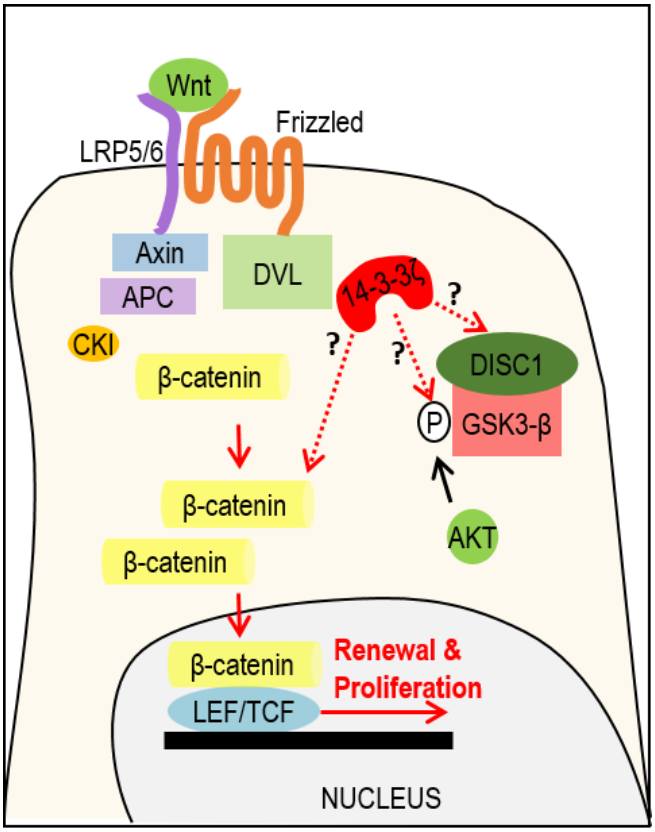

Figure 5. 10: A model for the stabilization mechanism of β-catenin by 14-3-3ζ to regulate neural stem/progenitor proliferation.

14-3-3ζ may enhance β-catenin stabilisation through direct interaction or through maintenance of GSK-3β in a phosphorylated form. Alternatively, it may interact indirectly through DISC1 in maintaining GSK-3β phosphorylation. Red broken arrows represent potential 14-3-3ζ function; red arrows represent positive function; black arrows represent negative function.

Chapter Six:

General Discussion and Conclusion

6.1 Discussion

The anatomy of the hippocampus complements its function, and its disruption contributes to several neurological diseases such as Alzheimer's disease, epilepsy, depression and schizophrenia (Tamminga et al., 2010). Although there is extensive evidence regarding schizophrenia susceptibility genes, the precise cellular and molecular underpinnings of the disease remain unclear. Recently, 14-3-3ζ has been associated with schizophrenia at the genetic, mRNA and protein level (discussed in section 1.2.2). Therefore, in hope of shedding light on the aetiology of schizophrenia and related neurodevelopmental disorders, this thesis assessed the neurodevelopment and neurobiology of the hippocampus in the absence of 14-3-3ζ, and the cellular and molecular mechanisms through which 14-3-3ζ may control hippocampal development and function.

Hippocampal development proceeds through a series of well characterised stages (section 1.3.2) involving: 1) proliferation of neural stem precursor cells that give rise to immature neurons which migrate to their allocated position within the hippocampal plate, 2) differentiation and specialisation of neurons, and 3) maturation of neurons into functional networks. The birth-date of each neuron determines its final position within the hippocampal layers, therefore the timing of neurogenesis contributes to their identity (Belvindrah et al., 2014). Schizophrenia patients have been reported to have reduced hippocampal volume (Nelson et al., 1998, Shenton et al., 2001), correlating with the degree of cognitive dysfunction (Gur et al., 2000, Sanfilipo et al., 2002). Moreover, post-mortem schizophrenia brain samples were reported to display significant reduction in hippocampal cell

proliferation and neurogenesis (Allen et al., 2015, Reif et al., 2006, Reif et al., 2007). Schizophrenia is a complex heterogeneous disorder with different subtypes where the onset of clinical symptoms can arise during early developmental stages or later during adulthood (Lewis and Levitt, 2002, Ross et al., 2006). Based on the current studies and heterogeneity between schizophrenia patients, the neuropathology of the disease may arise from disruptions of early patterning and neurogenesis or neuronal functioning during postnatal stages. Data presented here demonstrate that 14-3-3ζ is required at multiple stages of hippocampal development including the processes of neurogenesis, migration, maturation and integration into functional networks.

Analyses of 14-3-3ζ KO in three independent mouse backgrounds, presented in chapter 3, demonstrated that the hippocampal lamination defects observed in Cheah et al. (2012) resulted from 14-3-3ζ deficiency and not from epistatic interaction with other genetic variation within the 129/sv background. These defects were characterised by a bilaminar distribution of pyramidal cells in CA3, ectopically positioned pyramidal neurons at the stratum oriens, diffusely packed DG granule cells, reduced DG size and aberrant DG structure (Figure 3.1). The hippocampal lamination defects in the 14-3-3ζ KO mice were akin to those seen in 14-3-3ε, Ndel1 and Lis1 deficient mice (Fleck et al., 2000, Hirotsune et al., 1998, Sasaki et al., 2005, Toyo-oka et al., 2003). However, additional hippocampal lamination defects seen in the CA1 region of 14-3-3ε, Ndel1 and Lis1 deficient mice such as fragmentation, bilaminar layering and ectopically positioned pyramidal neurons were absent in 14-3-3ζ KO mice (Fleck et al., 2000, Hirotsune et al., 1998, Sasaki et al., 2005, Toyo-oka et al., 2003). From a developmental point of view,

migration of CA3 cells is more complex than CA1 as they are required to migrate curved routes involving additional modes of migration and therefore may require additional cellular and molecular mechanisms (Belvindrah et al., 2014). Therefore, 14-3-3ζ may be more important in CA3 cell migration compared to CA1 cells.

Several studies have shown that disruption of molecules within the neuronal migration pathway lead to hippocampal lamination defects (section 1.6.1). Work undertaken in chapter 4 demonstrated an important role for 14-3-3ζ in proper neuronal migration (Figure 4.2) and nucleus-centrosome coupling (Figure 4.5). The role for 14-3-3ζ in neuronal migration was also found to be dose-dependent, similar to that reported for 14-3-3ε, Ndel1 and Lis1 (Gambello et al., 2003, Hirotsune et al., 1998, Sasaki et al., 2000, Tanaka et al., 2004a, Toyo-oka et al., 2003, Youn et al., 2009, Shu et al., 2004). My investigations into the molecular mechanisms through which 14-3-3ζ may control neuronal migration identified direct interaction with Cdk5/p35 phosphorylated Ndel1 (Figures 4.6). Given that the interaction between 14-3-3ζ and Ndel1 was dependent on Ndel1 phosphorylation and that Ndel1 phosphorylation is misregulated in the hippocampus of 14-3-3ζ KO mice, my data suggest that in normal circumstances 14-3-3ζ acts to maintain Ndel1 phosphorylation (Figures 4.8) and protect its dephosphorylation by phosphatases such as PP2A (Figures 4.7). Double KO of 14-3-3ζ and 14-3-3ε leads to severe cortical defects (Toyo-oka et al., 2014) compared to the single KO mice. Given that 14-3-3ε only functions as a heterodimer (Gardino et al., 2006) and plays a role in neuronal migration (Toyo-oka et al., 2003), this suggests that 14-3-3ζ may heterodimerise with 14-3-3ε to provide part of the

molecular machinery controlling neuronal migration and lamination within several brain structures, such as the hippocampus and cortex.

Abnormalities in mossy fibre connectivity are often correlated with aberrant hippocampal lamination (Belvindrah et al., 2014) which was also apparent in 14-3-3ζ KO mice. The integration of granular cell mossy fibres into the hippocampal circuitry of 14-3-3ζ KO mice was perturbed, affecting both synaptic input as indicated by reduced dendritic spine numbers (Figures 3.9 & 3.10), and synaptic output as indicated by aberrant mossy fibre projections (Figures 3.2) and reduced thorny excrescences on CA3 neurons (Cheah et al., 2012). Establishment of functional hippocampal circuitry requires proper synapse formation and therefore reduced dendritic spines would likely result in memory deficit in individual mice. In support of this notion, cognitive defects in learning and memory are one of the hallmark features of 14-3-3ζ KO mice in both the 129/sv and BALB/c backgrounds (Cheah et al., 2012, Xu et al., 2015).

Disruption at any stage of hippocampal neuron development can adversely affect another. For example, perturbed neural stem proliferation during embryonic neurogenesis can impact the timing of neuronal migration leading to mispositioning of neurons having functional implications. Using neurosphere assays, it was demonstrated in chapter 5 that 14-3-3ζ KO leads to reduced embryonic neural stem/progenitor cell proliferation and self-renewal (Figures 5.2-5.4). The latter was also observed in the 14-3-3ζ KO hippocampal DG where reduced cell proliferation was consistently seen in all ages examined (Figures 5.6). Given that the role of 14-3-3ζ in hippocampal neurogenesis is novel, there is still a

lot to learn about the cellular and molecular mechanism by which it regulates neurogenesis and what effects its deficiency at this stage of development have on later developmental stages and how these may be involved in the progression of diseases such as schizophrenia.

6.2 Future studies and conclusion

Given the complex genetic foundations and variable clinical phenotype to schizophrenia it is unrealistic that any animal could replicate the disorder in its entirety. The most rational approach to establishing face, construct and predictive validity (section 1.4.1) in animal model of this disorder is to focus on the most replicated symptoms (behavioural, structural and molecular components). In addition to recent publications from our laboratory, the work presented here identifies 14-3-3ζ KO mice as a robust model of schizophrenia as they fulfil many of these criteria. Face validity for positive and cognitive symptoms of schizophrenia were evident from deficits in prepulse inhibition (Cheah et al., 2012), spatial learning and memory (Cheah et al., 2012, Xu et al., 2015), and sensitivity to psychostimulant amphetamine (Ramshaw et al., 2013). Construct validity is met in terms of neuroanatomical alterations such as hippocampal neuronal disorganization, enlarged ventricles, decreased synaptic connections and locomotor hyperactivity arising from neurotransmitter changes (Cheah et al., 2012, Xu et al., 2015). Moreover, administration of the antipsychotic drug clozapine reversed the locomotor hyperactivity of 14-3-3ζ KO mice (Ramshaw et al., 2013) therefore providing evidence of predictive validity.

14-3-3 proteins are important for a variety of critical cellular processes and hence, future studies should include use of more sophisticated genetic manipulation such as conditional knockout only targeting the hippocampus and at different stages of development. The latter would help enhance the validity of the model and understanding of the neuropathology of schizophrenia. Our laboratory

has recently generated conditional 14-3-3ζ KO mice, where preliminary analysis showed hippocampal lamination defects when crossed to a ubiquitous Cre driver (unpublished). It would now be of interest to determine if the behavioural and cognitive defects are also present in these mice. Moreover, it will be imperative to determine the implications of removing 14-3-3ζ in the hippocampus at later stages of brain development, or in adulthood, to address if any of the schizophrenia-like deficiencies are also modelled in these mice.

In summary, data presented here illustrate that 14-3-3ζ crucially regulates multiple processes of brain development, which likely underpin aspects of the clinical presentations of schizophrenia. At a cellular level 14-3-3ζ deficiency led to defects in neural stem cells proliferation and self-renewal, neurogenesis, neuronal migration, nucleus-centrosome coupling, dendritic spine formation and mossy fibre axonal navigation. 14-3-3 proteins have many binding partners and their deficiency can adversely affect multiple signalling pathways which may lead to the development of schizophrenia, making it a central player in its neuropathology.

References

AITKEN, A., COLLINGE, D. B., VAN HEUSDEN, B. P., ISOBE, T., ROSEBOOM, P. H., ROSENFELD, G. & SOLL, J. 1992. 14-3-3 proteins: a highly conserved, widespread family of eukaryotic proteins. *Trends in biochemical sciences,* 17**,** 498-501.

AITKEN, A., HOWELL, S., JONES, D., MADRAZO, J. & PATEL, Y. 1995. 14-3-3 alpha and delta are the phosphorylated forms of raf-activating 14-3-3 beta and zeta. In vivo stoichiometric phosphorylation in brain at a Ser-Pro-Glu-Lys MOTIF. *The Journal of biological chemistry,* 270**,** 5706-9.

ALLEN, K. M., FUNG, S. J. & SHANNON WEICKERT, C. 2015. Cell proliferation is reduced in the hippocampus in schizophrenia. *Aust N Z J Psychiatry*.

ANGRAND, P. O., SEGURA, I., VOLKEL, P., GHIDELLI, S., TERRY, R., BRAJENOVIC, M., VINTERSTEN, K., KLEIN, R., SUPERTI-FURGA, G., DREWES, G., KUSTER, B., BOUWMEESTER, T. & ACKER-PALMER, A. 2006. Transgenic mouse proteomics identifies new 14-3-3-associated proteins involved in cytoskeletal rearrangements and cell signaling. *Mol Cell Proteomics,* 5**,** 2211-27.

ARIMURA, N. & KAIBUCHI, K. 2007. Neuronal polarity: from extracellular signals to intracellular mechanisms. *Nat Rev Neurosci,* 8**,** 194-205.

BAXTER, H. C., FRASER, J. R., LIU, W. G., FORSTER, J. L., CLOKIE, S., STEINACKER, P., OTTO, M., BAHN, E., WILTFANG, J. & AITKEN, A. 2002. Specific 14-3-3 isoform detection and immunolocalization in prion diseases. *Biochemical Society transactions,* 30**,** 387-91.

BELVINDRAH, R., NOSTEN-BERTRAND, M. & FRANCIS, F. 2014. Neuronal migration and its disorders affecting the CA3 region. *Front Cell Neurosci,* 8**,** 63.

BERG, D., HOLZMANN, C. & RIESS, O. 2003. 14-3-3 proteins in the nervous system. *Nat Rev Neurosci,* 4**,** 752-62.

BOSTON, P. F., JACKSON, P. & THOMPSON, R. J. 1982. Human 14-3-3 protein: radioimmunoassay, tissue distribution, and cerebrospinal fluid levels in patients with neurological disorders. *Journal of neurochemistry,* 38**,** 1475-82.

BRADSHAW, N. J. & PORTEOUS, D. J. 2010. DISC1-binding proteins in neural development, signalling and schizophrenia. *Neuropharmacology*.

BRANDON, N. J., HANDFORD, E. J., SCHUROV, I., RAIN, J. C., PELLING, M., DURAN-JIMENIZ, B., CAMARGO, L. M., OLIVER, K. R., BEHER, D., SHEARMAN, M. S. & WHITING, P. J. 2004. Disrupted in Schizophrenia 1 and Nudel form a neurodevelopmentally regulated protein complex: implications for schizophrenia and other major neurological disorders. *Mol Cell Neurosci,* 25**,** 42-55.

BRODKIN, E. S. 2007. BALB/c mice: low sociability and other phenotypes that may be relevant to autism. *Behav Brain Res,* 176**,** 53-65.

BURDICK, K. E., KAMIYA, A., HODGKINSON, C. A., LENCZ, T., DEROSSE, P., ISHIZUKA, K., ELASHVILI, S., ARAI, H., GOLDMAN, D., SAWA, A. & MALHOTRA, A. K. 2008. Elucidating the relationship between DISC1, NDEL1 and NDE1 and the risk for schizophrenia: evidence of epistasis and competitive binding. *Hum Mol Genet,* 17**,** 2462-73.

CAMARGO, L. M., COLLURA, V., RAIN, J. C., MIZUGUCHI, K., HERMJAKOB, H., KERRIEN, S., BONNERT, T. P., WHITING, P. J. & BRANDON, N. J. 2007. Disrupted in Schizophrenia 1 Interactome: evidence for the close connectivity of risk genes and a potential synaptic basis for schizophrenia. *Mol Psychiatry,* 12**,** 74-86.

CHALFIN, L., DAYAN, M., LEVY, D. R., AUSTAD, S. N., MILLER, R. A., IRAQI, F. A., DULAC, C. & KIMCHI, T. 2014. Mapping ecologically relevant social behaviours by gene knockout in wild mice. *Nat Commun,* 5**,** 4569.

CHANG, T. C., LIU, C. C., HSING, E. W., LIANG, S. M., CHI, Y. H., SUNG, L. Y., LIN, S. P., SHEN, T. L., KO, B. S., YEN, B. L., YET, S. F., WU, K. K. & LIOU, J. Y. 2012. 14-3-3sigma regulates beta-catenin-mediated mouse embryonic stem cell proliferation by sequestering GSK-3beta. *PLoS One,* 7**,** e40193.

CHEAH, P. S., RAMSHAW, H. S., THOMAS, P. Q., TOYO-OKA, K., XU, X., MARTIN, S., COYLE, P., GUTHRIDGE, M. A., STOMSKI, F., VAN DEN BUUSE, M., WYNSHAW-BORIS, A., LOPEZ, A. F. & SCHWARZ, Q. P. 2012. Neurodevelopmental and neuropsychiatric behaviour defects arise from 14-3-3zeta deficiency. *Mol Psychiatry,* 17**,** 451-66.

CHEN, Y., BALASUBRAMANIYAN, V., PENG, J., HURLOCK, E. C., TALLQUIST, M., LI, J. & LU, Q. R. 2007. Isolation and culture of rat and mouse oligodendrocyte precursor cells. *Nat Protoc,* 2**,** 1044-51.

CHEN, Y., REX, C. S., RICE, C. J., DUBE, C. M., GALL, C. M., LYNCH, G. & BARAM, T. Z. 2010. Correlated memory defects and hippocampal dendritic spine loss after acute stress involve corticotropin-releasing hormone signaling. *Proc Natl Acad Sci U S A,* 107**,** 13123-8.

CLAPCOTE, S. J., LIPINA, T. V., MILLAR, J. K., MACKIE, S., CHRISTIE, S., OGAWA, F., LERCH, J. P., TRIMBLE, K., UCHIYAMA, M., SAKURABA, Y., KANEDA, H., SHIROISHI, T., HOUSLAY, M. D., HENKELMAN, R. M., SLED, J. G., GONDO, Y., PORTEOUS, D. J. & RODER, J. C. 2007. Behavioral phenotypes of Disc1 missense mutations in mice. *Neuron,* 54**,** 387-402.

CRUSIO, W. E. & SCHWEGLER, H. 2005. Learning spatial orientation tasks in the radial-maze and structural variation in the hippocampus in inbred mice. *Behav Brain Funct,* 1**,** 3.

DANGLOT, L., TRILLER, A. & MARTY, S. 2006. The development of hippocampal interneurons in rodents. *Hippocampus,* 16**,** 1032-60.

DEPHOURE, N., GOULD, K. L., GYGI, S. P. & KELLOGG, D. R. 2013. Mapping and analysis of phosphorylation sites: a quick guide for cell biologists. *Mol Biol Cell,* 24**,** 535-42.

DOTTI, C. G., SULLIVAN, C. A. & BANKER, G. A. 1988. The establishment of polarity by hippocampal neurons in culture. *J Neurosci,* 8**,** 1454-68.

DOUGHERTY, M. K. & MORRISON, D. K. 2004. Unlocking the code of 14-3-3. *Journal of cell science,* 117**,** 1875-84.

ENGLISH, J. A., DICKER, P., FOCKING, M., DUNN, M. J. & COTTER, D. R. 2009. 2-D DIGE analysis implicates cytoskeletal abnormalities in psychiatric disease. *Proteomics,* 9**,** 3368-82.

ENGLISH, J. A., PENNINGTON, K., DUNN, M. J. & COTTER, D. R. 2011. The neuroproteomics of schizophrenia. *Biol Psychiatry,* 69**,** 163-72.

FENG, Y., OLSON, E. C., STUKENBERG, P. T., FLANAGAN, L. A., KIRSCHNER, M. W. & WALSH, C. A. 2000. LIS1 regulates CNS lamination by interacting with mNudE, a central component of the centrosome. *Neuron,* 28**,** 665-79.

FENG, Y. & WALSH, C. A. 2001. Protein-protein interactions, cytoskeletal regulation and neuronal migration. *Nat Rev Neurosci,* 2**,** 408-16.

FENG, Y. & WALSH, C. A. 2004. Mitotic spindle regulation by Nde1 controls cerebral cortical size. *Neuron,* 44**,** 279-93.

FLECK, M. W., HIROTSUNE, S., GAMBELLO, M. J., PHILLIPS-TANSEY, E., SUARES, G., MERVIS, R. F., WYNSHAW-BORIS, A. & MCBAIN, C. J. 2000. Hippocampal abnormalities and enhanced excitability in a murine model of human lissencephaly. *J Neurosci,* 20**,** 2439-50.

FLYNN, K. C. 2013. The cytoskeleton and neurite initiation. *Bioarchitecture,* 3**,** 86-109.

FOCKING, M., DICKER, P., ENGLISH, J. A., SCHUBERT, K. O., DUNN, M. J. & COTTER, D. R. 2011. Common proteomic changes in the hippocampus in schizophrenia and bipolar disorder and particular evidence for involvement of cornu ammonis regions 2 and 3. *Arch Gen Psychiatry,* 68**,** 477-88.

FROMER, M., POCKLINGTON, A. J., KAVANAGH, D. H., WILLIAMS, H. J., DWYER, S., GORMLEY, P., GEORGIEVA, L., REES, E., PALTA, P., RUDERFER, D. M., CARRERA, N., HUMPHREYS, I., JOHNSON, J. S., ROUSSOS, P., BARKER, D. D., BANKS, E., MILANOVA, V., GRANT, S. G., HANNON, E., ROSE, S. A., CHAMBERT, K., MAHAJAN, M., SCOLNICK, E. M., MORAN, J. L., KIROV, G., PALOTIE, A., MCCARROLL, S. A., HOLMANS, P., SKLAR, P., OWEN, M. J., PURCELL, S. M. & O'DONOVAN, M. C. 2014. De novo mutations in schizophrenia implicate synaptic networks. *Nature,* 506**,** 179-84.

FU, H., SUBRAMANIAN, R. R. & MASTERS, S. C. 2000. 14-3-3 proteins: structure, function, and regulation. *Annu Rev Pharmacol Toxicol,* 40**,** 617-47.

GAGE, G. J., KIPKE, D. R. & SHAIN, W. 2012. Whole animal perfusion fixation for rodents. *J Vis Exp*.

GAMBELLO, M. J., DARLING, D. L., YINGLING, J., TANAKA, T., GLEESON, J. G. & WYNSHAW-BORIS, A. 2003. Multiple dose-dependent effects of Lis1 on cerebral cortical development. *J Neurosci,* 23**,** 1719-29.

GARDINO, A. K., SMERDON, S. J. & YAFFE, M. B. 2006. Structural determinants of 14-3-3 binding specificities and regulation of subcellular localization of 14-3-3-ligand complexes: a comparison of the X-ray crystal structures of all human 14-3-3 isoforms. *Seminars in cancer biology,* 16**,** 173-82.

GEHLER, S., SHAW, A. E., SARMIERE, P. D., BAMBURG, J. R. & LETOURNEAU, P. C. 2004. Brain-derived neurotrophic factor regulation of retinal growth cone filopodial dynamics is mediated through actin depolymerizing factor/cofilin. *J Neurosci,* 24**,** 10741-9.

GEIGER, J. C., LIPKA, J., SEGURA, I., HOYER, S., SCHLAGER, M. A., WULF, P. S., WEINGES, S., DEMMERS, J., HOOGENRAAD, C. C. & ACKER-PALMER, A. 2014. The GRIP1/14-3-3 pathway coordinates cargo trafficking and dendrite development. *Dev Cell,* 28**,** 381-93.

GIACHINO, C., BASAK, O. & TAYLOR, V. 2009. Isolation and manipulation of mammalian neural stem cells in vitro. *Methods Mol Biol,* 482**,** 143-58.

GOHLA, A. & BOKOCH, G. M. 2002. 14-3-3 regulates actin dynamics by stabilizing phosphorylated cofilin. *Curr Biol,* 12**,** 1704-10.

GRAESER, R., GANNON, J., POON, R. Y., DUBOIS, T., AITKEN, A. & HUNT, T. 2002. Regulation of the CDK-related protein kinase PCTAIRE-1 and its possible role in neurite outgrowth in Neuro-2A cells. *J Cell Sci,* 115**,** 3479-90.

GUR, R. E., TURETSKY, B. I., COWELL, P. E., FINKELMAN, C., MAANY, V., GROSSMAN, R. I., ARNOLD, S. E., BILKER, W. B. & GUR, R. C. 2000. Temporolimbic volume reductions in schizophrenia. *Arch Gen Psychiatry,* 57**,** 769-75.

HARDOUIN, S. N. & NAGY, A. 2000. Mouse models for human disease. *Clin Genet,* 57**,** 237-44.

HARRISON, P. J. 2004. The hippocampus in schizophrenia: a review of the neuropathological evidence and its pathophysiological implications. *Psychopharmacology (Berl),* 174**,** 151-62.

HAYASHI, K., KUBO, K., KITAZAWA, A. & NAKAJIMA, K. 2015. Cellular dynamics of neuronal migration in the hippocampus. *Front Neurosci,* 9**,** 135.

HEVERIN, M., BRENNAN, G. P., KOEHLER, C. J., TREUMANN, A. & HENSHALL, D. C. 2012. Proteomic analysis of 14-3-3 zeta binding proteins in the mouse hippocampus. *Int J Physiol Pathophysiol Pharmacol,* 4**,** 74-83.

HIPPENMEYER, S., YOUN, Y. H., MOON, H. M., MIYAMICHI, K., ZONG, H., WYNSHAW-BORIS, A. & LUO, L. 2010. Genetic Mosaic Dissection of Lis1 and Ndel1 in Neuronal Migration. *Neuron,* 68**,** 695-709.

HIROKAWA, N. & TAKEMURA, R. 2005. Molecular motors and mechanisms of directional transport in neurons. *Nat Rev Neurosci,* 6**,** 201-14.

HIROTSUNE, S., FLECK, M. W., GAMBELLO, M. J., BIX, G. J., CHEN, A., CLARK, G. D., LEDBETTER, D. H., MCBAIN, C. J. & WYNSHAW-BORIS, A. 1998. Graded reduction of Pafah1b1 (Lis1) activity results in neuronal migration defects and early embryonic lethality. *Nat Genet,* 19**,** 333-9.

HIRSCH, S., AITKEN, A., BERTSCH, U. & SOLL, J. 1992. A plant homologue to mammalian brain 14-3-3 protein and protein kinase C inhibitor. *FEBS letters,* 296**,** 222-4.

HOOGENRAAD, C. C., MILSTEIN, A. D., ETHELL, I. M., HENKEMEYER, M. & SHENG, M. 2005. GRIP1 controls dendrite morphogenesis by regulating EphB receptor trafficking. *Nat Neurosci,* 8**,** 906-15.

HUMPHRIES, M. J. 2009. Cell adhesion assays. *Methods Mol Biol,* 522**,** 203-10.

ICHIMURA, T., ISOBE, T., OKUYAMA, T., TAKAHASHI, N., ARAKI, K., KUWANO, R. & TAKAHASHI, Y. 1988. Molecular cloning of cDNA coding for brain-specific 14-3-3 protein, a protein kinase-dependent activator of tyrosine and tryptophan hydroxylases. *Proceedings of the National Academy of Sciences of the United States of America,* 85**,** 7084-8.

IKEDA, M., HIKITA, T., TAYA, S., URAGUCHI-ASAKI, J., TOYO-OKA, K., WYNSHAW-BORIS, A., UJIKE, H., INADA, T., TAKAO, K., MIYAKAWA, T., OZAKI, N., KAIBUCHI, K. & IWATA, N. 2008. Identification of YWHAE, a gene encoding 14-3-3epsilon, as a possible susceptibility gene for schizophrenia. *Hum Mol Genet,* 17**,** 3212-22.

JAARO-PELED, H., AYHAN, Y., PLETNIKOV, M. V. & SAWA, A. 2010. Review of pathological hallmarks of schizophrenia: comparison of genetic models with patients and nongenetic models. *Schizophr Bull,* 36**,** 301-13.

JAEHNE, E. J., RAMSHAW, H., XU, X., SALEH, E., CLARK, S. R., SCHUBERT, K. O., LOPEZ, A., SCHWARZ, Q. & BAUNE, B. T. 2015. In-vivo administration of clozapine affects behaviour but does not reverse dendritic spine deficits in the 14-3-3zeta KO mouse model of schizophrenia-like disorders. *Pharmacol Biochem Behav,* 138**,** 1-8.

JAN, Y. N. & JAN, L. Y. 2010. Branching out: mechanisms of dendritic arborization. *Nat Rev Neurosci,* 11**,** 316-28.

JIA, Y., YU, X., ZHANG, B., YUAN, Y., XU, Q. & SHEN, Y. 2004. An association study between polymorphisms in three genes of 14-3-3 (tyrosine 3-monooxygenase/tryptophan 5-monooxygenase activation protein) family and paranoid schizophrenia in northern Chinese population. *Eur Psychiatry,* 19**,** 377-9.

JIANG, X. & NARDELLI, J. 2015. Cellular and molecular introduction to brain development. *Neurobiol Dis*.

JIN, Y., DAI, M. S., LU, S. Z., XU, Y., LUO, Z., ZHAO, Y. & LU, H. 2006. 14-3-3gamma binds to MDMX that is phosphorylated by UV-activated Chk1, resulting in p53 activation. *EMBO J,* 25**,** 1207-18.

JOHNSON, C., CROWTHER, S., STAFFORD, M. J., CAMPBELL, D. G., TOTH, R. & MACKINTOSH, C. 2010. Bioinformatic and experimental survey of 14-3-3-binding sites. *Biochem J,* 427**,** 69-78.

JOHNSON, M. 2012. Laboratory Mice and Rats. *Mater Methods,* 2**,** 113.

JOHNSTONE, M., THOMSON, P. A., HALL, J., MCINTOSH, A. M., LAWRIE, S. M. & PORTEOUS, D. J. 2011. DISC1 in schizophrenia: genetic mouse models and human genomic imaging. *Schizophr Bull,* 37**,** 14-20.

JONES, C. A., WATSON, D. J. & FONE, K. C. 2011. Animal models of schizophrenia. *Br J Pharmacol,* 164**,** 1162-94.

KAECH, S. & BANKER, G. 2006. Culturing hippocampal neurons. *Nat Protoc,* 1**,** 2406-15.

KAJIWARA, Y., BUXBAUM, J. D. & GRICE, D. E. 2009. SLITRK1 binds 14-3-3 and regulates neurite outgrowth in a phosphorylation-dependent manner. *Biol Psychiatry,* 66**,** 918-25.

KEAYS, D. A. 2007. Neuronal migration: unraveling the molecular pathway with humans, mice, and a fungus. *Mamm Genome,* 18**,** 425-30.

KHALAF-NAZZAL, R. & FRANCIS, F. 2013. Hippocampal development - old and new findings. *Neuroscience,* 248**,** 225-42.

KIRYUSHKO, D., BEREZIN, V. & BOCK, E. 2004. Regulators of neurite outgrowth: role of cell adhesion molecules. *Ann N Y Acad Sci,* 1014**,** 140-54.

KNOLL, B., KRETZ, O., FIEDLER, C., ALBERTI, S., SCHUTZ, G., FROTSCHER, M. & NORDHEIM, A. 2006. Serum response factor controls neuronal circuit assembly in the hippocampus. *Nat Neurosci,* 9**,** 195-204.

KOIKE, H., ARGUELLO, P. A., KVAJO, M., KARAYIORGOU, M. & GOGOS, J. A. 2006. Disc1 is mutated in the 129S6/SvEv strain and modulates working memory in mice. *Proceedings of the National Academy of Sciences of the United States of America,* 103**,** 3693-7.

KOLESKE, A. J. 2013. Molecular mechanisms of dendrite stability. *Nat Rev Neurosci,* 14**,** 536-50.

KOLOMEETS, N. S., ORLOVSKAYA, D. D. & URANOVA, N. A. 2007. Decreased numerical density of CA3 hippocampal mossy fiber synapses in schizophrenia. *Synapse,* 61**,** 615-21.

KULKARNI, V. A. & FIRESTEIN, B. L. 2012. The dendritic tree and brain disorders. *Mol Cell Neurosci,* 50**,** 10-20.

LAMBERT DE ROUVROIT, C. & GOFFINET, A. M. 2001. Neuronal migration. *Mech Dev,* 105**,** 47-56.

LAYFIELD, R., FERGUSSON, J., AITKEN, A., LOWE, J., LANDON, M. & MAYER, R. J. 1996. Neurofibrillary tangles of Alzheimer's disease brains contain 14-3-3 proteins. *Neuroscience letters,* 209**,** 57-60.

LEWIS, D. A. & LEVITT, P. 2002. Schizophrenia as a disorder of neurodevelopment. *Annu Rev Neurosci,* 25**,** 409-32.

LIPSKA, B. K., MITKUS, S. N., MATHEW, S. V., FATULA, R., HYDE, T. M., WEINBERGER, D. R. & KLEINMAN, J. E. 2006. Functional genomics in postmortem human brain: abnormalities in a DISC1 molecular pathway in schizophrenia. *Dialogues Clin Neurosci,* 8**,** 353-7.

LIU, D., BIENKOWSKA, J., PETOSA, C., COLLIER, R. J., FU, H. & LIDDINGTON, R. 1995. Crystal structure of the zeta isoform of the 14-3-3 protein. *Nature,* 376**,** 191-4.

LIU, F., ZHOU, Q., ZHOU, J., SUN, H., WANG, Y., ZOU, X., FENG, L., HOU, Z., ZHOU, A., ZHOU, Y. & LI, Y. 2015. 14-3-3tau promotes surface expression of Cav2.2 (alpha1B) Ca2+ channels. *J Biol Chem,* 290**,** 2689-98.

LUSIS, A. J., YU, J. & WANG, S. S. 2007. The problem of passenger genes in transgenic mice. *Arterioscler Thromb Vasc Biol,* 27**,** 2100-3.

MAO, Y., GE, X., FRANK, C. L., MADISON, J. M., KOEHLER, A. N., DOUD, M. K., TASSA, C., BERRY, E. M., SODA, T., SINGH, K. K., BIECHELE, T., PETRYSHEN, T. L., MOON, R. T., HAGGARTY, S. J. & TSAI, L. H. 2009. Disrupted in schizophrenia 1 regulates neuronal progenitor proliferation via modulation of GSK3beta/beta-catenin signaling. *Cell,* 136**,** 1017-31.

MARIN, O., VALIENTE, M., GE, X. & TSAI, L. H. 2010. Guiding neuronal cell migrations. *Cold Spring Harb Perspect Biol,* 2**,** a001834.

MARTIN, H., PATEL, Y., JONES, D., HOWELL, S., ROBINSON, K. & AITKEN, A. 1993. Antibodies against the major brain isoforms of 14-3-3 protein: an antibody specific for the N-acetylated amino-terminus of a protein. *FEBS letters,* 336**,** 189.

MARZINKE, M. A., MAVENCAMP, T., DURATINSKY, J. & CLAGETT-DAME, M. 2013. 14-3-3epsilon and NAV2 interact to regulate neurite outgrowth and axon elongation. *Arch Biochem Biophys,* 540**,** 94-100.

MIDDLETON, F. A., PENG, L., LEWIS, D. A., LEVITT, P. & MIRNICS, K. 2005. Altered expression of 14-3-3 genes in the prefrontal cortex of subjects with schizophrenia. *Neuropsychopharmacology,* 30**,** 974-83.

MING, G. L. & SONG, H. 2011. Adult neurogenesis in the mammalian brain: significant answers and significant questions. *Neuron,* 70**,** 687-702.

MIYAMOTO, S., LAMANTIA, A. S., DUNCAN, G. E., SULLIVAN, P., GILMORE, J. H. & LIEBERMAN, J. A. 2003. Recent advances in the neurobiology of schizophrenia. *Molecular interventions,* 3**,** 27-39.

MOORE, B. W. & PEREZ, V. J. 1967. Specific acidic proteins of the nervous system. . *In Physiological and Biochemical Aspects of Nervous Integration***,** 343-59.

MORI, D., YANO, Y., TOYO-OKA, K., YOSHIDA, N., YAMADA, M., MURAMATSU, M., ZHANG, D., SAYA, H., TOYOSHIMA, Y. Y., KINOSHITA, K., WYNSHAW-BORIS, A. & HIROTSUNE, S. 2007. NDEL1 phosphorylation by Aurora-A kinase is essential for centrosomal maturation, separation, and TACC3 recruitment. *Mol Cell Biol,* 27**,** 352-67.

MWANGI, S., ANITHA, M., FU, H., SITARAMAN, S. V. & SRINIVASAN, S. 2006. Glial cell line-derived neurotrophic factor-mediated enteric neuronal survival involves glycogen synthase kinase-3beta phosphorylation and coupling with 14-3-3. *Neuroscience,* 143**,** 241-51.

NELSON, M. D., SAYKIN, A. J., FLASHMAN, L. A. & RIORDAN, H. J. 1998. Hippocampal volume reduction in schizophrenia as assessed by magnetic resonance imaging: a meta-analytic study. *Arch Gen Psychiatry,* 55**,** 433-40.

NESTLER, E. J. & HYMAN, S. E. 2010. Animal models of neuropsychiatric disorders. *Nature neuroscience,* 13**,** 1161-9.

NIETHAMMER, M., SMITH, D. S., AYALA, R., PENG, J., KO, J., LEE, M. S., MORABITO, M. & TSAI, L. H. 2000. NUDEL is a novel Cdk5 substrate that associates with LIS1 and cytoplasmic dynein. *Neuron,* 28**,** 697-711.

NIMCHINSKY, E. A., SABATINI, B. L. & SVOBODA, K. 2002. Structure and function of dendritic spines. *Annu Rev Physiol,* 64**,** 313-53.

PAUL, C. A., BELTZ, B. & BERGER-SWEENEY, J. 2008. The nissl stain: a stain for cell bodies in brain sections. *CSH Protoc,* 2008**,** pdb prot4805.

PENZES, P., CAHILL, M. E., JONES, K. A., VANLEEUWEN, J. E. & WOOLFREY, K. M. 2011. Dendritic spine pathology in neuropsychiatric disorders. *Nat Neurosci,* 14**,** 285-93.

PILATI, N., BARKER, M., PANTELEIMONITIS, S., DONGA, R. & HAMANN, M. 2008. A rapid method combining Golgi and Nissl staining to study neuronal morphology and cytoarchitecture. *J Histochem Cytochem,* 56**,** 539-50.

RAMSER, E. M., BUCK, F., SCHACHNER, M. & TILLING, T. 2010a. Binding of alphaII spectrin to 14-3-3beta is involved in NCAM-dependent neurite outgrowth. *Mol Cell Neurosci,* 45**,** 66-74.

RAMSER, E. M., WOLTERS, G., DITYATEVA, G., DITYATEV, A., SCHACHNER, M. & TILLING, T. 2010b. The 14-3-3zeta protein binds to the cell adhesion molecule L1, promotes L1 phosphorylation by CKII and influences L1-dependent neurite outgrowth. *PLoS One,* 5**,** e13462.

RAMSHAW, H., XU, X., JAEHNE, E. J., MCCARTHY, P., GREENBERG, Z., SALEH, E., MCCLURE, B., WOODCOCK, J., KABBARA, S., WISZNIAK, S., WANG, T. Y., PARISH, C., VAN DEN BUUSE, M., BAUNE, B. T., LOPEZ, A. & SCHWARZ, Q.

2013. Locomotor hyperactivity in 14-3-3zeta KO mice is associated with dopamine transporter dysfunction. *Transl Psychiatry,* 3**,** e327.

REIF, A., FRITZEN, S., FINGER, M., STROBEL, A., LAUER, M., SCHMITT, A. & LESCH, K. P. 2006. Neural stem cell proliferation is decreased in schizophrenia, but not in depression. *Mol Psychiatry,* 11**,** 514-22.

REIF, A., SCHMITT, A., FRITZEN, S. & LESCH, K. P. 2007. Neurogenesis and schizophrenia: dividing neurons in a divided mind? *Eur Arch Psychiatry Clin Neurosci,* 257**,** 290-9.

REINER, O. 2013. LIS1 and DCX: Implications for Brain Development and Human Disease in Relation to Microtubules. *Scientifica (Cairo),* 2013**,** 393975.

REINER, O., CARROZZO, R., SHEN, Y., WEHNERT, M., FAUSTINELLA, F., DOBYNS, W. B., CASKEY, C. T. & LEDBETTER, D. H. 1993. Isolation of a Miller-Dieker lissencephaly gene containing G protein beta-subunit-like repeats. *Nature,* 364**,** 717-21.

RIVERA, J. & TESSAROLLO, L. 2008. Genetic background and the dilemma of translating mouse studies to humans. *Immunity,* 28**,** 1-4.

RONG, J., LI, S., SHENG, G., WU, M., COBLITZ, B., LI, M., FU, H. & LI, X. J. 2007. 14-3-3 protein interacts with Huntingtin-associated protein 1 and regulates its trafficking. *J Biol Chem,* 282**,** 4748-56.

ROSENQUIST, M., ALSTERFJORD, M., LARSSON, C. & SOMMARIN, M. 2001. Data mining the Arabidopsis genome reveals fifteen 14-3-3 genes. Expression is demonstrated for two out of five novel genes. *Plant physiology,* 127**,** 142-9.

ROSS, C. A., MARGOLIS, R. L., READING, S. A., PLETNIKOV, M. & COYLE, J. T. 2006. Neurobiology of schizophrenia. *Neuron,* 52**,** 139-53.

SANFILIPO, M., LAFARGUE, T., RUSINEK, H., ARENA, L., LONERAGAN, C., LAUTIN, A., ROTROSEN, J. & WOLKIN, A. 2002. Cognitive performance in schizophrenia: relationship to regional brain volumes and psychiatric symptoms. *Psychiatry Res,* 116**,** 1-23.

SASAKI, S., MORI, D., TOYO-OKA, K., CHEN, A., GARRETT-BEAL, L., MURAMATSU, M., MIYAGAWA, S., HIRAIWA, N., YOSHIKI, A., WYNSHAW-BORIS, A. & HIROTSUNE, S. 2005. Complete loss of Ndel1 results in neuronal migration defects and early embryonic lethality. *Mol Cell Biol,* 25**,** 7812-27.

SASAKI, S., SHIONOYA, A., ISHIDA, M., GAMBELLO, M. J., YINGLING, J., WYNSHAW-BORIS, A. & HIROTSUNE, S. 2000. A LIS1/NUDEL/cytoplasmic dynein heavy chain complex in the developing and adult nervous system. *Neuron,* 28**,** 681-96.

SCHUBERT, K. O., FOCKING, M. & COTTER, D. R. 2015. Proteomic pathway analysis of the hippocampus in schizophrenia and bipolar affective disorder implicates 14-3-3 signaling, aryl hydrocarbon receptor signaling, and glucose metabolism: Potential roles in GABAergic interneuron pathology. *Schizophr Res,* 167**,** 64-72.

SEABOLD, G. K., DAUNAIS, J. B., RAU, A., GRANT, K. A. & ALVAREZ, V. A. 2010. DiOLISTIC labeling of neurons from rodent and non-human primate brain slices. *J Vis Exp*.

SELLERS, R. S. 2012. The gene or not the gene--that is the question: understanding the genetically engineered mouse phenotype. *Vet Pathol,* 49**,** 5-15.

SETOU, M., SEOG, D. H., TANAKA, Y., KANAI, Y., TAKEI, Y., KAWAGISHI, M. & HIROKAWA, N. 2002. Glutamate-receptor-interacting protein GRIP1 directly steers kinesin to dendrites. *Nature,* 417**,** 83-7.

SHENTON, M. E., DICKEY, C. C., FRUMIN, M. & MCCARLEY, R. W. 2001. A review of MRI findings in schizophrenia. *Schizophr Res,* 49**,** 1-52.

SHOLL, D. A. 1953. Dendritic organization in the neurons of the visual and motor cortices of the cat. *J Anat,* 87**,** 387-406.

SHU, T., AYALA, R., NGUYEN, M. D., XIE, Z., GLEESON, J. G. & TSAI, L. H. 2004. Ndel1 operates in a common pathway with LIS1 and cytoplasmic dynein to regulate cortical neuronal positioning. *Neuron,* 44**,** 263-77.

SIVAGNANASUNDARAM, S., FLETCHER, D., HUBANK, M., ILLINGWORTH, E., SKUSE, D. & SCAMBLER, P. 2007. Differential gene expression in the hippocampus of the Df1/+ mice: a model for 22q11.2 deletion syndrome and schizophrenia. *Brain Res,* 1139**,** 48-59.

SKOULAKIS, E. M. & DAVIS, R. L. 1998. 14-3-3 proteins in neuronal development and function. *Molecular neurobiology,* 16**,** 269-84.

ST CLAIR, D., BLACKWOOD, D., MUIR, W., CAROTHERS, A., WALKER, M., SPOWART, G., GOSDEN, C. & EVANS, H. J. 1990. Association within a family of a balanced autosomal translocation with major mental illness. *Lancet,* 336**,** 13-6.

STILES, J. & JERNIGAN, T. L. 2010. The basics of brain development. *Neuropsychol Rev,* 20**,** 327-48.

SUN, J., JIA, P., FANOUS, A. H., VAN DEN OORD, E., CHEN, X., RILEY, B. P., AMDUR, R. L., KENDLER, K. S. & ZHAO, Z. 2010. Schizophrenia gene networks and pathways and their applications for novel candidate gene selection. *PLoS One,* 5**,** e11351.

TAKAHASHI, Y. 2003. The 14-3-3 proteins: gene, gene expression, and function. *Neurochemical research,* 28**,** 1265-73.

TAMMINGA, C. A., STAN, A. D. & WAGNER, A. D. 2010. The hippocampal formation in schizophrenia. *Am J Psychiatry,* 167**,** 1178-93.

TANAKA, T., SERNEO, F. F., HIGGINS, C., GAMBELLO, M. J., WYNSHAW-BORIS, A. & GLEESON, J. G. 2004a. Lis1 and doublecortin function with dynein to mediate coupling of the nucleus to the centrosome in neuronal migration. *J Cell Biol,* 165**,** 709-21.

TANAKA, T., SERNEO, F. F., TSENG, H. C., KULKARNI, A. B., TSAI, L. H. & GLEESON, J. G. 2004b. Cdk5 phosphorylation of doublecortin ser297 regulates its effect on neuronal migration. *Neuron,* 41**,** 215-27.

TANG, S. J., SUEN, T. C., MCINNES, R. R. & BUCHWALD, M. 1998. Association of the TLX-2 homeodomain and 14-3-3eta signaling proteins. *J Biol Chem,* 273**,** 25356-63.

TAYA, S., SHINODA, T., TSUBOI, D., ASAKI, J., NAGAI, K., HIKITA, T., KURODA, S., KURODA, K., SHIMIZU, M., HIROTSUNE, S., IWAMATSU, A. & KAIBUCHI, K. 2007. DISC1 regulates the transport of the NUDEL/LIS1/14-3-3epsilon complex through kinesin-1. *J Neurosci,* 27**,** 15-26.

TIAN, Q., FEETHAM, M. C., TAO, W. A., HE, X. C., LI, L., AEBERSOLD, R. & HOOD, L. 2004. Proteomic analysis identifies that 14-3-3zeta interacts with beta-catenin and facilitates its activation by Akt. *Proc Natl Acad Sci U S A,* 101**,** 15370-5.

TOMA, C., TORRICO, B., HERVAS, A., VALDES-MAS, R., TRISTAN-NOGUERO, A., PADILLO, V., MARISTANY, M., SALGADO, M., ARENAS, C., PUENTE, X. S., BAYES, M. & CORMAND, B. 2014. Exome sequencing in multiplex autism families suggests a major role for heterozygous truncating mutations. *Mol Psychiatry,* 19**,** 784-90.

TOYO-OKA, K., SASAKI, S., YANO, Y., MORI, D., KOBAYASHI, T., TOYOSHIMA, Y. Y., TOKUOKA, S. M., ISHII, S., SHIMIZU, T., MURAMATSU, M., HIRAIWA, N., YOSHIKI, A., WYNSHAW-BORIS, A. & HIROTSUNE, S. 2005. Recruitment of katanin p60 by phosphorylated NDEL1, an LIS1 interacting protein, is essential for mitotic cell division and neuronal migration. *Human molecular genetics,* 14**,** 3113-28.

TOYO-OKA, K., SHIONOYA, A., GAMBELLO, M. J., CARDOSO, C., LEVENTER, R., WARD, H. L., AYALA, R., TSAI, L. H., DOBYNS, W., LEDBETTER, D., HIROTSUNE, S. & WYNSHAW-BORIS, A. 2003. 14-3-3epsilon is important for neuronal migration by binding to NUDEL: a molecular explanation for Miller-Dieker syndrome. *Nat Genet,* 34**,** 274-85.

TOYO-OKA, K., WACHI, T., HUNT, R. F., BARABAN, S. C., TAYA, S., RAMSHAW, H., KAIBUCHI, K., SCHWARZ, Q. P., LOPEZ, A. F. & WYNSHAW-BORIS, A. 2014. 14-3-3epsilon and zeta regulate neurogenesis and differentiation of neuronal progenitor cells in the developing brain. *J Neurosci,* 34**,** 12168-81.

TSAI, L. H. & GLEESON, J. G. 2005. Nucleokinesis in neuronal migration. *Neuron,* 46**,** 383-8.

URBAN, N. & GUILLEMOT, F. 2014. Neurogenesis in the embryonic and adult brain: same regulators, different roles. *Front Cell Neurosci,* 8**,** 396.

VAN DEN BUUSE, M. 2010. Modeling the positive symptoms of schizophrenia in genetically modified mice: pharmacology and methodology aspects. *Schizophr Bull,* 36**,** 246-70.

VARELA-NALLAR, L. & INESTROSA, N. C. 2013. Wnt signaling in the regulation of adult hippocampal neurogenesis. *Front Cell Neurosci,* 7**,** 100.

VIESSELMANN, C., BALLWEG, J., LUMBARD, D. & DENT, E. W. 2011. Nucleofection and primary culture of embryonic mouse hippocampal and cortical neurons. *J Vis Exp*.

WADE, C. M. & DALY, M. J. 2005. Genetic variation in laboratory mice. *Nat Genet,* 37**,** 1175-80.

WALSH, T., MCCLELLAN, J. M., MCCARTHY, S. E., ADDINGTON, A. M., PIERCE, S. B., COOPER, G. M., NORD, A. S., KUSENDA, M., MALHOTRA, D., BHANDARI, A., STRAY, S. M., RIPPEY, C. F., ROCCANOVA, P., MAKAROV, V., LAKSHMI, B., FINDLING, R. L., SIKICH, L., STROMBERG, T., MERRIMAN, B., GOGTAY, N., BUTLER, P., ECKSTRAND, K., NOORY, L., GOCHMAN, P., LONG, R., CHEN, Z., DAVIS, S., BAKER, C., EICHLER, E. E., MELTZER, P. S., NELSON, S. F., SINGLETON, A. B., LEE, M. K., RAPOPORT, J. L., KING, M. C. & SEBAT, J. 2008. Rare structural variants disrupt multiple genes in neurodevelopmental pathways in schizophrenia. *Science,* 320**,** 539-43.

WANG, W. & SHAKES, D. C. 1996. Molecular evolution of the 14-3-3 protein family. *Journal of molecular evolution,* 43**,** 384-98.

WHO 2008. The global burden of disease: 2004 update. *Geneva, Switerland: World Health Organization Libaray Cataloging-in-Publication Data*.

WILKE, S. A., RAAM, T., ANTONIOS, J. K., BUSHONG, E. A., KOO, E. H., ELLISMAN, M. H. & GHOSH, A. 2014. Specific disruption of hippocampal mossy fiber synapses in a mouse model of familial Alzheimer's disease. *PLoS One,* 9**,** e84349.

WILSON, C. & TERRY, A. V., JR. 2010. Neurodevelopmental animal models of schizophrenia: role in novel drug discovery and development. *Clin Schizophr Relat Psychoses,* 4**,** 124-37.

WONG, A. H., LIKHODI, O., TRAKALO, J., YUSUF, M., SINHA, A., PATO, C. N., PATO, M. T., VAN TOL, H. H. & KENNEDY, J. L. 2005. Genetic and post-mortem mRNA analysis of the 14-3-3 genes that encode phosphoserine/threonine-binding regulatory proteins in schizophrenia and bipolar disorder. *Schizophr Res,* 78**,** 137-46.

WU, Q., LI, Y. & XIAO, B. 2013. DISC1-related signaling pathways in adult neurogenesis of the hippocampus. *Gene,* 518**,** 223-30.

WYNSHAW-BORIS, A. & GAMBELLO, M. J. 2001. LIS1 and dynein motor function in neuronal migration and development. *Genes Dev,* 15**,** 639-51.

XIAO, B., SMERDON, S. J., JONES, D. H., DODSON, G. G., SONEJI, Y., AITKEN, A. & GAMBLIN, S. J. 1995. Structure of a 14-3-3 protein and implications for coordination of multiple signalling pathways. *Nature,* 376**,** 188-91.

XU, X., JAEHNE, E. J., GREENBERG, Z., MCCARTHY, P., SALEH, E., PARISH, C. L., CAMERA, D., HENG, J., HAAS, M., BAUNE, B. T., RATNAYAKE, U., VAN DEN BUUSE, M., LOPEZ, A. F., RAMSHAW, H. S. & SCHWARZ, Q. 2015. 14-3-3zeta deficient mice in the BALB/c background display behavioural and anatomical defects associated with neurodevelopmental disorders. *Sci Rep,* 5**,** 12434.

YOUN, Y. H., PRAMPARO, T., HIROTSUNE, S. & WYNSHAW-BORIS, A. 2009. Distinct dose-dependent cortical neuronal migration and neurite extension defects in Lis1 and Ndel1 mutant mice. *J Neurosci,* 29**,** 15520-30.

YOUNG, J. W., ZHOU, X. & GEYER, M. A. 2010. Animal models of schizophrenia. *Curr Top Behav Neurosci,* 4**,** 391-433.

YUAN, Z., AGARWAL-MAWAL, A. & PAUDEL, H. K. 2004. 14-3-3 binds to and mediates phosphorylation of microtubule-associated tau protein by Ser9-

phosphorylated glycogen synthase kinase 3beta in the brain. *J Biol Chem,* 279**,** 26105-14.

ZENG, C., PAN, F., JONES, L. A., LIM, M. M., GRIFFIN, E. A., SHELINE, Y. I., MINTUN, M. A., HOLTZMAN, D. M. & MACH, R. H. 2010. Evaluation of 5-ethynyl-2'-deoxyuridine staining as a sensitive and reliable method for studying cell proliferation in the adult nervous system. *Brain Res,* 1319**,** 21-32.

Appendix

A.1 General solutions and buffers

General solutions

Solution		Ingredients		Storage
1x PBS (Phosphate-buffer saline)	50ml	1x PBS (Gibco) Baxter water	10ml of 10x 90ml	RT
4% PFA (Paraformaldehyde)	500ml	PFA MilliQ water (heat stir to dissolve)	20g 500ml	-20°C (10ml aliquots)

Staining solutions

Solution		Ingredients		Storage
20% Sucrose solution	10ml	20% Sucrose 1x PBS	2g 10ml	Make fresh (filtered)
10% Tween-20	50ml	10% Tween-20 1x PBS	5ml of 100% 45ml	RT (alfoil covered)
1X PBT	50ml	0.1% Tween-20 1x PBS	1.5ml of 10% 48.5ml	RT
10% Normal goat serum	10ml	10% NGS (Invitrogen) 1x PBT	1ml of 100% 9ml	Make fresh
10% TTX (Trion X-100)	50ml	10% Trion X-100 (Merck) 1x PBS	5ml of 100% 45ml	RT (alfoil covered)
1x PBST	50ml	0.3% TTX 1x PBS	1.5ml of 10% 48.5ml	RT (alfoil covered)

A.2 Genotyping of mice

Mice genotype was determined by PCR amplification of genomic tail DNA or DNA from the E18.5 brains (sections 2.7.1 & 2.7.2). Two PCRs were run one consisting of primers for amplification of the wild type (WT) allele, while the other for the knockout (KO) gene trapped allele (see Table 2.1 for primer sets).

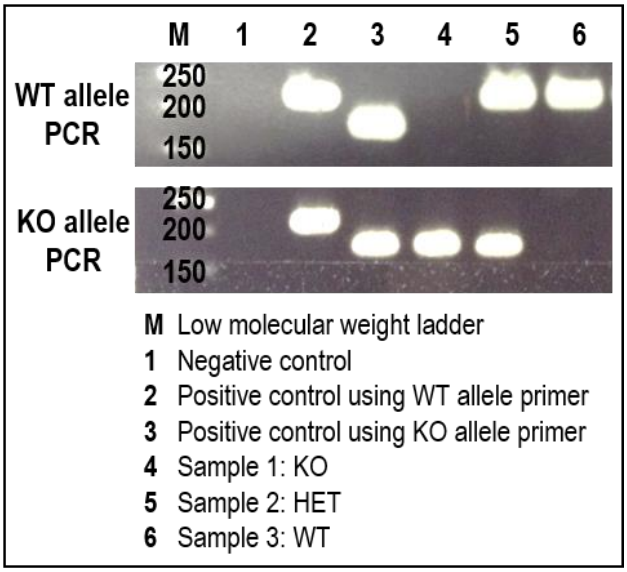

Agarose gel of mice genotyping.
The top gel shows PCR products of WT allele (exception lane 3 which is of KO allele loading control), while the bottom show amplification KO gene trapped allele (exception lane 2 which is of WT allele loading control). The higher band indicates WT allele (288bp), while lower band indicates KO gene trapped allele (165bp).

The above figure shows an example of PCR for identification of the mouse genotype. WT samples show a single 288bp band (lane 6), KO samples show a single 165bp band (lane 4), while HET samples show double bands of 288bp and 165bp (lane 5).

A.3 Hippocampal primary DIV21 neurons for dendritic spine density analysis

Hippocampal neurons isolated from E18.5 14-33ζ WT and KO mice were co-cultured with glia for 21 days *in vitro* (DIV21) (sections 2.51-2.5.5), followed by labelling with lipohilic fluorescent dye using a gene gun approach (section 2.4.4). Dendritic spine density tends to be heavily sensitive to culture conditions and may produce large variability. In my DIV21 (mass) culture system, the individual neurons were innervated by neighbouring cells and therefore cell density had a profound influence on dendritic spine density. Autaptic neuronal cultures, where single isolated cell innervates itself, are commonly used to study dendritic spine density. For future studies of *in vitro* hippocampal dendritic spine density, use of autaptic neuronal cultures may be more appropriate.

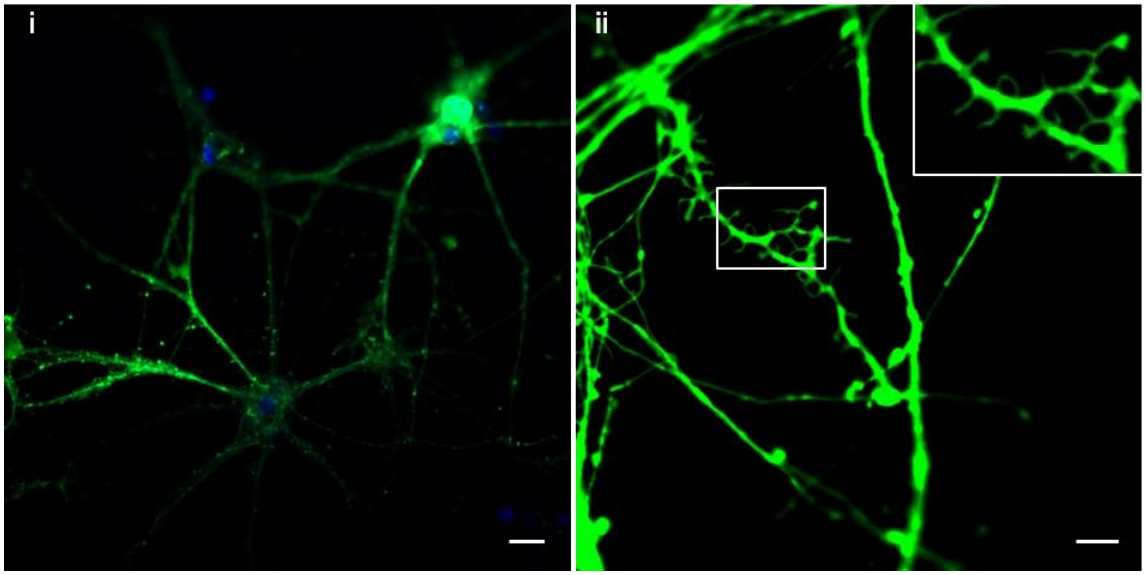

Biolistic labelling of DIV21 hippocampal neurons. (i) Low-magnification image showing DIV21 hippocampal neurons innervating neighbouring cells. The nucleus is labelled with DAPI (blue). Scale bar 20μm. (ii) High magnification of z-stack image of dendritic spines of DIV21 hippocampal neurons. Rectangular box shows zoomed image of dendritic spines. Scale bar 5μm.

A.4 Preliminary analysis of dendritic spine in the 14-3-3ζ KO hippocampus via transmission electron microscopy revealed increase size compared to WT

To examine the dendritic synaptic density and the type of synapses in the CA3 region of the hippocampus a protocol used by Kolomeets et al. (2007) was adapted with a few modifications. Mice were perfuse fixed in a 1:1 ratio of 2% PFA and 2% glutaraldehyde, as described in section 2.3.1. Brains were isolated and postfixed in the same fixative solution for 2-4 days. Coronal sections 1mm and 200μm thick, in sequence, were taken through the anterior part of the hippocampus using a vibratome (section 2.3.3). The 200μm sections were Nissl stained (section 2.4.1) and used as a quick guide to locate the CA3 region. Once the preferred CA3 region was found, a 1x1mm block was dissected from the CA3 region. The blocks were stained in osmium tetroxide and embedded into epoxy-resin. Blocks were semi-thin sectioned (1μm) and stained with 1% toluidine blue to help orient the blocks before final trimming. Blocks were then ultrathin sectioned and placed on carbon-stabilized, formvar-coated copper slot grids. The ultrathin sections were then stained with uranyl acetate and lead citrate before observation under the transmission electron microscope (CM100, Philips) at the Adelaide Microscopy Facility.

Unfortunately, thefollowing transmission electron microscope experiment was not completed due to lack of time. However, even with the small amount of staining that I was able to complete I noticed that 14-3-3ζ KO leads to an increase in dendritic spine size in the hippocampus compared to WT. It would be of interest to determine if there was a difference in excitatory or inhibitory synapses in the 14-3-3ζ KO mice compare to WT.

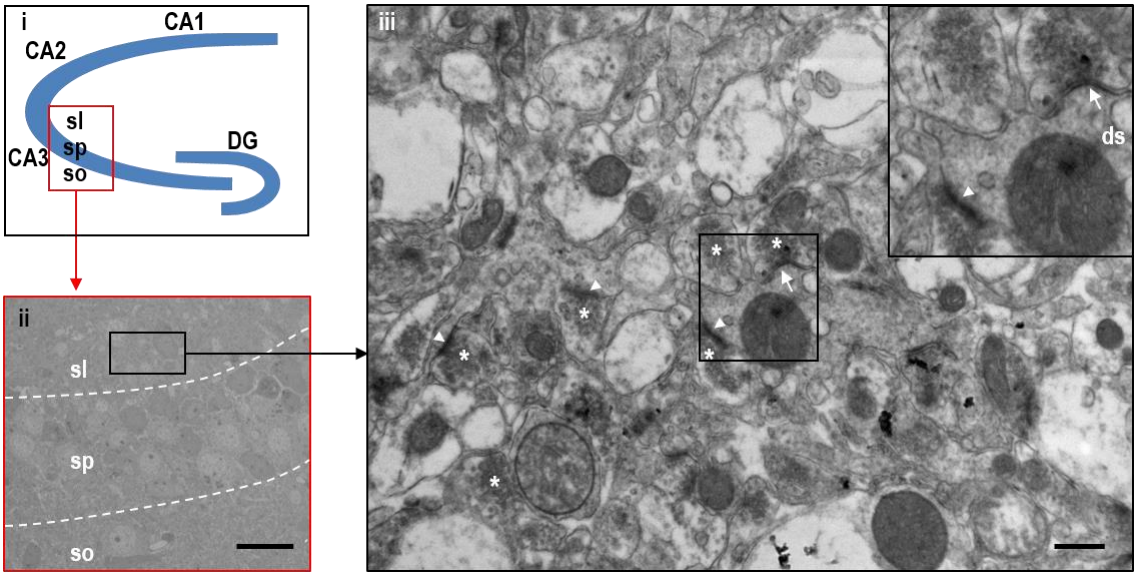

Electron micrographs of the adult mice hippocampal dendritic spines. (i) Schematic of the hippocampus to show location of interest. (ii) Low magnification image of the hippocampus CA3 region. Scale bar 25µm. (iii) High magnification image of the dendritic spines at the stratum lucidum of adult mice. Rectangular box shows close up of excitatory (arrowhead) and inhibitory synapses (arrow). Scale bar 0.5µm. CA: cornus ammonus, DG: dentate gyrus, so: stratum oriens, sp: stratum pyramidale, sl: stratum lucidum, arrowheads: excitatory synapses, arrow: inhibitory synapses. Asterisks highlight mossy fiber terminal.

A.5 Additional migration distance rescue experiments

The rescue experiments were undertaken towards the end of this project. Briefly, neuronal progenitor cells isolated from E18.5 hippocampi of 14-3-3ζ WT and KO mice were cultured as neurospheres (section 2.6.1). Neurospheres from the third passage were transfected with vectors consisting of either GFP alone, 14-3-3ζ IRES GFP, Ndel1 3E IRES GFP, Ndel1 4A IRES GFP or native Ndel1 GFP tagged (section 2.6.7), followed by neurosphere migration assay (section 2.6.2) and live imaging (section 2.6.4). The number of neurospheres and neurons analysed for each experimental condition is listed in the table below. It is noteworthy that the GFP positive cell number varied among the experimental condition and hence the number of migrating neurons measured also varied.

Experimental condition		Biological replicates	Total neurosphere no.	Avg. neurons no. measured/ neurosphere
Genotype	Transfection			
WT	UT	3	116	12998
KO	UT	3	113	7906
WT	GFP + UT	4	120	8671
KO	GFP + UT	4	117	5277
WT	GFP	1	4	19
KO	GFP	1	4	19
WT	14-3-3ζ IRES GFP	1	4	13
KO	14-3-3ζ IRES GFP	1	4	16
WT	Ndel1 3E IRES GFP	2	9	23
KO	Ndel1 3E IRES GFP	4	15	25
WT	Ndel1 4A IRES GFP	2	6	9
KO	Ndel1 4A IRES GFP	3	14	39
WT	Ndel1 GFP tagged	3	8	14
KO	Ndel1 GFP tagged	3	8	14

UT: untransfected, GFP: green fluroscent protein,
Ndel1 3E: Ndel1 phosphomimetic, Ndel1 4A: Ndel1 quadruple mutant.

Quantification of the mean migration distance of the GFP alone transfected 14-3-3ζ KO neuronal progenitor cells did not identify a significant difference in migration distance (Figure A.5 i) as observed in previous experiments using untransfected cells (Figures 4.2 viii & 4.3 v). By looking at the table below, it is obvious that the number of GFP positive cells measure were significantly lower than that of untransfected cells. Therefore, in chapter 4 (section 4.2.8) quantification of the mean migration distance of 14-3-3ζ WT and KO control neuronal progenitor cells transfected with GFP were pooled together with the untransfected data (Figure 4.9 iii). Figures A.5 ii & iii present data using the 14-3-3ζ WT and KO controls of GFP alone. Further experiments are required to increase GFP positive cell numbers, which is expected to provide enough power to obtain significant results. In this study transient transfection was a limitation given that it resulted in low numbers of GFP positive cells. For future studies an alternative method would be the use of lentivirus systems for transduction of the gene of interest.

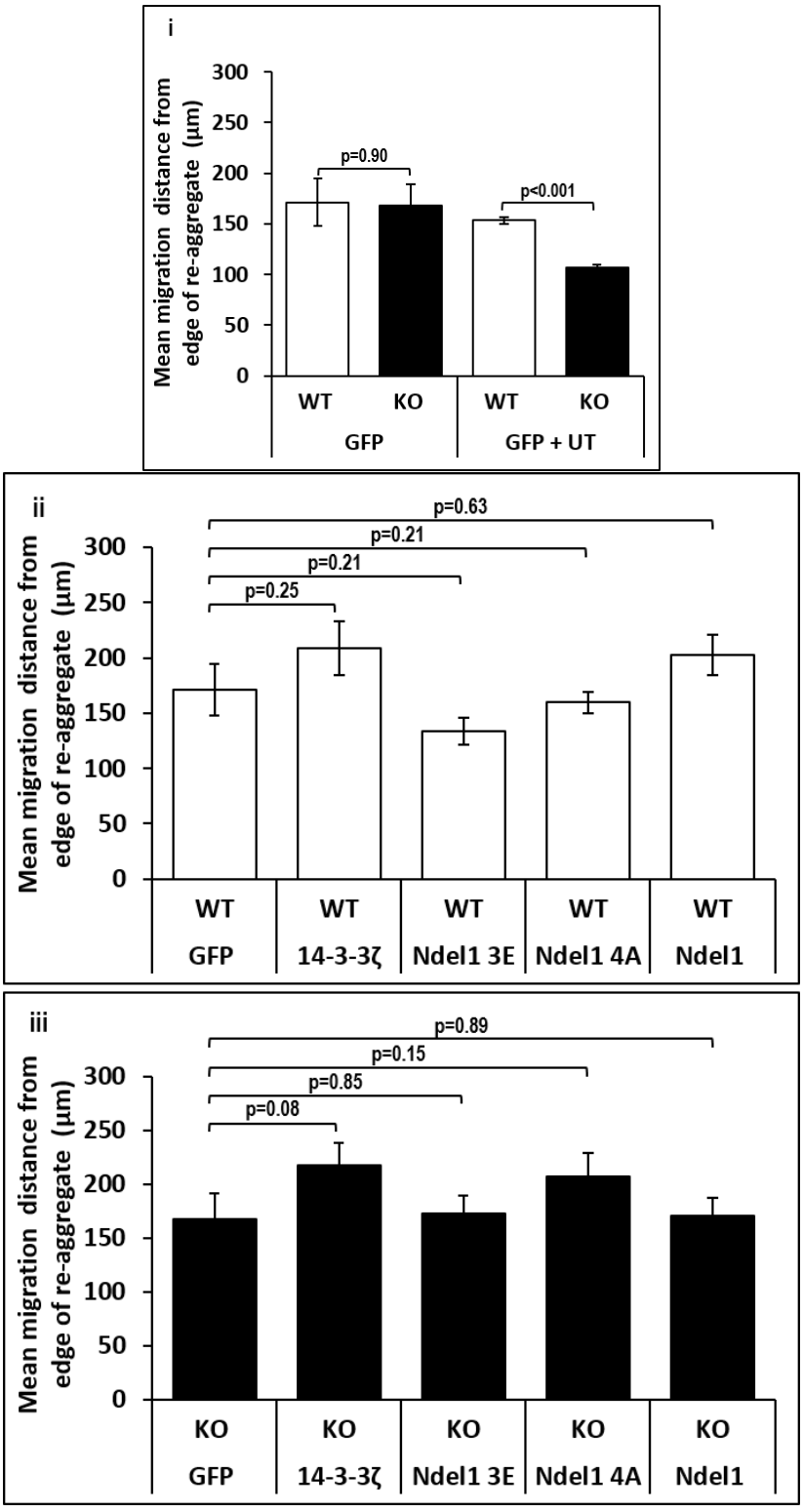

Figure A.5: Migration assay for rescue study. (i) Quantification of the mean migration distance using either GFP transfected cells alone or a combination of transfected and untransfected cells. Quantification of WT (ii) and KO (iii) neural progenitor cells transfected with either 14-3-3ζ, Ndel1 3E, Ndel1 4A or Ndel1. Error bars indicate SEM of neurosphere number (see table). GFP: Green fluorescent protein, Ndel1 3E: Ndel1 phosphomimetic, Ndel1 4A: Ndel1 quadruple mutant.

A.6 Additional migration velocity data

Initial analysis of the mean migration velocity in chapter 4 (Figure 4.4 i) resulted in a significant reduction in the mean migration velocity. However, the plots of the GFP transfected cells alone or data pooled together with the untransfected cells did not result in a significant reduction in migration velocity (Figure A.6 i). As present in the table below, the neuron number measure was smaller compared to initial experiment using untransfected cells alone. As discussed above (Appendix A.5) there is a need to increase the number of GFP positive cells.

Experimental Condition		Biological replicates	Total neurosphere no.	Avg. neurons no. measured/ neurosphere
Genotype	Transfection			
WT	UT	1	3	53
KO	UT	1	3	43
WT	GFP + UT	2	7	63
KO	GFP + UT	2	7	53
WT	GFP	1	4	19
KO	GFP	1	4	19
WT	14-3-3ζ IRES GFP	1	4	13
KO	14-3-3ζ IRES GFP	1	4	16
WT	Ndel1 3E IRES GFP	2	9	23
KO	Ndel1 3E IRES GFP	4	15	25
WT	Ndel1 4A IRES GFP	2	6	9
KO	Ndel1 4A IRES GFP	3	14	39
WT	Ndel1 GFP tagged	3	8	14
KO	Ndel1 GFP tagged	3	8	14

UT: untransfected, GFP: green fluroscent protein,
Ndel1 3E: Ndel1 phosphomimetic, Ndel1 4A: Ndel1 quadruple mutant.

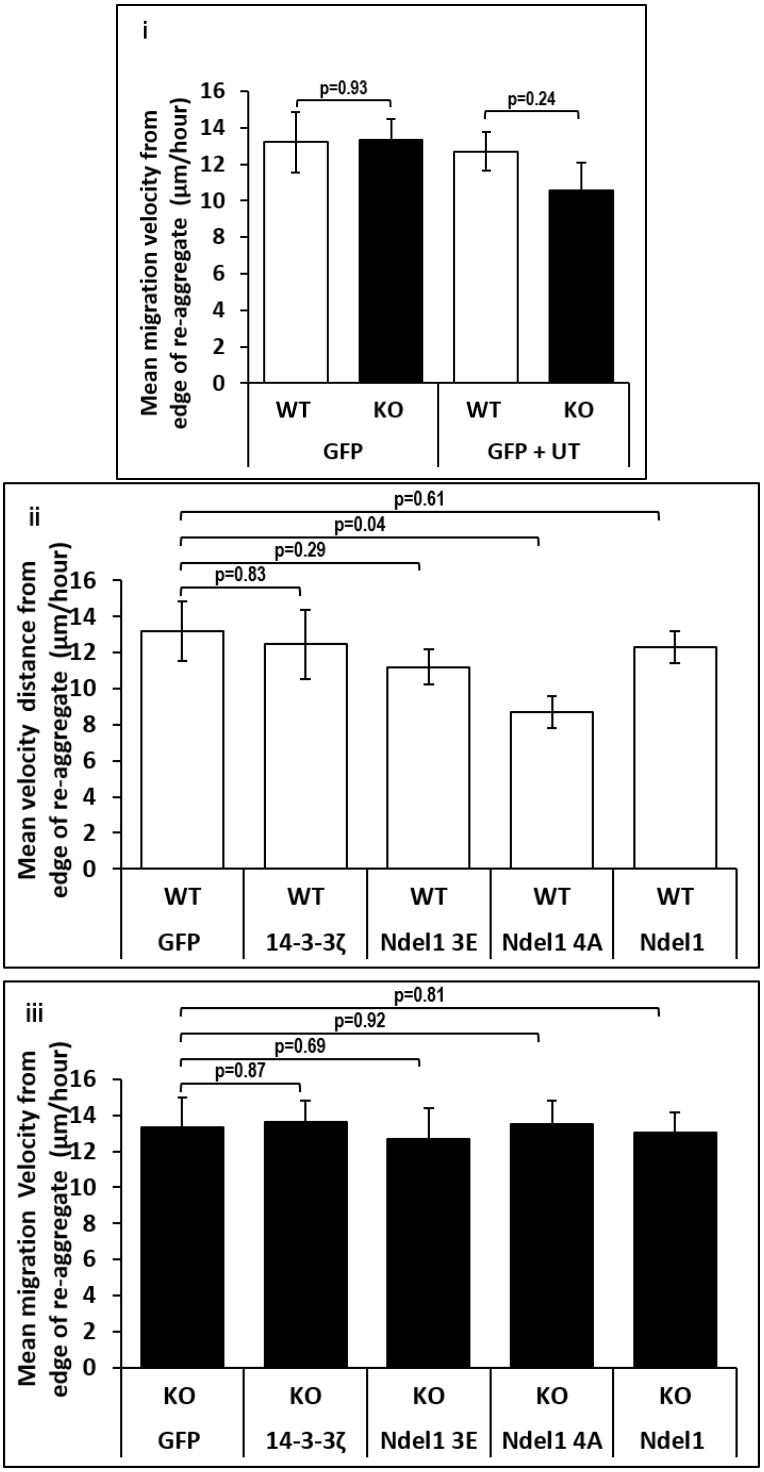

Figure A.6: Migration velocity. (i) Quantification of the mean migration velocity using either GFP transfected cells alone or a combination of transfected and untransfected cells. Quantification of WT (ii) and KO (iii) neural progenitor cells transfected with either 14-3-3ζ, Ndel1 3E, Ndel1 4A or Ndel1. Error bars indicate SEM of neurosphere number (see table). GFP: Green fluorescent protein, Ndel1 3E: Ndel1 phosphomimetic, Ndel1 4A: Ndel1 quadruple mutant.

A.7 BALB/c derived 14-3-3ζ deficient stem/progenitor cells also show reduced self-renewal *in vitro*

Neural stem/progenitor cells were isolated from 14-3-3ζ WT, HET and KO E18.5 mice from the BALB/c background and 10,000cells/well were cultured in a 24-well plate (section 2.6.8). The total neurosphere number generated from 10,000 cells showed a trend towards reduced neurosphere number in the 14-3-3ζ deficient cultures compared to WT (i). The likely reason that it was not significant was because the cell density in this experiment was higher (10,000 cells instead of 500 cells) compared to the experiment of the 129/sv derived cells in section 5.2.2 (Figure 5.2 ii). Increased cell number results in higher neurosphere number, given the nature of the analysis the accuracy of the measurement was affected. Therefore, since these experiments were actually undertaken before the 129/sv background derived neural stem/progenitor cells, based on these findings it was decided to use 500 cells rather than 10,000 cells for this experiment. Similar to the 129/sv background derived cells (Figure 5.2 iii), the total neural stem/progenitors cell number was reduced in the BALB/c derived 14-3-3ζ deficient cell compared to WT (ii).

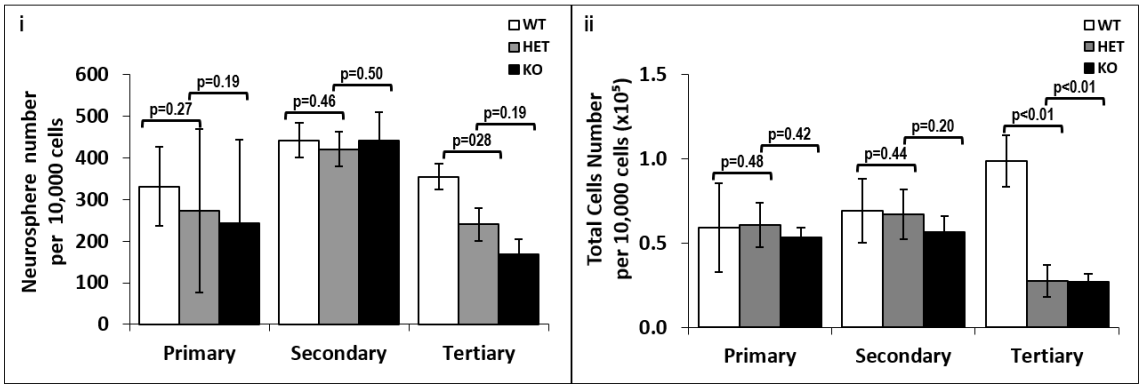

Figure A.7: 14-3-3ζ KO results in reduced stem/progenitor cell self-renewal in vitro. (i) Quantification of the number of neurospheres forming from 500 stem/progenitors cells reveals reduced neurosphere number in the 14-3-3ζ KO compared to WT (mean± SEM; WT n=3, HET=8, KO n=11; three wells/sample were analysed). (ii) Quantification of the total cell number of stem/progenitor cells per well reveals reduced stem/progenitor in 14-3-3ζ KO culture compared to WT (mean± SEM; WT n=3, HET=8, KO n=11; two wells/sample were analysed).

Published Papers

OPEN

Citation: Transl Psychiatry (2013) **3**, e327; doi:10.1038/tp.2013.99
© 2013 Macmillan Publishers Limited All rights reserved 2158-3188/13
www.nature.com/tp

ORIGINAL ARTICLE

Locomotor hyperactivity in 14-3-3ζ KO mice is associated with dopamine transporter dysfunction

H Ramshaw[1,4], X Xu[1,4], EJ Jaehne[2], P McCarthy[1], Z Greenberg[1], E Saleh[1], B McClure[1], J Woodcock[1], S Kabbara[1], S Wiszniak[1], Ting-Yi Wang[3], C Parish[3], M van den Buuse[3], BT Baune[2], A Lopez[1] and Q Schwarz[1]

Dopamine (DA) neurotransmission requires a complex series of enzymatic reactions that are tightly linked to catecholamine exocytosis and receptor interactions on pre- and postsynaptic neurons. Regulation of dopaminergic signalling is primarily achieved through reuptake of extracellular DA by the DA transporter (DAT) on presynaptic neurons. Aberrant regulation of DA signalling, and in particular hyperactivation, has been proposed as a key insult in the presentation of schizophrenia and related neuropsychiatric disorders. We recently identified 14-3-3ζ as an essential component of neurodevelopment and a central risk factor in the schizophrenia protein interaction network. Our analysis of 14-3-3ζ-deficient mice now shows that baseline hyperactivity of knockout (KO) mice is rescued by the antipsychotic drug clozapine. 14-3-3ζ KO mice displayed enhanced locomotor hyperactivity induced by the DA releaser amphetamine. Consistent with 14-3-3ζ having a role in DA signalling, we found increased levels of DA in the striatum of 14-3-3ζ KO mice. Although 14-3-3ζ is proposed to modulate activity of the rate-limiting DA biosynthesis enzyme, tyrosine hydroxylase (TH), we were unable to identify any differences in total TH levels, TH localization or TH activation in 14-3-3ζ KO mice. Rather, our analysis identified significantly reduced levels of DAT in the absence of notable differences in RNA or protein levels of DA receptors D1–D5. Providing insight into the mechanisms by which 14-3-3ζ controls DAT stability, we found a physical association between 14-3-3ζ and DAT by co-immunoprecipitation. Taken together, our results identify a novel role for 14-3-3ζ in DA neurotransmission and provide support to the hyperdopaminergic basis of pathologies associated with schizophrenia and related disorders.

Translational Psychiatry (2013) **3,** e327; doi:10.1038/tp.2013.99; published online 3 December 2013

Keywords: 14-3-3ζ; dopamine neurotransmission; dopamine transporter; schizophrenia; schizophrenia mouse model

INTRODUCTION

Schizophrenia and related neuropsychiatric disorders are widely believed to arise from neurodevelopmental defects that affect synaptic transmission.[1] Indeed, neuropharmacological studies with antipsychotic drugs suggest that many of the positive symptoms associated with schizophrenia arise from increased dopamine (DA) signalling.[2,3] Neuroimaging studies following amphetamine treatment add strong support to this notion[4,5] and further implicate the mesolimbic pathway in the hyperdopaminergic hypothesis. Within the mesolimbic pathway, DA is produced by neurons predominantly located in the ventral tegmental area (VTA) and the substantia nigra (SN) of the midbrain. Central to the function of these neurons is the expression and activity of the rate-limiting catecholamine biosynthesis enzyme, tyrosine hydroxylase (TH), which catalyses the synthesis of DA from its precursor L-tyrosine. Following exocytosis from presynaptic neurons, DA binds to G-protein-coupled DA receptors D1–D5 to initiate signalling cascades in postsynaptic neurons. The activity of DA is tightly regulated by the DA transporter (DAT) that mediates reuptake of DA by presynaptic neurons where it is either recycled to the vesicular pool or degraded.[6,7]

Recent studies have shown that the family of 14-3-3 regulatory proteins bind to TH to enhance phosphorylation of serine 31 (Ser-31) and Ser-40 to positively regulate its enzymatic activity.[8,9] Indeed, 14-3-3 proteins were originally identified as archetypical TH co-factors.[10,11] The 14-3-3 family comprises seven isoforms in mammals (β, ζ, ε, γ, η, τ and σ) that bind to phospho-serine/threonine residues on target proteins to modify their function and/or localization. In this manner, 14-3-3 proteins have been described to mediate a range of cell functions including cell cycle regulation, proliferation, migration, differentiation and apoptosis.[10,12–14] Although multiple 14-3-3 isoforms have the ability to bind TH *in vitro*, knockdown studies in midbrain-derived MN9D cells suggest that 14-3-3ζ is the major isoform involved in DA synthesis.[15] In support of these findings, 14-3-3ζ is also the major isoform expressed in regions containing termini of dopaminergic neurons such as the striatum.[16] However, the role of 14-3-3ζ in TH activity *in vivo,* or in other stages of DA neurotransmission, has not been explored.

We recently reported that 14-3-3ζ knockout (KO) mice have schizophrenia-like behavioural deficits such as hyperactivity and disrupted sensorimotor gating that are accompanied by aberrant neuronal migration and axonal guidance defects in the hippocampus.[17] 14-3-3ζ KO mice therefore represent a novel neurodevelopmental model of schizophrenia and associated disorders. In strong support of this notion, 14-3-3ζ is downregulated in post-mortem schizophrenia brain samples at the mRNA level[18,19] and is one of only 24 proteins downregulated across multiple

[1]Centre for Cancer Biology, SA Pathology, Adelaide, South Australia, Australia; [2]Department of Psychiatry, University of Adelaide, Adelaide, South Australia, Australia and [3]Florey Institute for Neuroscience and Mental Health, University of Melbourne, Melbourne, Victoria, Australia. Correspondence: Dr Q Schwarz, Centre for Cancer Biology, SA Pathology, Frome Road, Adelaide 5000, South Australia, Australia.
E-mail: quenten.schwarz@health.sa.gov.au
[4]These authors contributed equally to this work.
Received 3 October 2013; accepted 7 October 2013

neuroproteomic studies on schizophrenia patient samples.[20–22] In addition, significant linkage to 14-3-3ζ has been identified through analysis of single-nucleotide polymorphisms from control and schizophrenia patient samples.[23] Further support for a role in schizophrenia is derived from the recent finding that 14-3-3ζ is represented as a central hub within the schizophrenia-specific interaction network.[24] At the molecular level, 14-3-3ζ interacts with several proteins essential for neuronal development that are also implicated in the pathogenesis of schizophrenia, including DISC1, NUDEL, LIS1 and TH.[17,25]

Here we have explored the physiological and molecular basis of schizophrenia-like behavioural deficits by analyzing locomotor hyperactivity in 14-3-3ζ KO mice. We found that baseline hyperactivity of KO mice is rescued by the antipsychotic drug clozapine and that KO mice are hypersensitive to the DA releaser amphetamine. In strong support of DA underpinning some of the schizophrenia-like behavioural defects, in this model we found that total tissue DA levels were increased in KO mice. Our analysis of the dopaminergic signalling pathway indicates that 14-3-3ζ has an essential role in modulating protein levels of DAT. Our finding that 14-3-3ζ interacts with DAT provides insight into the molecular regulation of DAT stability. Unexpectedly, TH-positive neurons, TH expression and TH activation were unaffected in KO mice. Moreover, DA receptors were also expressed at similar levels to wild-type (WT) mice. Our results therefore implicate 14-3-3ζ as an essential component in the DA neurotransmission pathway by modulating the abundance of DAT.

MATERIALS AND METHODS

Mice

14-3-3$\zeta^{Gt(OST062)Lex}$ (or 14-3-3ζ KO) mice on a SV129 background carrying a gene trap construct that contains the βGeo reporter gene disrupting 14-3-3ζ expression, have been described previously.[17] *14-3-3ζ* Genotype was determined by PCR amplification of genomic tail DNA as described.[17] Animal experiments were conducted in accordance with the guidelines of the Animal Ethics Committee of the Institute of Medical and Veterinary Sciences, the University of Adelaide and the Florey Institute for Neuroscience and Mental Health, University of Melbourne.

Behavioural assays

All procedures were carried out under normal light conditions (60–100 Lux) between 0800 and 1200 hours. Behavioural phenotyping was performed on the 14-3-3ζ KO line as previously described.[26–28] One cohort of mice was used for the psychotropic drug-induced open field test at 30 weeks of age (11 WT, 5 females and 6 males; 11 KO, 5 females and 6 males). A separate cohort of mice was used at the age of 35 weeks for clozapine treatments and locomotor function tests (12 WT, 8 males and 4 females; 12 KO, 8 males and 4 females).

Clozapine treatment and locomotor function test

Clozapine was obtained from Sigma Aldrich (St Louis, MO, USA) and was dissolved in 10 mM HCl and diluted in sterile water.[29] Vehicle was prepared in an identical manner without the addition of clozapine. Concentrated aliquots of both clozapine and vehicle were stored at $-20\,^{\circ}C$. Aliquots were thawed and diluted to their final concentration in sterile saline on the day of dosing. Solutions were buffered with NaOH to achieve a final pH of 6.5–7.5. Mice were given clozapine (5 mg kg^{-1}) or vehicle daily for 14 days before behavioural testing. Dosing was continued for a further 11 days throughout the behavioural testing period, with dosing always conducted between 1530 and 1700 hours, following any behavioural testing. In all, 10 WT (3 males + 7 females) and 9 KO (3 males + 6 females) mice were given vehicle, whereas 10 WT (4 males + 6 females) and 8 KO (4 males + 4 females) mice were given clozapine. Mice were tested in a brightly lit square arena, 40 × 40 cm (Stoelting, Wood Dale, IL, USA), with clear walls 35 cm high for 5 min according to published protocols.[30,31] The floor was divided into inner and outer zones. Time spent in each zone was measured and total distance travelled was measured as an indication of baseline locomotor activity. An imaging program (ANY-maze, Wood Dale, IL, USA) was used to track movements and measure time in zones.

Amphetamine-induced locomotor hyperactivity

Baseline locomotor activity and amphetamine-induced locomotor activity were assessed using a TruScan Photobeam Activity system (Coulbourn Instruments, Whitehall, PA, USA). This system consists of a mouse enclosure (25.4 × 25.4 × 40.6 cm) surrounded by a sensor-ring that included a 16 × 16 array of photobeams and a computerized data acquisition system. After 30 min of baseline locomotor activity and habituation to the test environment, the animals received either saline or 5 mg kg^{-1} of amphetamine by intraperitoneal injection and activity was monitored over a subsequent 90-min period.

Production of 14-3-3ζ monoclonal antibodies

Anti-14-3-3ζ monoclonal antibodies were generated in a female BALB/c 14.3.3ζ KO mouse, which was injected three times, each with 10 μg purified recombinant 14.3.3ζ protein, over a period of 6 weeks. Enzyme-linked immunoassay of serum was performed to verify immunoreactivity to 14-3-3ζ. Splenocytes were isolated and fused with NS1 myeloma cells. Hybridomas were selected by incubating the cells at 37 °C with humidified 5% CO_2 atmosphere in hypoxanthine–aminopterin–thymidine containing media. Immunoreactivity of these hybridomas was determined using a modified enzyme-linked immunoassay in which recombinant 14-3-3ζ was adsorbed to the surface of 96-well tissue culture plates. Positive lines were then clonally expanded. From this screen, we identified 35 positive hybridoma cell lines. Monoclonal antibodies were purified from eight lines detailed in Supplementary Figure S1. Purified antibodies were tested by western blot against each 14-3-3 isoform obtained from overexpression of His-tagged pGEX-expression constructs in bacteria in comparison with a commercially available 14-3-3ζ polyclonal antibody (C-16, Santa Cruz, CA, USA). Antibodies M6 (for western blots) and G1-7 for immunoprecipitation (IPs) were grown up and purified by the Walter Eliza Hall Institute Antibody facility for use in this study.

Histology and immunohistochemistry

For all anatomical analyses, postnatal mice were perfuse fixed with fresh 4% paraformaldehyde dissolved in phosphate-buffered saline as previously described.[32] Brains were rapidly dissected free from other tissue and post fixed in 4% paraformaldehyde for an additional 24 h at 4 °C. Tissue was cryopreserved in 20% sucrose at room temperature (RT) overnight and frozen in Tissue-Tek OCT (Sakura Finetek, Torrance, CA, USA). Sections were cut at a thickness of 10 μm on a CM1850 cryostat (Leica, North Ryde, Australia) and air-dried for 60 min before staining.

For immunohistochemistry, sections were blocked in 10% non-immune goat serum or 1% bovine serum albumin in PBST (0.1 M phosphate-buffered saline, 0.3% Triton X-100, 1% bovine serum albumin) for 1 h at RT and subsequently incubated with primary antibodies for 1 h at RT. Primary antibodies and dilutions: rabbit polyclonal to TH (1:200; Millipore, Billerica, MA, USA), rat monoclonal to DAT (1:20, Santa Cruz). Sections were washed several times with PBST and then incubated with 1:200 dilution of Alexa Fluor-labelled secondary antibodies (Molecular Probes, Mullgrave, VIC, Australia) or streptavidin-labelled secondary antibodies (Jackson Laboratories, Bar Harbor, ME, USA) for 1 h at RT. After three washes in PBST, fluorescent sections were mounted in Prolong Gold antifade reagent with 4,6-diamidino-2-phenylindole (Molecular Probes) and streptavidin-labelled sections were developed with DAB substrate (Sigma, Castle Hill, NSW, Australia).

Image analysis

Low-resolution images were recorded on an SZX10 stereo microscope (Olympus, Edwardstown, SA, Australia) equipped with a Micropublisher 3.3 digital camera (Q-Imaging, Waltham, MA, USA) and processed with OpenLab 2.2 software (Improvision, Waltham, MA, USA). High-resolution images were recorded on an IX81 inverted microscope (Olympus) equipped with an OCRA-ER digital CCD camera (Hamamatsu, Hamamatsu, Japan) and processed with CellR software (Olympus). DAT and TH immunofluorescence was captured on a LSM700 confocal microscope (Zeiss, North Ryde, NSW, Australia). All figures were constructed in Adobe Photoshop CS3 (Adobe Systems, San Jose, CA, USA). Quantitation of DAT and TH expression from confocal immunofluorescence images was completed as described previously.[33] Briefly, images were split into separate channels for TH or DAT, converted to binary images and used for fluorescence intensity calculations with an Image J area calculator macro designed to detect staining in confocal image slices.

© 2013 Macmillan Publishers Limited

Cell culture

The dopaminergic neuronal progenitor cell line, SN4741,[34] was maintained in Dulbecco's modified Eagle's medium containing 10% fetal bovine serum (HyClone, South Logan, UT, USA), 1% glutamine and antibiotics. FLAG-His-DAT (generously provided by Alexander Sorkin) and Myc-14-3-3ζ (generously provided by Joanna Woodcock) were transiently transfected into cells with Lipofectamine 2000 (Life Sciences, Mullgrave, VIC, Australia) and allowed to grow for 48 h before extracting protein lysates.

Immunoprecipitation

All protein extracts were prepared by lysis in NP40 lysis buffer composed of 137 mM NaCl, 10 mM Tris-HCl (pH 7.4), 10% glycerol, 1% Nonidet P-40, and protease and phosphatase inhibitors (4.5 U of aprotinin per ml, 1 μg of leupeptin per ml, 1 mM phenylmethylsulfonyl fluoride, 10 mM sodium fluoride, 10 mM β-glycerol phosphate, 10 mM sodium pyrophosphate and 10 mM sodium vanadate). Samples were lysed for 60 min at 4 °C, then centrifuged at 10 000 *g* for 15 min. The supernatants were precleared with mouse Ig-coupled Sepharose beads for 30 min at 4 °C. The precleared lysates were incubated for 2 h at 4 °C with 2 μg ml^{-1} of anti-TH antibody (Millipore), monoclonal anti-1433ζ antibody (G1-7), anti-DAT (6-5G10, Santa Cruz; and MAB369, Millipore), anti-Flag (Sigma) and control immunoglobulin G (Sigma) absorbed to protein G-Sepharose (Amersham Biosciences, Amersham, UK). The sepharose beads were washed three times with lysis buffer before being boiled for 5 min in sodium dodecyl sulphate–polyacrylamide gel electrophoresis sample buffer. The immunoprecipitated proteins and lysates were separated by sodium dodecyl sulphate–polyacrylamide gel electrophoresis, electrophorectically transferred to a polyvinylidene difluoride (Hybond-P, Amersham, UK) membrane (GE Health, Rydalmere, NSW, Australia) and analysed by immunoblotting.

Immunoblotting

Polyvinylidene difluoride membranes were blocked with 5% skim milk powder in TBST and immunoblotted with polyclonal rabbit anti-14-3-3ζ C-16 (Santa Cruz) at 1:1000, rabbit anti-TH (Millipore) at 1:1000, rabbit anti-phospho-serine-31 TH (Cell Signalling Anibodies, Danvers, MA, USA) at 1:1000, rabbit anti-phospho-serine-40 TH (Cell Signalling Anibodies) at 1:1000, rat anti-DAT (6–5G10; Santa Cruz) at 1:200, mouse anti-Flag-M2 (Sigma-Aldrich) at 1:1000, mouse anti-Myc (9B11; Cell Signalling Technologies) at 1:1000 and mouse anti-HA (6E2; Cell Signalling Technologies) at 1:1000. Rabbit polyclonal against β-actin (1:5000, Millipore) was used as a loading control. Bound antibodies were detected with horseradish peroxidase-conjugated secondary antibody (1:5,000, Pierce-Thermo Scientific, Rockford, IL, USA). Immunoreactive proteins were visualized by ECL (Luminescent Image Analyzer LAS-4000, Fujifilm, Tokyo, Japan). The images were analysed with Multi Gauge Ver3.0 (Fujifilm).

Detection of DA levels and metabolism

DA, and the metabolite 3,4-dihydroxyphenylacetic acid (DOPAC), levels in the striatum, prefrontal cortex and hippocampus of 7 WT and 7 KO animals were determined using reverse-phase high-performance liquid chromatography (HPLC) as previously described. For tissue preparation, small biopsies were dissected on a chilled plate, weighed, and stabilized in 200 μl 0.4 M perchloric acid ($HClO_4$) containing 0.05% sodium metabisulphate ($Na_2S_2O_5$) and 0.01% disodium EDTA. The sample tissue was then homogenized, cellular and vesicular membranes disrupted using a sonicator and finally stored at 70 °C. On the day of analysis, all samples were centrifuged at 10 500 *g* for 10 min and filtered though minispin filters for additional 3 min at 10 000 r.p.m. before being injected into the HPLC. For each sample, 10 μl was injected by a cooled autosampler (SIL 20A, Shimadzu, Rydalmere, NSW, Australia) and Shimadzu LC-AT pumpon to a reverse-phase C18 column (4.6 mm diameter, 150 mm length; CHROMPACK, Croydon, UK) coupled with an electrochemical detector (Decade II, Antec Leyden, Rydalmere, NSW, Australia). The mobile phase, comprises the following (mM): (KH_2PO_4, 70; EDTA di-sodium salt, 0.5; octane-sulphonic acid, sodium salt, 8; with 17% HPLC grade methanol, pH 3) was delivered at a flow rate of 500 μl min^{-1}. The peaks were processed using LC solutions software (Antec Leyden). Concentrations of DA and its metabolite DOPAC were calculated for each sample.

Quantitative reverse transcriptase-PCR

Total RNA was isolated from cells using Trizol (Ambion, Austin, TX, USA) and single-stranded complementary DNA was synthesized using the QuantiTect Reverse transcription kit (Qiagen, Frankfurt, Germany). Quantitative PCR was performed with SYBR Green reagent (Qiagen) using the Rotor-Gene 6000 real-time PCR system (Corbett Life Science, Frankfurt, Germany). Primers used were: *glyceraldehyde 3-phosphate dehydrogenase* F: 5′-ACCCAGAAGACTGTGGATGG-3′, R: 5′-CAGTGAGCTTCCCGTTCA-3′; *DA receptor D1* F: 5′-AACTGTATGGTGCCCTTCTGTGG-3′, R: 5′-CATTCGTAGTT GTTGTTGCCCCG-3′; *DA receptor D2* F: 5′-CACTCCGCCACTTCTTGACATA CA-3′, R: 5′-TCTCCTCCGACACCTACCCCGA-3′; *DA receptor D3* F: 5′-GTCCT GCCCTCTCCTCTTTGGTTT-3′, R: 5′-AGTCTACGGTGCCCTGTTTAC-3′; *DA receptor D4* F: 5′-TGCCCTCAACCCCATCATCTACAC-3′, R: 5′-AATACTTCCGAC CCCCAACCCT-3′; *DA receptor D5* F: 5′-GGGAGATCGCTGCTGCCTATGTC-3′, R: 5′-TTTTAGAGTGGTGAGTGGGGGTTA-3′; *DAT* F: 5′-ACGCTCAAAATACTCAG CAG-3′, R: 5′-TACCGAGAGGACAGCATTCC-3′. Relative mRNA levels were quantified using the comparative quantitation method in Rotor-Gene 6000 Series Software. Relative mRNAs levels were then normalized to *glyceraldehyde 3-phosphate dehydrogenase*. Each PCR was performed in technical triplicates, and each experiment was performed in at least three biological replicates. Error bars represent s.e.m. between biological replicates.

Statistical analysis

All data are presented as mean ± s.e.m. Behavioural experiments were analysed using two-way analysis of variance (ANOVA) with repeated measures where appropriate (Systat, version 9.0, SPSS software; SPSS, Armonk, NY, USA). Neurochemical data were analysed using ANOVA and Student's *t*-test. In all studies, a *P*-value of <0.05 was considered to be statistically significant.

RESULTS

Baseline hyperactivity of 14-3-3ζ KO mice is rescued with clozapine

Our previous studies identified several schizophrenia-like behavioural deficits in 14-3-3ζ KO mice, including a reduced capacity to learn and remember, hyperactivity and disrupted sensorimotor gating. To further test the relevance of this mouse model to schizophrenia and related disorders, we completed behavioural analyses with the antipsychotic drug clozapine, an antagonist of DA and serotonin receptors. Consistent with our previous report, we found that 14-3-3ζ KO mice have baseline hyperactivity over a 30-min test period. Following 2 weeks of daily intraperitoneal injections of 5 mg kg^{-1} clozapine, we found that baseline locomotor hyperactivity of 14-3-3ζ KO mice returned to levels similar to WT mice (Figure 1). ANOVA revealed main effects of genotype ($F(1, 31) = 7.2$, $P = 0.012$) and of clozapine treatment

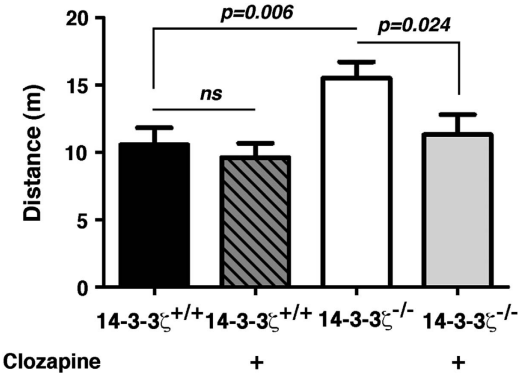

Figure 1. Clozapine rescues baseline hyperactivity of 14-3-3ζ knockout (KO) mice. 14-3-3ζ KO mice (white bar; $n = 8$; 5 males and 3 females) have greater baseline exploratory behaviour than 14-3-3ζ wild-type (WT) mice (closed bar; $n = 10$; 6 males and 4 females) in an open field test. Treatment with the antipsychotic clozapine has no effect on WT mice (dark grey hashed bar; $n = 10$; 6 males and 4 females) but reduces baseline exploratory behaviour of 14-3-3ζ KO mice (light grey bar; $n = 8$; 5 males and 3 females) to levels similar to WT.

© 2013 Macmillan Publishers Limited

($F(1,31)=4.3$, $P=0.046$) and a trend towards a genotype × clozapine interaction ($F(1,31)=3.3$, $P=0.078$). Further pairwise comparison confirmed the expected baseline locomotor hyperactivity in 14-3-3ζ KO mice compared with controls ($F(1,16)=9.9$, $P=0.006$) but there was no difference between clozapine-treated 14-3-3ζ KO mice and WT controls (Figure 1). Distance moved was significantly reduced in clozapine-treated compared with saline-treated 14-3-3ζ KO mice ($F(1,14)=6.4$, $P=0.024$) but there was no clozapine effect in WT controls (Figure 1). This functional rescue of hyperactivity was independent of sex.

14-3-3ζ KO mice are hypersensitive to amphetamine

A defining feature of human psychiatric conditions is enhanced behavioural effects of amphetamine.[35–37] To further validate 14-3-3ζ KO mice as a robust schizophrenia-like mouse model, we completed analysis of amphetamine-induced hyperactivity. Amphetamine is a potent psychostimulant that enhances the release of DA from presynaptic dopaminergic terminals.[38] Consistent with previous findings, we found that 14-3-3ζ KO mice showed hyperactivity relative to WT mice in the 20-min habituation phase before drug or after saline administration (Figure 2a; WT, $n=12$; KO, $n=11$). Indeed, ANOVA showed a significant main effect of genotype after injection of saline ($F(1,22)=11.0$, $P=0.003$). WT and KO mice also demonstrated a decline in activity with habituation to the test arena. Subcutaneous injection of amphetamine-induced (5 mg kg^{-1}) hyperactivity in both 14-3-3ζ WT and KO mice (WT, $n=12$; KO, $n=11$), however, this effect was significantly enhanced in the KO mice that had reduced time to become maximally hyperactive and also covered a greater distance than WT controls particularly in the first 45 min of the 90-min testing period (Figure 2b). The genotype-dependent difference in amphetamine time-course was reflected by a significant ANOVA amphetamine × genotype × time interaction ($F(17,374=2.8$, $P<0.001$). During the first 45 min after amphetamine injection, there was also a genotype × amphetamine interaction ($F(1,22)=6.0$, $P=0.023$), which was absent for the second 45 min after injection (Figure 2b). Induced hyperactivity was similar for both males and females with no sex bias ($P>0.05$).

DA levels and DA turnover are aberrant in 14-3-3ζ KO mice

Given the rescue of baseline hyperactivity with clozapine and the increased hyperactivity to the DA releaser amphetamine, we next investigated the levels of total tissue DA and DOPAC in the striatum, cortex and hippocampus by HPLC/EC. Our analysis found that tissue content of DA was significantly increased by 30% in the striatum of P100 14-3-3ζ KO mice when compared with WT controls (Figure 3a; WT, mean = 135 pmol mg^{-1}, $n=6$; KO, mean = 178 pmol mg^{-1}, $n=6$; $P=0.038$). Although not reaching levels of significance this trend was also observed in the cortex and hippocampus of 14-3-3ζ KO mice (Supplementary Figures S1a and d). We also observed an increase of DOPAC in the striatum of 14-3-3ζ KO mice when compared with WT controls (Figure 3b; WT, mean = 14.7 pmol mg^{-1}; KO, mean = 20.9 pmol mg^{-1}) that was not observed in the cortex (Supplementary Figure S1b). This increase of DOPAC resulted in a similar level of DA turnover (DOPAC/DA ratio) in 14-3-3ζ KO and WT mice (Figure 3c).

TH is preserved in 14-3-3ζ KO mice

Our previous findings raised the hypothesis that DA neurotransmission is affected in 14-3-3ζ KO mice. DA is produced by dopaminergic neurons that primarily reside in the VTA/SN and send their processes to the dorsal and ventral striatum,

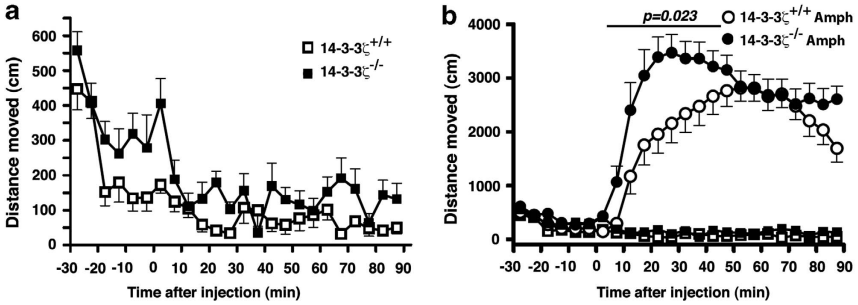

Figure 2. 14-3-3ζ Knockout (KO) mice are hypersensitive to amphetamine. (**a**) 14-3-3ζ KO mice (closed square; $n=11$; 6 males and 5 females) have greater baseline exploratory behaviour than 14-3-3ζ wild-type (WT) mice (open square; $n=12$; 8 males and 4 females) in an open field test. (**b**) 14-3-3ζ KO mice (closed circle; $n=11$; 6 males and 5 females) have increased hyperactivity in response to amphetamine (5 mg kg^{-1}) than 14-3-3ζ WT mice (open circle; $n=12$; 8 males and 4 females) in an open field test. Note difference in vertical scale.

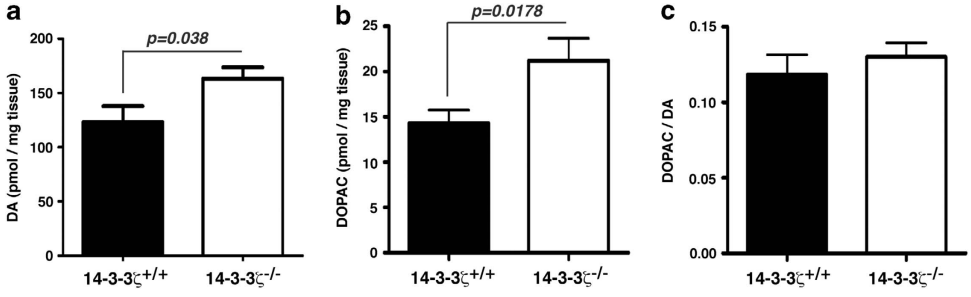

Figure 3. Altered baseline dopamine (DA) in the striatum of 14-3-3ζ knockout (KO) mice. (**a**) Baseline DA and 3,4-dihydroxyphenylacetic acid (DOPAC) levels were measured in the striatum by high-performance liquid chromatography (HPLC)/EC. 14-3-3ζ KO mice (white bar; $n=6$; 4 males and 2 females) have increased DA compared with 14-3-3ζ wild-type (WT) mice (closed bar; $n=6$; 3 males and 3 females). (**b**) 14-3-3ζ KO mice (white bar) also have increased DOPAC compared with 14-3-3ζ WT mice (closed bar). (**c**) DA turnover (DOPAC/DA ratio) is conserved in 14-3-3ζ KO mice (white bar) compared with 14-3-3ζ WT mice (closed bar).

© 2013 Macmillan Publishers Limited

respectively. 14-3-3ζ Has previously been suggested to have an essential role in DA synthesis by interacting with TH to promote its phosphorylation and activity.[15] To investigate the interactions and functions of 14-3-3ζ, we generated a suite of 14-3-3ζ monoclonal antibodies by immunizing 14-3-3ζ KO mice with recombinant 14-3-3ζ protein. Western blot analysis of recombinant 14-3-3 proteins expressed in bacteria shows that anti-14-3-3ζ M6, D1-4 and N4 predominantly interact with 14-3-3ζ while also recognizing 14-3-3τ (Supplementary Figure S2). However, as 14-3-3τ is not expressed in brain tissue[16] these antibodies provide an ideal resource to specifically address the role of 14-3-3ζ in brain function. Using anti-14-3-3ζ M6 on a western blot of proteins co-immunoprecipitated with anti-TH from P35 mouse brain lysates, we were able to confirm the interaction of 14-3-3ζ and TH *in vivo* (Figure 4a).

We next analysed the abundance of total TH in sagittal and coronal brain sections by immunohistochemistry. Our analysis identified similar levels of expression in the striatum, VTA and SN and further showed that 14-3-3ζ KO mice have an equivalent number of TH-positive dopaminergic neurons as WT controls (Figure 4b; WT, $n=4$; KO, $n=4$). As TH activity is controlled through the phosphorylation of Ser-31 and Ser-40, we next explored the abundance of active TH with phospho-specific antibodies. Our immunoblotting analysis was unable to identify any significant differences in the levels of total or active TH in 14-3-3ζ KO brains (Figure 4c and Supplementary Figure S3; WT, $n=6$; KO, $n=6$).

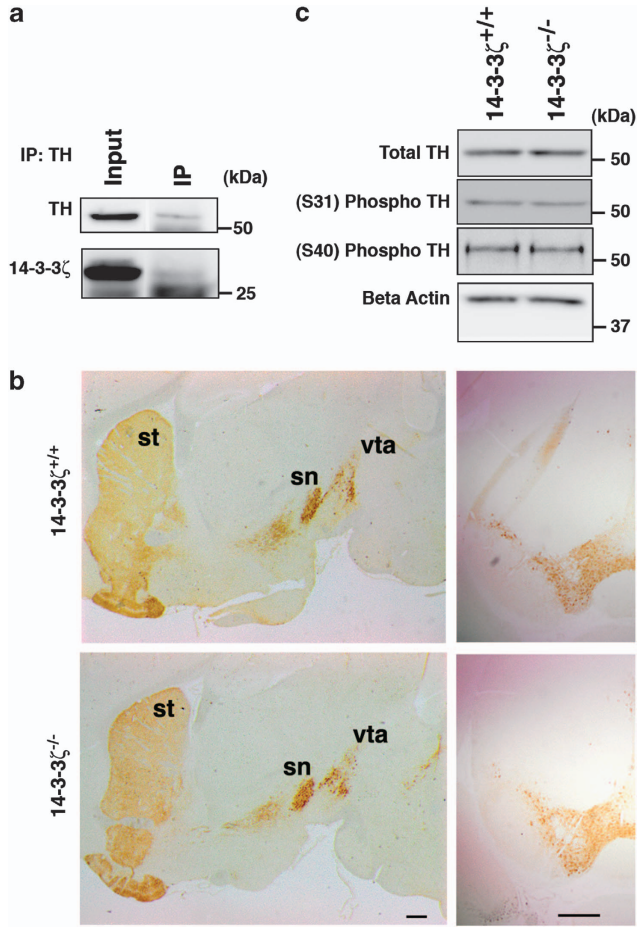

Figure 4. Tyrosine hydroxylase (TH) is activated normally in 14-3-3ζ knockout (KO) mice. (**a**) TH was precipitated from P35 whole-brain lysates with anti-TH antibody. TH immunoprecipitates were probed with anti-TH and monoclonal antibodies against 14-3-3ζ (M6). (**b**) Sagittal sections and (i, ii) coronal sections (iii iv) show that the abundance of TH-positive dopaminergic neurons in the substantia nigra (sn) and ventral tegmental area (vta), and their projections to the striatum (st) are similar in 14-3-3ζ KO and wild-type (WT) mice. Scale bars = 500 μm. (**c**) Western blot analysis of brain lysates shows that total TH, phospho serine 31 (Ser-31) and phospho Ser-40 are present at similar levels in 14-3-3ζ KO and WT mice. Load control used for quantitating western blots was α tubulin. A representative blot of all four samples is shown in this figure that is quantitated in Supplementary Figure S3.

DAT density is reduced in 14-3-3ζ KO mice

Following release of DA into the synaptic cleft it initiates signalling cascades in postsynaptic neurons by interacting with the G-protein-coupled DA receptors D1–D5. Regulation of this interaction is primarily achieved through the reuptake of DA by presynaptic neurons with DAT. Given the distinct possibility of a DA signalling dysfunction in 14-3-3ζ KO mice, we therefore explored the abundance of DA receptors and DAT in 14-3-3ζ KO brain samples. Quantitative reverse transcriptase-PCR analysis from P35 whole-brain RNA shows that each of these receptors is expressed normally at the transcript level (Figure 5a). Furthermore, analysis of the DA receptors by immunoblotting of P35 whole-brain lysates shows that the major isoforms of D1–D5 are present at normal levels in 14-3-3ζ KO mice (Figure 5b and Supplementary Figure S4; WT, $n=4$; KO, $n=4$).

We next analysed the localization and abundance of DAT by co-labelling sagittal brain sections with anti-DAT and anti-TH antibodies. In comparison with 14-3-3ζ WT mice, we observed a reduction in DAT within the SN-VTA of KO mice (Figure 6a). Upon closer examination, 14-3-3ζ WT showed evenly distributed DAT staining throughout the cell body and neurites of dopaminergic neurons within the midbrain, whereas KO neurons had sparse staining in neuronal processes and irregular localization within the cell body (Figure 6b). Within these KO mice, DAT localization was predominantly polarized to one side of the nucleus (Figure 6b). Expression of DAT was quantified by measuring the fluorescence intensity of anti-DAT in SN-VTA neurons relative to that of anti-TH antibodies. Our analysis shows that DAT levels are reduced by approximately 30% in the SN-VTA of 14-3-3ζ KO mice (Figure 6c; WT, $n=4$; KO, $n=4$; $P=0.043$). Using the same immunostaining method, we also found a significant reduction of DAT in the striatum (Figure 7). Analysis of low magnification images shows that DAT is uniformly reduced across the entire striatum (Figure 7a). Higher magnification further identifies distinct TH-positive fibres within the striatum that lack DAT (arrowheads, Figure 7b). Quantitation of this staining shows that DAT levels are

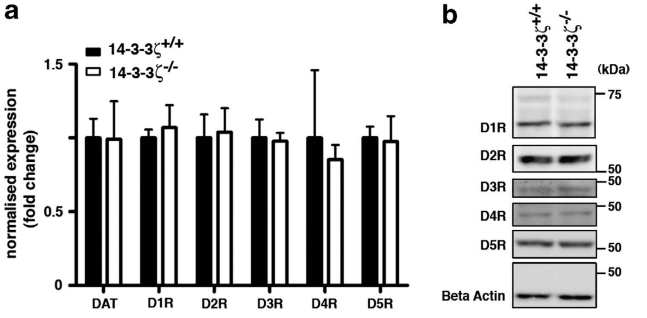

Figure 5. Expression of dopamine (DA) receptors in 14-3-3ζ knockout (KO) mice. (**a**) Quantitative reverse transcriptase-PCR (qRT-PCR) of *DA receptors D1–D5* and *DA transporter* (*DAT*) show that transcript levels of these genes are present at the same level in 14-3-3ζ KO (open bars; $n=4$) and 14-3-3ζ wild-type (WT) brains (closed bars; $n=4$). (**b**) Western blot analysis of whole-brain lysate shows that protein levels of DA receptors D1–D5 are present at the same level in 14-3-3ζ KO ($n=4$) and 14-3-3ζ WT brains ($n=4$). A representative blot of all four samples is shown in this figure that is quantitated in Supplementary Figure S4.

© 2013 Macmillan Publishers Limited

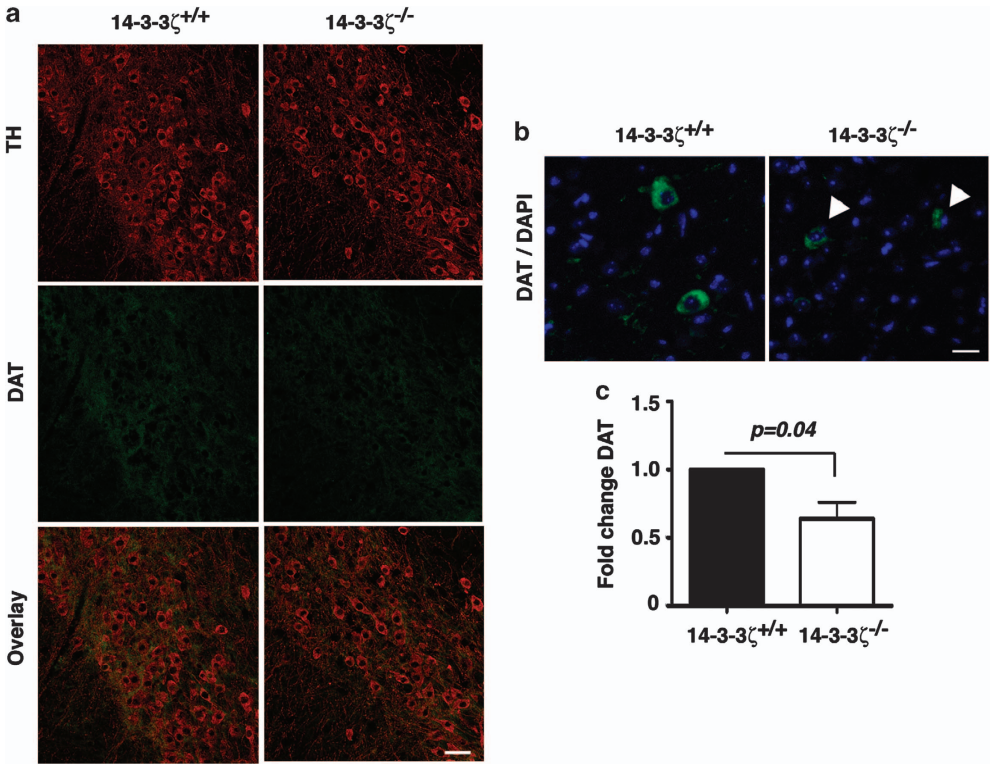

Figure 6. 14–3-3ζ Regulates dopamine transporter (DAT)expression in the substantia nigra (SN)-ventral tegmental area (VTA). (**a**) Sagittal brain sections stained with anti-tyrosine hydroxylase (TH; red) and anti-DAT (green) show reduced levels of DAT in the SN-VTA of 14-3-3ζ knockout (KO) mice compared with wild-type (WT) littermates. Blue, 4,6-diamidino-2-phenylindole (DAPI); scale bars = 50 um. (**b**) Higher magnification of anti-DAT immunostaining (green) in SN-VTA shows that DAT is mislocalized in the cell bodies of dopaminergic neurons (white arrowheads). Scale bar = 20 um. (**c**) Quantitation of anti-DAT immunostaining normalized to anti-TH confirms that 14-3-3ζ KO (open bar) have an approximately 30% reduction of DAT compared with WT mice (closed bar).

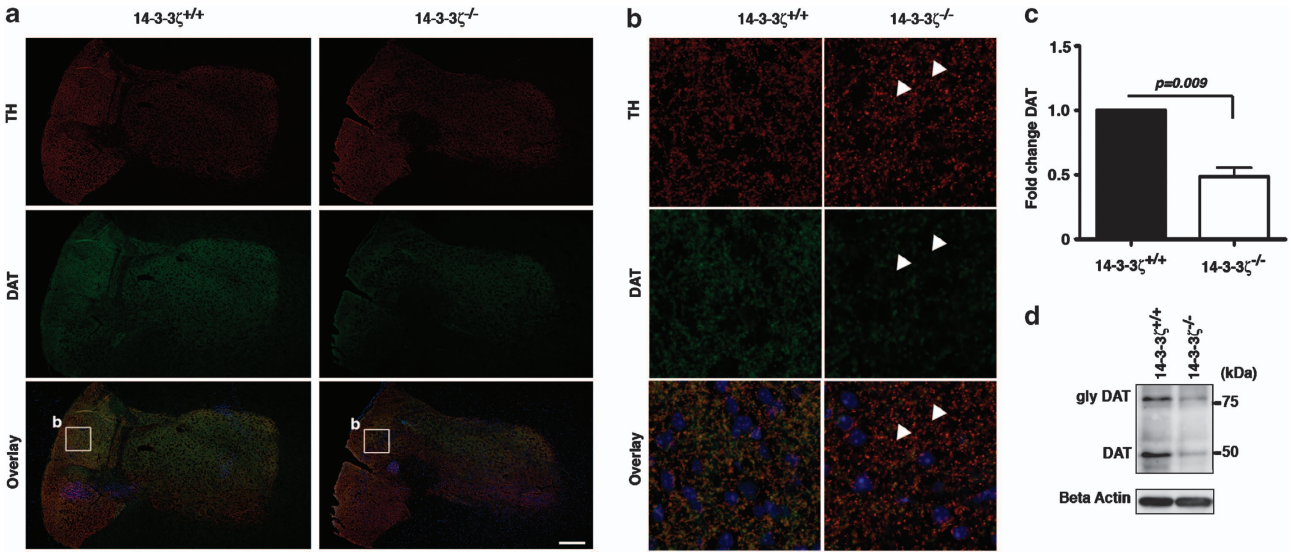

Figure 7. 14–3-3ζ Regulates dopamine transporter (DAT) expression in the striatum. (**a**) Sagittal brain sections stained with anti-tyrosine hydroxylase (TH; red) and anti-DAT (green) show reduced levels of DAT in the striatum of 14-3-3ζ knockout (KO) mice compared with wild-type (WT) littermates. Blue, 4,6-diamidino-2-phenylindole (DAPI); scale bars = 200 um. (**b**) Higher magnification of anti-DAT immunostaining (boxed region in **a**) shows that DAT is missing in the axonal terminals of dopaminergic neurons (white arrowheads). Blue, DAPI; scale bar = 10 um. (**c**) Quantitation of anti-DAT immunostaining normalized to anti-TH confirms that 14-3-3ζ KO (open bar) have an approximately 50% reduction of DAT compared with WT mice (closed bar). (**d**) Western blot analysis of whole-brain lysate shows that proteins levels of unglycosylated DAT (50 kDa) and glycosylated DAT (80 kDa) are reduced in 14-3-3ζ KO ($n = 4$) compared with 14-3-3ζ WT mice ($n = 4$).

© 2013 Macmillan Publishers Limited

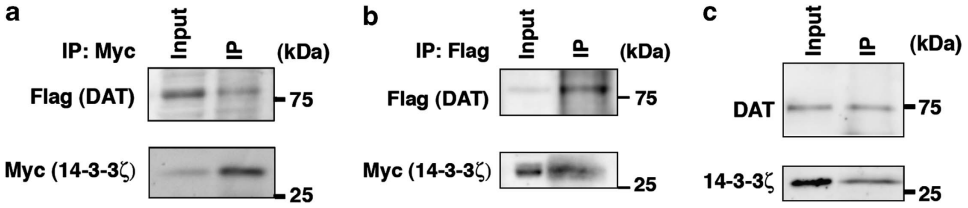

Figure 8. 14–3-3ζ Associates with dopamine transporter (DAT). (**a**) SN4741 cells were transiently transfected with Flag-His-DAT and Myc-14-3-3ζ. 14-3-3ζ was precipitated from protein lysates with anti-Myc antibody. 14-3-3ζ Immunoprecipitates were probed with anti-Myc monoclonal antibody to recognise 14-3-3ζ and anti-Flag to recognize DAT. (**b**) DAT was precipitated from protein lysates as in (**a**) with anti-Flag antibody. DAT immunoprecipitates were probed with anti-Myc monoclonal antibody to recognise 14-3-3ζ and anti-Flag to recognize DAT (**c**) 14-3-3ζ Was precipitated from P35 striatum lysates with anti-14-3-3ζ G1-7 monoclonal antibody. 14-3-3ζ Immunoprecipitates were probed with anti-14-3-3ζ (C16) and antibodies against DAT.

reduced by approximately 50% in the striatum of 14-3-3ζ KO mice (Figure 7c; WT, $n = 4$; KO, $n = 4$; $P = 0.009$).

Analysis of P35 whole-brain lysates by immunoblotting further identified robust deficiency of the non-glycosylated form of DAT (approximately 50 kDa band) in KO mice and in around half the cases also deficiency of the glycosylated form (approximately 75 kDa band; Figure 7d). To confirm that 14-3-3ζ is expressed in dopaminergic neurons, and in appropriate regions to have a role in DAT function, we co-immunostained sagittal brain sections with anti-14-3-3ζ M6 and anti-TH antibodies. Our analysis found that 14-3-3ζ is widely expressed in the midbrain, and importantly, within TH-positive neurons in the SN/VTA and their terminals in the striatum (Supplementary Figure S5). The lack of staining in 14-3-3ζ KO brain sections further confirms the specificity of this antibody and the expression of 14-3-3ζ in dopaminergic neurons.

DAT associates with 14-3-3ζ

As DAT is phosphorylated on several serine and threonine residues by CAMKII/protein kinase C and contains putative 14-3-3 binding sites (data not shown), we next investigated if 14-3-3ζ interacts with this transporter. By transiently expressing Flag-His-DAT and Myc-14-3-3ζ in the SN-derived mouse neuronal cell line SN4741, we were able to identify an interaction between these proteins by co-immuoprecipitation. In these experiments, purification of 14-3-3ζ with anti-Myc antibodies also co-precipitated Flag-His-tagged DAT (Figure 8a). In addition, purification of DAT with anti-Flag antibodies co-precipitated Myc-tagged 14-3-3ζ (Figure 8b). In contrast, co-immunoprecipitation with an immunoglobulin G isotype control antibody was unable to purify either 14-3-3ζ or DAT from protein lysates in which purification of DAT with anti-Flag antibodies co-precipitated Myc-tagged 14-3-3ζ (Supplementary Figure S6). To confirm the interaction between these proteins *in vivo*, we next completed co-immunoprecipitation experiments with our G1-7 monoclonal antibody in striatal protein extracts from P35 WT mice. Consistent with our overexpression study, we found that antibodies recognizing 14-3-3ζ also precipitate DAT from these complex protein extracts (Figure 8c).

DISCUSSION

Over the past 50 years, there have been many clinical and pharmacological studies implicating aberrant DA signalling in the pathology of psychosis associated with schizophrenia and related disorders.[5,39–42] Animal models with deficits in each component of the dopaminergic pathway, such as DA biosynthesis, DA receptors and DAT have provided valuable insight to the role of aberrant DA signalling in the presentation of psychosis-like behavioural defects.[43] However, many of these models have also shown paradoxical effects when compared with the human condition. We recently described 14-3-3ζ KO mice as a novel neurodevelopmental schizophrenia-like mouse model that has many anatomical and behavioural defects associated with the human condition.[17] This notion is supported by genetic linkage analysis[23] and the observations that 14-3-3ζ is downregulated at the mRNA[18] and protein[20,21,44] levels in post-mortem schizophrenia brain samples. Further support for a role in schizophrenia is derived from the recent finding that 14-3-3ζ is represented as a central hub within the schizophrenia-specific protein interaction network.[24] At the molecular level, 14-3-3ζ also interacts with several putative risk factors for schizophrenia that are essential for neuronal development, such as NdeL1, LIS1 and DISC1.[17,45] In this study, we have significantly advanced our understanding of the role of 14-3-3ζ in the presentation of schizophrenia-like deficits by identifying part of the molecular defects underpinning locomotor hyperactivity. First, we specifically identify dysregulated DA signalling as a cause of hyperactivity in 14-3-3ζ KO mice. Second, we have shown that DAT dysregulation occurs in the absence of any obvious change in abundance of TH or DA receptors. Finally, we found a reduction in the abundance of DAT in the brains of adult 14-3-3ζ KO mice, and show that in the WT setting, 14-3-3ζ and DAT interact.

A defining feature of schizophrenia is hypersensitivity to drugs that increase synaptic DA levels.[35–37] To test the validity of 14-3-3ζ KO mice as a model for the human condition, we therefore analysed both this feature and the ability of antipsychotics to ameliorate psychosis-like symptoms in our mouse model *in vivo*.

In support of 14-3-3ζ KO mice modelling the behavioural deficits associated with schizophrenia and associated disorders, we found that the antipsychotic drug clozapine was able to rescue baseline hyperactivity. However, although a 2-week treatment regime with clozapine had dramatic pharmacological effects on hyperactivity it was unable to modify the neurodevelopmental and anatomical defects associated with the disorder, including lamination and mossy fibre navigation in the hippocampus (data not shown).

Consistent with behavioural responses in patients with schizophrenia and related psychiatric disorders, we found that 14-3-3ζ KO mice are hypersensitive to the effects of amphetamine in a test of locomotor function. Taken together with our findings of baseline hyperactivity, disrupted senorimotor gating and developmental defects in the hippocampus,[17] these analyses implicate 14-3-3ζ KO mice as a highly applicable neurodevelopmental model of schizophrenia and related disorders.

As amphetamine acts as a substrate for DAT to promote DA efflux from presynaptic neurons, and clozapine can antagonise DA receptors, our results further suggest that some of the psychosis-like behavioural defects of 14-3-3ζ KO mice may arise from defects in the dopaminergic pathway. Indeed, our analysis of total tissue DA levels found that DA is significantly increased in the striatum of KO mice and strongly supports a role for 14-3-3ζ in the DA signalling pathway. 14-3-3ζ Has been implicated as a regulator of

© 2013 Macmillan Publishers Limited

DA signalling by interacting with TH through phosphorylation of Ser-19 to enhance activation of TH enzymatic activity by promoting further phosphorylation of Ser-31 and Ser-40.[15] Our analysis of 14-3-3ζ KO mice not only shows that 14-3-3ζ is indispensable for the formation of dopaminergic neurons in the brain, it also shows that TH levels and TH activation are maintained in the absence of 14-3-3ζ. In contrast to the proposal that 14-3-3ζ is the major isoform controlling TH activity,[15] our results suggest that 14-3-3 isoforms are likely to act redundantly in promoting TH activity *in vivo*. Indeed, multiple 14-3-3 isoforms have been shown to bind TH, and 14-3-3γ has recently been suggested to promote localization of TH to membrane fractions to preserve enzymatic activity.[46] Although our data fit with the idea that DA production is normal in 14-3-3ζ KO mice, it will now be important to measure the rate of DA synthesis *in vivo*.

To determine the nature of the dopaminergic dysfunction in our schizophrenia-like mouse model, we therefore analysed later stages of signalling post-secretion of DA from presynaptic vesicles. DA interacts with receptors on postsynaptic neurons to initiate a myriad of downstream signalling events by modulating activity of adenylate cyclase. Our analysis of the abundance of DA receptor by quantitative reverse transcriptase-PCR and western blotting was unable to detect any differences in the levels of either total RNA or protein from whole-brain samples. This finding identifies important differences between our schizophrenia-like mouse model and that of the DISC1 mouse models. DISC1 mutant mice also display DA dysfunction, however, in these mice the primary defect has been attributed to excessive levels of DA receptor D2.[47] Although the techniques used in our study provide a high level of quantitation, future experiments will be best directed at completing receptor binding studies to confirm our results and to analyse the levels and binding capacity of the DA receptors in more detail.

In the absence of gross defects in DA receptor levels, we next analysed the abundance of DAT that is expressed in presynaptic dopaminergic neurons to regulate levels of DA in the synaptic cleft. Our finding that DAT levels are reduced at the protein level and not at the RNA level suggests that the deficiency of DAT occurs via post-transcriptional mechanisms. In support of DAT dysfunction having a central role in the behavioural defects of our 14-3-3ζ mouse model, DAT KO mice have also been shown to have baseline hyperactivity.[48] At steady-state levels DAT is constitutively internalized, recycled to the plasma membrane or degraded in the lysosome through the activity of the E3 ubiquitin ligase Nedd4-2.[49] Although the precise mechanisms of this trafficking pathway are unclear it is reliant on amino acids 587–597 in the c-terminus of the protein[50] and on the ubiquitination of three lysine residues in the N-terminus.[51] DAT function is also heavily regulated by several kinases that primarily phosphorylate serine and threonine residues in its n-terminus.[52] Upon pharmacological stimulation of DAT with amphetamine, several serine and threonine residues in this n-terminal region are phosphorylated by protein kinase C and CAMKII to induce DA efflux from presynaptic neurons.[52] Our finding that DAT levels are reduced in 14-3-3ζ KO mice and also mislocalized in dopaminergic neurons therefore raises the hypothesis that 14-3-3ζ may have a role in modulating DAT phosphorylation, trafficking and/or degradation. In support of this notion, 14-3-3ζ has previously been found to bind to and inhibit the function of Nedd4-2 to positively regulate the abundance of other substrates such as amiloride-sensitive epithelial $Na+$ channel.[53] Whether 14-3-3ζ also binds Nedd4-2 to regulate levels of DAT is currently unknown, however, as Nedd4-2 is proposed to modulate membrane associated DAT (that is, the glycosylated form) our finding of reduced non-glycosylated DAT may argue against a primary role in regulating DAT levels through this pathway. A role for 14-3-3ζ in modulating DAT phosphorylation or function may also help to explain the ability of amphetamine to increase hyperactivity of KO mice over and above that of WT controls albeit in the presence of a 30% reduction of total DAT levels. Thus, dysregulation of receptor phosphorylation and/or activity may promote degradation in the resting state but retain DAT in a primed state for activation upon pharmacological stimulation. In support of this notion, phosphorylation of DAT Ser-7 has previously been found to hold DAT in a primed state for amphetamine-induced DA efflux.[52] It will now be of interest to examine the response of 14-3-3ζ KO mice to alternative stimulants of DAT such as cocaine and to test the ability of 14-3-3ζ to reduce amphetamine-induced DA efflux, for example by micro-dialysis.

In this study, we also identified an interaction between DAT and 14-3-3ζ in SN4741 cells and striatum brain extracts. However, as we were only able to co-purify a small proportion of total input protein in our co-immunoprecipitation experiments this further suggests that the interaction between DAT and 14-3-3ζ is quite weak and/or unstable. Whether this interaction is direct or mediated by an intermediate adaptor protein and whether this has a role in DAT function is currently unknown. Our *in silico* analysis of DAT identifies several high stringency phospho-serine/threonine 14-3-3 binding motifs in the c-terminus of the protein. Interestingly, these sites are located near the regions predicted to act as interaction sites for CAMKII and in the regions predicted to be essential for DAT internalization. It will now be of interest to determine the interaction dynamics of 14-3-3ζ and DAT and to determine if this has any role in kinase binding and receptor phosphorylation.

Finally, consistent with a functional abnormality in DAT physiology we found that total tissue DA levels are increased in 14-3-3ζ KO mice. Our study also found an increase in the DA degradation by-product, DOPAC. Although a 30% reduction in DAT may be expected to result in reduced DA degradation, our finding is in agreement with that observed in DAT KO mice that also have abundant levels of DOPAC.[54] Our findings therefore add strong support to the notion that DOPAC represents a by-product of newly synthesized DA rather than a by-product of DA recycled from the synaptic cleft.[54] Thus, although TH levels and activation are normal in 14-3-3ζ KO mice it will be of interest to determine the rate of DA synthesis in this model.

In conclusion, our data supports a model in which 14-3-3ζ interacts with DAT to modulate its activity and stability and thereby control the availability of DA in the synaptic cleft. This finding has important implications to the physiological basis of schizophrenia-like behavioural defects, the mechanisms controlling DAT function and the potential modulation of this pathway in the treatment of disorders with a hyperdopaminergic basis.

CONFLICT OF INTEREST

The authors declare no conflict of interest.

ACKNOWLEDGMENTS

We thank Rebecca Krake for genotyping mice and maintaining the mouse colonies. This work was funded by grants from the National Health and Medical Research Council of Australia (NHMRC) and Medvet Laboratories. HR is the recipient of the Peter Nelson Leukemia Research Fellowship and QS is the recipient of a NHMRC Career Development Award. MvdB is a NHMRC Senior Research Fellow. CLP is the recipient of a Viertel charitable foundation senior medical research fellowship.

REFERENCES

1 Tamminga CA, Stan AD, Wagner AD. The hippocampal formation in schizophrenia. *Am J Psychiatry* 2010; **167**: 1178–1193.
2 Carpenter WT, Koenig JI. The evolution of drug development in schizophrenia: past issues and future opportunities. *Neuropsychopharmacology* 2008; **33**: 2061–2079.

© 2013 Macmillan Publishers Limited

3 Leucht S, Wahlbeck K, Hamann J, Kissling W. New generation antipsychotics versus low-potency conventional antipsychotics: a systematic review and meta-analysis. *Lancet* 2003; **361**: 1581–1589.
4 Drevets WC, Gautier C, Price JC, Kupfer DJ, Kinahan PE, Grace AA *et al.* Amphetamine-induced dopamine release in human ventral striatum correlates with euphoria. *Biol Psychiatry* 2001; **49**: 81–96.
5 Laruelle M, Abi-Dargham A, Gil R, Kegeles L, Innis R. Increased dopamine transmission in schizophrenia: relationship to illness phases. *Biol Psychiatry* 1999; **46**: 56–72.
6 Amara SG, Kuhar MJ. Neurotransmitter transporters: recent progress. *Annu Rev Neurosci* 1993; **16**: 73–93.
7 Giros B, Caron MG. Molecular characterization of the dopamine transporter. *Trends Pharmacol Sci* 1993; **14**: 43–49.
8 Itagaki C, Isobe T, Taoka M, Natsume T, Nomura N, Horigome T *et al.* Stimulus-coupled interaction of tyrosine hydroxylase with 14-3-3 proteins. *Biochemistry* 1999; **38**: 15673–15680.
9 Toska K, Kleppe R, Armstrong CG, Morrice NA, Cohen P, Haavik J. Regulation of tyrosine hydroxylase by stress-activated protein kinases. *J Neurochem* 2002; **83**: 775–783.
10 Aitken A. 14-3-3 proteins: a historic overview. *Semin Cancer Biol* 2006; **16**: 162–172.
11 Ichimura T, Isobe T, Okuyama T, Yamauchi T, Fujisawa H. Brain 14-3-3 protein is an activator protein that activates tryptophan 5-monooxygenase and tyrosine 3-monooxygenase in the presence of Ca2+,calmodulin-dependent protein kinase II. *FEBS Lett* 1987; **219**: 79–82.
12 Berg D, Holzmann C, Riess O. 14-3-3 proteins in the nervous system. *Nat Rev Neurosci* 2003; **4**: 752–762.
13 Fu H, Subramanian RR, Masters SC. 14-3-3 Proteins: structure, function, and regulation. *Annu Rev Pharmacol Toxicol* 2000; **40**: 617–647.
14 Rosner M, Hengstschlager M. 14-3-3 Proteins are involved in the regulation of mammalian cell proliferation. *Amino Acids* 2006; **30**: 105–109.
15 Wang J, Lou H, Pedersen CJ, Smith AD, Perez RG. 14-3-3Zeta contributes to tyrosine hydroxylase activity in MN9D cells: localization of dopamine regulatory proteins to mitochondria. *J Biol Chem* 2009; **284**: 14011–14019.
16 Baxter HC, Liu WG, Forster JL, Aitken A, Fraser JR. Immunolocalisation of 14-3-3 isoforms in normal and scrapie-infected murine brain. *Neuroscience* 2002; **109**: 5–14.
17 Cheah PS, Ramshaw HS, Thomas PQ, Toyo-Oka K, Xu X, Martin S *et al.* Neurodevelopmental and neuropsychiatric behaviour defects arise from 14-3-3zeta deficiency. *Mol Psychiatry* 2012, Picture solicited for cover **17**: 451–466.
18 Middleton FA, Peng L, Lewis DA, Levitt P, Mirnics K. Altered expression of 14-3-3 genes in the prefrontal cortex of subjects with schizophrenia. *Neuropsychopharmacology* 2005; **30**: 974–983.
19 Wong AH, Likhodi O, Trakalo J, Yusuf M, Sinha A, Pato CN *et al.* Genetic and post-mortem mRNA analysis of the 14-3-3 genes that encode phosphoserine/threonine-binding regulatory proteins in schizophrenia and bipolar disorder. *Schizophr Res* 2005; **78**: 137–146.
20 English JA, Dicker P, Focking M, Dunn MJ, Cotter DR. 2-D DIGE analysis implicates cytoskeletal abnormalities in psychiatric disease. *Proteomics* 2009; **9**: 3368–3382.
21 English JA, Pennington K, Dunn MJ, Cotter DR. The neuroproteomics of schizophrenia. *Biol Psychiatry* 2011; **69**: 163–172.
22 Sivagnanasundaram S, Crossett B, Dedova I, Cordwell S, Matsumoto I. Abnormal pathways in the genu of the corpus callosum in schizophrenia pathogenesis: a proteome study. *Proteomics Clin Appl* 2007; **1**: 1291–1305.
23 Jia Y, Yu X, Zhang B, Yuan Y, Xu Q, Shen Y. An association study between polymorphisms in three genes of 14-3-3 (tyrosine 3-monooxygenase/tryptophan 5-monooxygenase activation protein) family and paranoid schizophrenia in northern Chinese population. *Eur Psychiatry* 2004; **19**: 377–379.
24 Sun J, Jia P, Fanous AH, van den Oord E, Chen X, Riley BP *et al.* Schizophrenia gene networks and pathways and their applications for novel candidate gene selection. *PLoS One* 2010; **5**: e11351.
25 Toyo-oka K, Shionoya A, Gambello MJ, Cardoso C, Leventer R, Ward HL *et al.* 14-3-3epsilon is important for neuronal migration by binding to NUDEL: a molecular explanation for Miller-Dieker syndrome. *Nat Genet* 2003; **34**: 274–285.
26 Coyle P, Tran N, Fung JN, Summers BL, Rofe AM. Maternal dietary zinc supplementation prevents aberrant behaviour in an object recognition task in mice offspring exposed to LPS in early pregnancy. *Behav Brain Res* 2009; **197**: 210–218.
27 Summers BL, Rofe AM, Coyle P. Prenatal zinc treatment at the time of acute ethanol exposure limits spatial memory impairments in mouse offspring. *Pediatr Res* 2006; **59**: 66–71.
28 van den Buuse M, Wischhof L, Lee RX, Martin S, Karl T. Neuregulin 1 hypomorphic mutant mice: enhanced baseline locomotor activity but normal psychotropic drug-induced hyperlocomotion and prepulse inhibition regulation. *Int J Neuropsychopharmacol* 2009; **12**: 1383–1393.
29 Williams AA, Ingram WM, Levine S, Resnik J, Kamel CM, Lish JR *et al.* Reduced levels of serotonin 2A receptors underlie resistance of Egr3-deficient mice to locomotor suppression by clozapine. *Neuropsychopharmacology* 2012; **37**: 2285–2298.
30 Baune BT, Wiede F, Braun A, Golledge J, Arolt V, Koerner H. Cognitive dysfunction in mice deficient for TNF- and its receptors. *Am J Med Genet B Neuropsychiatr Genet* 2008; **147B**: 1056–1064.
31 Hart PC, Bergner CL, Smolinsky AN, Dufour BD, Egan RJ, Laporte JL *et al.* Experimental models of anxiety for drug discovery and brain research. *Methods Mol Biol* 2010; **602**: 299–321.
32 Koike H, Arguello PA, Kvajo M, Karayiorgou M, Gogos JA. Disc1 is mutated in the 129S6/SvEv strain and modulates working memory in mice. *Proc Natl Acad Sci USA* 2006; **103**: 3693–3697.
33 Samuel MS, Lopez JI, McGhee EJ, Croft DR, Strachan D, Timpson P *et al.* Actomyosin-mediated cellular tension drives increased tissue stiffness and beta-catenin activation to induce epidermal hyperplasia and tumor growth. *Cancer Cell* 2011; **19**: 776–791.
34 Son JH, Chun HS, Joh TH, Cho S, Conti B, Lee JW. Neuroprotection and neuronal differentiation studies using substantia nigra dopaminergic cells derived from transgenic mouse embryos. *J Neurosci* 1999; **19**: 10–20.
35 Levy DL, Smith M, Robinson D, Jody D, Lerner G, Alvir J *et al.* Methylphenidate increases thought disorder in recent onset schizophrenics, but not in normal controls. *Biol Psychiatry* 1993; **34**: 507–514.
36 Lieberman JA, Alvir J, Geisler S, Ramos-Lorenzi J, Woerner M, Novacenko H *et al.* Methylphenidate response, psychopathology and tardive dyskinesia as predictors of relapse in schizophrenia. *Neuropsychopharmacology* 1994; **11**: 107–118.
37 Lieberman JA, Kane JM, Alvir J. Provocative tests with psychostimulant drugs in schizophrenia. *Psychopharmacology (Berl)* 1987; **91**: 415–433.
38 Sulzer D. How addictive drugs disrupt presynaptic dopamine neurotransmission. *Neuron* 2011; **69**: 628–649.
39 Abi-Dargham A, Gil R, Krystal J, Baldwin RM, Seibyl JP, Bowers M *et al.* Increased striatal dopamine transmission in schizophrenia: confirmation in a second cohort. *Am J Psychiatry* 1998; **155**: 761–767.
40 Breier A, Su TP, Saunders R, Carson RE, Kolachana BS, de Bartolomeis A *et al.* Schizophrenia is associated with elevated amphetamine-induced synaptic dopamine concentrations: evidence from a novel positron emission tomography method. *Proc Natl Acad Sci USA* 1997; **94**: 2569–2574.
41 Laruelle M. Imaging dopamine transmission in schizophrenia. A review and meta-analysis. *Q J Nucl Med* 1998; **42**: 211–221.
42 van Rossum JM. The significance of dopamine-receptor blockadefor the mechanism of action of neuroleptic drugs. *Arch Int de Pharmacodynamie et de Thérapie* 1966; **160**: 492–494.
43 van den Buuse M. Modeling the positive symptoms of schizophrenia in genetically modified mice: pharmacology and methodology aspects. *Schizophr Bull* 2010; **36**: 246–270.
44 Sivagnanasundaram S, Fletcher D, Hubank M, Illingworth E, Skuse D, Scambler P. Differential gene expression in the hippocampus of the Df1/+ mice: a model for 22q11.2 deletion syndrome and schizophrenia. *Brain Res* 2007; **1139**: 48–59.
45 Toyo-Oka K, Sasaki S, Yano Y, Mori D, Kobayashi T, Toyoshima YY *et al.* Recruitment of katanin p60 by phosphorylated NDEL1, an LIS1 interacting protein, is essential for mitotic cell division and neuronal migration. *Hum Mol Genet* 2005; **14**: 3113–3128.
46 Halskau Jr. O, Ying M, Baumann A, Kleppe R, Rodriguez-Larrea D, Almas B *et al.* Three-way interaction between 14-3-3 proteins, the N-terminal region of tyrosine hydroxylase, and negatively charged membranes. *J Biol Chem* 2009; **284**: 32758–32769.
47 Jaaro-Peled H, Niwa M, Foss CA, Murai R, de Los Reyes S, Kamiya A *et al.* Subcortical dopaminergic deficits in a DISC1 mutant model: a study in direct reference to human molecular brain imaging. *Hum Mol Genet* 2013; **22**: 1574–1580.
48 Giros B, Jaber M, Jones SR, Wightman RM, Caron MG. Hyperlocomotion and indifference to cocaine and amphetamine in mice lacking the dopamine transporter. *Nature* 1996; **379**: 606–612.
49 Vina-Vilaseca A, Sorkin A. Lysine 63-linked polyubiquitination of the dopamine transporter requires WW3 and WW4 domains of Nedd4-2 and UBE2D ubiquitin-conjugating enzymes. *J Biol Chem* 2010; **285**: 7645–7656.
50 Holton KL, Loder MK, Melikian HE. Nonclassical distinct endocytic signals dictate constitutive and PKC-regulated neurotransmitter transporter internalization. *Nat Neurosci* 2005; **8**: 881–888.
51 Miranda M, Dionne KR, Sorkina T, Sorkin A. Three ubiquitin conjugation sites in the amino terminus of the dopamine transporter mediate protein kinase C-dependent endocytosis of the transporter. *Mol Biol Cell* 2007; **18**: 313–323.

© 2013 Macmillan Publishers Limited

52 Khoshbouei H, Sen N, Guptaroy B, Johnson L, Lund D, Gnegy ME *et al*. N-terminal phosphorylation of the dopamine transporter is required for amphetamine-induced efflux. *PLoS Biol* 2004; **2**: E78.

53 Ichimura T, Yamamura H, Sasamoto K, Tominaga Y, Taoka M, Kakiuchi K *et al*. 14-3-3 proteins modulate the expression of epithelial Na+ channels by phosphorylation-dependent interaction with Nedd4-2 ubiquitin ligase. *J Biol Chem* 2005; **280**: 13187–13194.

54 Jones SR, Gainetdinov RR, Jaber M, Giros B, Wightman RM, Caron MG. Profound neuronal plasticity in response to inactivation of the dopamine transporter. *Proc Natl Acad Sci USA* 1998; **95**: 4029–4034.

This work is licensed under a Creative Commons Attribution-NonCommercial-ShareAlike 3.0 Unported License. To view a copy of this license, visit http://creativecommons.org/licenses/by-nc-sa/3.0/

Supplementary Information accompanies the paper on the Translational Psychiatry website (http://www.nature.com/tp)

© 2013 Macmillan Publishers Limited

SCIENTIFIC REPORTS

OPEN

Received: 23 February 2015
Accepted: 14 April 2015
Published: 24 July 2015

14-3-3ζ deficient mice in the BALB/c background display behavioural and anatomical defects associated with neurodevelopmental disorders

Xiangjun Xu[1], Emily J. Jaehne[2], Zarina Greenberg[1], Peter McCarthy[1], Eiman Saleh[1], Clare L. Parish[3], Daria Camera[4], Julian Heng[5,6], Matilda Haas[7], Bernhard T. Baune[2], Udani Ratnayake[3], Maarten van den Buuse[3,7], Angel F. Lopez[1], Hayley S. Ramshaw[1,*] & Quenten Schwarz[1,*]

Sequencing and expression analyses implicate 14-3-3ζ as a genetic risk factor for neurodevelopmental disorders such as schizophrenia and autism. In support of this notion, we recently found that 14-3-3ζ$^{-/-}$ mice in the Sv/129 background display schizophrenia-like defects. As epistatic interactions play a significant role in disease pathogenesis we generated a new congenic strain in the BALB/c background to determine the impact of genetic interactions on the 14-3-3ζ$^{-/-}$ phenotype. In addition to replicating defects such as aberrant mossy fibre connectivity and impaired spatial memory, our analysis of 14-3-3ζ$^{-/-}$ BALB/c mice identified enlarged lateral ventricles, reduced synaptic density and ectopically positioned pyramidal neurons in all subfields of the hippocampus. In contrast to our previous analyses, 14-3-3ζ$^{-/-}$ BALB/c mice lacked locomotor hyperactivity that was underscored by normal levels of the dopamine transporter (DAT) and dopamine signalling. Taken together, our results demonstrate that dysfunction of 14-3-3ζ gives rise to many of the pathological hallmarks associated with the human condition. 14-3-3ζ-deficient BALB/c mice therefore provide a novel model to address the underlying biology of structural defects affecting the hippocampus and ventricle, and cognitive defects such as hippocampal-dependent learning and memory.

Neurodevelopmental disorders arise from aberrant embryonic and postnatal brain development and encompass a wide spectrum of pathologies such as schizophrenia, autism and intellectual disability. Although heterogeneous in nature, recent sequencing analyses have shown that many of these disorders, in particular schizophrenia and autism, arise from mutations in overlapping molecular pathways thereby suggesting they share similar pathophysiological origins[1–3]. Indeed, this notion is further supported by

[1]Centre for Cancer Biology, SA Pathology and University of South Australia, Frome Road, Adelaide, 5000, Australia. [2]Discipline of Psychiatry, University of Adelaide, Adelaide, SA 5005, Australia. [3]The Florey Institute of Neuroscience and Mental Health, The University of Melbourne, Parkville, 3010, Australia. [4]School of Medical Sciences, RMIT University, Bundoora, 3083, Australia. [5]Harry Perkins Institute of Medical Research, Perth, Australia. [6]School of Medicine and Pharmacology, University of Western Australia, Crawley, 6009, Australia. [7]Australian Regenerative Medicine Institute, Monash University, Clayton, Australia. [8]School of Psychological Science, La Trobe University, Melbourne, Australia. *These authors contributed equally to this work. Correspondence and requests for materials should be addressed to Q.S. (email: quenten.schwarz@health.sa.gov.au)

the finding that these disorders often share similar anatomical features including structural anomalies of the hippocampus, enlarged ventricles and reduced synaptic density[4–7].

The family of 14-3-3 proteins comprise seven distinct isoforms (β, ζ, ε, γ, η, τ, σ) that are expressed abundantly throughout development and in adult tissue[8]. This family of proteins comprise over 1% of total soluble brain protein[9] and have been implicated in several neurological disorders such as epilepsy[10], bipolar disorder[11,12], mental retardation[13] and lissencephaly. Notably, non-synonomous *14-3-3ζ* mutations have recently been identified in both schizophrenia and autistic patients[14,15]. Taken together with the findings that this gene is consistently down-regulated in post-mortem brain samples at the mRNA[11,16] and protein levels[17–19], these data collectively identify *14-3-3ζ* as a potential risk factor for neurodevelopmental disorders.

Mouse models of schizophrenia and autism have been paramount in our understanding of genetic risk factors and in the identification of biological pathways underlying neurobehavioural deficits. To define the role of 14-3-3ζ in neurodevelopmental disorders we recently characterised some of the anatomical, physiological and behavioural defects of 14-3-3ζ$^{-/-}$ mice in the Sv/129 background[20,21]. Our findings demonstrated that 14-3-3ζ is required for normal brain development and brain function. Thus, 14-3-3ζ$^{-/-}$ mice have schizophrenia-like behavioural defects including hyperactivity and disrupted sensorimotor gating that are accompanied by aberrant neuronal migration and axonal guidance defects in the hippocampus[20]. We further demonstrated that baseline hyperactivity of 14-3-3ζ$^{-/-}$ mice arises from aberrant dopamine signaling as a result of decreased levels of the dopamine transporter (DAT). Given that 14-3-3ζ$^{-/-}$ mice respond favourably to the frontline antipsychotic drug clozapine, our previous findings suggest that 14-3-3ζ$^{-/-}$ mice represent a novel neurodevelopmental model of schizophrenia and associated disorders.

One of the major confounding factors in interpreting findings from neurodevelopmental mouse models is the epistatic effects of the background strain. For example, the phenotypes of mice lacking DAT vary dramatically depending on genetic background[22] and even wild type mice from different backgrounds have profoundly different behavioural phenotypes[23,24]. To establish the role of candidate genes in the pathophysiology of any particular disorder it is therefore essential to examine the role of any mutations in multiple genetic backgrounds.

To investigate the contribution of genetic backgrounds to the 14-3-3ζ$^{-/-}$ phenotype we have derived a new congenic strain in the BALB/c background by back-crossing to this line for over 10 generations. BALB/c mice were chosen as they are a widely used inbred mouse strain that breeds well and shows markedly different behavioural phenotypes to the Sv/129 strain[21,23,24]. Moreover, as BALB/c mice are reported to respond differently to psychostimulants acting on the dopamine pathway[23] this line provides an ideal model to test the role of 14-3-3ζ in dopamine signalling.

Here we report that 14-3-3ζ$^{-/-}$ mice in the BALB/c genetic background replicate all of the anatomical defects previously reported in the Sv/129 strain and uncover additional hallmark phenotypes of neurodevelopmental disorders. In the absence of profound structural brain defects BALB/c mice lacking 14-3-3ζ display mispatterning of hippocampal pyramidal neurons and misrouting of dentate mossy fibres. Importantly, we show for the first time that 14-3-3ζ is essential for correct formation of the lateral ventricles and for hippocampal synaptic connections. Consistent with physiological dysfunction of the hippocampus we found that 14-3-3ζ$^{-/-}$ mice had striking neurobehavioural deficits in spatial learning and memory. In contrast, we failed to observe alterations in anxiety or locomotor function, a finding that is underscored by normal levels of DAT and dopaminergic signaling. Our analysis therefore shows that 14-3-3ζ is essential for neurodevelopment and for higher-order brain function. Although 14-3-3ζ$^{-/-}$ mice have variable behavioural phenotypes depending on the genetic background, each of the lines present unique features of human neurodevelopmental disorders and identify a key role for deficiency of the 14-3-3ζ molecular pathway in the pathophysiology of schizophrenia and associated disorders.

Results

14-3-3ζ-deficient mice in the BALB/c background display hippocampal defects. We have previously shown that 14-3-3ζ$^{-/-}$ mice in the Sv/129 background display anatomical and behavioural defects reminiscent to neurodevelopmental disorders such as schizophrenia[20,21]. To determine if different genetic backgrounds affect the 14-3-3ζ$^{-/-}$ phenotype we back-crossed these mice in to the BALB/c background for over 10 generations. Quantitative RT-PCR and western blot analysis on embryonic and adult tissue confirmed that BALB/c 14-3-3ζ$^{-/-}$ mice completely lacked *14-3-3ζ* expression (Supplementary Fig. 1). Inter-crosses of BALB/c 14-3-3ζ heterozygous mice gave rise to homozygous mice at the expected Mendelian ratio at birth indicating that 14-3-3ζ$^{-/-}$ mice are embryonically viable (25.5% 14-3-3ζ$^{+/+}$, 53.2% 14-3-3ζ$^{+/-}$, 21.2% 14-3-3ζ$^{-/-}$; $n = 470$, $P = 0.1772$). Notably, back-crossing into the BALB/c background rescued the growth retardation and postnatal death of 14-3-3ζ$^{-/-}$ mice that was evident in the Sv/129 background. Regardless of the genetic background 14-3-3ζ$^{-/-}$ males and females were infertile. Tests of olfaction, vision, balance, self-righting, eye blink, eye twitch, whisker orientation and neuromuscular strength were normal in 14-3-3ζ$^{-/-}$ compared to 14-3-3ζ$^{+/+}$ controls (summarised in Table S1) further indicating that there are no outwardly abnormal phenotypes in these mice.

Nissl staining of coronal brain sections from adult mice indicated that laminar organisation of several brain regions, implicated in neurodevelopmental disorders, such as the prefrontal cortex, cingulate cortex, hypothalamus, motor cortex and striatum formed normally in BALB/c 14-3-3ζ$^{-/-}$ mice (Fig. 1).

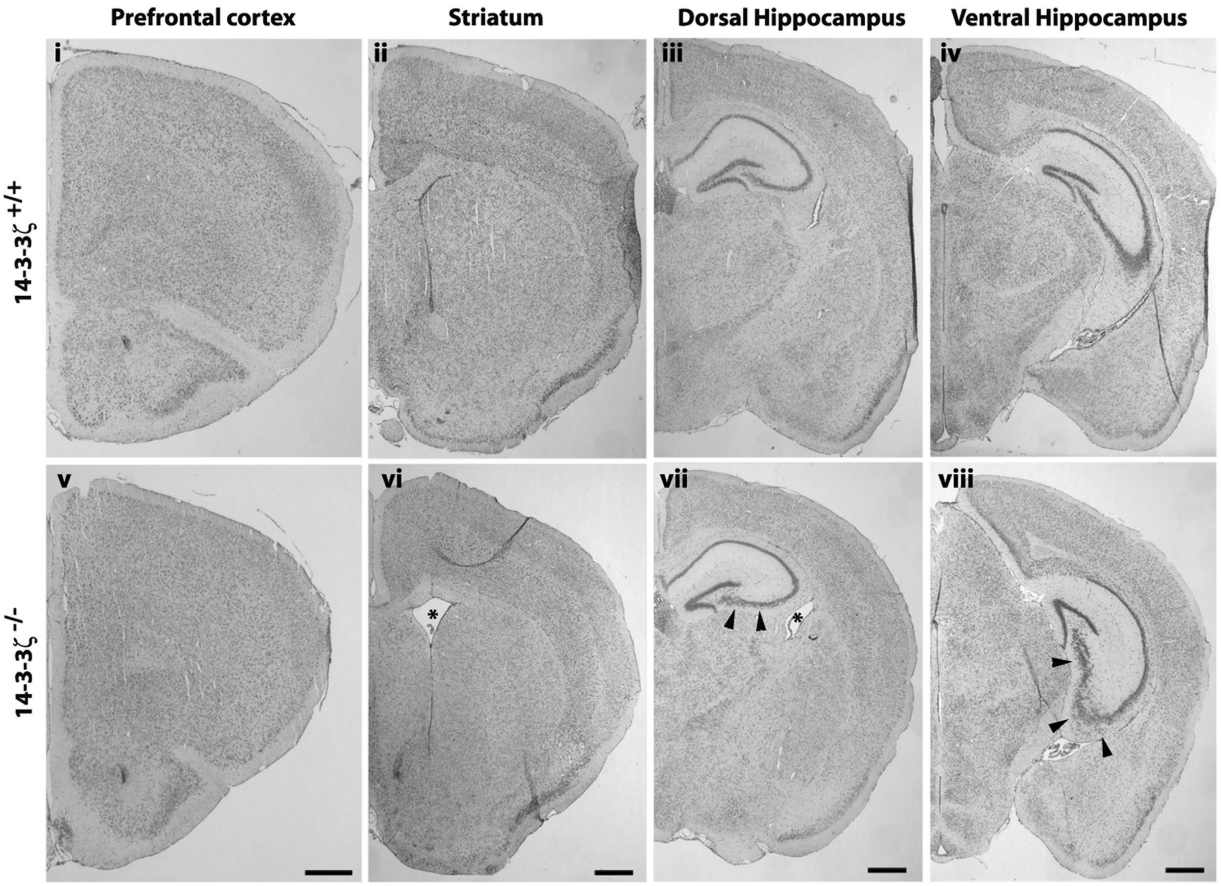

Figure 1. Structural brain defects in 14-3-3ζ-deficient mice. Nissl staining of coronal brain sections from 5 month old adult 14-3-3$\zeta^{+/+}$ (i–iv) and 14-3-3$\zeta^{-/-}$ mice (v–viii). Images show that lamination of the prefrontal cortex (i and v), motor cortex and cingulate cortex (i–iii and v–vii), thalamus (iii and vii) and amygdala (iii and vii) are normal in 14-3-3$\zeta^{-/-}$ mice. Lamination defects were identified in the dorsal and ventral hippocampus of 14-3-3$\zeta^{-/-}$ mice (iii and vii, iv and viii respectively; arrowhead). The lateral ventricle was also enlarged in 14-3-3$\zeta^{-/-}$ mice (ii–iii and vi–vii; asterisk). Scale bar = 100 μm.

In contrast, pyramidal neurons of the dorsal and ventral hippocampus in cornu ammonis (CA) subfields CA1, CA2 and CA3 were ectopically positioned (arrowheads, Fig. 1 iii,iv,vii,viii). Consistent with the notion that 14-3-3$\zeta^{-/-}$ mice model schizophrenia-like symptoms, Nissl staining also uncovered enlargement of the lateral ventricle in 14-3-3$\zeta^{-/-}$ adult mice compared to wildtypes, that was fully penetrant and not previously identified in other genetic backgrounds (Fig. 1vi,vii and ii,iii respectively; n = 5/genotype).

We next asked if the neuronal mispatterning and enlarged ventricles arose from developmental defects. Ectopically positioned pyramidal neurons in CA1-3 were first identified prior to hippocampal maturation at postnatal day (P) 7 and this was maintained throughout all postnatal stages (asterisk, Fig. 2A; 3/3 at P7, 5/5 at P14 and 5/5 at P56). Similar to our observations in the Sv/129 background, pyramidal neurons within the CA3 subfield split into a bilaminar stratum while pyramidal neurons within the CA2/3 boundary were ectopically positioned in the stratum radiatum and stratum oriens. In addition, we identified ectopically positioned neurons in the stratum oriens of the CA1 subfield that was not previously described in Sv/129 14-3-3$\zeta^{-/-}$ mice[20] (Fig. 2Avi–viii). Analysis of Nissl-stained sections was unable to detect any notable differences at embryonic day (E) 17.5, a stage at which the pyramidal neurons are starting to condense in to a bonafide stratum (Fig. 2Ai and v). Enlargement of the lateral ventricles was also identified during developmental stages, first being detected at P14 with no notable defects at P7 (Fig. 2Avi–viii) or in additional mice examined at P10 (data not shown).

To determine if ectopically-positioned pyramidal cells formed mature neurons we next immunostained coronal sections with antibodies against the neuronal marker NeuN. At all ages examined the ectopically positioned cells were positive for NeuN (Fig. 2B) indicating that these neurons likely form functional connections. At E17.5 when pyramidal neurons are condensing in to the stratum of the CA in the 14-3-3$\zeta^{+/+}$ controls, mature neurons were identified in the superficial layers juxtaposing the subventricular zone of 14-3-3$\zeta^{-/-}$ embryos (Fig. 2Bi,ii). Taken together, and in light of our previous work in the Sv/129 background, these findings identify a clear role for 14-3-3ζ during hippocampal morphogenesis and pyramidal neuron migration.

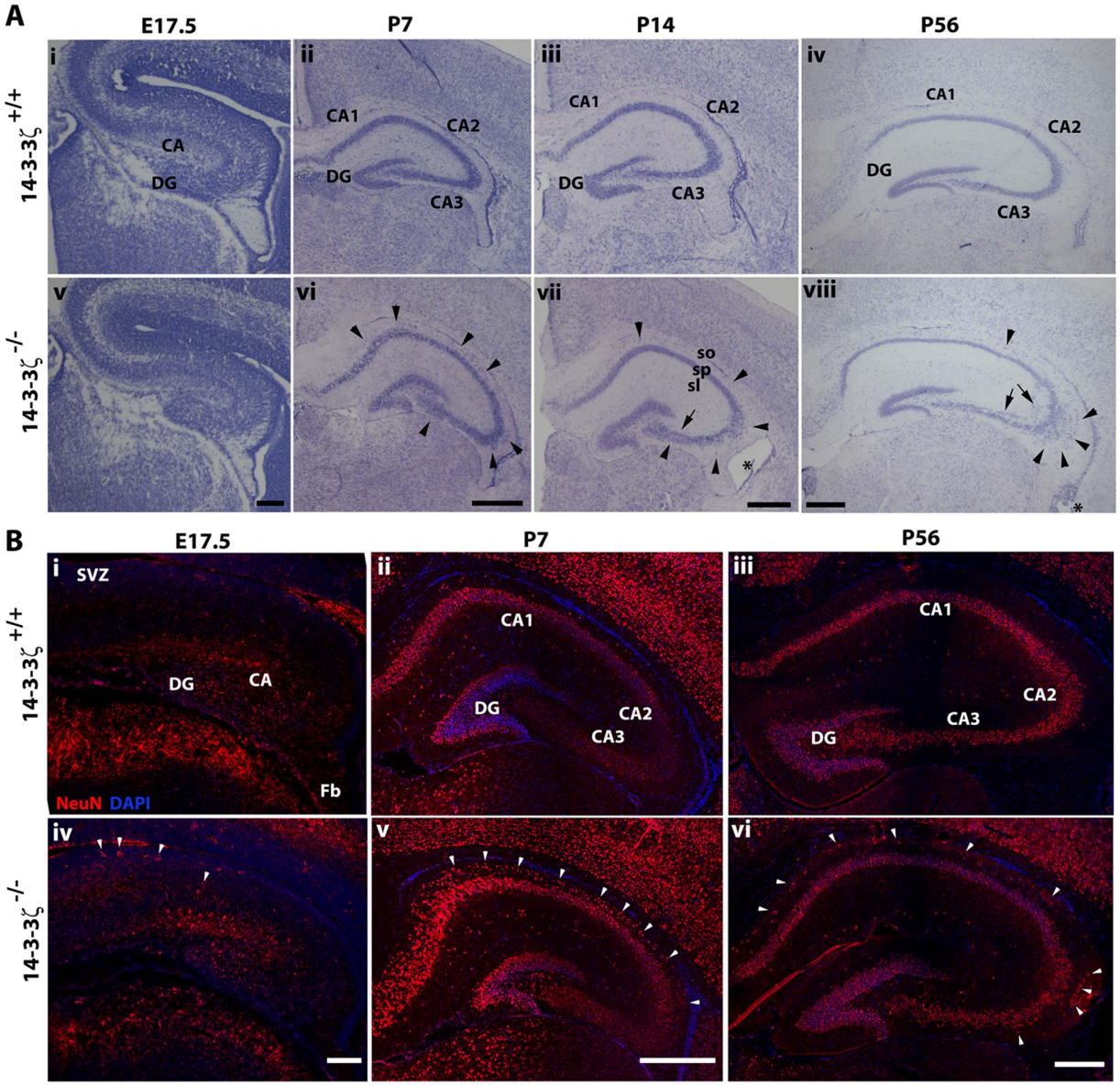

Figure 2. Hippocampal lamination defects in 14-3-3ζ-deficient mice. (**A**) Nissl staining shows the hippocampal development of 14-3-3$\zeta^{+/+}$ (i–iv) and 14-3-3$\zeta^{-/-}$ (v–viii) mice from embryonic day (E) 17.5 until post natal day (P) 56. During embryonic development no gross structural defects could be seen in 14-3-3$\zeta^{-/-}$ mice (**i** and **v**). Pyramidal neurons in the cornu ammonis (CA) subfields, CA1-3, were dispersed in the stratum pyramidale (sp) and stratum oriens (arrowheads) layer in 14-3-3$\zeta^{-/-}$ mice. Arrows highlight the duplicated layer of hippocampal pyramidal neurons in stratum radiatum (sr). Scale bar = 100 μm. (**B**) Coronal sections of the hippocampus obtained from E17.5 (**i** and **iv**), P7 (**ii** and **v**) and P56 (iii and vi) 14-3-3$\zeta^{+/+}$ and14-3-3$\zeta^{-/-}$ mice. At E17.5 the stratum pyramidale is populated by NeuN-positive pyramidal cells in 14-3-3$\zeta^{+/+}$ hippocampi forming a uniform mature zone in the developing CA. In 14-3-3$\zeta^{-/-}$ hippocampi, the maturation zone was less uniform with some NeuN-positive mature pyramidal cells ectopically positioned in the superficial zone of the stratum pyramidale in the CA and others in the sub ventricular zone (SVZ; white arrowheads). In P7 and P56 14-3-3-$\zeta^{-/-}$ mice, NeuN immunostaining identifies mature pyramidal neurons ectopically positioned in the stratum oriens of CA1-3 (arrowheads). Scale bars: 100 μm.

Aberrant hippocampal connectivity in 14-3-3ζ-deficient mice. Functional connectivity within the hippocampus is essential for high-order brain function[25]. Given the ectopic positions of neurons within the CA of 14-3-3$\zeta^{-/-}$ mice we next asked if the mossy fibre connections between the dentate granular neurons and CA3 pyramidal neurons were also affected. Immunostaining with antibodies against calbindin showed that the suprapyramidal and infrapyramidal mossy fibre tracts were aberrantly aligned in the 14-3-3$\zeta^{-/-}$ mice, compared to wildtype littermates (Fig. 3i–iv). Whereas the suprapyramidal tract

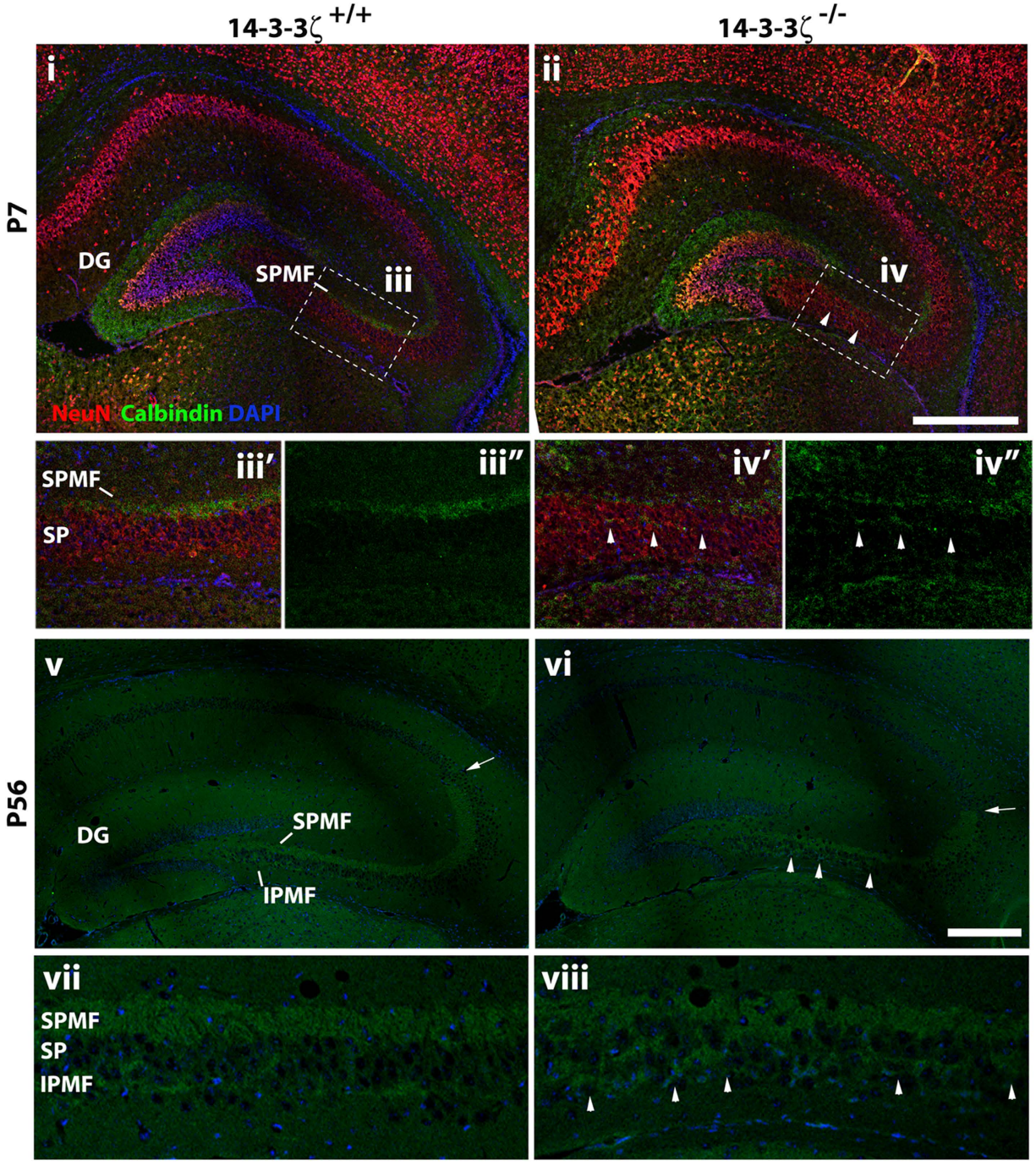

Figure 3. Abnormal connectivity of the hippocampus in 14-3-3ζ-deficient mice. Calbindin immunostaining of the infrapyramidal (IPMF) and the suprapyramidal (SPMF) mossy fibre trajectories. At P7 (i–iv) the calbindin mossy fibres are seen along the SPMF branch navigating away from the dentate gyrus (DG) in both 14-3-3$\zeta^{+/+}$ and 14-3-3$\zeta^{-/-}$ mice. In 14-3-3$\zeta^{-/-}$ mice the SPMF (green) branch aberrantly navigates among the NeuN positive (red) pyramidal cell somata (sp, arrowheads) in CA3. (iii') higher magnification of boxed area in (i) and (iii") higher magnification of calbindin staining from boxed area in (i). (iv') Higher magnification of boxed area in (ii) and (iv") higher magnification of calbindin staining from boxed area in (ii). At P56 (v-viii) the SPMF and IPMF branches of 14-3-3$\zeta^{-/-}$ mice navigate aberrantly among the pyramidal cell somata (arrowheads) in CA3 and, the SPMF is shorter than in 14-3-3$\zeta^{+/+}$ mice (arrow). (vii and viii) higher magnification of the boxed regions in (v) and (vi), respectively. Scale bars = 100 μm.

formed tight axonal bundles along the apical surface of the CA3 pyramidal neurons in 14-3-3$\zeta^{+/+}$ mice, these mossy fibres navigated within the CA3 pyramidal layer of 14-3-3$\zeta^{-/-}$ mice at P7 (Fig. 3iii,iv).

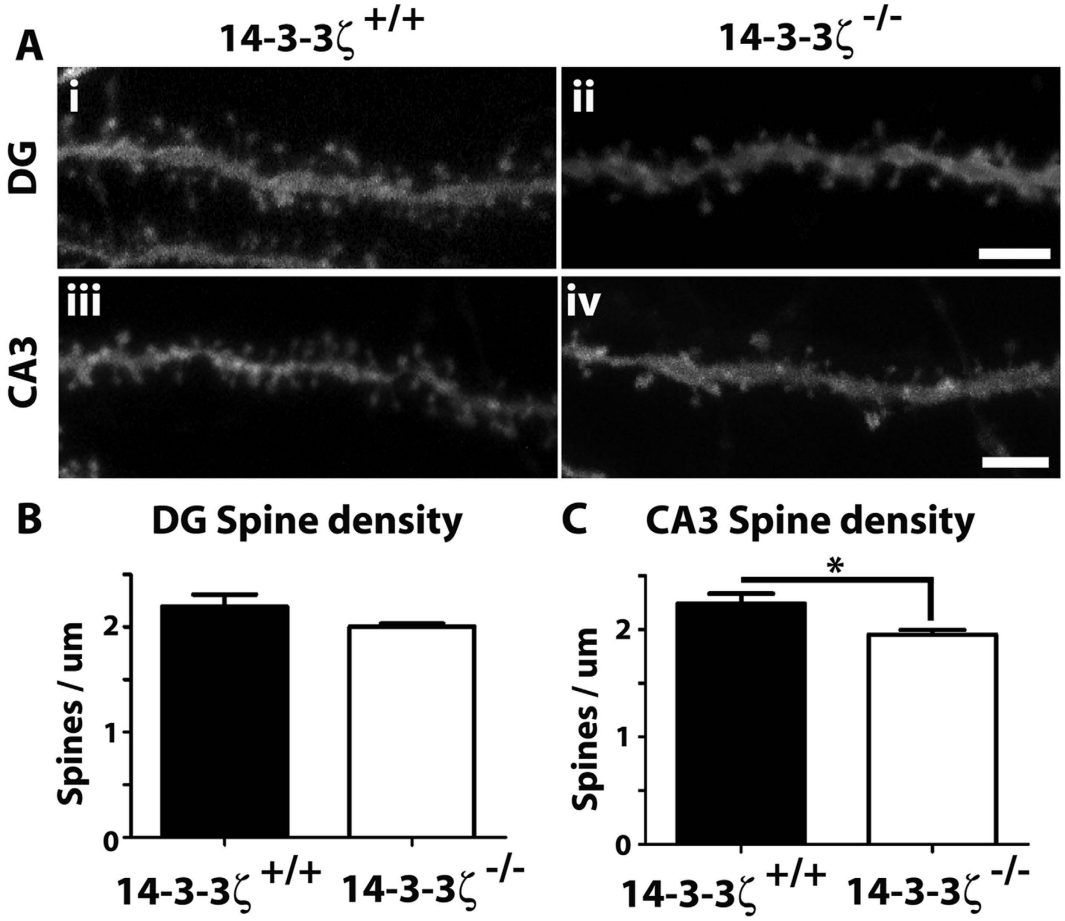

Figure 4. 14–3–3ζ-deficient mice have reduced spine density. (**A**) Biolistic labelling of dendritic spines in the dentate gyrus (DG) and cornu ammonis layer 3 (CA3) of 14-3-3$\zeta^{+/+}$ and 14-3-3$\zeta^{-/-}$ mice. (**B**) Granular neurons in the DG have similar numbers of dendritic spines in 14-3-3$\zeta^{-/-}$ (open bar) and 14-3-3$\zeta^{+/+}$ mice (closed bar; n = 3 mice/genotype, >50 dendrites quantified/mouse). (**C**) Pyramidal neurons in CA3 have significantly reduced dendritic spine density in 14-3-3$\zeta^{-/-}$ mice (open bar) compared to 14-3-3$\zeta^{+/+}$ mice (closed bar; n = 3 mice/genotype, >50 dendrites counted/mouse). * <0.05. Scale bar = 5μm.

In adult 14-3-3$\zeta^{+/+}$ brains, mossy fibres split into tightly bundled infrapyramidal and suprapyramidal branches lining the CA3 pyramidal layer. However, in 14-3-3$\zeta^{-/-}$ mice the suprapyramidal fibres were diffuse and the infrapyramidal branch aberrantly navigated among the pyramidal cell layer and ectopically fused with the suprapyramidal branch (Fig. 3v–viii). Moreover, analysis of calbindin staining showed that the suprapyramidal branch failed to extend to the boundary of CA2/3 in 14-3-3$\zeta^{-/-}$ adult brains (arrowheads, Fig. 3v,vi).

Given the aberrant axonal navigation within the hippocampus we next asked if the granular and pyramidal neurons had altered synaptic density. Dendritic spines are small membranous protrusions on neuronal dendrites that mark the sites of contact between pre- and post-synaptic neurons. As over 90% of excitatory synapses form on these spines their density and morphology are considered a direct correlation of synaptic strength and activity[26,27]. Furthermore, altered spine formation is associated with several human conditions showing deficits in social interaction, cognition and memory function, including schizophrenia, autism and intellectual disability[28–31]. To analyse spine density we labelled individual neurons in fixed vibratome sections with biolistic delivery of lipophilic fluorescent dyes (DiI and DiO). Spines from secondary apical dendrites on CA3 pyramidal neurons and basal dendrites from dentate granular neurons were quantitated from 3D-reconstructed confocal images. In comparison to 14-3-3$\zeta^{+/+}$ adult mice, we identified reduced spine density in 14-3-3$\zeta^{-/-}$ mice that was specific to the CA3 region of the hippocampus (Fig. 4; n = 3/genotype with over 50 dendrites counted/mouse, P = 0.04). 14-3-3ζ is therefore required for the formation of functional connections within the hippocampus.

14-3-3ζ-deficient mice display cognitive defects. As the anatomical defects of 14-3-3$\zeta^{-/-}$ mice are conserved across genetic backgrounds we next asked if the BALB/c model recapitulates the

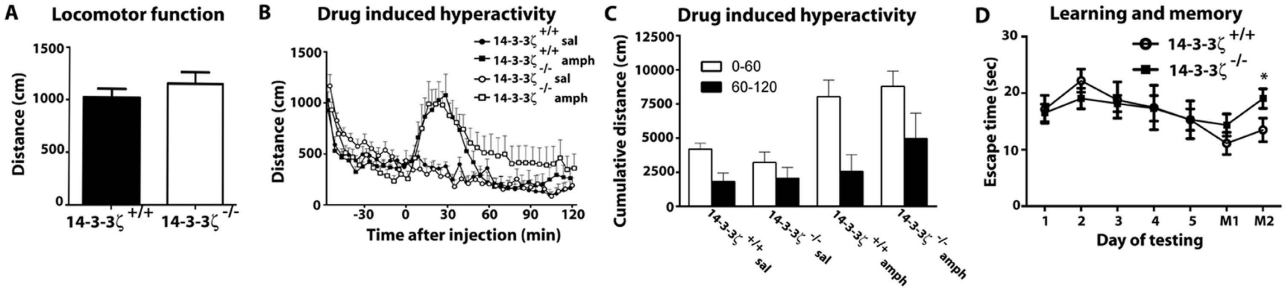

Figure 5. 14–3–3ζ-deficient mice in the BALB/c background demonstrate abnormal cognitive traits. (**A**) 14-3-3$\zeta^{-/-}$ mice (open bars; n = 12; 5 male and 7 female) have similar exploratory behaviour at 3 months of age compared to 14-3-3$\zeta^{+/+}$ littermates (filled bars; n = 10; 5 male and 5 female) in an open field test. (**B**) 14-3-3$\zeta^{-/-}$ mice (open circle; n = 12; 5 male and 7 female) have similar baseline exploratory behaviour compared to 14-3-3$\zeta^{+/+}$ littermates (closed circle; n = 10; 5 male and 5 female) in an open field test over 120 mins. 14-3-3$\zeta^{-/-}$ mice and 14-3-3$\zeta^{+/+}$ mice display similar hyperactivity in response to amphetamine (5 mg/kg). 14-3-3$\zeta^{-/-}$ mice showed a trend towards increased hyperactivity in the 60–120 min post amphetamine injection compared to 14-3-3$\zeta^{+/+}$ mice. (**C**) 14-3-3$\zeta^{-/-}$ mice and 14-3-3$\zeta^{+/+}$ mice have no significant differences in amphetamine-induced hyperactivity in the 0–60 min or 60–120 min post amphetamine injection. Error bars are presented as mean ± SEM. (**D**) 14-3-3$\zeta^{-/-}$ mice (closed squares; n = 12; 8 male and 4 female) and 14-3-3$\zeta^{+/+}$ mice (open circles; n = 8; 4 male and 4 female) have similar capacity for spatial learning (Day1-5) in a cross maze escape task test. In contrast, 14-3-3$\zeta^{-/-}$ mice have reduced capacity to remember (M1 and M2) in the cross maze escape task.

schizophrenia-like behavioural defects observed in the Sv/129 background. We first tested the locomotor function of 14-3-3$\zeta^{-/-}$ mice in an open field environment. In contrast to the robust hyperactivity seen in the Sv/129 background, 14-3-3$\zeta^{-/-}$ in the BALB/c background showed no differences in distance travelled over the test period (Fig. 5A), or across sexes (data not shown). We next performed an analysis of amphetamine-induced hyperactivity. Both WT 14-3-3$\zeta^{+/+}$ and 14-3-3$\zeta^{-/-}$ mice demonstrated a decline in activity in the test arena during the 60 min habituation phase. Consistent with previous reports suggesting that BALB/c mice respond poorly to psychostimulants of the dopamine signalling pathway[23], subcutaneous injection of amphetamine (5 mg/kg) induced only mild and variable hyperactivity in both 14-3-3$\zeta^{+/+}$ (n = 10; 5 male, 5 female) and 14-3-3$\zeta^{-/-}$ mice (n = 12; 5 male, 7 female), with similar time to become maximally hyperactive and similar degree of hyperactivity being reached across both genotypes and sexes (Fig. 5B). 14-3-3$\zeta^{-/-}$ mice trended toward covering a greater distance in the 60–120 min post amphetamine injection, however the accumulated distance travelled in this period was not significantly different between genotypes (Fig. 5C).

To test the levels of anxiety, we next analysed the mice on the elevated zero maze. 14-3-3$\zeta^{-/-}$ mice and 14-3-3$\zeta^{+/+}$ mice showed similar preference for the closed quadrants over the open quadrants of the maze (Supp. Fig. 2A). As the anxiety levels of BALB/c mice are heightened under normal lighting conditions compared to other strains[32], we also completed the elevated plus maze test under low-level lighting. Consistent with our previous test of anxiety, we found that 14-3-3$\zeta^{-/-}$ mice and 14-3-3$\zeta^{+/+}$ mice showed similar preference for the closed arm to the open arms of the maze in the 5 min test period with no change in rearing or head dipping (Supp. Fig. 2B). Therefore, in contrast to our previous findings in the Sv/129 background, mice lacking 14-3-3ζ in the BALB/c background do not display disturbances of hyperactivity or anxiety.

Given the structural defects in the hippocampus we next completed a series of tests to investigate cognitive behaviours of learning and memory. Short-term memory of 14-3-3$\zeta^{-/-}$ mice was first explored by performing an object recognition task. Overall both the 14-3-3$\zeta^{+/+}$ and 14-3-3$\zeta^{-/-}$ mice had limited interactions with the novel and familiar objects with 14-3-3$\zeta^{-/-}$ mice trending towards spending less time interacting with the objects compared to controls (Supp Fig. 3A). However, both genotypes showed the same preference for the novel object compared to the familiar object, as indicated by an equivalent preference index (Supp. Fig. 3B). We next explored working memory-dependent learning and memory using a cross-maze escape task under low-level lighting to reduce anxiety levels of the BALB/c mice. After 5 days of training to identify the correct arm of a cross-maze containing a submerged escape platform, we found that 14-3-3$\zeta^{-/-}$ mice learned at the same rate as 14-3-3$\zeta^{+/+}$ mice (Fig. 5D), showing the same amount of latency to find the escape platform. However, only the 14-3-3$\zeta^{+/+}$ mice had a significant change in escape latency during the learning phase, suggesting that they learned better than 14-3-3$\zeta^{-/-}$ mice (Fig. 5D, One-way ANOVA, P = 0.0116). The ability to remember the correct arm of the maze was then tested after a 14- and 28-day rest period (M1 and M2, respectively). Consistent with defects in hippocampal-dependent memory, we found that 14-3-3$\zeta^{-/-}$ mice

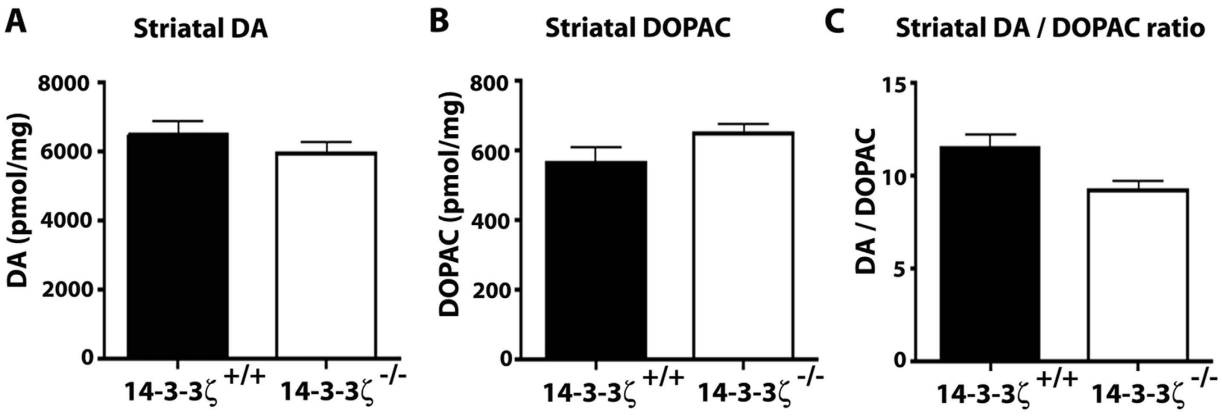

Figure 6. Baseline dopamine levels are conserved in 14-3-3ζ-deficient BALB/c mice. (**A**) Baseline DA and DOPAC levels, measured in the striatum by HPLC. 14-3-3ζ$^{-/-}$ mice (open bar; n = 12; 7 male and 5 female), were not significantly different from 14-3-3ζ$^{+/+}$ mice (closed bar; n = 10; 5 male and 5 female). (**B**) 14-3-3ζ$^{-/-}$ mice have the same levels of DOPAC compared to 14-3-3ζ$^{+/+}$ mice. (**C**) Dopamine turnover (DOPAC/DA ratio) was conserved in 14-3-3ζ$^{-/-}$ mice compared to 14-3-3ζ$^{+/+}$ mice.

had significantly increased escape latency compared to 14-3-3ζ$^{+/+}$ mice after the 28-day rest period (Fig. 5D; student t-test, P = 0.04).

Dopamine signalling is preserved in BALB/c mice lacking 14-3-3ζ. We have previously shown that baseline hyperactivity of 14-3-3ζ$^{-/-}$ mice in the Sv/129 background correlates with reduced levels of the dopamine transporter DAT and increased levels of dopamine[21]. As 14-3-3ζ$^{-/-}$ in the BALB/c background lacked hyperactivity, we tested the notion that DAT and dopamine are also preserved in this model. Notably, both dopamine signalling and DAT function have been reported to be altered in BALB/c mice[23,33]. Dopamine signalling is usually balanced by reuptake from the synaptic space through DAT, which promotes recycling to the presynaptic vesicular pool or degradation to DOPAC and other by-products. Total tissue levels of dopamine and DOPAC were measured in the striatum, cortex and hypothalamus by reverse phase high performance liquid chromatography with electrochemical detection (HPLC). Our analysis found that tissue content of dopamine, DOPAC and dopamine turnover (ratio of dopamine/DOPAC) were preserved across genotypes in all regions examined (Fig. 6A–C and Supp. Fig. 4), supporting our previous behavioural analyses (Fig. 5).

We next examined the localisation and abundance of DAT by co-labelling sagittal brain sections with anti-DAT and anti-TH antibodies. In contrast to our previous findings in the Sv/129 model, we observed no changes in the expression levels or localisation of DAT within the SN-VTA of 14-3-3ζ$^{-/-}$ mice (Fig. 7A). Thus, DAT was distributed evenly throughout the cell body and neurites of dopaminergic neurons within the midbrain in both 14-3-3ζ$^{+/+}$ and 14-3-3ζ$^{-/-}$ mice. Expression of DAT was quantified by measuring the fluorescence intensity of anti-DAT in the termini of dopaminergic neurons within the striatum relative to that of anti-TH antibodies. Our analysis shows that DAT levels are similar in both 14-3-3ζ$^{+/+}$ and 14-3-3ζ$^{-/-}$ mice (Fig. 7B,C). Analysis of adult whole-brain lysates by immunoblotting further confirmed that DAT levels were preserved in BALB/c mice lacking 14-3-3ζ (Fig. 7D).

Discussion

Neurodevelopmental disorders such as schizophrenia and autism are highly prevalent clinical syndromes affecting over 2% of the population[34]. Although these disorders are known to arise from neurodevelopmental insults, their complex genetic nature has provided a major obstacle in elucidating the molecular and cellular deficiencies underlying their aetiology. Indeed, schizophrenia and autism are considered prototypic complex genetic traits with pathogenesis arising from synergistic defects in multiple genes within connected molecular pathways. As such, the genetic background of any affected individual plays a significant role in the pathophysiology, fecundity and severity of disease presentation. Through the use of deep sequencing technologies, several recent publications have highlighted the presence of overlapping genetic mutations in both schizophrenia and autism[1], suggesting that many neurodevelopmental disorders share common molecular origins. Of note, exome sequencing of afflicted patients and their unaffected parents has recently identified *de novo* loss of function mutations in *14-3-3ζ* in both schizophrenia and autism[14,15], strongly implicating this gene as a risk factor for neurodevelopmental disorders. Our previous analysis of 14-3-3ζ-deficient mice in the Sv/129 background provided strong support to this notion, showing that complete abrogation of 14-3-3ζ expression gives rise to schizophrenia-like behavioural, physiological and anatomical defects[20,21]. Importantly, our current study now shows that many of these defects are conserved across other genetic backgrounds, thereby demonstrating that these traits arise as a direct consequence of 14-3-3ζ deficiency.

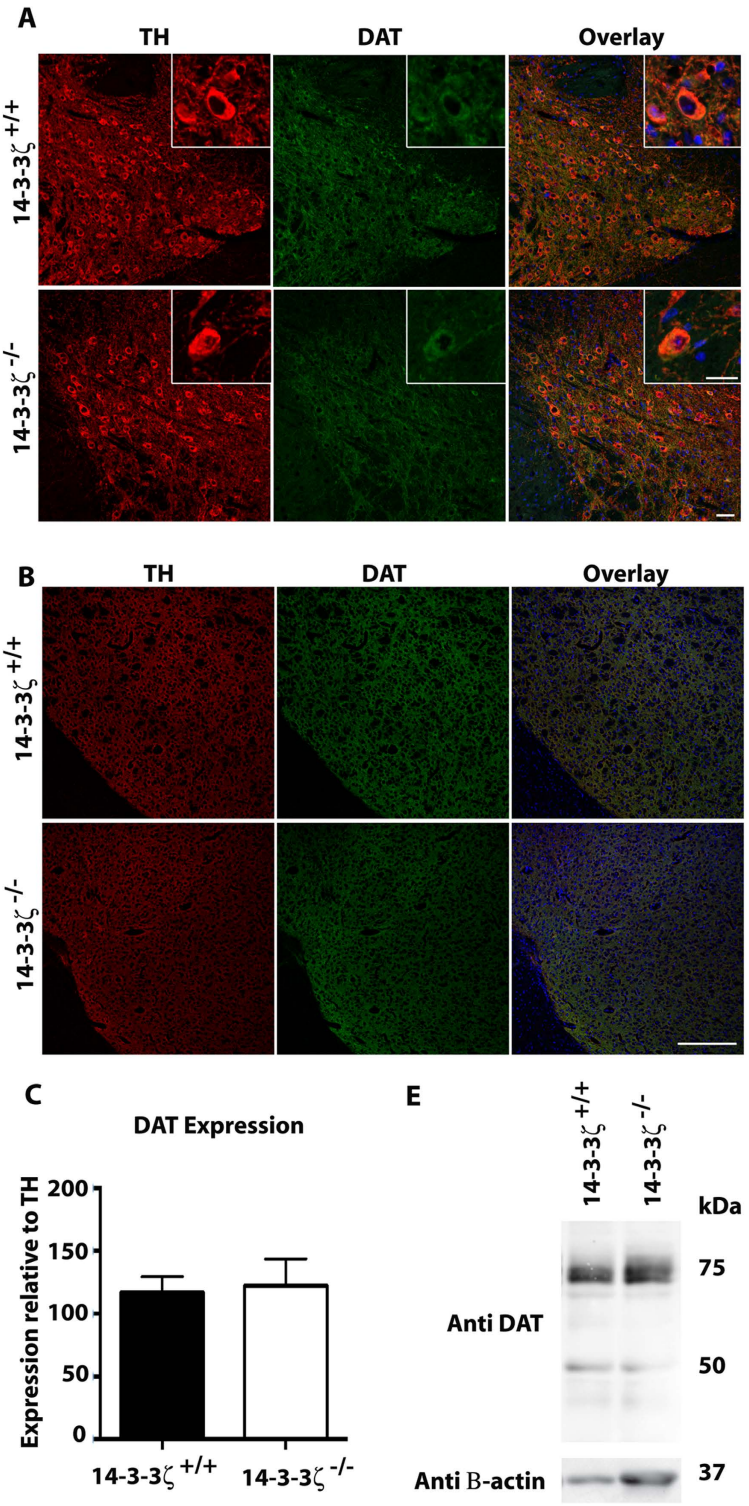

Figure 7. Expression of DAT is conserved in 14-3-3ζ-deficient mice in the BALB/c background. (**A**) Sagittal brain sections stained with anti-TH (red) and anti-DAT (green) show similar levels of DAT in the VTA/SN of 14-3-3$\zeta^{-/-}$ mice compared to 14-3-3$\zeta^{+/+}$ littermates. Higher magnification of anti-DAT immunostaining (inserts) in VTA/SN shows that DAT is localised normally in dopaminergic neurons. Scale bars = 50 μm in main figure and 20μm in the higher magnification inset figure. (**B**) Sagittal brain sections show similar levels of DAT in the striatum of 14-3-3$\zeta^{-/-}$ mice compared to 14-3-3$\zeta^{+/+}$ littermates. Scale bars = 200μm. (C) Quantitation of anti-DAT immunostaining in the striatum normalised to anti-TH confirms that 14-3-3$\zeta^{-/-}$ (open bar; n = 4) had equivalent expression of DAT compared to 14-3-3$\zeta^{+/+}$ mice (closed bar; n = 4). (D) Western blot analysis of whole brain lysate shows that proteins levels of unglycosylated DAT (50 kDa) and glycosylated DAT (80 kDa) are equivalent in 14-3-3$\zeta^{-/-}$ (n = 2) 14-3-3$\zeta^{+/+}$ mice (n = 2).

In addition to replicating the hippocampal structural defects, mossy fibre navigation defects and cognitive defects previously seen in the Sv/129 background, our current study identified critical roles for 14-3-3ζ in promoting formation of the lateral ventricle and excitatory synapses. 14-3-3 regulatory proteins lack enzymatic activity but instead exert their functions by binding to substrate proteins that are phosphorylated on serine/threonine residues to modify their localisation, stabilisation and/or biological property. Our finding that pyramidal neurons of the hippocampus are ectopically positioned in 14-3-3ζ$^{-/-}$ mice suggests that the role of 14-3-3ζ in promoting pyramidal neuron migration is conserved across genetic backgrounds. Moreover, the interactions of 14-3-3ζ with DISC1 and Ndel1[20,35] further implicate this protein as a key component of the migratory machinery within this cell type. BALB/c 14-3-3ζ$^{-/-}$ mice also had reduced dendritic spine density demonstrating that the number of excitatory synapses is reduced in these mice. Consistent with 14-3-3ζ playing an essential role in synapse formation, transgenic mice over-expressing 14-3-3ζ have been shown to have increased spine density[36]. Although it is currently unknown how 14-3-3ζ regulates spine density, it binds to several proteins found in the post synaptic density including HOMER, DISC1 and SPIN90[20,37,38], and plays a critical role in modulating actin polymerisation by binding to cofilin[39]. Notably, mice lacking cofilin or other 14-3-3ζ interacting partners such as DAT, Ndel1 and Lis1 have reduced dendritic spine density reminiscent of what is reported here[40,41].

Retrospective analysis of sections from 14-3-3ζ$^{-/-}$ mice in the Sv/129 background confirmed that the enlarged lateral ventricle is specific to the BALB/c background (data not shown), indicating that there is a genetic modifier in one of these backgrounds that either ameliorates or enhances this defect. Alternatively, as the brain size of BALB/c mice has been reported to be larger in comparison to other backgrounds[42], the enlarged ventricles in the 14-3-3ζ$^{-/-}$ mice may be exacerbated in this background. Ventricular enlargement is a common occurrence in many neurodevelopmental disorders and thought to arise from aberrant cell death or reduced neurogenesis[43]. Although we can not rule out aberrant cell death as the mechanism driving ventricular enlargement, its foundations during a time at which the brain is rapidly expanding fits best with a primary defect in neurogenesis, possibly through interactions with 14-3-3ε and δ-catenin[44].

The learning and memory defects previously identified in the Sv/129 background are also conserved in the BALB/c model[20] and are consistent with the anatomical and synaptic defects identified in the hippocampus, a major brain centre essential for these functions. However, in contrast to these cognitive defects we did not observe altered locomotor function in the BALB/c model. Our previous analyses demonstrated that hyperactivity in 14-3-3ζ$^{-/-}$ mice arose from aberrant DAT biogenesis and increased dopamine levels[21]. BALB/c mice have known differences in the dopamine signalling pathway that may arise from reduced expression of the monoamine oxidase enzymes MAO-A and MAO-B that also play a role in dopamine turnover[45]. Due to reduced activity of monamine oxidases, the tissue content of dopamine is increased in the BALB/c background, a defect that is thought to underpin some of the increased anxiolytic behavioural defects of these mice[46]. In addition, BALB/c mice respond poorly to psychostimulants such as amphetamine[23]. Given amphetamines primary mode of action is to block dopamine reuptake by DAT and subsequently promote dopamine efflux, there also appears to be fundamental differences in either the activity or biogenesis of DAT in the BALB/c background. In our current study we found that dopamine levels, DAT and locomotor function were normal in mice lacking 14-3-3ζ. Notably, in comparison to our previous study we found that BALB/c mice have a dramatic increase in total tissue content of dopamine (i.e. Sv/129 mice had approximately 125 pmol/mg tissue[21] compared with BALB/c mice that had approximately 6200 pmol/mg tissue) that may also mask any effects of 14-3-3ζ in regulating the dopamine pathway. By showing that DAT levels are unaltered in the current model, our results further suggest that the genetic background of BALB/c mice is somehow protective against the loss of DAT expression observed in other 14-3-3ζ-deficient backgrounds, such as 14-3-3ζ$^{-/-}$ Sv/129 mice. Thus, the mechanisms by which 14-3-3ζ plays a role in DAT biogenesis may be genetically heterogeneous, or there may be potentially greater redundancy for 14-3-3ζ function with respect to DAT biogenesis in BALB/c mice.

Taken together our data provide further support to the notion that deficiencies of the synapse are a key insult in the pathogenesis of behavioural deficits associated with neurodevelopmental disorders. Importantly, our analyses of 14-3-3ζ-deficiency in diverse genetic backgrounds, now demonstrates that 14-3-3ζ is essential for brain development and higher order brain function. Absence of the 14-3-3ζ molecular pathway during critical times of neuronal development is therefore predicted to underlie at least some of the anatomical and neurobehavioral deficits associated with neurodevelopmental disorders such as schizophrenia.

Materials and Methods

Mice. 14-3-3ζ$^{Gt(OST062)Lex}$ (or 14-3-3ζ$^{-/-}$) mice carrying a gene trap construct that contains the βGeo reporter gene disrupting 14-3-3ζ expression have been described previously[20]. In this study we back-crossed 14-3-3ζ KO mice onto the BALB/c background for over 10 generations. *14-3-3ζ* genotype was determined by PCR amplification of genomic tail DNA as described[20]. All experiments were approved by and conducted in accordance with the guidelines of the Animal Ethics Committee of the Central Adelaide Local Health Network, the University of Adelaide and Florey Institute of Neuroscience and Mental Health.

General health and basic sensorimotor characteristics. General physical attributes and basic sensorimotor characteristics of all animals were evaluated as previously described[47,48]. In brief, at the time body weight was measured, the appearance of fur and body posture were also examined. Vision was tested by placing mice on a visual cliff apparatus and by testing the ability of mice to stretch their arms to the surface upon being lowered from a 30 cm height. Olfaction was tested by the ability to locate buried cat food pellets in a clean cage in a period of 2 minutes. Balance was tested by the ability to remain standing in a shaking cage. Self-righting was tested by the ability to immediately return to a standing position after being placed on their back. Eye blink, ear twitch and whisker orientation were tested by touching the eyeball, ear or whiskers with a cotton swab. The wire-hang test was completed by placing mice on a wire cage lid and measuring the latency to fall after being inverted and held 15 cm above fresh bedding (maximum time of 60 sec).

Behavioural assays. Except where indicated, all procedures were carried out under normal light conditions (60–100 Lux) between 8.00 am and 12.00 pm. Behavioural phenotyping was performed on the 14-3-3$\zeta^{-/-}$ and 14-3-3$\zeta^{+/+}$ BALB mice as previously described[49–51]. One cohort of mice was used for locomotor hyperactivity testing and measurements of dopamine/DOPAC levels at 3 months of age (14-3-3$\zeta^{+/+}$: n = 5 male and n = 5 female; 14-3-3$\zeta^{-/-}$: n = 5 males and n = 7 females). Separate cohorts of mice were used at the age of 35 weeks for the novel-object recognition test and elevated zero maze (14-3-3$\zeta^{+/+}$: n = 9 male and n = 6 female; 14-3-3$\zeta^{-/-}$: n = 7 males and n = 6 females) and at 28 weeks for the elevated plus maze and cross escape water maze (14-3-3$\zeta^{+/+}$: n = 4 male and n = 4 female; 14-3-3$\zeta^{-/-}$: n = 8 males and n = 4 females).

Psychotropic drug-induced test of locomotor activity. Baseline locomotor activity and psychotropic drug-induced locomotor hyperactivity were assessed using an automated photobeam system (Med Associates, St. Albans, VT, USA). The system consisted of a mouse enclosure (25.4 × 25.4 × 40.6 cm) surrounded by a sensor-ring that included a 16 × 16 array of photobeams, and a computerized data-acquisition system. After 60 min of baseline locomotor activity and habituation to the test environment, amphetamine (5 mg/kg) or saline vehicle was injected intraperitoneally and behavioural activity monitored over a subsequent 120 min period.

Novel-object recognition test. The novel-object recognition test was completed in the same apparatus as the open-field test as previously reported[52–54]. In brief, mice were first habituated to the apparatus for three sessions of 5 minutes each (open field test). The following day, mice were placed back into the arena for a period of 3 minutes, for the training session with 2 identical objects. Objects were black painted wooden cubes or spheres, approximately 4 cm in diameter. Following the training session (15 min), mice were placed back into the arena, for the retention session with 1 familiar object (the same as used in the training session) and 1 novel object (different shape). Time spent interacting with the 2 objects (defined as mice touching the object, or sniffing the object within a distance of 2 cm) was recorded. Total time spent interacting with objects was used as a measure of exploratory behaviour, and time spent interacting with the novel object compared to the familiar object was used as a measure of retention memory. A preference index, a ratio of the amount of time spent exploring the novel object over the total time spent exploring both objects, was used to measure recognition memory. A preference index approaching 1 was regarded as successful learning and retention memory.

Escape water maze test. Spatial learning and memory was assessed using a cross-maze escape task as previously described[49]. The cross maze was made of clear plastic (length, 72 cm; arm dimensions, length 26 cm x width 20 cm) and placed in a circular pool of water (1 m diameter) maintained at 23°C. Milk powder was mixed with water-soluble black paint in the water to conceal a submerged (0.5 cm below the water surface) escape platform placed in the distal north arm of the maze. The pool was enclosed by a black plastic wall (height, 90 cm). Constant spatial cues were arranged at each arm of the maze and the experimenter always stood at the southern end of the apparatus during the training and testing procedures. Mice were individually habituated to the maze environment by being placed into the pool without the escape platform and allowed to swim for 60 s 2 days prior to learning. Learning trials were then conducted over a 5-day training period in which mice were required to learn the position of the submerged escape platform from the other three (East, South, West) arms that did not contain an escape platform. Each mouse was given six daily trials (two blocks of three trials separated by a 30 min rest interval), in which each of the three arms was chosen as a starting point in a randomized pattern (twice daily). For each trial, the mouse was placed in the distal end of an arm facing the wall and allowed 60 s to reach the escape platform where it remained for 10 s. Mice that did not climb onto the escape platform in the given time were placed on the platform for 10 s. The mouse was then placed in a clean holding cage before subsequent trials. Mice were assessed on their long-term retention of the escape platform location, which was placed in the same position as during the learning phase. Memory was tested 14 (M1) and 28 (M2) days after the final day of learning and consisted of a single day of 6 trials as described for the learning period. Data were recorded for each mouse for each trial on their escape latency (i.e. time (s) taken to swim to the platform), number of correct trials (i.e. if a mouse found the

platform on the first arm entry) and number of incorrect entries/reentries (i.e. the number of times that a mouse went into an arm that did not contain the escape platform).

Elevated Zero Maze. The elevated zero maze consisted of an elevated circular platform, 50 cm diameter, with a 5 cm wide platform 40 cm above ground. The zero was divided into four quadrants with two quadrants of the maze open and two enclosed with 15 cm high walls. Mice were placed into an open quadrant of the maze and were allowed to explore the apparatus for 5 minutes[55]. Time spent in the open quadrants was measured as an indication of anxiety-like behaviour.

Elevated plus maze test. The elevated plus-maze was completed as previously described[56,57]. Briefly, the apparatus was made in the shape of a cross from black plexiglass and consisted of two open arms (25 cm x 5 cm) and two closed arms (25 cm x 5 cm x 16 cm) that crossed in the middle perpendicular to each other. The plus maze was raised 1 m from the ground. Individual mice were introduced to the centre of the apparatus, facing the open arm opposite to the experimenter, and were observed by video recording for 5 minutes. The number of entries into the open and closed arms, and the time in exploring both types of arm were scored. Naturalistic behaviour of the mouse, such as the number of head dipping, number of rearing and number of stretch-attended postures were also counted. After each trial, the maze was thoroughly cleaned with alcohol to remove any scents cues.

Histology and Immunohistochemistry. For all anatomical analyses, postnatal mice were perfuse fixed with fresh 4% paraformaldehyde (PFA) dissolved in PBS as previously described[58]. Brains were rapidly dissected free from other tissue and post fixed in 4% PFA for an additional 24 hrs at 4°C. Tissue was cryopreserved in 20% sucrose at room temperature (RT) overnight and frozen in Tissue-Tek O.C.T. (Sakura Finetek, Torrance, CA). Sections were cut at a thickness of 10μm on a CM1850 cryostat (Leica) and air-dried for 60 min before staining.

Nissl staining and determination of β-galactosidase activity was performed using previously described methods[59,60]. For immunohistochemistry, sections were blocked in 10% non-immune goat serum or 1% bovine serum albumin in PBST (0.1 M PBS, 0.3% Triton X-100, 1% BSA) for 1 h at RT and subsequently incubated with primary antibodies for 1 h at RT. Primary antibodies and dilutions: rabbit polyclonal to calbindin-D28K (1:1000, Chemicon), mouse monoclonal to NeuN (1:500, Chemicon), rabbit polyclonal to TH (1:200; Millipore), rat monoclonal to DAT (1:20, Santa Cruz). Sections were washed several times with PBST and then incubated with 1:200 dilution of Alexa Fluor labelled secondary antibodies (Molecular Probes) or streptavidin labelled secondary antibodies (Jackson Laboratories) for 1 h at RT. After 3 washes in PBST, fluorescent sections were mounted in Prolong® Gold antifade reagent with DAPI (Molecular Probes).

Image analysis. Low resolution images were recorded on an SZX10 stereo microscope (Olympus) equipped with a Micropublisher 3.3 digital camera (Q-Imaging) and processed with OpenLab 2.2 software (Improvision). High resolution images were captured on a LSM700 confocal microscope (Zeiss). All figures were constructed in Adobe Photoshop CS3 (Adobe Systems, Inc.). Quantification of DAT and TH expression from confocal immunofluoresecence images was completed as described previously[61]. Briefly, images were split into separate channels for TH or DAT, converted to binary images and used for fluorescence intensity calculations with an Image J area calculator macro designed to detect staining in confocal image slices.

Immunoblotting. Nitrocellulose membranes were blocked with 2% skim milk powder in PBST and immunoblotted with Rat anti-DAT (1:500, Santa Cruz) and Mouse anti-14-3-3ζ (1:1000, Santa Cruz) (Ramshaw *et al.*, 2013). Rabbit polyclonal against β-actin (1:5000, Millipore) was used as a loading control. Bound antibodies were detected with HRP-conjugated secondary antibody (1:5,000, Pierce-Thermo Scientific). Immunoreactive proteins were visualized by ECL (Luminescent Image Analyzer LAS-4000, Fujifilm, Japan). The images were analysed with Multi Gauge Ver3.0 (Fujifilm, Japan).

Detection of Dopamine. Dopamine and DOPAC levels in the striatum, hypothalamus and cortex were determined using HPLC as previously described[62]. For tissue preparation, small biopsies were dissected out on a chilled plate, weighed, and placed in 200 μl 0.4 M perchloric acid ($HClO_4$) containing 0.05% sodium metabisulphate ($Na_2S_2O_5$) and 0.01% disodium EDTA. The sample tissue was homogenized, cellular and vesicular membranes disrupted using a sonicator and finally stored at 70 °C. On the day of analysis, all samples were centrifuged at 10,500 *g* for 10 minutes and filtered though minispin filters for an additional 3 minutes at 10,000 rpm. The resultant supernatant was transferred to HPLC vials and placed in an autosampler for injection onto the HPLC. The HPLC consisted of a LC-20AT pump (Shimadzu), SIL-20A Autosampler (Shimadzu) and C18 reverse phase column (Bio-Rad, Hercules, USA). Detection was via a 3 mm VT-03 flow cell with glassy carbon working electrode (Antec Leyden) and Decade II Electrochemical Detector (Antec Leyden). The mobile phase consisted of 17% v/v methanol in purified deionized water containing 70 mM KH2PO4 (Merck), 0.5 mM EDTA (Merck) and 8.0 mM sulfonic acid (Merck), pH 3.0 and was run at a flow rate of 0.5 ml/min.

Biolistic gene gun labelling and quantitation of dendritic spines. Perfused brain samples were sliced at 200 μm with a Leica VT1200 vibratome (Leica) and shot with 30 μm gold particles labelled with lipophilic tracers DiI and DiO as previously described[63]. Images were acquired at 100X magnification on an LSM 700 Zeiss confocal microscope (Zeiss) using z-stack settings overlapping at least 10% between images. Spines were counted from over 50 3D reconstructed images from between 100–500 um from the cell body from each mouse using Neuron Studio and confirmed by manual counting[64]. Spines were counted from both the CA3 subfield and dentate gyrus from 3 adult mice/genotype. The CA3 subfield and dentate gyrus regions were identified through gross morphology after staining with DAPI.

Quantitative RT-PCR. Total RNA was isolated from total brains using Trizol (Ambion) and single stranded cDNA synthesised using the QuantiTect Reverse transcription kit (Qiagen). qPCR was performed with SYBR Green reagent (Qiagen) using the Rotor-Gene 6000 real-time PCR system (Corbett Life Science). Primers used were: *GAPDH* F: ACCCAGAAGACTGTGGATGG, R: CAGTGAGCTTCCCGTTCA; *14-3-3ζ* F: AACTGTATGGTGCCCTTCTGTGG, R: CATTCGTAGTTGTTGTTGCCCCG. Relative mRNA levels were quantified using the comparative quantitation method in Rotor-Gene 6000 Series Software. Relative mRNA levels were normalised to *GAPDH*. Each PCR was performed in technical triplicates, and each experiment was performed in at least three biological replicates for each genotype.

Statistical analysis. All data were presented as mean ± SEM. Behavioural experiments were analysed using two-way analysis of variance (ANOVA) with repeated measures where appropriate (Systat, version 9.0, SPSS software; SPSS Inc., USA). Neurochemical data and expression analyses were analysed using ANOVA and Student's t-test. In all studies a p value of <0.05 was considered to be statistically significant.

References

1. Hu, W. F., Chahrour, M. H. & Walsh, C. A. The diverse genetic landscape of neurodevelopmental disorders. *Annu Rev Genomics Hum Genet*. **15,** 195–213 (2014).
2. Casanova, E. L. & Casanova, M. F. Genetics studies indicate that neural induction and early neuronal maturation are disturbed in autism. *Front Cell Neurosci*. **8,** 397 (2014).
3. Iossifov, I. *et al.* The contribution of de novo coding mutations to autism spectrum disorder. *Nature*. **515,** 216–221 (2014).
4. Wegiel, J. *et al.* The neuropathology of autism: defects of neurogenesis and neuronal migration, and dysplastic changes. *Acta Neuropathol*. **119,** 755–770 (2010).
5. Jia, F. *et al.* Core symptoms of autism improved after vitamin d supplementation. *Pediatrics*. **135,** e196–198 (2015).
6. Chen, J., Yu, S., Fu, Y. & Li, X. Synaptic proteins and receptors defects in autism spectrum disorders. *Front Cell Neurosci*. **8,** 276 (2014).
7. Jaaro-Peled, H., Ayhan, Y., Pletnikov, M. V. & Sawa, A. Review of pathological hallmarks of schizophrenia: comparison of genetic models with patients and nongenetic models. *Schizophr Bull*. **36,** 301–313 (2010).
8. Aitken, A. 14-3-3 proteins: a historic overview. *Semin Cancer Biol*. **16,** 162–172 (2006).
9. Berg, D., Holzmann, C. & Riess, O. 14-3-3 proteins in the nervous system. *Nat Rev Neurosci*. **4,** 752–762 (2003).
10. Tenney, J. R., Hopkin, R. J. & Schapiro, M. B. Deletion of 14-3-3{varepsilon} and CRK: a clinical syndrome with macrocephaly, developmental delay, and generalized epilepsy. *J Child Neurol*. **26,** 223–227 (2011).
11. Wong, A. H. *et al.* Genetic and post-mortem mRNA analysis of the 14-3-3 genes that encode phosphoserine/threonine-binding regulatory proteins in schizophrenia and bipolar disorder. *Schizophr Res*. **78,** 137–146 (2005).
12. Grover, D. *et al.* Family-based association of YWHAH in psychotic bipolar disorder. *Am J Med Genet B Neuropsychiatr Genet*. **150B,** 977–983 (2009).
13. Schiff, M. *et al.* Further delineation of the 17p13.3 microdeletion involving YWHAE but distal to PAFAH1B1: four additional patients. *Eur J Med Genet*. **53,** 303–308 (2010).
14. Fromer, M. *et al.* De novo mutations in schizophrenia implicate synaptic networks. *Nature*. **506,** 179–184 (2014).
15. Toma, C. *et al.* Exome sequencing in multiplex autism families suggests a major role for heterozygous truncating mutations. *Mol Psychiatry*. **19,** 784–790 (2013).
16. Middleton, F. A., Peng, L., Lewis, D. A., Levitt, P. & Mirnics, K. Altered expression of 14-3-3 genes in the prefrontal cortex of subjects with schizophrenia. *Neuropsychopharmacology*. **30,** 974–983 (2005).
17. English, J. A., Dicker, P., Focking, M., Dunn, M. J. & Cotter, D. R. 2-D DIGE analysis implicates cytoskeletal abnormalities in psychiatric disease. *Proteomics*. **9,** 3368–3382 (2009).
18. English, J. A., Pennington, K., Dunn, M. J. & Cotter, D. R. The neuroproteomics of schizophrenia. *Biol Psychiatry*. **69,** 163–172 (2011).
19. Sivagnanasundaram, S., Crossett, B., Dedova, I., Cordwell, S. & Matsumoto, I. Abnormal pathways in the genu of the corpus callosum in schizophrenia pathogenesis: a proteome study. *Proteomics Clin Appl*. **1,** 1291–1305 (2007).
20. Cheah, P. S. *et al.* Neurodevelopmental and neuropsychiatric behaviour defects arise from 14-3-3zeta deficiency. *Mol Psychiatry*. **17,** 451–466 (2012).
21. Ramshaw, H. *et al.* Locomotor hyperactivity in 14-3-3zeta KO mice is associated with dopamine transporter dysfunction. *Transl Psychiatry*. **3,** e327 (2013).
22. Morice, E., Denis, C., Giros, B. & Nosten-Bertrand, M. Phenotypic expression of the targeted null-mutation in the dopamine transporter gene varies as a function of the genetic background. *Eur J Neurosci*. **20,** 120–126 (2004).
23. Kitahama, K. & Valatx, J. L. Strain differences in amphetamine sensitivity in mice. I. A diallel analysis of open field activity. *Psychopharmacology (Berl)*. **66,** 189–194 (1979).
24. Van Den Buuse, M. Modeling the positive symptoms of schizophrenia in genetically modified mice: pharmacology and methodology aspects. *Schizophr Bull*. **36,** 246–270 (2010).
25. Ergorul, C. & Eichenbaum, H. Essential role of the hippocampal formation in rapid learning of higher-order sequential associations. *J Neurosci*. **26,** 4111–4117 (2006).
26. Kasai, H., Matsuzaki, M., Noguchi, J., Yasumatsu, N. & Nakahara, H. Structure-stability-function relationships of dendritic spines. *Trends Neurosci*. **26,** 360–368 (2003).
27. Yuste, R. & Bonhoeffer, T. Morphological changes in dendritic spines associated with long-term synaptic plasticity. *Annu Rev Neurosci*. **24,** 1071–1089 (2001).

28. Glantz, L. A. & Lewis, D. A. Decreased dendritic spine density on prefrontal cortical pyramidal neurons in schizophrenia. *Arch Gen Psychiatry*. **57,** 65–73 (2000).
29. Hutsler, J. J. & Zhang, H. Increased dendritic spine densities on cortical projection neurons in autism spectrum disorders. *Brain Res*. **1309,** 83–94 (2010).
30. Nimchinsky, E. A., Sabatini, B. L. & Svoboda, K. Structure and function of dendritic spines. *Annu Rev Physiol*. **64,** 313–353 (2002).
31. Tackenberg, C., Ghori, A. & Brandt, R. Thin, stubby or mushroom: spine pathology in Alzheimer's disease. *Curr Alzheimer Res*. **6,** 261–268 (2009).
32. Chapillon, P. & Debouzie, A. BALB/c mice are not so bad in the Morris water maze. *Behav Brain Res*. **117,** 115–118 (2000).
33. Yochum, C. L., Medvecky, C. M., Cheh, M. A., Bhattacharya, P. & Wagner, G. C. Differential development of central dopaminergic and serotonergic systems in BALB/c and C57BL/mice. *Brain Res*. **1349,** 97–104 (2010).
34. Castren, E., Elgersma, Y., Maffei, L. & Hagerman, R. Treatment of neurodevelopmental disorders in adulthood. *J Neurosci*. **32,** 14074–14079 (2012).
35. Toyo-oka, K. *et al.* 14-3-3epsilon is important for neuronal migration by binding to NUDEL: a molecular explanation for Miller-Dieker syndrome. *Nat Genet*. **34,** 274–285 (2003).
36. Angrand, P. O. *et al.* Transgenic mouse proteomics identifies new 14-3-3-associated proteins involved in cytoskeletal rearrangements and cell signaling. *Molecular & cellular proteomics: MCP*. **5,** 2211–2227 (2006).
37. Heverin, M., Brennan, G. P., Koehler, C. J., Treumann, A. & Henshall, D. C. Proteomic analysis of 14-3-3 zeta binding proteins in the mouse hippocampus. *International journal of physiology, pathophysiology and pharmacology*. **4,** 74–83 (2012).
38. Ayhan, Y. *et al.* Differential effects of prenatal and postnatal expressions of mutant human DISC1 on neurobehavioral phenotypes in transgenic mice: evidence for neurodevelopmental origin of major psychiatric disorders. *Mol Psychiatry*. **16,** 293–306 (2011).
39. Gohla, A. & Bokoch, G. M. 14-3-3 regulates actin dynamics by stabilizing phosphorylated cofilin. *Current biology : CB*. **12,** 1704–1710 (2002).
40. Berlanga, M. L. *et al.* Multiscale imaging characterization of dopamine transporter knockout mice reveals regional alterations in spine density of medium spiny neurons. *Brain Res*. **1390,** 41–49 (2011).
41. Sudarov, A., Gooden, F., Tseng, D., Gan, W. B. & Ross, M. E. Lis1 controls dynamics of neuronal filopodia and spines to impact synaptogenesis and social behaviour. *EMBO molecular medicine*. **5,** 591–607 (2013).
42. Brodkin, E. S. BALB/c mice: low sociability and other phenotypes that may be relevant to autism. *Behav Brain Res*. **176,** 53–65 (2007).
43. Ishihara, K. *et al.* Enlarged brain ventricles and impaired neurogenesis in the Ts1Cje and Ts2Cje mouse models of Down syndrome. *Cereb Cortex*. **20,** 1131–1143 (2009).
44. Toyo-oka, K. *et al.* 14-3-3epsilon and zeta regulate neurogenesis and differentiation of neuronal progenitor cells in the developing brain. *J Neurosci*. **34,** 12168–12181 (2014).
45. Siesser, W. B. *et al.* Tryptophan hydroxylase 2 genotype determines brain serotonin synthesis but not tissue content in C57Bl/6 and BALB/c congenic mice. *Neurosci Lett*. **481,** 6–11 (2010).
46. Anderzhanova, E. A. *et al.* Strain differences in profiles of dopaminergic neurotransmission in the prefrontal cortex of the BALB/C vs. C57Bl/6 mice: consequences of stress and afobazole. *Eur J Pharmacol*. **708,** 95–104 (2013).
47. Crawley, J. N. Behavioral phenotyping of transgenic and knockout mice: experimental design and evaluation of general health, sensory functions, motor abilities, and specific behavioral tests. *Brain Res*. **835,** 18–26 (1999).
48. Crawley, J. N. *et al.* Behavioral phenotypes of inbred mouse strains: implications and recommendations for molecular studies. *Psychopharmacology (Berl)*. **132,** 107–124 (1997).
49. Coyle, P., Tran, N., Fung, J. N., Summers, B. L. & Rofe, A. M. Maternal dietary zinc supplementation prevents aberrant behaviour in an object recognition task in mice offspring exposed to LPS in early pregnancy. *Behav Brain Res*. **197,** 210–218 (2009).
50. Summers, B. L., Rofe, A. M. & Coyle, P. Prenatal zinc treatment at the time of acute ethanol exposure limits spatial memory impairments in mouse offspring. *Pediatr Res*. **59,** 66–71 (2006).
51. Van Den Buuse, M., Wischhof, L., Lee, R. X., Martin, S. & Karl, T. Neuregulin 1 hypomorphic mutant mice: enhanced baseline locomotor activity but normal psychotropic drug-induced hyperlocomotion and prepulse inhibition regulation. *Int J Neuropsychopharmacol*. **12,** 1383–1393 (2009).
52. Baune, B. T. *et al.* Cognitive dysfunction in mice deficient for TNF- and its receptors. *Am J Med Genet B Neuropsychiatr Genet*. **147B,** 1056–1064 (2008).
53. Bevins, R. A. & Besheer, J. Object recognition in rats and mice: a one-trial non-matching-to-sample learning task to study 'recognition memory'. *Nat Protoc*. **1,** 1306–1311 (2006).
54. Hart, P. C. *et al.* Experimental models of anxiety for drug discovery and brain research. *Methods Mol Biol*. **602,** 299–321 (2010).
55. Shepherd, J. K., Grewal, S. S., Fletcher, A., Bill, D. J. & Dourish, C. T. Behavioural and pharmacological characterisation of the elevated "zero-maze" as an animal model of anxiety. *Psychopharmacology (Berl.)*, **116,** 56–64 (1994).
56. Komada, M., Takao, K. & Miyakawa, T. Elevated plus maze for mice. *J Vis Exp*. doi: 10.3791/1088 (2008).
57. Walf, A. A. & Frye, C. A. The use of the elevated plus maze as an assay of anxiety-related behavior in rodents. *Nat Protoc*. **2,** 322–328 (2007).
58. Koike, H., Arguello, P. A., Kvajo, M., Karayiorgou, M. & Gogos, J. A. Disc1 is mutated in the 129S6/SvEv strain and modulates working memory in mice. *Proc Natl Acad Sci USA*. **103,** 3693–3697 (2006).
59. Komiyama, N. H. *et al.* SynGAP regulates ERK/MAPK signaling, synaptic plasticity, and learning in the complex with postsynaptic density 95 and NMDA receptor. *J Neurosci*. **22,** 9721–9732 (2002).
60. Schwarz, Q. P. & Cox, T. C. Complementation of a yeast CYC3 deficiency identifies an X-linked mammalian activator of apocytochrome c. *Genomics*. **79,** 51–57 (2002).
61. Samuel, M. S. *et al.* Actomyosin-mediated cellular tension drives increased tissue stiffness and beta-catenin activation to induce epidermal hyperplasia and tumor growth. *Cancer Cell*. **19,** 776–791 (2011).
62. Parish, C. L. *et al.* Wnt5a-treated midbrain neural stem cells improve dopamine cell replacement therapy in parkinsonian mice. *J Clin Invest*. **118,** 149–160 (2008).
63. Gan, W. B., Grutzendler, J., Wong, W. T., Wong, R. O. & Lichtman, J. W. Multicolor "DiOlistic" labeling of the nervous system using lipophilic dye combinations. *Neuron*. **27,** 219–225 (2000).
64. Wearne, S. L. *et al.* New techniques for imaging, digitization and analysis of three-dimensional neural morphology on multiple scales. *Neuroscience*. **136,** 661–680 (2005).

Acknowledgements

We thank Rebecca Wright and Melanie Pudney for genotyping mice and SA Pathology ACF staff maintaining the mouse colonies. This work was funded by grants from the National Health and Medical Research Council of Australia and Medvet Laboratories. The Florey Institute of Neuroscience and Mental

Health acknowledges the support from the Victorian Government's Operational Infrastructure Support Grant. HR is the recipient of the Peter Nelson Leukaemia Research Fellowship. CLP was supported by a Senior Medical Research Fellowship provided by the Viertel Charitable Foundation, Australia.

Author Contributions

H.R., A.L. and Q.S. designed all of the work, X.X., Q.S., Z.G., E.S. and P.M. completed all anatomical analyses, X.X., E.J., B.B., U.R., M.V., D.C. and Q.S. completed all behavioural analyses, C.P. and P.M. completed all biochemical analyses, M.H and J.H provided expertise in quantitation, Q.S., H.R., P.M., M.V., C.P. and J.H. wrote the manuscript.

Additional Information

Supplementary information accompanies this paper at http://www.nature.com/srep

Competing financial interests: The authors declare no competing financial interests.

How to cite this article: Xu, X. *et al.* 14-3-3ζ deficient mice in the BALB/c background display behavioural and anatomical defects associated with neurodevelopmental disorders. *Sci. Rep.* **5**, 12434; doi: 10.1038/srep12434 (2015).

This work is licensed under a Creative Commons Attribution 4.0 International License. The images or other third party material in this article are included in the article's Creative Commons license, unless indicated otherwise in the credit line; if the material is not included under the Creative Commons license, users will need to obtain permission from the license holder to reproduce the material. To view a copy of this license, visit http://creativecommons.org/licenses/by/4.0/

Pharmacology, Biochemistry and Behavior 138 (2015) 1–8

Contents lists available at ScienceDirect

Pharmacology, Biochemistry and Behavior

journal homepage: www.elsevier.com/locate/pharmbiochembeh

In-vivo administration of clozapine affects behaviour but does not reverse dendritic spine deficits in the 14-3-3ζ KO mouse model of schizophrenia-like disorders

Emily J. Jaehne [a], Hayley Ramshaw [b], Xiangjun Xu [b], Eiman Saleh [b], Scott R. Clark [a], Klaus Oliver Schubert [a], Angel Lopez [b], Quenten Schwarz [b,1], Bernhard T. Baune [a,*,1]

[a] Discipline of Psychiatry, University of Adelaide, Adelaide, South Australia, Australia
[b] Centre for Cancer Biology, SA Pathology and University of South Australia, Adelaide, South Australia, Australia

ARTICLE INFO

Article history:
Received 26 May 2015
Received in revised form 4 September 2015
Accepted 7 September 2015
Available online 10 September 2015

Keywords:
Clozapine
14-3-3ζ
Anxiety
Cognition
Depression
Dendritic spines

ABSTRACT

Clozapine is an atypical antipsychotic drug used in the treatment of schizophrenia, which has been shown to reverse behavioural and dendritic spine deficits in mice. It has recently been shown that deficiency of 14-3-3ζ has an association with schizophrenia, and that a mouse model lacking this protein displays several schizophrenia-like behavioural deficits. To test the effect of clozapine in this mouse model, 14-3-3ζ KO mice were administered clozapine (5 mg/kg) for two weeks prior to being analysed in a test battery of cognition, anxiety, and despair (depression-like) behaviours. Following behavioural testing brain samples were collected for analysis of specific anatomical defects and dendritic spine formation. We found that clozapine reduced despair behaviour of 14-3-3ζ KO mice in the forced swim test (FST) and altered the behaviour of wild types and 14-3-3ζ KO mice in the Y-maze task. In contrast, clozapine had no effects on hippocampal laminar defects or decreased dendritic spine density observed in 14-3-3ζ KO mice. Our results suggest that clozapine may have beneficial effects on clinical behaviours associated with deficiencies in the 14-3-3ζ molecular pathway, despite having no effects on morphological defects. These findings may provide mechanistic insight to the action of this drug.

© 2015 Elsevier Inc. All rights reserved.

1. Introduction

Clozapine is an atypical antipsychotic and is considered the most effective treatment for schizophrenia (Leucht et al., 2013). Due to its high risk of serious side effects and the need for clinical monitoring, it is only used in patients who are resistant or intolerant to other antipsychotic drugs (Essali et al., 2009; Meltzer, 2010; Fakra and Azorin, 2012). The exact pharmacological, morphological, and molecular mechanisms through which clozapine exerts its antipsychotic action are not fully understood. It is clear that in addition to its known neurochemical activity at several dopaminergic, serotonergic and cholinergic sites (Fakra and Azorin, 2012), additional effects on molecular pathways and brain cell morphology contribute to clozapine's superior clinical efficacy (Ertugrul et al., 2009) (Ozcelik-Eroglu et al., 2014) (Sharp et al., 2013) (Rizig et al., 2012).

Recent evidence from animal models of schizophrenia-like disorders (Jones et al., 2011; Pratt et al., 2012) suggests that trophic effects on dendritic spine morphology and function could represent an important and clinically relevant mechanism of clozapine action. Dendritic spine deficits are a neuropathological hallmark of schizophrenia and related disorders in humans (Glantz and Lewis, 2000; Penzes et al., 2011; Konopaske et al., 2014). Clozapine has been shown to rescue the dendritic spine deficiency observed in cultured neurons of Erb/B2/B4-deficient mice (Barros et al., 2009), increases dendritic spine density in rat hippocampal neurons in vitro (Critchlow et al., 2006), and enhances neurite growth in PC12 cells (Lu and Dwyer, 2005). Additionally, clozapine appears to reverse some behavioural deficits observed in mouse models associated with dendritic spine deficits, including the Erb/B2/B4- and Kalirin-knock out models (Barros et al., 2009; Cahill et al., 2009).

Our group has recently developed the 14-3-3ζ knock-out (KO) model of schizophrenia-like disorders. The 14-3-3 family of proteins consist of seven isoforms (β, γ, ε, η, ζ, σ *and* θ) that are abundantly expressed in the developing and adult brain. 14-3-3 proteins lack enzymatic activity but exert their effects by binding to specific phosphoserine/threonine residues on target proteins to modulate their activity and/or localisation. Several studies have shown that the isoform14-3-3ζ has an association with schizophrenia and related neurodevelopmental disorders on the gene- (Jia et al., 2004; Fromer et al., 2014; Toma et al., 2014), gene expression- (Middleton et al., 2005; Wong et al., 2005), and protein level (Sivagnanasundaram et al.,

* Corresponding author at: School of Medicine, University of Adelaide, Adelaide, South Australia 5005, Australia.
E-mail address: Bernhard.Baune@Adelaide.edu.au (B.T. Baune).
[1] Equal contribution and are to be considered joint last authors.

http://dx.doi.org/10.1016/j.pbb.2015.09.006
0091-3057/© 2015 Elsevier Inc. All rights reserved.

2007; English et al., 2009; Focking et al., 2011; Schubert et al., 2015). We found that 14-3-3ζ KO mice display several schizophrenia-like behavioural deficits such as hyperactivity and disrupted sensorimotor gating, impaired novel object recognition, impaired learning in a water cross-maze escape task, and lower levels of anxiety in the elevated plus maze (Cheah et al., 2012). As previously reported, we found that clozapine ameliorated hyperactivity in 14-3-3ζ KO mice (Ramshaw et al., 2013). Anatomically, we have identified neuronal migration defects, disrupted mossy fibre circuits, and aberrant synaptic terminals in the hippocampi of 14-3-3ζ KO mice (Cheah et al., 2012). Molecular investigations suggest that 14-3-3ζ forms a central hub within the schizophrenia protein interaction network through interactions with schizophrenia risk genes including disrupted-in-schizophrenia 1 (DISC1), Ndel1, Lis1 and tyrosine hydroxylase (Toyo-oka et al., 2003; Cheah et al., 2012; Toma et al., 2014), and that 14-3-3ζ plays an essential role in dopamine neurotransmission by controlling the abundance of the dopamine transporter DAT (Ramshaw et al., 2013).

The first aim of the present study was to determine whether 14-3-3ζ KO mice display the dendritic spine pathology found in other animal models of schizophrenia-like disorders, and whether such changes could be rescued by clozapine. Secondly, we explored the effect of 14-3-3ζ deficiency on a comprehensive battery of behavioural tests for cognition-, anxiety- and depression-like behaviours, and examined whether clozapine would reverse any changes seen in these behavioural tests. We hypothesised that we would find changes in dendritic spine morphology in 14-3-3ζ KO mice, and that clozapine would reverse both the neurobehavioural and anatomical defects demonstrated in these animals.

2. Materials and methods

2.1. Mice

$14\text{-}3\text{-}3\zeta^{Gt(OST062)Lex}$(14-3-3ζ KO) mice on a SV129 background carrying a gene trap construct that contains the βGeo reporter gene disrupting 14-3-3ζ expression, have been described previously (Cheah et al., 2012). *14-3-3ζ* genotype was determined by PCR amplification of genomic tail DNA as described (Cheah et al., 2012). 37 mice were used for drug treatment experiments of which all took part in behavioural studies and 24 used for structural analyses. A parallel non-drug treatment and non-behavioural tested cohort of 8 (WT, n = 4, 2 male and 2 female; KO, n = 4, 2 male and 2 female) animals was also used to quantitate dendritic spines. The mean age of each treatment group was 28.8 ± 3.8, 31.4 ± 3.4, 25.9 ± 4.3 and 31.8 ± 4.0 weeks old respectively for WT-vehicle, WT-clozapine, KO-vehicle and KO-clozapine. All experimental mice were housed in groups of 2–6 in individually ventilated cages during the experimental period, with food and water available ad libitum. Ambient temperature of the housing and testing rooms was 22 ± 1 °C. Mice were housed under a 12-h light–dark cycle, lights on at 07:00 h, and all behavioural testing was conducted between 08:00 and 16:00 h. All experimentation was approved by and conducted in accordance with the guidelines of the University of Adelaide Animal Ethics Committee and Animal Ethics Committee of the SA Pathology/Central Adelaide Local Health Network (CALHN) and followed the Australian code of practice for the care and use of animals for scientific purposes.

2.2. Drug preparation

Clozapine was obtained from Sigma Aldrich (St Louis, MO) and was dissolved in HCl and diluted in sterile water (Williams et al., 2012). Vehicle was prepared in an identical manner without the addition of clozapine. Concentrated aliquots of both clozapine and vehicle were stored at −20 °C. Aliquots were thawed and diluted to their final concentration in sterile saline on the day of dosing. Solutions were buffered with NaOH to achieve a final pH of 6.5–7.5.

2.3. Experimental plan

Mice were given clozapine (5 mg/kg) or vehicle (i.p. at a dose volume of 10 ml/kg) daily for 14 days prior to behavioural testing based on previous papers which showed similar doses were able to decrease motor activity (Wolf et al., 2007; Dawe et al., 2010), while higher doses can lead to increased inflammation which could produce illness behaviour and interfere with behavioural testing (Wang et al., 2008). Dosing was continued for a further 11 days throughout the behavioural testing period, with dosing always conducted between 3:30 and 5 pm, following any behavioural testing. Of the 37 mice used 10 WT (3 male + 7 female) and 9 KO (3 male + 6 female) mice were given vehicle while 10 WT (4 male + 6 female) and 8 KO (4 male + 4 female) mice were given clozapine. Mice were tested in a variety of cognition, anxiety and depression-like behavioural tests in the order open field, elevated zero maze (EZM), Y-maze, tail suspension test (TST) and forced swim test (FST), with more stressful tests completed at the end, similar to previous studies (Jaehne and Baune, 2014). All mice underwent testing in each behavioural test, with 1–2 days of rest between each test. An imaging programme (ANY-maze, USA) was used to track movements, and was used for all behavioural testing. All behavioural equipment was purchased from Stoelting Co (USA). Following behavioural testing mice were culled and brains collected for analysis of anatomical defects in the hippocampus (WT, n = 6, 3 vehicle, 3 clozapine treated, 1 male and 2 females per group; KO, n = 6, 3 vehicle, 3 clozapine treated, 1 male and 2 females per group) or dendritic spine analysis (WT, n = 6, 3 vehicle, 3 clozapine treated, 1 male and 2 females per group; KO, n = 6, 3 vehicle, 3 clozapine treated, 1 male and 2 females per group).

2.4. Histology and immunohistochemistry

Following behavioural analyses, all mice were perfuse fixed with fresh 4% paraformaldehyde (PFA) dissolved in PBS as previously described (Cheah et al., 2012). Brains were rapidly dissected free from other tissue and post fixed in 4% PFA for an additional 24 h at 4 °C. Tissue was cryopreserved in 20% sucrose at room temperature (RT) overnight and frozen in Tissue-Tek O.C.T. (Sakura Finetek, Torrance, CA). Sections were cut at a thickness of 10 μm on a CM1850 cryostat (Leica) and air-dried for 60 min before staining.

For immunohistochemistry, hippocampal sections were blocked in 10% non-immune goat serum or 1% bovine serum albumin in PBST (0.1 M PBS, 0.3% Triton X-100, 1% BSA) for 1 h at RT and subsequently incubated with primary antibodies for 1 h at RT. Primary antibodies and dilutions: rabbit polyclonal to calbindin (1:500; Millipore). Sections were washed several times with PBST and then incubated with 1:200 dilution of Alexa Fluor labelled secondary antibodies (Molecular Probes) for 1 h at RT. After 3 washes in PBST, fluorescent sections were mounted in Prolong® Gold antifade reagent with DAPI (Molecular Probes).

Golgi stains were completed using the FD Rapid GolgiStain kit (NeuroTechnologies), according to the manufacturer's protocol. Briefly, brains were rapidly dissected from animals and placed into impregnation solution for 2 weeks before being sliced at 200 μm with a Leica VT1200 vibratome (Leica). Hippocampal tissue slices were stained and mounted in Leica CV mount (Leica). Images were captured with a 40× objective plus 1.6× magnification on an IX81 inverted microscope (Olympus) with bright field settings. For spine density quantification, the number of spines along equivalent lengths of dendritic segments proximal to the cell body was counted on layer V cortex neurons. All counts were performed on de-identified samples. The hippocampal brain region was chosen for these analyses as prior studies had identified structural defects in this region in the absence of gross anatomical defects in other regions of the brain (Cheah et al., 2012). In addition, the hippocampus plays central roles in cognition and emotion-like behaviour (Sweatt, 2004).

2.5. Biolistic labelling and quantitation of dendritic spines

Perfused brain samples were sliced at 200 μm with a Leica VT1200 vibratome (Leica) and shot with 30 μm gold particles labelled with lipophilic tracers DiI, DiA or DiO as previously described (Gan et al., 2000). Images were taken at 100× magnification on an LSM 700 Zeiss confocal microscope (Zeiss). Spines were counted from over 30 3D reconstructed images from between 100 and 500 μm from the cell body from each mouse.

2.6. Behavioural testing procedures

2.6.1. Emotion-like behaviour

2.6.1.1. Tail suspension test: despair (depression-like) behaviour. The TST consists of a horizontal bar with a large hook hanging below which the mouse is attached to by the tail using tape. Mice, which climb their tail, are excluded from results. Mice are attached to the apparatus for 6 min, and immobility is measured as an indication of despair and depression-like behaviour according to published protocols (O'Leary and Cryan, 2009).

2.6.1.2. Forced swim test: despair (depression-like) behaviour. The FST consists of a circular container, 45 cm high, with a diameter of 20 cm, which is filled with water to approximately halfway. Mice were placed in the water for 6 min and immobility time was measured as an indication of despair and depression-like behaviour according to published protocols (Porsolt et al., 1977; Petit-Demouliere et al., 2005).

2.6.1.3. Open field. Mice were placed into a brightly lit square arena, 40 × 40 cm, with clear walls 35 cm high for 5 min according to published protocols (Gould et al., nd; Baune et al., 2008; Hart et al., 2010). The floor was divided into inner and outer zones. Time spent in the centre of the open field was measured as an indication of anxiety-like behaviour.

2.6.1.4. Elevated zero maze: anxiety-like behaviour. Mice were placed in an open quadrant of the EZM, which is an elevated circular platform, 50 cm diameter, with a 5 cm wide platform 40 cm above ground. 2 quadrants are open, and 2 are enclosed with walls 15 cm high. Mice were allowed to explore the apparatus for 5 min according to published protocols (Shepherd et al., 1994), and time spent in the open quadrants was measured as an indication of anxiety-like behaviour (time in open arms is calculated as: time in open arm − latency to enter closed arm). Mice that spend more time in the open arms are considered to be less anxious. Distance travelled and number of head dips, defined as mice stretching their head out of a closed arm and dipping it over the edge of an open arm toward the floor, were also measured.

2.6.2. Cognition-like behaviour

2.6.2.1. Y-maze: spatial recognition memory. Mice were placed in the start arm of the Y-maze, which is a Y-shaped apparatus, with three arms (start arm and 2 test arms), each 35 cm long and 5 cm wide, with walls 10 cm high. The arms are at a 120° angle from each other, and the 2 test arms have different coloured pieces of tape on the inside walls. The left arm had horizontal, black stripes while the right arm had vertical yellow stripes of tape on the light grey walls. Testing was conducted according to published protocols (Dellu et al., 1992). During the training phase, one of the test arms was blocked off, and mice were allowed to explore the start arm and open test arm for 10 min. Half of the mice had access to the right test arm, while the other half had access to the left test arm to control for any possible side preference. 30 min later, they were placed back in the Y-maze for 5 min, with all 3 arms open. Time spent in the novel arm was used as a measure of spatial recognition memory. A preference index, a ratio of the amount of time spent in the novel test arm over the total time spent in the novel and familiar test arms, was used to measure recognition memory. A preference index approaching 1 was regarded as successful learning and retention memory. As all mice started the test in the same arm (start arm) time spent in this arm was not analysed.

2.7. Statistical analysis

Analyses were completed with GraphPad Prism statistical software (version 5.01). Comparisons between groups for results of behavioural data were performed using two-way ANOVA, with Bonferroni post hoc analysis when a significant effect was seen, as stated throughout the results. Histology and immunohistochemistry results were compared using Student's t-test. Results are presented as mean ± SEM and $p < 0.05$ taken as significant.

3. Results

3.1. 14-3-3ζ KO mice display dendritic spine defects and neurodevelopmental changes in the CA3 and dentate gyrus regions of the hippocampus and cortex

To analyse spine morphology we labelled individual neurons in fixed vibratome sections with biolostic delivery of lipohilic fluorescent dyes (DiI, DiD and DiO). Spines from secondary apical dendrites on hippocampus CA3 pyramidal neurons were quantitated from 3D reconstructed confocal images. Consistent with 14-3-3ζ KO mice modelling the phenotype of schizophrenia and related disorders, our analysis identified significant decreases in spine formation at P45 (Fig. 1A-B; WT, n = 4; KO, n = 4; P = 0.002). Neuronal complexity was also visualised by golgi stain in thick vibratome sections. Our analysis confirmed synaptic defects in the hippocampus and further revealed notable spine differences in cortical layer V pyramidal neurons (Fig. 1C).

We have previously shown that 14-3-3ζ KO mice have mild neuronal positioning and axonal guidance defects that are restricted to the hippocampus (Cheah et al., 2012), and confirmed these findings in the hippocampus of 14-3-3ζ KO mice examined for the present study.

3.2. In-vivo treatment with clozapine does not rescue dendritic spine deficits and neuronal lamination defects in 14-3-3ζ KO mice

As clozapine has been hypothesised to rescue dendritic spine deficits in some animal models of schizophrenia-like disorders (Barros et al., 2009) we examined the drug's effects on spine morphology in 14-3-3ζ KO mice. Our analysis of hippocampal pyramidal neurons shows that a 25-day treatment regime with clozapine does not modify spine density in either WT or KO neurons (Fig. 2A–B).

Additionally, analysis of Nissl staining (Fig. 3A) and immunostaining of calbindin (Fig. 3B) found that misplaced pyramidal neurons and mossy fibre navigation are not affected by clozapine treatment in either WT (n = 6, vehicle 3, clozapine treated 3, 1 male and 2 females per group) or KO mice (n = 6, vehicle 3, clozapine treated 3, 1 male and 2 females per group).

3.3. Despair (depression-like) behaviour is not affected by 14-3-3ζ KO; clozapine affects despair behaviour in 14-3-3ζ KO but not in WT mice

3.3.1. Despair (depression-like) behaviour: tail suspension and forced swim tests

Two-way ANOVA of TST immobility time (Interaction $F_{(1,27)} = 0.62$, P = 0.44, treatment $F_{(1,27)} = 2.76$, P = 0.11, Genotype $F_{(1,27)} = 0.50$, P = 0.49) showed no significant differences in despair-type behaviour between groups (Fig. 4A). However, two-way ANOVA of FST immobility time (Fig. 4B) showed significant effects of interaction ($F_{(1,30)} = 6.04$, P = 0.02), treatment ($F_{(1,30)} = 4.39$, P = 0.04) and genotype ($F_{(1,30)} = 5.89$, P = 0.02). Bonferroni post hoc analysis of treatment effect showed that clozapine decreased immobility time in KO mice (P =

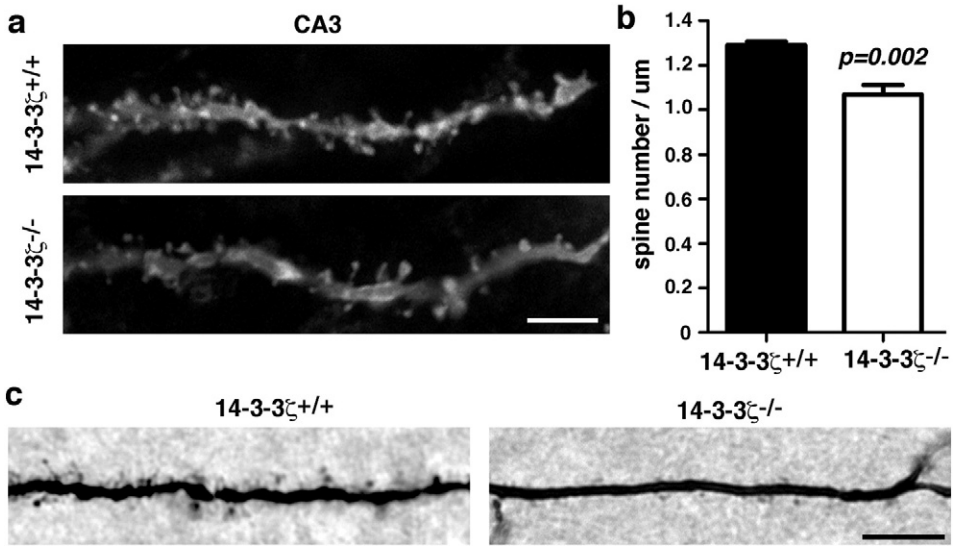

Fig. 1. A) Pyramidal neurons in the cornu ammonis layer 3 (CA3) of the hippocampus have reduced dendritic spines in 14-3-3ζ KO mice. Scale bar = 5um. B) Quantitation of data in A) shows that 14-3-3ζ KO mice (open bar; n = 4, 2 female, 2 male, over 30 dendrites counted/mouse) have significantly reduced dendritic spines compared to WT (closed bar; n = 4, 2 female, 2 male). C) High magnification of dendritic spines of layer V cortical pyramidal neurons with golgi stain reveals reduced spine numbers. Scale bar = 5um.

0.0076) but not WT mice (P > 0.99), while post hoc analysis of genotype effect showed that clozapine treated KO mice had a significantly lower immobility time than clozapine treated WT mice (P = 0.0026). These results indicate that clozapine may reduce despair behaviours specifically in 14-3-3ζ KO mice; however, we found significant effects only in one of the two despair tests carried out.

3.4. Anxiety-like behaviours are not affected by 14-3-3ζ KO or clozapine treatment

3.4.1. Open field: anxiety-like behaviour

In the open field test (Fig. 4C) there were no significant differences in time spent in the centre of the open field between any groups as analysed by two-way ANOVA (Interaction $F_{(1,29)} = 0.54$, P = 0.47, Treatment $F_{(1,29)} = 0.30$, P = 0.59, Genotype $F_{(1,29)} = 0.78$, P = 0.38), indicating no differences in anxiety levels in this test.

3.4.2. Elevated zero maze: anxiety-like behaviour

In the EZM, no differences were seen in anxiety levels as shown by (Fig. 4D) two-way ANOVA of time in open arms (Interaction $F_{(1,33)} = 1.16$, P = 0.29, Treatment $F_{(1,33)} = 0.001$, P = 0.97, Genotype $F_{(1,33)} = 0.05$,P = 0.83). There was also no difference in total distance travelled (WT-vehicle 11.1 ± 0.93, WT-clozapine 10.8 ± 1.06, KO-vehicle 12.3 ± 1.21, KO-clozapine 10.7 ± 1.12 m; two-way ANOVA: Interaction $F_{(1,33)} = 0.39$, P = 0.54, Treatment $F_{(1,33)} = 0.76$, P = 0.39, Genotype $F_{(1,33)} = 0.31$, P = 0.58). Number of head dips did show a significant effect of genotype (WT-vehicle 22.6 ± 3.51, WT-clozapine 18.8 ± 1.98, KO-vehicle 32.2 ± 4.14, KO-clozapine 28.6 ± 5.15; two-way ANOVA: Interaction $F_{(1,33)} = 0.01$, P = 0.92, Treatment $F_{(1,33)} = 1.28$, P = 0.27, Genotype $F_{(1,33)} = 7.58$, P = 0.0095), however Bonferroni post hoc analysis of genotype effect showed no significant differences. These results indicate no overall differences in anxiety between both vehicle groups and treatment groups in this test.

3.5. Clozapine treatment affects spatial recognition memory differentially in wild type and 14-3-3ζ KO mice

Fig. 5A compares the time spent in the novel compared to familiar arm of the Y-maze. Repeated measures two-way ANOVA shows a significant Interaction effect ($F_{(3,31)} = 6.35$, P = 0.0017) but no significant effect of other measures (Group $F_{(3,31)} = 1.13$, P = 0.35, Arm $F_{(1,31)} = 0.05$, P = 0.83). Bonferroni post hoc tests show that only clozapine treated WT mice spend significantly more time in the novel arm compared to the familiar (P = 0.033). Further information about the preference of mice can be gained from looking at the preference index for novel arm compared to familiar arm (Fig. 5B). Vehicle treated WT mice and clozapine treated KO mice have a preference index <0.5 (WT-vehicle 0.36 ± 0.07, KO-clozapine 0.39 ± .07), indicating a preference for the familiar arm, while clozapine treated WT mice and vehicle treated KO mice have a preference index >0.5 (WT-clozapine 0.78 ±

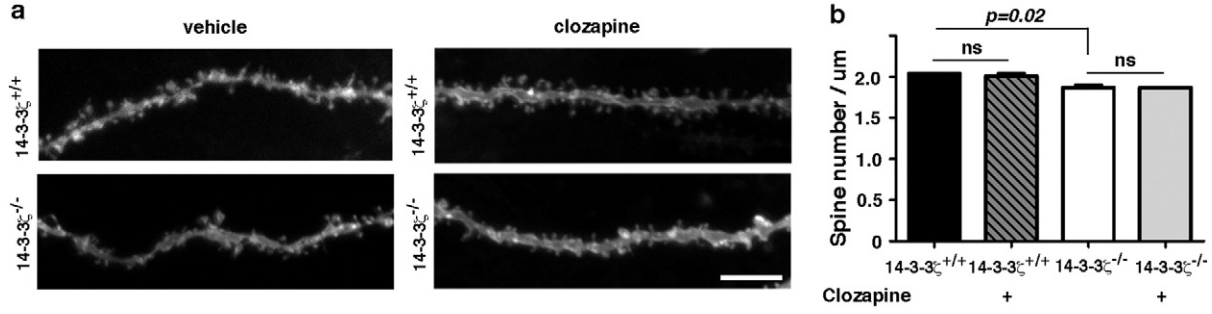

Fig. 2. A) Pyramidal neurons in the cornu ammonis layer 3 (CA3) of the hippocampus have reduced dendritic spines in 14-3-3ζ KO mice. Treatment with clozapine does not rescue the deficiency in spine formation of KO mice. B) Quantitation of data in *a*) shows that while 14-3-3ζ KO mice (open bar; n = 3 over 30 dendrites counted/mouse) have significantly reduced dendritic spines compared to WT (closed bar; n = 3). Clozapine treatment does not affect spine density in either WT (dark grey hashed bar; n = 3, 1 male, 2 females) or 14-3-3ζ KO mice (light grey bar; n = 3, 1 male, 2 females). Scale bar = 5um.

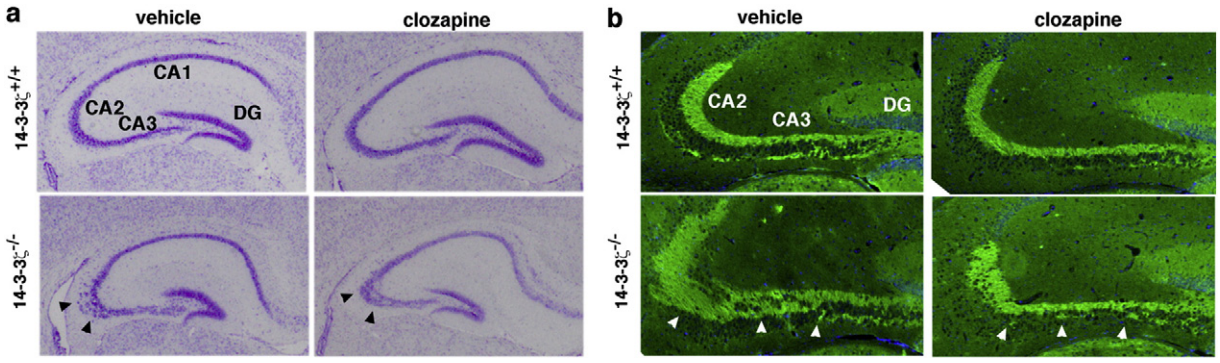

Fig. 3. A) Nissl staining highlights mispositioning of pyramidal neurons in the cornu ammonis region 2 (CA2) and 3 (CA3) of 14-3-3ζ KO mice (black arrowheads). Clozapine treatment is unable the rescue this positioning defect. B) Calbindin staining (green) identifies mossy fibre navigation defects in the CA3 of 14-3-3ζ KO mice (white arrowheads) that are not rescued by clozapine treatment.

0.06, KO-vehicle 0.69 ± 0.10), indicating a preference for the novel arm. Two-way ANOVA of preference index (Interaction $F_{(1,31)} = 20.0$, $P < 0.0001$, Treatment $F_{(1,31)} = 0.55$, $P = 0.46$, Genotype $F_{(1,31)} = 0.20$, $P = 0.60$) with Bonferroni post hoc analysis of genotype effect shows that vehicle control KO mice had a higher preference than WT control mice ($P = 0.017$). Bonferroni post hoc analysis of treatment effect showed that this difference between WT and KO mice was reversed by clozapine (KO vehicle vs clozapine $P = 0.033$), and that clozapine also significantly increased preference index in WT mice ($P = 0.0011$), suggesting clozapine had opposing effects on WT and KO mice.

4. Discussion

In-depth investigations of medication effects on anatomical and behavioural characteristics in animal models of psychiatric disorders have the potential to unveil novel biological processes contributing to treatment efficacy. Here, we demonstrate that 14-3-3ζ KO mice, representing a novel mouse model of schizophrenia, display dendritic spine abnormalities similar to other animal models of the disease. Clozapine, the most effective antipsychotic used for the treatment of schizophrenia, does not reverse these changes in our model, contrary to our initial hypothesis. On a behavioural level, clozapine reduced despair-like behaviour in 14-3-3ζ KO mice but not in wild-type animals. In a spatial recognition memory task (Y-maze), we found that 14-3-3ζ KO mice behave differently to WT mice on the Y-maze memory task, and that clozapine reversed these behavioural differences. We show that 14-3-3ζ KO or clozapine treatment have no effect on anxiety behaviours, or exploratory behaviour.

The loss of hippocampal dendritic spines in the 14-3-3ζ KO model is consistent with findings in human schizophrenia post-mortem brain (Garey et al., 1998; Harrison, 1999; Glantz and Lewis, 2000; Glausier and Lewis, 2013) and in other animal models of schizophrenia-like disorders (Barros et al., 2009; Cahill et al., 2009), and supports the utility of the 14-3-3ζ model for the study of these conditions. Our finding is also consistent with the fact that transgenic mice overexpressing 14-3-3ζ have increased spine density (Angrand et al., 2006) and that 14-3-3ζ KO mice in the BalBC genetic background have spine deficiency (Xu et al., 2015). Spine deficits in experimental models are thought to be associated with impairments in working memory, attention, sensorymotor processing, and sociability (Liston et al., 2006; Cahill et al., 2009; Hains et al., 2009; Brennaman et al., 2011), We have previously demonstrated that 14-3-3ζ KO mice also display deficits in several of

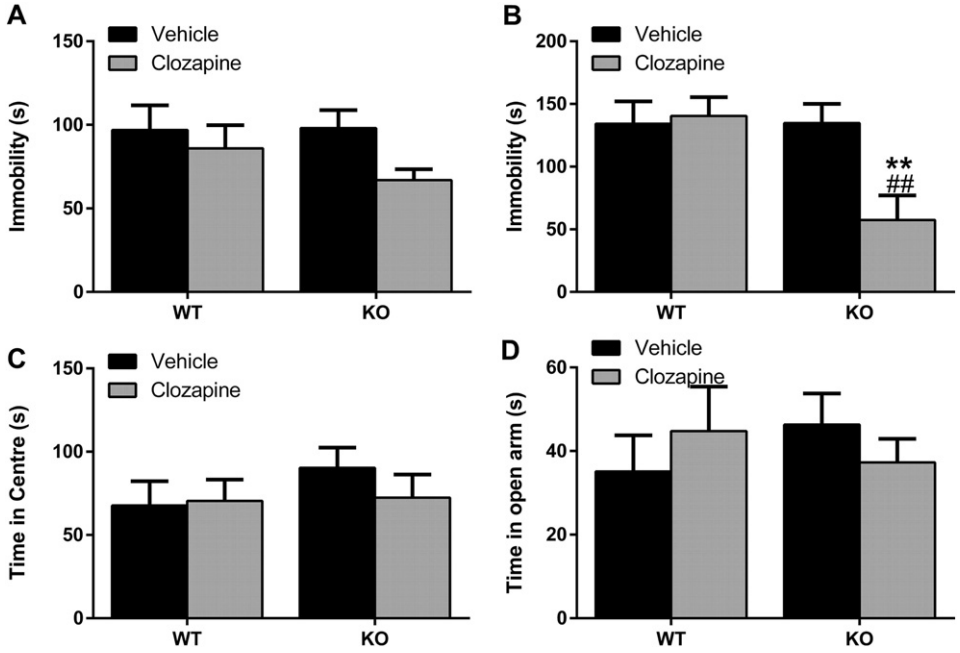

Fig. 4. A) Total time spent immobile during the tail suspension test and, B) total time spent immobile during the forced swim test. C) Time spent in the centre of the open field. D) Time spent in open arms of the elevated zero maze. Data compared using two-way ANOVA with Bonferroni post hoc test. **P < 0.01 c.f. WT (same treatment), # c.f. vehicle (same strain) (n = 8–10/group).

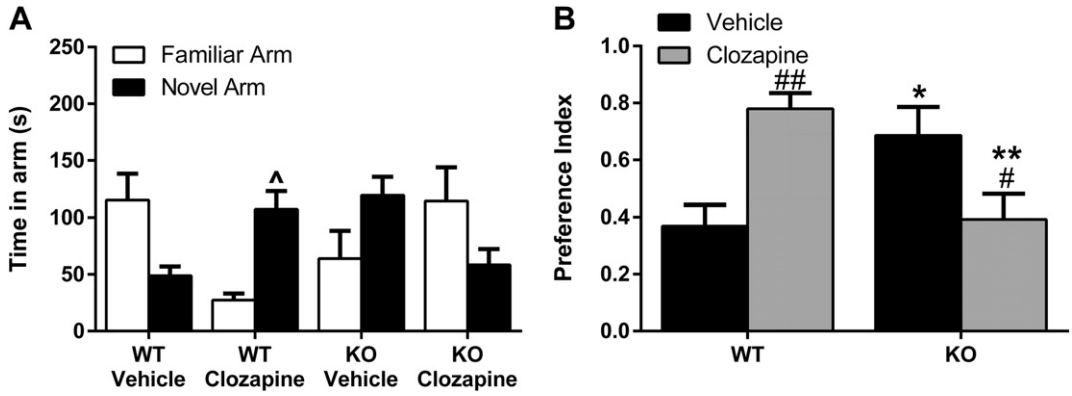

Fig. 5. A) Time spent in the novel and familiar arms in the retention phase of the Y-maze, B) preference index for novel arm, C) time spent interacting with familiar and novel object in retention phase of NOR test and D) preference index for novel object. Data compared using repeated measures two-way ANOVA with Bonferroni post hoc test. ^P < 0.05 c.f. novel arm. Data for preference index compared using two-way ANOVA with Bonferroni post hoc test. *c.f. WT, #c.f. vehicle. * P < 0.05, ** P < 0.01. (n = 8–10/group).

these cognitive domains (Cheah et al., 2012). It is therefore possible that dendritic spine abnormalities contribute to the behavioural phenotype observed in the 14-3-3ζ model.

The formation and stabilisation of dendritic spines is heavily dependent on many signalling events that modify the actin cytoskeleton (Schubert and Dotti, 2007). 14-3-3ζ has previously been shown to modulate actin polymerisation by binding to cofilin (Gohla and Bokoch, 2002), a molecule that has recently been implicated as a central mediator of dendritic spine dynamics (Shi et al., 2009). Consistent with the idea that 14-3-3ζ plays a role in regulating spine dynamics, cell fractionation experiments have shown that it is located in the synapse (Rajan et al., 2002), and biochemical studies have shown that it complexes with proteins required for stability of the postsynaptic density such as SPIN90 (Heverin et al., 2012). Spine density has also been analysed in a number of mouse mutants lacking proteins that interact with 14-3-3ζ. Consistent with our findings, DAT, Ndel1 and Lis1 deficient mice have reduced dendritic spine density (Berlanga et al., 2011; Sudarov et al., 2013). A detailed analysis of 14-3-3ζ localisation in pre- and post-synaptic neurons, and the analysis of spine development in 14-3-3ζ KO mice, is now required to define the mechanisms through which it controls spine formation.

In the present study, the in-vivo administration of clozapine for 25 days did not rescue or reverse dendritic spine abnormalities in 14-3-3ζ KO mice. This finding contrasts previous in- vitro experiments suggesting trophic effects of clozapine on dendritic spine morphology (Lu and Dwyer, 2005; Critchlow et al., 2006; Barros et al., 2009). It is possible that the *in vivo* environment examined in our study prevented or procrastinated the morphological changes seen *in vitro*. Differences between *in vivo* and *in vitro* observations of dendritic spine function are well recognised in the field (Rochefort and Konnerth, 2012). Alternatively, a longer treatment period or higher doses of clozapine may have led to different results.

On the other hand, it is possible that spine abnormalities caused by different molecular lesions have differential sensitivity to clozapine treatment. For example, dendritic spine abnormalities induced by Erb/B2/B4-deficiency may benefit from clozapine, whereas 14-3-3ζ KO-associated abnormalities do not. Such differential response to clozapine is plausible from a clinical perspective, since the clinical benefits to patients treated with this drug also differ vastly (Lieberman et al., 1994). Differential findings in animal models may therefore open the door to pharmacogenetic studies to identify potential biomarkers of clozapine treatment response.

In the present study, we investigated the effects of 14-3-3ζ KO and clozapine on tests for cognition-, anxiety- and despair (depression-like) behaviours. These behaviours are relevant for schizophrenia: cognitive deficits are a well-recognised feature of schizophrenia and are thought to have particularly devastating consequences on patients' functioning (Keefe and Harvey, 2012); depression and anxiety co-morbidly occur in a large proportion of people with schizophrenia, and have been shown to correlate with symptom severity and treatment outcomes (Gozdzik-Zelazny et al., 2011; Braga et al., 2013).

Results of the FST indicate that clozapine may reduce despair-like behaviours in 14-3-3ζ KO mice, but not in wild type animals. 14-3-3ζ KO status alone did not significantly impact on baseline FST performance. Results of the TST showed a similar pattern but did not reach statistical significance between groups. Previous animal studies have shown despair-reducing effects of clozapine in the FST (Weiner et al., 2003), and reductions in anhedonia-like behaviours in the sucrose preference test (Vardigan et al., 2010). Given the negative results in wild-type animals, our findings are only partially consistent with these studies. Therefore, it remains unclear whether clozapine indeed reduces depression-like behaviours in rodents. At best, the results of our study provide a preliminary indication that such effects could be mediated by specific molecular lesions such as 14-3-3ζ deficiency.

For anxiety-like behaviours, we observed a trend toward KO mice displaying decreased levels of anxiety, as measured by increased time spent in open arms in the EZM. This finding contrasts the increased time spent in the open arms of the elevated plus maze (EPM) reported by Cheah et al. (2012). Discrepant findings may be at least in part due to the different maze apparatus used, as KO mice also spent less time in the centre area on the EPM (Cheah et al., 2012). The EZM and EPM apparatus both measure the same behavioural phenotype, however the EZM removes the issue of ambiguity with time spent in the centre of the EPM (Shepherd et al., 1994), which may lead to different anxiety results being seen in some studies. In the current study, there were also no significant differences in anxiety seen in the open field, as measured by time spent in the centre of the test arena, although there was a similar trend to that seen in the EZM. In both tests there was also a trend for clozapine to reverse the differences seen in KO mice. However, overall these results indicate that anxiety was not a robust characteristic of KO mice compared to WT mice and that clozapine may not exert relevant effects on anxiety via 14-3-3ζ-related pathways.

Tests of cognition-like behaviours yielded unexpected results in this study. In contrast to the expected behaviour in the Y-maze, where control mice show a preference for the novel arm, our Y-maze analysis showed that 14-3-3ζ WT mice on the SV129 background had a preference for the familiar arm, suggesting either experimental problems or impaired memory in these animals. Vehicle treated KO mice showed the expected behaviour with a significantly higher preference index for the novel arm. Clozapine treatment decreased preference for the novel arm in KO mice, possibly as a result of sedative side effects. Clozapine also reversed the unexpected baseline behaviour in WT mice. As these results are difficult to interpret due to the unexpected behaviour of WT mice, further studies should now be completed with different

cognition tests to definitively determine whether clozapine can rescue the cognition and memory impairments previously reported in these mice (Cheah et al., 2012).

The findings of this study underscore the importance of comprehensive behavioural testing and result reporting when characterising animal models of mental diseases and their response to common treatments. Previous studies in *14-3-3ζ* -depleted mice have reported a beneficial effect of clozapine on isolated behavioural paradigms such as hyperactivity (Ramshaw et al., 2013; Foote et al., 2015) and prepulse inhibition (Foote et al., 2015). The incorporation of a more comprehensive test battery in our study shows that clozapine effects are not clear-cut in this model. In fact, the replicated finding of reversed hyperactivity, as well as some of the findings of the present study, could also be explained by sedative effects, given that clozapine is the most sedating antipsychotic on the market (Leucht et al., 2013).

In conclusion, our study demonstrates that *14-3-3ζ* KO mice display a reduction of dendritic spines in the hippocampus, mirroring findings in human post-mortem schizophrenia brain and in other animal models of schizophrenia-like disorders. Our finding supports the utility of *14-3-3ζ* KO animal model in these disorders, and implicates dendritic changes as a potential common morphological endpoint of various molecular alterations associated with schizophrenia. Contrary to our initial hypothesis, our behavioural findings indicate that *14-3-3* proteins may play only a modest role in mediating cognition-, depression-, and anxiety-like behaviours and clinical responses to clozapine in schizophrenia.

Acknowledgements

This study is supported by the National Health and Medical Research Council Australia (APP1003788 to BTB) and Medvet Laboratories (QPS). The funders had no role in study design, data collection and analysis, decision to publish, or preparation of the manuscript.

We thank Rebecca Krake for genotyping mice and maintaining the mouse colony, and Frances Corrigan and Catherine Toben for assistance with clozapine dosing.

References

Angrand, P.O., Segura, I., Volkel, P., Ghidelli, S., Terry, R., Brajenovic, M., Vintersten, K., Klein, R., Superti-Furga, G., Drewes, G., Kuster, B., Bouwmeester, T., Acker-Palmer, A., 2006. Transgenic mouse proteomics identifies new 14-3-3-associated proteins involved in cytoskeletal rearrangements and cell signaling. Mol. Cell. Proteomics 5, 2211–2227.

Barros, C.S., Calabrese, B., Chamero, P., Roberts, A.J., Korzus, E., Lloyd, K., Stowers, L., Mayford, M., Halpain, S., Muller, U., 2009. Impaired maturation of dendritic spines without disorganization of cortical cell layers in mice lacking NRG1/ErbB signaling in the central nervous system. Proc. Natl. Acad. Sci. U. S. A. 106, 4507–4512.

Baune, B.T., Wiede, F., Braun, A., Golledge, J., Arolt, V., Koerner, H., 2008. Cognitive dysfunction in mice deficient for TNF- and its receptors. Am J Med Genet B Neuropsychiatr Genet 147B, 1056–1064.

Berlanga, M.L., Price, D.L., Phung, B.S., Giuly, R., Terada, M., Yamada, N., Cyr, M., Caron, M.G., Laakso, A., Martone, M.E., Ellisman, M.H., 2011. Multiscale imaging characterization of dopamine transporter knockout mice reveals regional alterations in spine density of medium spiny neurons. Brain Res. 1390, 41–49.

Braga, R.J., Reynolds, G.P., Siris, S.G., 2013. Anxiety comorbidity in schizophrenia. Psychiatry Res. 210, 1–7.

Brennaman, L.H., Kochlamazashvili, G., Stoenica, L., Nonneman, R.J., Moy, S.S., Schachner, M., Dityatev, A., Maness, P.F., 2011. Transgenic mice overexpressing the extracellular domain of NCAM are impaired in working memory and cortical plasticity. Neurobiol. Dis. 43, 372–378.

Cahill, M.E., Xie, Z., Day, M., Photowala, H., Barbolina, M.V., Miller, C.A., Weiss, C., Radulovic, J., Sweatt, J.D., Disterhoft, J.F., Surmeier, D.J., Penzes, P., 2009. Kalirin regulates cortical spine morphogenesis and disease-related behavioral phenotypes. Proc. Natl. Acad. Sci. U. S. A. 106, 13058–13063.

Cheah, P.S., Ramshaw, H.S., Thomas, P.Q., Toyo-Oka, K., Xu, X., Martin, S., Coyle, P., Guthridge, M.A., Stomski, F., Van Den Buuse, M., Wynshaw-Boris, A., Lopez, A.F., Schwarz, Q.P., 2012. Neurodevelopmental and neuropsychiatric behaviour defects arise from 14 to 3-3zeta deficiency. Mol. Psychiatry 17, 451–466.

Critchlow, H.M., Maycox, P.R., Skepper, J.N., Krylova, O., 2006. Clozapine and haloperidol differentially regulate dendritic spine formation and synaptogenesis in rat hippocampal neurons. Mol. Cell. Neurosci. 32, 356–365.

Dawe, G.S., Nagarajah, R., Albert, R., Casey, D.E., Gross, K.W., Ratty, A.K., 2010. Antipsychotic drugs dose-dependently suppress the spontaneous hyperactivity of the chakragati mouse. Neuroscience 171, 162–172.

Dellu, F., Mayo, W., Cherkaoui, J., Le Moal, M., Simon, H., 1992. A two-trial memory task with automated recording: study in young and aged rats. Brain Res. 588, 132–139.

English, J.A., Dicker, P., Focking, M., Dunn, M.J., Cotter, D.R., 2009. 2-D DIGE analysis implicates cytoskeletal abnormalities in psychiatric disease. Proteomics 9, 3368–3382.

Ertugrul, A., Volkan-Salanci, B., Basar, K., Karli Oguz, K., Demir, B., Ergun, E.L., Senturk, S., Erbas, B., Cila, A., Ulug, B., 2009. The effect of clozapine on regional cerebral blood flow and brain metabolite ratios in schizophrenia: relationship with treatment response. Psychiatry Res. 174, 121–129.

Essali, A., Haasan, N.a.H., Li, C., Rathbone, J., 2009. Clozapine Versus Typical Neuroleptic Medication for Schizophrenia. Cochrane Database of Systematic Reviews.

Fakra, E., Azorin, J.M., 2012. Clozapine for the treatment of schizophrenia. Expert. Opin. Pharmacother. 13, 1923–1935.

Focking, M., Dicker, P., English, J.A., Schubert, K.O., Dunn, M.J., Cotter, D.R., 2011. Common proteomic changes in the hippocampus in schizophrenia and bipolar disorder and particular evidence for involvement of cornu ammonis regions 2 and 3. Arch. Gen. Psychiatry 68, 477–488.

Foote, M., Qiao, H., Graham, K., Wu, Y., Zhou, Y., 2015. Inhibition of 14-3-3 proteins leads to schizophrenia-related behavioral phenotypes and synaptic defects in mice. Biol. Psychiatry.

Fromer, M., Pocklington, A.J., Kavanagh, D.H., Williams, H.J., Dwyer, S., Gormley, P., Georgieva, L., Rees, E., Palta, P., Ruderfer, D.M., Carrera, N., Humphreys, I., Johnson, J.S., Roussos, P., Barker, D.D., Banks, E., Milanova, V., Grant, S.G., Hannon, E., Rose, S.A., Chambert, K., Mahajan, M., Scolnick, E.M., Moran, J.L., Kirov, G., Palotie, A., Mccarroll, S.A., Holmans, P., Sklar, P., Owen, M.J., Purcell, S.M., O'donovan, M.C., 2014. De novo mutations in schizophrenia implicate synaptic networks. Nature 506, 179–184.

Gan, W.B., Grutzendler, J., Wong, W.T., Wong, R.O., Lichtman, J.W., 2000. Multicolor "DiOlistic" labeling of the nervous system using lipophilic dye combinations. Neuron 27, 219–225.

Garey, L.J., Ong, W.Y., Patel, T.S., Kanani, M., Davis, A., Mortimer, A.M., Barnes, T.R., Hirsch, S.R., 1998. Reduced dendritic spine density on cerebral cortical pyramidal neurons in schizophrenia. J. Neurol. Neurosurg. Psychiatry 65, 446–453.

Glantz, L.A., Lewis, D.A., 2000. Decreased dendritic spine density on prefrontal cortical pyramidal neurons in schizophrenia. Arch. Gen. Psychiatry 57, 65–73.

Glausier, J.R., Lewis, D.A., 2013. Dendritic spine pathology in schizophrenia. Neuroscience 251, 90–107.

Gohla, A., Bokoch, G.M., 2002. 14-3-3 regulates actin dynamics by stabilizing phosphorylated cofilin. Curr. Biol. 12, 1704–1710.

Gould, T.D., Dao, D.T., and Kovacsics, C.E. "The Open Field Test."), 1–20 nd.

Gozdzik-Zelazny, A., Borecki, L., Pokorski, M., 2011. Depressive symptoms in schizophrenic patients. Eur J Med Res 16, 549–552.

Hains, A.B., Vu, M.A., Maciejewski, P.K., Van Dyck, C.H., Gottron, M., Arnsten, A.F., 2009. Inhibition of protein kinase C signaling protects prefrontal cortex dendritic spines and cognition from the effects of chronic stress. Proc. Natl. Acad. Sci. U. S. A. 106, 17957–17962.

Harrison, P.J., 1999. The neuropathology of schizophrenia. A critical review of the data and their interpretation. Brain 122 (Pt 4), 593–624.

Hart, P.C., Bergner, C.L., Smolinsky, A.N., Dufour, B.D., Egan, R.J., Laporte, J.L., Kalueff, A.V., 2010. Experimental models of anxiety for drug discovery and brain research. Methods Mol. Biol. 602, 299–321.

Heverin, M., Brennan, G.P., Koehler, C.J., Treumann, A., Henshall, D.C., 2012. Proteomic analysis of 14-3-3 zeta binding proteins in the mouse hippocampus. Int J Physiol Pathophysiol Pharmacol 4, 74–83.

Jaehne, E.J., Baune, B.T., 2014. Effects of chemokine receptor signalling on cognition-like, emotion-like and sociability behaviours of CCR6 and CCR7 knockout mice. Behav. Brain Res. 261, 31–39.

Jia, Y., Yu, X., Zhang, B., Yuan, Y., Xu, Q., Shen, Y., Shen, Y., 2004. An association study between polymorphisms in three genes of 14-3-3 (tyrosine 3-monooxygenase/tryptophan 5-monooxygenase activation protein) family and paranoid schizophrenia in northern Chinese population. Eur Psychiatry 19, 377–379.

Jones, C.A., Watson, D.J., Fone, K.C., 2011. Animal models of schizophrenia. Br. J. Pharmacol. 164, 1162–1194.

Keefe, R.S., Harvey, P.D., 2012. Cognitive impairment in schizophrenia. Handb. Exp. Pharmacol. 11-37.

Konopaske, G.T., Lange, N., Coyle, J.T., Benes, F.M., 2014. Prefrontal cortical dendritic spine pathology in schizophrenia and bipolar disorder. JAMA Psychiatry 71, 1323–1331.

Leucht, S., Cipriani, A., Spineli, L., Mavridis, D., Orey, D., Richter, F., Samara, M., Barbui, C., Engel, R.R., Geddes, J.R., Kissling, W., Stapf, M.P., Lassig, B., Salanti, G., Davis, J.M., 2013. Comparative efficacy and tolerability of 15 antipsychotic drugs in schizophrenia: a multiple-treatments meta-analysis. Lancet 382, 951–962.

Lieberman, J.A., Safferman, A.Z., Pollack, S., Szymanski, S., Johns, C., Howard, A., Kronig, M., Bookstein, P., Kane, J.M., 1994. Clinical effects of clozapine in chronic schizophrenia: response to treatment and predictors of outcome. Am. J. Psychiatry 151, 1744–1752.

Liston, C., Miller, M.M., Goldwater, D.S., Radley, J.J., Rocher, A.B., Hof, P.R., Morrison, J.H., Mcewen, B.S., 2006. Stress-induced alterations in prefrontal cortical dendritic morphology predict selective impairments in perceptual attentional set-shifting. J Neurosci 26, 7870–7874.

Lu, X.H., Dwyer, D.S., 2005. Second-generation antipsychotic drugs, olanzapine, quetiapine, and clozapine enhance neurite outgrowth in PC12 cells via PI3K/AKT, ERK, and pertussis toxin-sensitive pathways. J. Mol. Neurosci. 27, 43–64.

Meltzer, H.Y., 2010. Role of clozapine in treatment-resistant schizophrenia. In: Elkis, H., Meltzer, H.Y. (Eds.), Therapy-Resistant Schizophrenia. Karger, Basel, pp. 114–128.

Middleton, F.A., Peng, L., Lewis, D.A., Levitt, P., Mirnics, K., 2005. Altered expression of 14-3-3 genes in the prefrontal cortex of subjects with schizophrenia. Neuropsychopharmacology 30, 974–983.

O'leary, O.F., Cryan, J.F., 2009. The tail-suspension test: a model for characterizing antidepressant activity in mice #. T Mood and Anxiety Related Phenotypes in Mice, pp. 119–137.
Ozcelik-Eroglu, E., Ertugrul, A., Oguz, K.K., Has, A.C., Karahan, S., Yazici, M.K., 2014. Effect of clozapine on white matter integrity in patients with schizophrenia: a diffusion tensor imaging study. Psychiatry Res. 223, 226–235.
Penzes, P., Cahill, M.E., Jones, K.A., Vanleeuwen, J.E., Woolfrey, K.M., 2011. Dendritic spine pathology in neuropsychiatric disorders. Nat. Neurosci. 14, 285–293.
Petit-Demouliere, B., Chenu, F., Bourin, M., 2005. Forced swimming test in mice: a review of antidepressant activity. Psychopharmacology 177, 245–255.
Porsolt, R.D., Bertin, A., Jalfre, M., 1977. Behavioral despair in mice: a primary screening test for antidepressants. Arch. Int. Pharmacodyn. Ther. 229, 327–336.
Pratt, J., Winchester, C., Dawson, N., Morris, B., 2012. Advancing schizophrenia drug discovery: optimizing rodent models to bridge the translational gap. Nat. Rev. Drug Discov. 11, 560–579.
Rajan, S., Preisig-Muller, R., Wischmeyer, E., Nehring, R., Hanley, P.J., Renigunta, V., Musset, B., Schlichthorl, G., Derst, C., Karschin, A., Daut, J., 2002. Interaction with 14-3-3 proteins promotes functional expression of the potassium channels TASK-1 and TASK-3. J. Physiol. 545, 13–26.
Ramshaw, H., Xu, X., Jaehne, E.J., Mccarthy, P., Greenberg, Z., Saleh, E., Mcclure, B., Woodcock, J., Kabbara, S., Wiszniak, S., Wang, T.Y., Parish, C., Van Den Buuse, M., Baune, B.T., Lopez, A., Schwarz, Q., 2013. Locomotor hyperactivity in 14-3-3zeta KO mice is associated with dopamine transporter dysfunction. Transl Psychiatry 3, e327.
Rizig, M.A., Mcquillin, A., Ng, A., Robinson, M., Harrison, A., Zvelebil, M., Hunt, S.P., Gurling, H.M., 2012. A gene expression and systems pathway analysis of the effects of clozapine compared to haloperidol in the mouse brain implicates susceptibility genes for schizophrenia. J. Psychopharmacol. 26, 1218–1230.
Rochefort, N.L., Konnerth, A., 2012. Dendritic spines: from structure to in vivo function. EMBO Rep. 13, 699–708.
Schubert, K.O., Focking, M., Cotter, D.R., 2015. Proteomic pathway analysis of the hippocampus in schizophrenia and bipolar affective disorder implicates 14-3-3 signaling, aryl hydrocarbon receptor signaling, and glucose metabolism: potential roles in GABAergic interneuron pathology. Schizophr. Res.
Schubert, V., Dotti, C.G., 2007. Transmitting on actin: synaptic control of dendritic architecture. J. Cell Sci. 120, 205–212.
Sharp, S.I., Hu, Y., Weymer, J.F., Rizig, M., Mcquillin, A., Hunt, S.P., Gurling, H.M., 2013. The effect of clozapine on mRNA expression for genes encoding G protein-coupled receptors and the protein components of clathrin-mediated endocytosis. Psychiatr. Genet. 23, 153–162.
Shepherd, J.K., Grewal, S.S., Fletcher, A., Bill, D.J., Dourish, C.T., 1994. Behavioural and pharmacological characterisation of the elevated "zero-maze" as an animal model of anxiety. Psychopharmacology 116, 56–64.
Shi, Y., Pontrello, C.G., Defea, K.A., Reichardt, L.F., Ethell, I.M., 2009. Focal adhesion kinase acts downstream of EphB receptors to maintain mature dendritic spines by regulating cofilin activity. J Neurosci 29, 8129–8142.
Sivagnanasundaram, S., Crossett, B., Dedova, I., Cordwell, S., Matsumoto, I., 2007. Abnormal pathways in the genu of the corpus callosum in schizophrenia pathogenesis: a proteome study. Proteomics Clin. Appl. 1, 1291–1305.
Sudarov, A., Gooden, F., Tseng, D., Gan, W.B., Ross, M.E., 2013. Lis1 controls dynamics of neuronal filopodia and spines to impact synaptogenesis and social behaviour. EMBO Mol Med 5, 591–607.
Sweatt, J.D., 2004. Hippocampal function in cognition. Psychopharmacology 174, 99–110.
Toma, C., Torrico, B., Hervas, A., Valdes-Mas, R., Tristan-Noguero, A., Padillo, V., Maristany, M., Salgado, M., Arenas, C., Puente, X.S., Bayes, M., Cormand, B., 2014. Exome sequencing in multiplex autism families suggests a major role for heterozygous truncating mutations. Mol. Psychiatry 19, 784.
Toyo-Oka, K., Shionoya, A., Gambello, M.J., Cardoso, C., Leventer, R., Ward, H.L., Ayala, R., Tsai, L.H., Dobyns, W., Ledbetter, D., Hirotsune, S., Wynshaw-Boris, A., 2003. 14-3-3epsilon is important for neuronal migration by binding to NUDEL: a molecular explanation for Miller–Dieker syndrome. Nat. Genet. 34, 274–285.
Vardigan, J.D., Huszar, S.L., Mcnaughton, C.H., Hutson, P.H., Uslaner, J.M., 2010. MK-801 produces a deficit in sucrose preference that is reversed by clozapine, D-serine, and the metabotropic glutamate 5 receptor positive allosteric modulator CDPPB: relevance to negative symptoms associated with schizophrenia? Pharmacol. Biochem. Behav. 95, 223–229.
Wang, J.F., Min, J.Y., Hampton, T.G., Amende, I., Yan, X., Malek, S., Abelmann, W.H., Green, A.I., Zeind, J., Morgan, J.P., 2008. Clozapine-induced myocarditis: role of catecholamines in a murine model. Eur. J. Pharmacol. 592, 123–127.
Weiner, I., Schiller, D., Gaisler-Salomon, I., Green, A., Joel, D., 2003. A comparison of drug effects in latent inhibition and the forced swim test differentiates between the typical antipsychotic haloperidol, the atypical antipsychotics clozapine and olanzapine, and the antidepressants imipramine and paroxetine. Behav. Pharmacol. 14, 215–222.
Williams, A.A., Ingram, W.M., Levine, S., Resnik, J., Kamel, C.M., Lish, J.R., Elizalde, D.I., Janowski, S.A., Shoker, J., Kozlenkov, A., Gonzalez-Maeso, J., Gallitano, A.L., 2012. Reduced levels of serotonin 2A receptors underlie resistance of Egr3-deficient mice to locomotor suppression by clozapine. Neuropsychopharmacology 37, 2285–2298.
Wolf, R., Paelchen, K., Matzke, K., Dobrowolny, H., Bogerts, B., Schwegler, H., 2007. Acute or subchronic clozapine treatment does not ameliorate prepulse inhibition (PPI) deficits in CPB-K mice with low levels of hippocampal NMDA receptor density. Psychopharmacology 194, 93–102.
Wong, A.H., Likhodi, O., Trakalo, J., Yusuf, M., Sinha, A., Pato, C.N., Pato, M.T., Van Tol, H.H., Kennedy, J.L., 2005. Genetic and post-mortem mRNA analysis of the 14-3-3 genes that encode phosphoserine/threonine-binding regulatory proteins in schizophrenia and bipolar disorder. Schizophr. Res. 78, 137–146.
Xu, X., Jaehne, E.J., Greenberg, Z., Mccarthy, P., Saleh, E., Parish, C.L., Camera, D., Heng, J., Haas, M., Baune, B.T., Ratnayake, U., Buuse, M., Lopez, A.F., Ramshaw, H.S., Schwarz, Q., 2015. 14-3-3zeta deficient mice in the BALB/c background display behavioural and anatomical defects associated with neurodevelopmental disorders. Sci. Rep. 5, 12434.